RESEARCH WORK SUBMITTED TO THE DEPARTMENT OF ENERGY ENGINEERING,
HIGHER TECHNICAL SCHOOL OF ENGINEERING,
IN PARTIAL FULFILMENT OF THE REQUIREMENTS FOR THE DEGREE OF
DOCTOR OF PHILOSOPHY

Theoretical Analysis of High Efficient Multi-Effect Distillation Processes and their Integration into Concentrating Solar Power Plants

by

Bartolomé Ortega Delgado

ALMERÍA
September 2016

UNIVERSITY OF SEVILLE
Department of Energy Engineering

In collaboration with

SOLAR DESALINATION UNIT
CIEMAT - PLATAFORMA SOLAR DE ALMERÍA

Ciemat
Centro de Investigaciones Energéticas, Medioambientales y Tecnológicas

Theoretical Analysis of High Efficient Multi-Effect Distillation Processes and their Integration into Concentrating Solar Power Plants

Author:

Bartolomé Ortega Delgado

Supervisors:

DR. DIEGO-CÉSAR ALARCÓN PADILLA	DR. PATRICIA PALENZUELA ARDILA	DR. LOURDES GARCÍA RODRÍGUEZ
SENIOR RESEARCHER AT CIEMAT	RESEARCH SCIENTIST AT CIEMAT	PROFESSOR AT UNIVERSITY OF SEVILLE

UNIVERSITY OF SEVILLE
Department of Energy Engineering

In collaboration with

SOLAR DESALINATION UNIT
CIEMAT - PLATAFORMA SOLAR DE ALMERÍA

Ciemat
Centro de Investigaciones Energéticas, Medioambientales y Tecnológicas

El Dr. Diego-César Alarcón Padilla, Científico Titular de OPIS CIEMAT,
la Dra. Patricia Palenzuela Ardila, Investigador Titulado Superior CIEMAT y
la Dra. Lourdes García Rodríguez, Catedrática de la Universidad de Sevilla

INFORMAN:

Que el trabajo descrito en la presente memoria, titulado: "Theoretical Analysis of High Efficient Multi-Effect Distillation Processes and their Integration into Concentrating Solar Power Plants" ha sido realizado por D. Bartolomé Ortega Delgado bajo su dirección.

Dicha tesis reúne los requisitos necesarios para su presentación y defensa.

Y para que conste y surta los efectos oportunos, firma el presente en Sevilla, a ____ de _____ de _____.

El Director (1) La Directora (2) La Directora (3) y tutora

Fdo.:Diego-César Alarcón Padilla Fdo.:Patricia Palenzuela Ardila Fdo.:Lourdes García Rodríguez

Agradecimientos / acknowledgements

Me gustaría en primer lugar expresar mi agradecimiento a Julián Blanco por la oportunidad que me ofreció para comenzar este período como estudiante predoctoral en el CIEMAT, a finales del 2012.

Quiero agradecer muy especialmente a mis directores de tesis, Lourdes García, Diego Alarcón y Patricia Palenzuela, la completa dedicación, inestimable ayuda y amable generosidad que me han prestado y con la que me han tratado a lo largo de estos inolvidables años. Sus siempre acertados comentarios y oportuna guía han sido fundamentales para la realización de esta memoria.

También quiero acordarme de mi excompañera de despacho Alba, por su apoyo y comprensión, con la que tan buenos momentos he compartido; y del resto de integrantes de la Unidad de Desalación Solar, Guillermo Zaragoza, Juan Antonio y Rafa, que siempre me han brindado su valiosa ayuda.

Y, cómo no, quiero agradecer a las chicas de Tratamiento Solares del Agua, María, Isa, Margarita, Melina, Samira, Mercedes, Inma, Ana, Irene, Laura, Eli, Sara, Estefanía … por su amistad y por permitirme compartir con ellas tantos buenos ratos. También al resto de compañeros y personal de la PSA, Isa Oller, Pilar, Nacho, Carmen, Merche, Víctor, Luis, Laura, Elena, Asma, Aicha, David, Juanjo, Álex, Diego, Rafa, Lucía, Arantxa, Lidia, Javi… Y aunque no quiero olvidar a nadie, la lista de personas que he conocido durante mi estancia en la PSA es demasiado grande como para plasmarla aquí, por ello quiero mostrar mi mayor agradecimiento hacia todas y cada una de ellas.

Y lo más importante, mi familia, por su gran ayuda durante esta etapa.

A mis padres,
José y Carmen,

y hermanos,
José y María del Carmen

"Consider your origin: you were not made to live like brutes, but to follow virtue and knowledge."

Dante Alighieri,
Inferno Canto XXVI:85-142
Ulysses's last voyage

Resumen

La escasez de agua y el abastecimiento energético son actualmente dos de los mayores retos a los que se enfrenta la sociedad global. El crecimiento de la población mundial junto con el aumento de las actividades industriales, especialmente en los países en vía de desarrollo, está provocando un rápido incremento del consumo energético y, en consecuencia, de la construcción de nuevas plantas de producción de potencia. La mayoría de dichas plantas están basadas en la utilización de combustibles fósiles, los cuales emiten en su combustión gases de efecto invernadero (principalmente CO_2), contribuyendo al calentamiento global del planeta. Las tecnologías de producción de potencia que emplean energías renovables (solar, eólica, geotérmica, etc.) como fuente energética representan una alternativa limpia y respetuosa con el medio ambiente, en particular las plantas solares de concentración, las cuales han demostrado ser un sistema fiable para la generación de energía eléctrica. Por otra parte, aunque más del 70% de la superficie terrestre es agua, el agua dulce representa sólo el 2.5% del volumen total de la hidrosfera, siendo el resto agua salada. Además, de dicho porcentaje de agua dulce, alrededor del 69% está contenida en glaciares y nieves permanentes, siendo su extracción poco viable, tanto desde un punto de vista económico como medioambiental. Por lo tanto, la producción de agua dulce mediante la desalación de agua de mar puede ayudar a resolver los problemas de abastecimiento de agua, en especial en las zonas áridas del planeta, como ha sido probado en los países de Oriente Medio desde la segunda mitad del siglo XX. Asimismo, aquellas regiones del mundo que sufren problemas de estrés hídrico presentan habitualmente altos niveles de irradiación solar, lo que refuerza la idea de emplear dicha fuente de energía renovable para producir agua dulce mediante la desalación de agua de mar en dichas zonas con acceso directo a la costa. Existe también una conexión entre los problemas asociados al abastecimiento de agua y energía, debido a que la generación de electricidad, ya sea por medios convencionales o tecnologías renovables, requiere grandes cantidades de agua (en particular para la refrigeración del ciclo de potencia), y a su vez, la producción de agua mediante desalación de agua de mar precisa de un alto consumo energético. De los anteriores razonamientos puede concluirse que la cogeneración de agua y electricidad mediante la integración de procesos de desalación de agua de mar y plantas termosolares de concentración, podría ayudar a resolver, al menos parcialmente, los problemas de suministro energético y de agua dulce en dichas zonas del planeta.

Los principales objetivos de este trabajo de investigación son el desarrollo de una herramienta de simulación (en funcionamiento nominal y a carga parcial) para procesos de destilación multiefecto (*Multi-Effect Distillation*, MED) con compresión térmica de vapor (*Thermal Vapor Compression*, TVC), integrados en una planta termosolar de concentración para generación eléctrica (*Concentrating Solar Power*, CSP) con tecnología de captadores cilindroparabólicos

(*Parabolic Trough*, PT). Dicha herramienta permitirá determinar la eficiencia de la producción conjunta de agua y electricidad y el análisis de procesos MED de alta eficiencia integrados en plantas PT-CSP. A este fin, primero se ha llevado a cabo una revisión bibliográfica pormenorizada para presentar el estado actual de la tecnología propuesta y los diferentes acercamientos a este concepto. Posteriormente, se ha realizado un estudio termoeconómico preliminar para un caso particular de la integración de una planta de termosolar de captadores cilindroparabólicos con generación directa de vapor y dos tecnologías de desalación: ósmosis inversa y destilación multiefecto. Los resultados han revelado que la ósmosis inversa es la mejor opción de integración ya que genera los menores costes anualizados de producción de agua. Además, se recomienda la integración indirecta con la planta termosolar, conectándose directamente a la red eléctrica local. De dichos análisis se ha concluido que no existe acuerdo entre la comunidad científica en cuanto a la tecnología de desalación más adecuada para su acoplamiento con una planta termosolar de concentración. Además, debido al potencial mostrado por la destilación multiefecto para la integración con plantas CSP, se requiere una investigación más profunda sobre las posibilidades de aumento de eficiencia de esta tecnología.

En esta línea, dos métodos para incrementar la eficiencia del proceso de destilación multiefecto han sido evaluados: el aumento del número de efectos, que conduce a un incremento de la temperatura máxima de salmuera, y la introducción de la compresión térmica de vapor. En el primer caso, el aumento de la temperatura máxima de salmuera sin aparición de incrustaciones salinas en los tubos de los intercambiadores de calor (*scaling*) precisa la utilización de un pretratamiento del agua de mar tal como la nanofiltración, la cual elimina los iones bivalentes causantes de dicho efecto. Para este propósito se ha desarrollado un modelo matemático detallado del proceso de destilación multiefecto con alimentación frontal (o hacia delante), el cual ha sido implementado en el entorno *Engineering Equation Solver* (EES). Dicha configuración ha sido elegida para minimizar los riesgos de aparición de incrustaciones en los tubos de los intercambiadores de calor. Los resultados han mostrado que la eficiencia térmica del proceso, medida mediante el *Gain Output Ratio* (GOR), se incrementa considerablemente (hasta en un 70%), mientras que el área específica de transferencia y consumo energético específico se reducen significativamente (en un 11 y 45%, respectivamente). A pesar del gran potencial mostrado por esta mejora del proceso MED, no se ha analizado su integración en plantas CSP debido a que no existen unidades MED comerciales utilizando dicha configuración y además el aumento del consumo auxiliar causado por el pretratamiento de nanofiltración podría no ser adecuado para aplicaciones solares. La mayoría de plantas MED comerciales presentan una configuración de flujo paralelo/cruzado con compresión térmica de vapor, la cual presenta ventajas para su acoplamiento con plantas CSP. Una primera evaluación de esta integración ha sido realizada para un caso particular de estudio, simulando la producción conjunta de agua y electricidad en una planta PT-CSP de 50 MW_e, con características similares a la planta comercial Andasol-I en Granada (España), y una unidad

MED-TVC de 10,000 m^3/d, basada en la planta comercial de Trapani (Italia), durante tres días representativos de invierno y tres días de verano. Se han considerado dos extracciones diferentes de turbina para alimentar la planta desalinizadora, una del cuerpo de turbina de alta presión y otra del cuerpo de turbina de baja presión. El modelo del campo solar de la planta CSP se ha tomado de la literatura científica y ha sido implementado en el entorno MATLAB, mientras que el bloque de potencia, implementado en EES, se ha desarrollado para simular condiciones de operación a carga parcial. De este estudio se ha concluido que se requieren diferentes esquemas de integración para cumplir con los diferentes perfiles de demanda de agua y electricidad durante el año, de manera que se otorgue mayor prioridad a la producción de agua o la generación de energía eléctrica.

Posteriormente se ha realizado un estudio paramétrico de la integración de una planta desalinizadora MED-TVC, basada en la configuración de la planta comercial de Trapani, con un ciclo de potencia Rankine similar al de la planta CSP Andasol-1, con objeto de identificar el mejor acoplamiento, desde el punto de vista de eficiencia y área de intercambio de calor mínima. A este fin, se ha desarrollado un modelo matemático detallado del proceso MED-TVC con alimentación en paralelo/cruzado y se ha validado con datos de una planta real. Se ha encontrado que el máximo GOR y la mínima área específica se obtienen para una posición particular del termocompresor, dependiendo de la presión del vapor motriz que alimenta al termocompresor. Además, se ha desarrollado un modelo de operación del proceso MED-TVC, basado en el modelo de diseño, y se ha utilizado para determinar los límites de operación de la integración con ciclos de potencia Rankine tales que permitirían trabajar a la unidad MED en condiciones nominales (lo cual fue posible considerando termocompresores de área variable), para cuatro extracciones de vapor diferentes. Para este propósito, se ha simulado la operación del bloque de potencia a diferentes cargas y se ha introducido un algoritmo de control para mantener la salinidad máxima de la salmuera en valores por debajo de 70,000 ppm y la temperatura del condensador final alrededor de su valor de diseño (37 °C).

Para finalizar, se han efectuado simulaciones anuales de la integración de una unidad de destilación multiefecto con compresión térmica de vapor (en flujo paralelo/cruzado) y una planta termosolar de captadores cilindroparabólicos, considerando Almería (España) como la localización geográfica de la hipotética planta de cogeneración. Los modelos presentados previamente del campo solar, bloque de potencia y unidad de desalación (modelos para la operación a carga nominal y parcial) han sido utilizados en las simulaciones. Como un caso particular de estudio, se ha estimado la producción diaria, mensual y anual de electricidad y agua considerando dos extracciones de vapor de diferentes presiones, iguales a las identificadas en el estudio anterior: una perteneciente a la turbina de alta presión, a 45.4 bar, y otra de la turbina de baja presión, a 3.63 bar, las cuales se han utilizado alternativamente para alimentar

la unidad MED-TVC dependiendo de la demanda mensual de electricidad y agua en dicha localización.

Abstract

Water scarcity and energy supply are currently two of the major problems faced by the global society. The growth of the world's population along with the rise of industrial activities, especially in developing countries, is leading to a rapid increase of the energy consumption and the construction of new power plants. Most of these plants are based on fossil fuels, which emit harmful greenhouse gases (mainly CO_2) and contribute to global warming on Earth. Power production technologies which use renewable energies (solar, wind, geothermal, etc.) as energy source represent clean and environmentally friendly alternatives to traditional methods, particularly Concentrating Solar Power (CSP) plants, which have been proved as a reliable system for power generation. On the other hand, although more than 70% of the Earth's surface is water, fresh water represents only 2.5% of the total volume in the hydrosphere, approximately, being the rest saline water. Furthermore, of that fresh water percentage, a 69% is contained in form of glaciers and ice sheets, from which its extraction does not result neither economically nor environmentally viable. Therefore, the fresh water production by means of seawater desalination can help to solve water supply problems in arid areas of the world, as it has been proved in Middle East countries since the middle of the twentieth century. In addition, regions of the world suffering from water stress habitually have high levels of solar irradiation and access to the sea, which reinforces the idea of using this renewable energy source to produce fresh water by seawater desalination in those regions. Also, the power and water supply issues are linked, because power generation, either by conventional or renewable technologies, need great amounts of water (particularly for the cooling requirements of the power cycle), and fresh water production by seawater desalination require high amounts of energy. Therefore, the combined generation of power and fresh water by integrating desalination processes and concentrating solar power plants, concept known as CSP+D, may help to solve the issues emerged regarding the power and water supply in such regions of the world.

The specific objectives and goals set out in the present research work are to develop a simulation tool (in nominal and partial-load conditions) for the Multi-Effect Distillation (MED) seawater desalination process with Thermal Vapour Compression (TVC) (variable nozzle thermocompressors) integrated in a CSP plant. This tool will allow to determine the plant performance regarding both, electricity and water production, and to analyse high efficient MED processes and their integration within parabolic trough concentrating solar power plants. To that end, firstly a detailed literature review on CSP+D has been performed to present the state-of-the-art of this technology and different approaches to this concept. Then, a preliminary thermo-economic study has been carried out for a particular case of the combination of a parabolic trough CSP plant with direct steam generation and two different desalination

technologies, Reverse Osmosis (RO) and multi-effect distillation. Results obtained show that the bet coupling option, which produce the lower levelised cost of water, is the RO process. Also, it is recommended its indirect integration with the CSP plant, connected directly to the local grid. It is concluded that, in view of the lack of agreement among scientific community about the most suitable technology for integrating with a CSP plant and due to the potential of the combined freshwater and power production with MED and CSP, further investigation with higher efficient MED plants is needed.

In this regard, two methods to improve the efficiency of MED processes have been investigated: the increase of the number of effects, which leads to an increase in the Top Brine Temperature (TBT), and its coupling with thermocompressors. The first case has been assessed by using seawater pretreatments that permit to elevate the temperature of the MED process without scale formation, like the nanofiltration membranes. For this purpose, a detailed mathematical model has been developed for a MED plant with forward-feed configuration and the model was implemented within Engineering Equation Solver (EES) software environment. Such feed arrangement has been selected in order to minimize the scale risk on the tubes of the heat exchangers. Results show that the Gain Output Ratio (GOR) is greatly improved (up to a 70%), while the specific heat transfer area and specific energy consumption are significantly reduced (11 and 45%, respectively). Despite of the great potential of this improvement to the MED process, the analysis of its integration into a CSP plant has been not pursued because there are not commercial MED plants using the forward feed scheme. Moreover, the increase of auxiliary consumption attributable to nanofiltration pretreatment may be not suitable for solar applications. Most commercial MED plants present a parallel/cross feed arrangement with thermal vapour compression, which presents several advantages for its coupling with power plants. Therefore, this technology has been selected for the analysis of its coupling with CSP plants. A preliminary evaluation has been performed for a particular case study, simulating the power and water productions of a parabolic trough CSP plant of 50 MW_e, with features similar to commercial Andasol-I CSP plant, and a MED-TVC unit of 10,000 m^3/d, based on commercial Trapani plant (Italy), during three representative days in winter and summer periods. Two different steam extractions have been considered to feed the MED-TVC unit, one from the high pressure turbine, and other from the low pressure turbine. The CSP model has been taken from the literature and implemented in MATLAB software environment, and the power block model, implemented in EES, has been developed to simulate part load conditions. From this assessment it is concluded that different integration schemes are needed to accomplish for the different profile demands of power and water during the year, in order to promote the power generation or the water production.

Later, a parametric study of the integration of a parallel/cross MED-TVC, based on Trapani commercial plant, with a Rankine cycle power block similar to that one of Andasol-1 has been

carried out in order to identify the best coupling arrangement, in terms of efficiency and minimum specific heat transfer area. To that end, a detailed design mathematical model of the MED-TVC unit has been developed and validated against actual data. It is found that the maximum GOR and minimum specific area are reached for a particular thermocompressor location, depending on the motive steam pressure fed into the thermocompressor. Also, an operation MED-TVC model has been developed, based on the design model, and used to determine the operational limits of the integration with a Rankine cycle power block that would allow the MED unit to work in nominal conditions (which has been possible by considering variable nozzle thermocompressors), for four different steam extractions of the turbines. For this purpose, the power block has been simulated at different loads, and a control algorithm has been also introduced in order to maintain the maximum brine salinity under 70,000 ppm and the end condenser temperature around its design value (37 °C).

Finally, annual simulations of the coupling between a parallel/cross MED-TVC unit and a parabolic trough CSP have been performed, considering Almería (Spain) as the geographical location of the cogeneration plant. The models previously presented for the solar field, power block and desalination unit (nominal and off-design models) have been used. As a particular case study, the daily, monthly and yearly power and water productions have been estimated, using two different steam extractions, equal to those ones identified in the previous analyses: one from the high pressure turbine, at 45.4 bar, and other from the low pressure turbine, at 3.63 bar, which have been used alternatively to feed the MED-TVC unit depending on the monthly power demand for that location.

Table of contents

Chapter 1. Objectives and Justification

Contents

List of figures

Nomenclature

Acronyms and abbreviations

ABHP	Absorption Heat Pump
ADHP	Adsorption Heat Pump
BRIICS	Brazil, Russia, India, Indonesia, China and South Africa
CD	Capacitive Deionization
CR	Central Receiver
CSP	Concentrating Solar Power
ED	Electrodialysis
EDS	European Desalination Society
EES	Engineering Equation Solver
FF	Forward Feed
FM	Freezing-Melting
FO	Forward Osmosis
GOR	Gain Output Ratio
HDH	Humidification-Dehumidification
HTF	Heat Transfer Fluid
IE	Ion Exchange
IWMI	International Water Management Institute
LT	Low Temperature
MD	Membrane Distillation
MED	Multi-Effect Distillation
MIGD	Million Imperial Gallons per Day
MSF	Multi-Stage Flash
MVC	Mechanical Vapour Compression
OECD	Organization for Economic Co-operation and Development
PF	Parallel Feed
PTC	Parabolic Trough Collectors
PVD	Passive Vacuum Desalination
RO	Reverse Osmosis
SEGS	Solar Electric Generation Station
ST	Solar Still
STE+D	Solar Thermal Electricity and Desalination
TVC	Thermal Vapour Compression

1.1 Presentation

Water is essential for the existence of life, constituting more than 70% of the Earth's surface and about 60% of total human body weight (Agogué et al., 2004; Altman and Katz, 1961). However, the fresh water resources available worldwide are scarce and limited. All water on Earth is contained in the hydrosphere, which includes the water of the surface, underground and the air, in liquid form (oceans, rivers, lakes, wells, aquifers, etc.), vapour phase (clouds, fog) or solid state (glaciers, icebergs, ice caps). But only 2.53% of the total volume of water present in the hydrosphere is fresh water, being the rest saltwater (Shiklomanov and Rodda, 2003). Within this percentage, 0.3% constitutes the liquid fresh water contained in rivers and lakes, which are the common sources of extraction, while a 30.8% is held on groundwater, soil moisture, swamp water and permafrost. The rest (68.9%) is stored in glaciers and ice sheets, which represents the largest volume of the total fresh water available. However, the water withdrawal from those reservoirs is difficult and hard to manage.

Also, the fresh water resources are not well distributed. Near 1.2 billion people live in regions where the absence of water is absolute, because of natural causes or overuse and mismanagement (IWMI, 2007). Poor infrastructures, bad handling and physical or economic water scarcity impede the fresh water to be accessible for millions of persons in the world. It is important to note that not always the cause of water scarcity is related to harsh climatic conditions (physical scarcity of fresh water). In many cases the lack of financial support, institutional assistance or adequate facilities to withdraw the existing fresh water resources are the cause of the water shortage, as occurs in central Africa, north-eastern India, north-eastern South America and South-East Asia (see Figure 1.1).

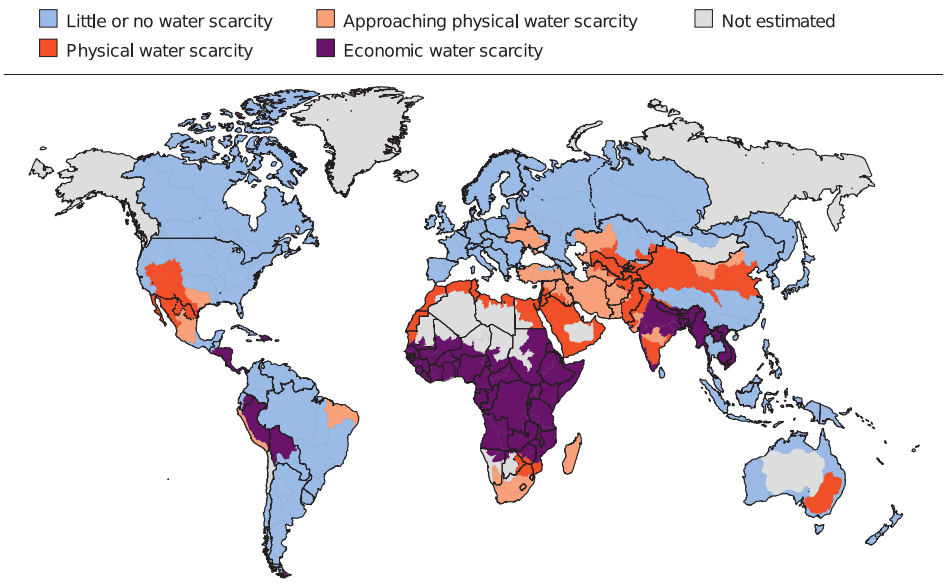

Figure 1.1. Areas with physical or economic water scarcity (IWMI, 2007).

One of the main causes of water scarcity is the rapid increase of the global population in the last decades, expecting an increase from 7 to over 9 billion by 2050 (OECD, 2012). Particularly, the amount of people living in areas with severe water stress has grown significantly and it is expected to follow this tendency in the near future. By 2050, the OCDE predicts a big increase of people (40% of the world's population) living in river basins under severe water stress, along with a global elevation of 55% in the water demand, especially within the BRIICS countries (Brazil, Russia, India, Indonesia, China and South Africa) (see Figure 1.2). It can be seen how manufacturing water demand is expected to increase by +400% in 2050, while the water used for thermal electricity generation would elevate +140%. On the contrary, it is predicted that the water used for irrigation will decrease, assuming the same irrigated land and more efficient irrigation systems.

The quality of the fresh water is also essential for the human consumption. Many diseases are caused and spread by the bad conditions of the fresh water, including the presence of bacteria, virus, toxic substances, suspended particles, etc. Different standards define the minimum quality required for the drinking water, that are defined by every country or region, like the Directive 98/83/EC of 1998 in Europe, the Royal Decree 140/2003 in Spain, or international norms like the Guidelines for drinking-water quality of the World Health Organization (2011) that are intended for general application, both developing and developed countries world-wide.

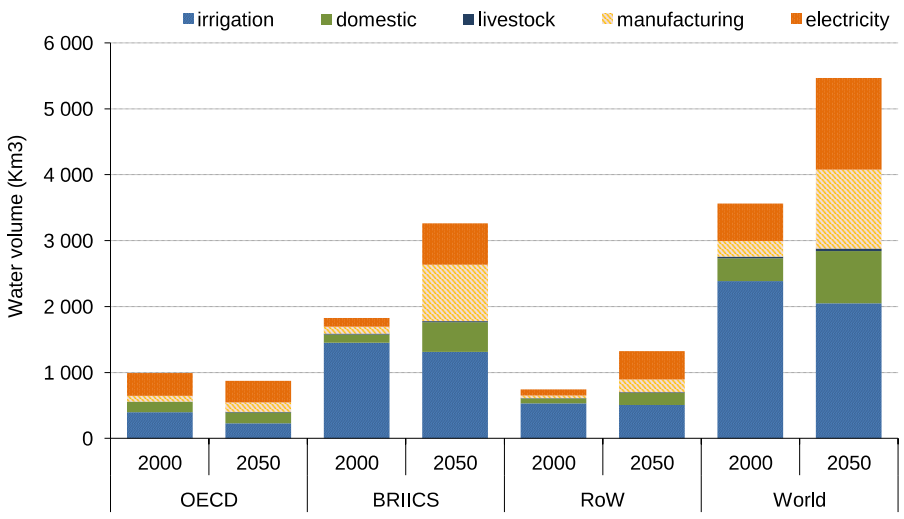

Figure 1.2. Global water demand by utilization, 2000 and 2050 (OECD, 2012).

Another issue regarding the fresh water resources is the utilization. The major consumers of fresh water are India, China, United States, Pakistan, Japan, Thailand, Indonesia, Bangladesh, Mexico and the Russian Federation, as reported by Unesco and World Water Assessment Programme (2009), and the main uses are, in average value: agriculture (70%), industry (20%) and domestic (10%) (Cosgrove et al., 2000). However, depending on the location those

percentages may vary, growing the share of the sector which has a major exploitation. A clear example is the case of Asia, the biggest consumer of freshwater worldwide due to the intense irrigation agriculture. Another example is the rapid drying suffered by the brackish lake known as Aral Sea, in Central Asia, during the last decades. Formerly being one of the biggest lakes of the world, its capacity has decreased up to 10% of the original content because of the water diversion projects planned by the Soviet Union since 1960s (see Figure 1.3), where the main two rivers feeding the lake were used for irrigation purposes in cotton and rice fields (Harriman, 2014).

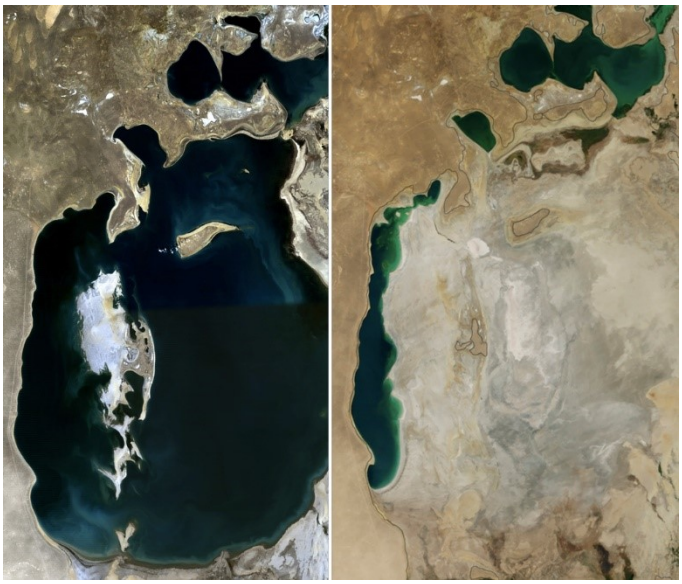

Figure 1.3. The Aral Sea in 1989 (left), and in 2014 (Lindsey, 2014).

There is a clear nexus between energy and water, as the energy generation at large scale need great amounts of water using the current existing technologies, and on the other hand, the fresh water production also requires an important amount of energy, in any of its forms (mechanical, thermal, chemical, etc.). Primary energy sources, such as oil, gas, coal and biofuels need water for their withdrawal, refining, irrigation (biofuels) and transport (International Energy Agency, 2012). But also power generation is a major water consumer process, which is mainly used for feeding the boiler and cooling the exhaust steam of the Rankine cycle in conventional power plants, based on fossil fuels and nuclear energy. Hydropower, concentrating solar power and geothermal plants also require water for other uses as storage in reservoirs, mirrors cleaning and water subsurface injection, respectively. It is important to note that not all the withdrawn water may be consumed, because in some cases could be returned to the source and being used again. The amount of water needed in power plants depends primarily on the cooling system employed, which is directly connected to the availability of natural cooling sources as lakes, rivers, etc. Basically there are four cooling methods, namely once-trough, evaporative wet cooling, dry-cooling and hybrid systems. Among them, the largest withdrawal of water is done

by the once-trough system, which also has the greatest environmental impact, while the biggest water consumption is done by the evaporative cooling tower.

Conventional methods for power generation based on fossil fuels are known to contribute for the global warming and environmental damage by emitting greenhouse gas emissions to the atmosphere (McMichael et al., 2006). By the end of 21st century, global temperature increments of 2 – 5.5 °C have been predicted (Betts et al., 2015), which would cause dramatic effect on human health and biosphere. Today, the consensus in the scientific community about the anthropogenic cause of the global warming is almost absolute, where about 97% of peer-reviewed scientific literature examined agreed in that relationship (Tol, 2014). On the other hand, nuclear energy has to deal with nuclear waste removal along with security risks which may lead to accidents, like the one occurred at Fukushima Nuclear power plant (Japan) on 11 March 2011. Following an earthquake, a tsunami destroyed the cooling system of the reactors, which melted and released radioactive materials to the environment (International Atomic Energy Agency, 2015), such as the isotope cesium-137, which was of major concern because of its high water solubility and rapid spread in the soil and atmosphere. Given that, clean and green alternatives based on renewable energy are ready for substituting those polluting technologies, as they have been proved as reliable and feasible methods for electricity production.

Regarding this energy–water issue, it is known that regions of the world that suffer from water stress usually present high levels of solar irradiation over the year. That means that there is a geographical coincidence between zones of the world with high demand of fresh water and a great solar potential. Moreover, those regions normally have coastal areas or access to the sea. This correspondence together with the fact that most of water in Earth is seawater leads to think about the use of solar irradiation to drive seawater desalination processes. Also, considering the mentioned benefits of the power generation driven by solar energy compared with traditional power plants based on fossil fuels, the integration of desalination plants and concentrating solar power plants could represent a sustainable and clean method for the combined production of water and electricity. As a result, the emission of greenhouse gases to the atmosphere and polluting risks would be avoided, and environmentally friendly technologies may be used instead.

Particularly, as depicted in Figure 1.4, the West coast of EEUU, Chile, North of Africa, South of Europe, Middle East, South Africa, India and Australia are world areas that present the required conditions for the integration of both the seawater desalination for fresh water production and the concentrating solar power for electricity generation.

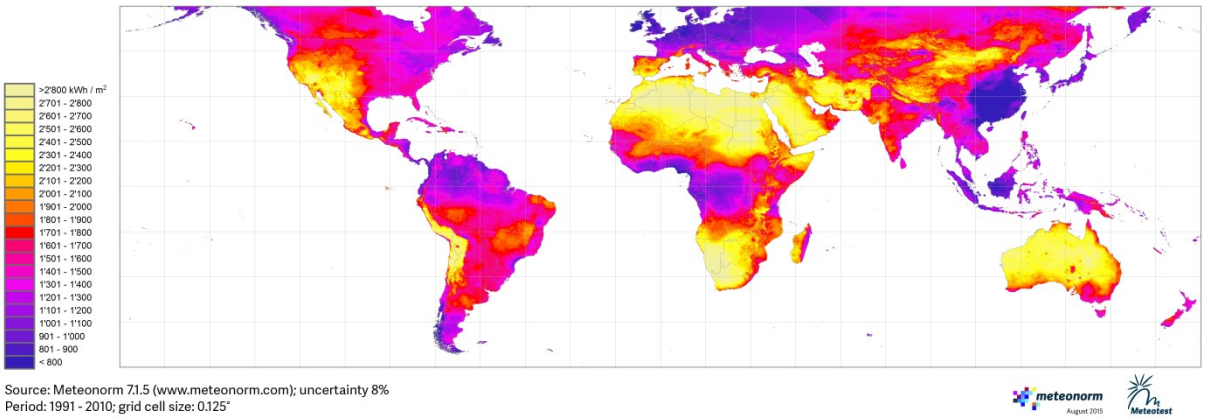

Figure 1.4. Yearly sum of direct normal irradiation global map (Meteonorm, 2015).

Among the different concentrating solar technologies for power production, the more mature and commercially proven is the one based on Parabolic Trough Collectors (PTC), which has been tested with success in the Mojave Desert (California) since early 80s, where nine Solar Electric Generation Station plants (SEGS) have been built, producing more than 350 MW_e (NREL, 2016). In 2013, it was inaugurated the largest parabolic trough solar plant in Arizona (EEUU), Solana Generating Station, with a net capacity of 250 MW_e and 6 h of thermal storage, using 2-tank indirect system of molten salts. This plant is able to meet the power demand of 71,000 households. Within the total concentrating solar power currently installed world-wide, near 5 GW at the end of 2015 (HeliosCSP, 2016), the majority (82%) belongs to this technology (Xu et al., 2016). Nevertheless, Central Receiver (CR) technology has gained share in the last years due to its higher solar-to-electric efficiency (theoretical operation temperatures around 1000 °C using Brayton power cycle) and lower levelized electricity cost. Global efficiencies between 10–16% and 10–22% are reported for PTC and CR technologies, respectively (Xu et al., 2016). The first solar tower commercial plant, PS10, was built in Seville (Spain) during 2007, with a capacity of 11 MW_e and 0.5 h of thermal storage. The tower produced steam at 250–300 °C for driving a steam turbine in a Rankine cycle and to provide electricity to 6000 households. In 2011, a solar tower power plant with 19.9 MW_e of gross capacity (17 MW_e net) started to operate in Fuentes de Andalucía (Seville, Spain), using molten salts as HTF, and with a thermal storage capacity of 15 h, which increases its annual capacity factor up to 74% (Dunn et al., 2012). It was the first commercial solar power plant applying central receiver technology and molten salts as HTF (Behar et al., 2013).

On the other hand, seawater desalination is a very traditional method for obtaining fresh water since the beginning of our civilization. From the ancient times it has been a common way for producing water using distillation processes. Aristotle (384-322 BC) by that time had already mentioned the seawater distillation process in his writings and described the natural water cycle as an open distiller (Kalogirou, 2005). The Multi-Effect Distillation (MED) process has

been widely used in the food and chemical industry as a method for producing sugar and other products, since 19th century (El-Dessouky and Ettouney, 2002). Later, during 20th century this process was first applied for seawater desalination. One of the first MED desalination plants was built in Jeddah (Saudi Arabia) in 1907, comprised of two distillation units, and using submerged tubes technology, which led to significant problems related with the appearance of scaling in the tubes of the heat exchangers. Shortly afterwards they were replaced for two new units, using the same submerged tubes technology, with a total capacity of 135 m^3/d. Other plants were installed but, the low productivity, maintenance stops, and low thermal efficiency led to look for other desalination alternatives, particularly Multi-Stage Flash (MSF) evaporation. That was one of the main reasons of the MSF desalination process growth, particularly in the Middle East countries. It was not until the 80s when new MED designs using high efficient falling-film evaporators and low operation temperatures (< 70 °C) re-activated the technology for desalination purposes, once the scale formation problems were controlled (Buros et al., 2000).

The desalination market has experienced a big expansion in the last years, as it can be seen in Figure 1.5, where it has been represented the additional and cumulative annual desalination capacity worldwide, from 1970 to 2014. The global economic crisis surged in EEUU during 2008 affected to the growing tendency for new desalination plants, mainly due to financing and funds raising difficulties.

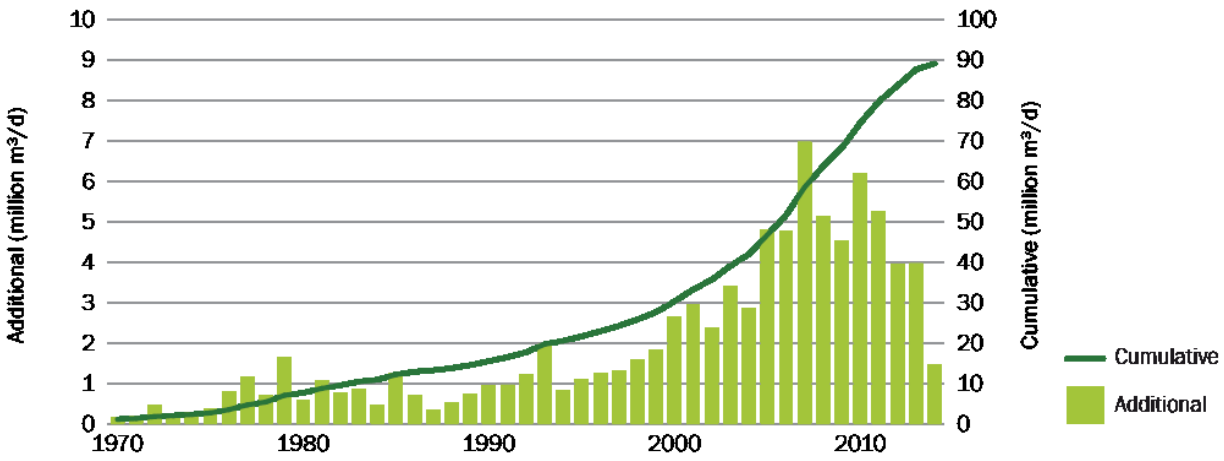

Figure 1.5. Annual additional and cumulative desalination capacity, 1970 – 2014 (Global Water Intelligence, 2016).

Currently, there are several desalination technologies and different classifications. Taking into account the element extracted from the process, water or salt, one categorization possible is the one illustrated in Figure 1.6. Within the processes based on water removal, two new categories can be proposed, with or without phase change. In the former group are Multi-Stage Flash, Multi-Effect Distillation, Solar Still (ST), Humidification-Dehumidification (HDH), Passive

Vacuum Desalination (PVD), Membrane Distillation (MD), Freezing-Melting (FM) and the techniques based on heat pumps: Mechanical Vapour Compression (MVC), Thermal Vapour Compression (TVC), Absorption Heat Pump (ABHP) and Adsorption Heat Pump (ADHP). In the second group, without phase change, are Reverse Osmosis (RO) and Forward Osmosis (FO). In the salt-collecting processes are found Electrodyalisis (ED), Ion Exchange (IE) and Capacitive Deionization (CD), which are habitually used with brackish water.

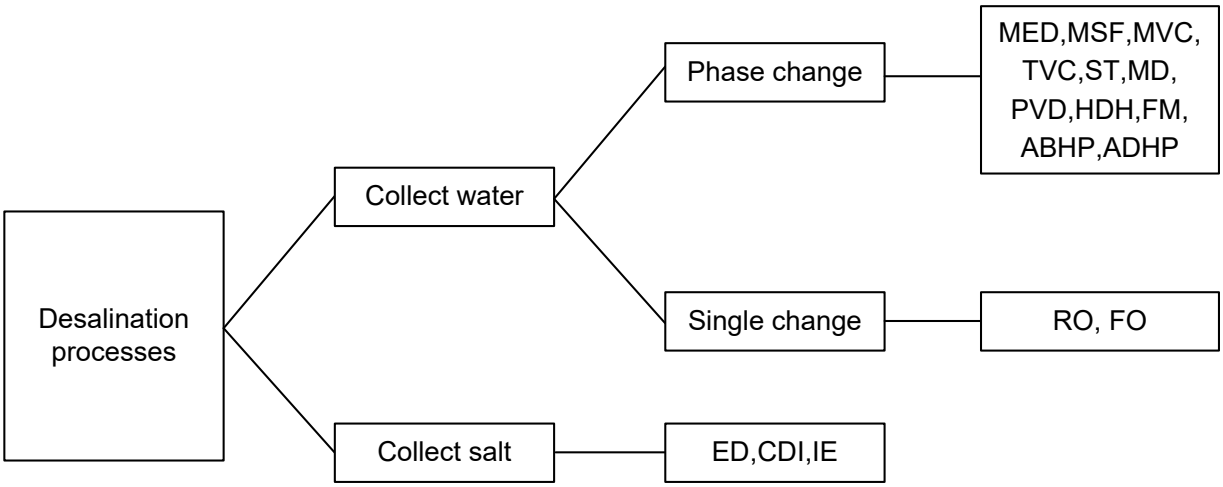

Figure 1.6. Main desalination technologies (adapted from (Li et al., 2013)).

Despite of the significant number of desalination processes available, not all are suitable for handling seawater desalination and large capacities. What is more, some are in research and experimental stages. The most common commercial desalination techniques, with the largest installed capacities, are, in this order (see Figure 1.7): reverse osmosis (63%), multi-stage flash (23%), multi-effect distillation (8%) and electrodialysis (3%) (Global Water Intelligence, 2016).

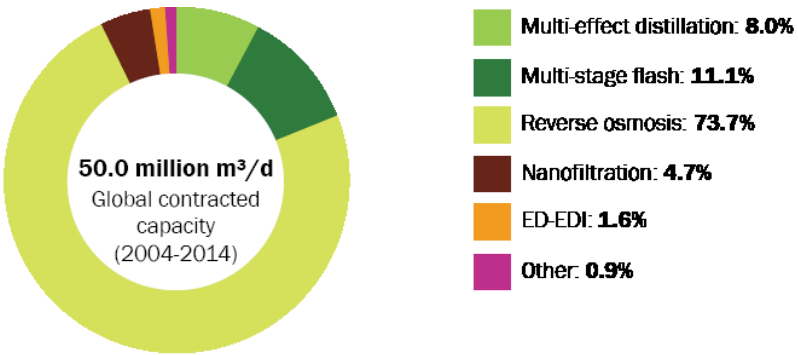

Figure 1.7. Total worldwide installed desalination capacity by technology (Global Water Intelligence, 2016).

At big scale, multi-effect distillation for seawater desalination is the most efficient technology for producing fresh water, among the thermal methods (Darwish and El-Dessouky, 1996), and RO the most used among the mechanical methods. Moreover, it is especially suitable for co-generation purposes (combined electricity and freshwater production) as only need steam at 70 ºC to operate, which could be obtained from process steam of any industrial application or from any steam extraction of the turbines of a power plant. The commercially available MED plants use the thermal vapour compression to increase their efficiency, by means of steam ejectors (also known as thermocompressors). These devices are very simple but at the same time are cheap, robust and easy to operate. They are based on the Venturi effect and basically compress low pressure vapour extracted from one effect of the MED unit, using high pressure vapour (motive steam) from a boiler or other external source, up to an intermediate pressure between the two inlets (compressed vapour). Single MED-TVC units have capacities up to 36,000 m^3/d (8 MIGD), like the plant at Layyah Power Station in United Arab Emirates, although the total daily capacity can be increased by the simultaneous operation of several units. For instance, Taweelah Power and Desalination Plant (Abu Dhabi - UAE) has 14 units of 17,143 m^3/d each, reaching a total capacity of 240,000 m^3/d (Veolia, 2016). The largest SWRO plant can handle up to 540,000 m^3/d (Sorek plant in Israel), due to the modularity of this kind of technology. The specific heat and electric consumption of the MED-TVC process are between 50–100 kWh_{th}/m^3 and 1–2 kWh_e/m^3, respectively, while the SWRO process have an electric consumption of about 3.9–5.6 kWh_e/m^3 (Khayet, 2013; Moser et al., 2011; Zak et al., 2013).

1.2 About the author

The author of this research work, with an Industrial Engineering degree and Energy specialization obtained at the University of Seville (Spain), was awarded with a scholarship by CIEMAT research centre to complete a PhD program within the Solar Desalination Unit at Plataforma Solar of Almería, from 1st December 2012 to 30th November 2016, in the framework of the National Plan for Scientific Research, Development and Technological Innovation ("National R+D+I Plan" 2011), dependent on the Ministry of Science and Innovation of Spain. The topic of doctorate program was the integration between concentrating solar power plants and desalination plants, particularly using parabolic trough solar thermal technology and multi-effect distillation with thermal vapour compression process, for the production of electricity and water, respectively.

The first year of the scholarship was dedicated in part to complete a Master Thesis in Thermal Energy Systems at University of Seville, as a previous requirement for joining the Doctorate program in Energy Engineering, Chemical and Environmental, which was done on 7th March

2013. The Final Project of the Master consisted in developing a steady-state mathematical model for a forward feed multi-effect distillation plant with a sensitivity analysis of different designs and performance variables.

Several papers resulting from his research activity at the Plataforma Solar de Almería have been submitted to conferences and journals, which are described in detail in Section 1.6. Also, the author has participated with oral presentations in two international conferences organised by the European Desalination Society (EDS) in Palermo and Rome (Italy) during 2015 and 2016. Oral presentations at SOLLAB in Germany, France and Switzerland during 2013, 2014 and 2015, respectively, have been done as well by the author.

This work has been developed under the framework of a European project, STAGE-STE, within Work Package (WP) 10, focused on the investigation of sustainable methods and technologies for the combined power and water production using concentrating solar energy (EERA, 2015). In addition, the author has collaborated within the Solar Desalination Unit for different works related to the STAGE-STE project. Particularly, in this WP, studies focused in the modelling and evaluation of different systems or processes have been carried out: multi-effect distillation plants, Rankine cycle power plants, parabolic trough solar fields, and steam jet ejectors.

1.3 Objectives and scope

The main objective of this work is the theoretical evaluation of high efficient multi-effect distillation processes and their combination with parabolic trough CSP plants. In particular, this research work investigates the best coupling arrangement between the desalination unit and the CSP plant, which minimizes the energy consumption of the MED-TVC process and meet the water and power demand, both daily and seasonally, for the location considered. This study makes sense only in arid or semi-arid regions of the world that present high irradiation levels and have access to the sea.

This research work is motivated as a continuation of the Thesis written by Patricia Palenzuela (2012), focusing in the MED-TVC technology and the use of thermocompressors for the coupling with Rankine cycle power blocks, as suggested in Palenzuela et al. (2011). Particularly, the study of the variable nozzle thermocompressors was analysed, due to their ability to maintain the MED efficiency near to the nominal even when the power plant is working at part load operation and the pressure level of the feeding vapour is reduced. The operational limits of the coupling between the two subsystems, solar thermal power plant and MED-TVC unit, working at part load operation, were thoroughly assessed and discussed in the present research work.

The specific objectives and goals set out in the present research work are:

1. The development of steady-state mathematical models of high efficient MED processes. Different feed arrangements were considered: forward feed and parallel/cross. Moreover, possible enhancements for the increase of the thermal efficiency of the MED process have been analysed, by raising the number of effects and top brine temperature using pretreatments such as nanofiltration membranes, and introducing thermocompression.

2. To implement a detailed model of a parabolic trough solar field based on a commercial PT-CSP plant (Andasol-2, Spain) configuration in order to simulate the yearly thermal energy production with the highest accuracy possible.

3. To develop a mathematical model for a Rankine cycle power block, similar to those existing in parabolic trough solar thermal power commercial plants, working at nominal and part load operation.

4. To determine the position of the thermocompressor in a MED-TVC unit that produces the highest thermal efficiency of the desalination plant with the minimum specific heat transfer area.

5. To investigate the different coupling arrangements between a multi-effect distillation unit with thermal vapour compression and a Rankine cycle power block similar to that of a commercial PT-CSP plant (Andasol-1, Spain), in terms of freshwater and power production.

6. To identify the operational limits of the coupling between a Rankine cycle power block similar to that of a commercial PT-CSP plant (Andasol-1, Spain) that allow to keep the motive steam mass flow rate constant using variable nozzle thermocompressors.

7. To develop a partial-load model for the MED-TVC process to be integrated into a Rankine power block that considers the control of the operation by the adjustment of key variables such as the maximum brine salinity and the condensation temperature.

8. To develop a mathematical model for integrated CSP+MED-TVC plant as a tool to simulate throughout the year the power and fresh water production under different freshwater and power profile demands.

1.4 Main contributions of this work

The number of works dedicated to perform quasi-dynamic analyses of the integration of multi-effect distillation processes for seawater desalination within concentrating solar power plants is scarce. The majority of the studies published in the literature either have been developed in steady-state conditions for a particular moment of the year, or assuming a 1-hour time step to simulate the yearly production of power and water (Casimiro et al., 2014; Ghobeity et al., 2011; Olwig et al., 2012), which makes the annual simulations less accurate because of the large difference between the time step and the solar irradiation variability. Other works use commercial simulation software with no access to governing physical equations (Iaquaniello et al., 2014; Wellmann et al., 2015). In the present research work, 10-s time step has been selected for the solar field performance simulation, which uses an accurate mathematical model developed by Llorente García et al. (2011) and validated against actual data from a commercial CSP plant. The simulations of the yearly power and water production have been done for 10-min time steps in order to save computational time, preserving a reasonable time difference to account for the instant variation of the solar irradiance.

Similarly, there is a lack of MED-TVC models in the literature able to simulate part load conditions, which is essential to perform time-dependent analyses of the coupling with CSP plants. The time-dependent MED models published in the literature (Aly and Marwan, 1997; Dardour et al., 2005; de la Calle et al., 2015; El-Nashar and Qamhiyeh, 1990) have as the main objective to develop control schemes that regulate the response of the main operational variables against certain disturbances, which are not suitable for the yearly simulation of complex systems such as CSP+MED plants. On the other hand, most of steady-state MED models found are used for design purposes, where the geometry of the plant is determined by the model (Al-Mutaz and Wazeer, 2014; Bin Amer, 2009; El-Dessouky et al., 2000; Kamali et al., 2009), and they are not either suitable to simulate the partial load operation. In this research work operation models are developed in order to perform the simulations of the integration of a fixed MED-TVC unit with a CSP plant under part load operation. In addition, the developed MED-TVC models try to investigate more in detail some phenomena occurring inside the multi-effect distillation process, such as the saturation temperature losses of the vapour from its generation in one effect up to its condensation inside the evaporator of the next effect, in contrast with most of the models reported where this effect is either neglected or assumed constant.

Also, other significant achievements of this work are:

- Identification of misunderstandings in some published models of MED units.

- Thorough parametric study on thermal efficiency of MED-TVC plants with determination of the optimal reduction of heat transfer areas of the evaporators after the thermocompressor location that minimizes the specific heat transfer area.
- Exhaustive parametric study on the operation of MED-TVC with the development of a specific control algorithm for the regulation of the maximum brine salinity produced and the condensation temperature.

1.5 Methodology

In order to meet the mentioned objectives, this research work has been structured as follows:

In Chapter 1, the justification and motivation of this research work is presented. Moreover, the main objectives and goals are described and the major contributions of this work in the scientific community are discussed. Finally, the publications derived from this work are shown.

In the second chapter, a literature review on concentrating solar power and desalination is firstly performed in order to set the state of the technology. Later, a thermoeconomic comparison of the integration of a desalination process into a concentrating solar power plant is shown, considering the leading seawater desalination technology in terms of capacity, reverse osmosis, and the most efficient one among the thermal methods, multi-effect distillation. As a result of this study and from the extensive literature review performed, it is concluded that there is not a clear agreement among scientific community about the suitability of the RO process compared with MED technology for its coupling with a CSP plant. Also, it is suggested that further investigation should be carried out regarding the coupling of MED-TVC units with CSP plants, due to the fact that this configuration permits to de-couple the water and power productions (in contrast to LT-MED+CSP scheme) and meet the profile demands during the year.

In Chapter 3, a highly efficient MED process is evaluated in order to investigate new methods for reducing the energy consumption and for improving the competitiveness of this technology against RO. The enhancement in the efficiency consists on the rise in the number of effects by increasing the top brine temperature, using specific seawater pretreatments such as nanofiltration membranes. In this case, forward feed configuration has been selected because, unlike the parallel feed, the maximum salinity takes place in the last effect, which has the lower temperature and therefore minimizes the scaling risks. The chapter also presents a detailed mathematical model for the FF-MED and a complete parametric study on the different design and operational parameters. Despite of the increase of the GOR and reduction of the energy consumption observed by elevating the heating steam temperature and number of effects, the

forward feed scheme is not commercially available yet and the model cannot be validated against actual data. Most of commercial plants are MED with thermal vapour compression and they are based on parallel feed configuration because their easier construction and operation. Therefore, next chapters are focused in developing and further improving the MED-TVC process in parallel feed configuration for its integration in CSP plants.

A first approach to the investigation on the coupling between CSP plants and MED-TVC units is performed in Chapter 4. Particularly, a parabolic trough solar thermal power plant of 50 MW_e with features similar to Andasol-1 is integrated with a MED-TVC unit of 10,000 m^3/d based on the commercial Trapani plant (Italy). An off-design model of the power block is implemented in EES, while the solar field model, taken from the literature (Llorente García et al., 2011), is implemented in MATLAB. A design MED-TVC model, which is explained in detail in Chapter 5, is used to identify the optimum thermocompressor position. Two coupling arrangements are considered, using a high/medium pressure steam extraction (20.6 bar) and a low pressure steam extraction (1.224 bar) to feed the MED-TVC unit. Simulations during three representative days in winter and three days in summer are performed in order to compare the water and power productions and identify the best coupling scheme depending on the demands curves. For these simulations, a black-box model of the MED-TVC unit is used. From this study it is found that different coupling schemes should be considered depending on the period of the year and environmental conditions.

Chapter 5 presents a parametric study of a Parallel Feed (PF) MED-TVC unit integrated with a Rankine cycle power block similar to that one in a commercial PT-CSP plant (Andasol-1, Spain), so as to identify the best coupling arrangement in terms of maximum thermal efficiency and minimum specific heat transfer area. A comprehensive design model for the PF-MED-TVC unit is developed and validated against actual data from the commercial plant located in Trapani (Italy). Four different steam extractions from the power block are selected in order to feed the MED-TVC unit, and the thermocompressor location is varied to investigate the position such as the minimum specific heat transfer area and maximum GOR are obtained. As a result, four different and optimized coupling arrangements between the MED-TVC unit and the CSP plant are achieved.

After the identification of the best coupling schemes between the CSP plant and the MED-TVC unit in nominal conditions, the operational limits of both the power block and the desalination plant are studied in Chapter 6. To that end, the power block is simulated at different loads to find the limits until which the MED-TVC can operate at nominal conditions. Also, an operation model for the MED-TVC unit is developed based on the former design model, and the simulation of the integrated plant (desalination unit into the Rankine power block) is performed for different coupling arrangements and loads of the power block.

In Chapter 7, as an application of the simulation tools developed beforehand in the previous chapters, annual simulations of the water and power productions for the integrated PT-CSP+MED-TVC plant using the off-design models are performed, taking Almería (Spain) as the location of the plant. Two of the proposed coupling arrangements are considered: one from the high pressure turbine at 45.4 bar and another from the low pressure turbine at 3.627 bar, which are used alternatively depending on the power demand profile for Andalusia (Spain) in 2015.

Finally, the main conclusions reached during the research work are shown along with future works.

1.6 Publishable results

The author has published and/or submitted for publication the following articles as a result of the work developed in the present research work:

1. Ortega-Delgado B., Palenzuela, P., Alarcón-Padilla, D.C., and García-Rodríguez, L. "Quasi-steady state simulations of thermal vapour compression multi-effect distillation plants coupled to parabolic trough solar thermal power plants", *Desalin. Water Treat.* (2016) 1–12. doi:10.1080/19443994.2016.1173377 [In press]. Presented at EuroMed 2015: Desalination for Clean Water and Energy, Palermo, Italy, 10–14 May 2015. Organized by the European Desalination Society.

2. Ortega-Delgado B., García-Rodríguez, L., and Alarcón-Padilla, D.C., "Thermoeconomic comparison of integrating seawater desalination processes in a concentrating solar power plant of 5 MW_e", *Desalination* 392 (2016) 102–117. doi:10.1016/j.desal.2016.03.016.

3. Ortega-Delgado, B., Palenzuela, P., Alarcón Padilla, D.-C., "Parametric study of a multi-effect distillation plant with thermal vapor compression for its integration into a Rankine cycle power block", *Desalination*. 394 (2016) 18–29. doi:10.1016/j.desal.2016.04.020.

4. Ortega-Delgado B., Cornali, M., Palenzuela, P., and Alarcón-Padilla, D.C., "Operational analysis of the coupling between a MED-TVC unit and a Rankine cycle power block using variable nozzle thermocompressors". (To be submitted) (Presented at the EDS Conference, Rome (Italy), May 22-26, 2016.).

5. Ortega-Delgado B., García-Rodríguez, L., and Alarcón-Padilla, D.C., "Opportunities of improvement of the MED seawater desalination process by pretreatments allowing high temperature operation", (To be submitted).

The author has also collaborated in the following works:

1. Palenzuela, P., Ortega-Delgado, B., Alarcón-Padilla, D.C., and Zaragoza, G., "Regeneration of concentrated solutions by multi-effect distillation in a RED close loop process". Presented at EuroMed 2016: Desalination for Clean Water and Energy, Rome, Italy, 22–26 May 2016. Organized by the European Desalination Society.

2. "Project deliverable 3.1: Low temperature regeneration assessment. Performance potentials of MED and MD processes using artificial aqueous solutions and effect of the addition of non-aqueous solvents". Project: "Conversion of Low Grade Heat to Power through closed-loop Reverse Electro-Dialysis". European Union's Horizon 2020 research and innovation programme.

3. "Project deliverable 10.1: State of the art and model development of multi-effect distillation with thermocompression" STAGE-STE Task 10.

Other studies carried out and presented by the doctorate at international conferences are listed below:

1. Ortega-Delgado B., Alarcón Padilla, D.C., and Blanco, J., "Modelling and optimization of integrated parabolic trough solar power and multi-effect desalination plants", presented at 9th SOLLAB Conference in Hornberg Castle, Black Forest, Germany (France), May 13-14, 2013.

2. Ortega-Delgado B., Alarcón Padilla, D.C., García-Rodríguez, L., Zaragoza, G., and Blanco, J., "Analysis of the step time influence in the yearly simulation of dual purpose solar thermal concentrating plants", Submitted to EuroMed 2014: Desalination for Clean Water and Energy, Limassol, Cyprus, 11–15 May 2014. Organized by the European Desalination Society.

3. Ortega-Delgado B., Palenzuela, P., Alarcón-Padilla, D.C., and García-Rodríguez, L., "Modelling and parametric study of thermal vapor compression multi-effect distillation plants", presented at 10th SOLLAB Conference in Odeillo (France), June 23-25, 2014.

4. Ortega-Delgado B., Palenzuela, P., Alarcón-Padilla, D.C., and García-Rodríguez, L., "Analysis of the coupling between multi-effect distillation plants with thermal vapour

compression and concentrating solar power plants", presented at 11th SOLLAB Conference in Melchsee Frutt (Switzerland), March 2-4, 2015.

5. Ortega-Delgado B., Palenzuela, P., Alarcón-Padilla, D.C., and García-Rodríguez, L. "Quasi-steady state simulations of thermal vapour compression multi-effect distillation plants coupled to parabolic trough solar thermal power plants", European Desalination Society Conference in Palermo, Italy, May 10-14, 2015

6. Ortega-Delgado B., Cornali, M., Palenzuela, P., and Alarcón-Padilla, D.C., "Operational analysis of the coupling between a MED-TVC unit and a Rankine cycle power block using variable nozzle thermocompressors", EDS Conference, Rome (Italy), May 22-26, 2016.

References

Agogué, H., Casamayor, E.O., Joux, F., Obernosterer, I., Dupuy, C., Lantoine, F., Catala, P., Weinbauer, M.G., Reinthaler, T., Herndl, G.J., Lebaron, P., 2004. Comparison of samplers for the biological characterization of the sea surface microlayer. Limnol. Oceanogr. Methods 2, 213–225. doi:10.4319/lom.2004.2.213

Al-Mutaz, I.S., Wazeer, I., 2014. Development of a steady-state mathematical model for MEE-TVC desalination plants. Desalination 351, 9–18. doi:10.1016/j.desal.2014.07.018

Altman, P.L., Katz, D.D., 1961. Blood and other body fluids. Federation of American Societies for Experimental Biology, Washington.

Aly, N.H., Marwan, M.A., 1997. Dynamic response of multi-effect evaporators. Desalination 114, 189–196. doi:10.1016/S0011-9164(98)00011-3

Behar, O., Khellaf, A., Mohammedi, K., 2013. A review of studies on central receiver solar thermal power plants. doi:10.1016/j.rser.2013.02.017

Betts, R.A., Golding, N., Gonzalez, P., Gornall, J., Kahana, R., Kay, G., Mitchell, L., Wiltshire, A., 2015. Climate and land use change impacts on global terrestrial ecosystems and river flows in the HadGEM2-ES Earth system model using the representative concentration pathways. Biogeosciences 12, 1317–1338. doi:10.5194/bg-12-1317-2015

Bin Amer, A.O., 2009. Development and optimization of ME-TVC desalination system. Desalination 249, 1315–1331. doi:10.1016/j.desal.2009.06.026

Buros, O.K., (IDA), I.D.A., (SWCC), S.W.C.C., 2000. The ABCs of desalting. International Desalination Association, Denver, CO.

Casimiro, S., Cardoso, J., Ioakimidis, C., Farinha Mendes, J., Mineo, C., Cipollina, A., 2014. MED parallel system powered by concentrating solar power (CSP). Model and case study: Trapani, Sicily. Desalin. Water Treat. 1–14. doi:10.1080/19443994.2014.940222

Cosgrove, W.J., Rijsberman, F.R., Council., W.W., 2000. World water vision : making water everybody's business. Earthscan Publications Ltd, London.

Dardour, S., Nisan, S., Charbit, F., 2005. Development of a computer-package for MED plant dynamics. Desalination 182, 229–237. doi:10.1016/j.desal.2005.02.028

Darwish, M.A., El-Dessouky, H., 1996. The heat recovery thermal vapour-compression desalting system: A comparison with other thermal desalination processes. Appl. Therm. Eng. 16, 523–537. doi:10.1016/1359-4311(95)00034-8

de la Calle, A., Bonilla, J., Roca, L., Palenzuela, P., 2015. Dynamic modeling and simulation of a solar-assisted multi-effect distillation plant. Desalination 357, 65–76. doi:10.1016/j.desal.2014.11.008

Dunn, R.I., Hearps, P.J., Wright, M.N., 2012. Molten-Salt Power Towers: Newly Commercial Concentrating Solar Storage. Proc. IEEE 100, 504–515. doi:10.1109/JPROC.2011.2163739

EERA, 2015. Concentrated Solar Power (CSP) | EERA [WWW Document]. URL http://www.eera-set.eu/eera-joint-programmes-jps/concentrated-solar-power-csp/ (accessed 2.8.16).

El-Dessouky, H.T., Ettouney, H.M., 2002. Reverse Osmosis Feed Treatment, Biofouling, and Membrane Cleaning, Fundamentals of Salt Water Desalination. Elsevier. doi:10.1016/B978-044450810-2/50010-5

El-Dessouky, H.T., Ettouney, H.M., Al-Juwayhel, F., 2000. Multiple Effect Evaporation—Vapour Compression Desalination Processes. Chem. Eng. Res. Des. 78, 662–676. doi:10.1205/026387600527626

El-Nashar, A.M., Qamhiyeh, A., 1990. Simulation of the performance of MES evaporators under unsteady state operating conditions. Desalination 79, 65–83. doi:10.1016/0011-9164(90)80071-I

Ghobeity, A., Noone, C.J., Papanicolas, C.N., Mitsos, A., 2011. Optimal time-invariant operation of a power and water cogeneration solar-thermal plant. Sol. Energy 85, 2295–2320. doi:10.1016/j.solener.2011.06.023

Global Water Intelligence, 2016. DesalData [WWW Document]. URL https://www.desaldata.com/

Harriman, L., 2014. The future of the Aral Sea lies in transboundary co-operation [WWW Document]. UNEP/DEWA/GRID-Sioux Falls. URL http://na.unep.net/geas/getUNEPPageWithArticleIDScript.php?article_id=108 (accessed 8.16.16).

HeliosCSP, 2016. HELIOSCSP - Concentrated Solar Power installed capacity increased to 4940 MW by the end of 2015 [WWW Document]. URL http://helioscsp.com/concentrated-solar-power-installed-capacity-increased-to-4940-mw-by-the-end-of-2015/ (accessed 9.6.16).

Iaquaniello, G., Salladini, A., Mari, A., Mabrouk, A.A., Fath, H.E.S., 2014. Concentrating solar power (CSP) system integrated with MED–RO hybrid desalination. Desalination 336, 121–128. doi:10.1016/j.desal.2013.12.030

International Atomic Energy Agency, 2015. The Fukushima Daiichi Accident [WWW Document]. URL http://www.world-nuclear.org/information-library/safety-and-security/safety-of-plants/fukushima-accident.aspx (accessed 8.13.16).

International Energy Agency, 2012. World Energy Outlook 2012.

IWMI, 2007. Water for food, water for life : a comprehensive assessment of water management in agriculture. Earthscan, London; Sterling, VA.

Kalogirou, S.A., 2005. Seawater desalination using renewable energy sources. Prog. Energy Combust. Sci. 31, 242–281. doi:10.1016/j.pecs.2005.03.001

Kamali, R.K., Abbassi, A., Sadough Vanini, S.A., 2009. A simulation model and parametric study of MED-TVC process 235, 340–351. doi:10.1016/j.desal.2008.01.019

Khayet, M., 2013. Solar desalination by membrane distillation: Dispersion in energy consumption analysis and water production costs (a review). Desalination 308, 89–101.

Li, C., Goswami, Y., Stefanakos, E., 2013. Solar assisted sea water desalination: A review. Renew. Sustain. Energy Rev. 19, 136–163. doi:http://0-dx.doi.org.fama.us.es/10.1016/j.rser.2012.04.059

Lindsey, R., 2014. World of Change: Shrinking Aral Sea : Feature Articles [WWW Document]. URL http://earthobservatory.nasa.gov/Features/WorldOfChange/aral_sea.php (accessed 9.16.16).

Llorente García, I., Álvarez, J.L., Blanco, D., 2011. Performance model for parabolic trough solar thermal power plants with thermal storage: Comparison to operating plant data. Sol. Energy 85, 2443–2460. doi:10.1016/j.solener.2011.07.002

McMichael, A.J., Woodruff, R.E., Hales, S., 2006. Climate change and human health: Present and future risks. doi:10.1016/S0140-6736(06)68079-3

Meteonorm, 2015. Meteonorm: Irradiation data for every place on Earth [WWW Document]. URL http://meteonorm.com/ (accessed 7.4.15).

Moser, M., Trieb, F., Scharfe, J., Savoldi, E., Tomasek, M.-L., Kern, J., Allal, H., Cottret, N., 2011. The MED-CSD Project: Potential for Concentrating Solar Power Desalination Development in Mediterranean Countries. J. Sol. Energy Eng. 133, 31012. doi:10.1115/1.4004352

National R+D+I Plan [WWW Document], 2011. URL http://www.idi.mineco.gob.es/portal/site/MICINN/menuitem.7eeac5cd345b4f34f09dfd1001432ea0/?vgnextoid=fe5aec1eb658c310VgnVCM1000001d04140aRCRD&lang_chosen=en (accessed 8.13.16).

NREL, 2016. NREL: Concentrating Solar Power Projects - Concentrating Solar Power Projects with Operational Plants [WWW Document]. URL http://www.nrel.gov/csp/solarpaces/projects_by_status.cfm?status=Operational (accessed 4.25.16).

OECD, 2012. OECD environmental outlook to 2050 : the consequences of inaction. OECD, Paris.

Olwig, R., Hirsch, T., Sattler, C., Glade, H., Schmeken, L., Will, S., Ghermandi, A., Messalem, R., 2012. Techno-economic analysis of combined concentrating solar power and desalination plant configurations in Israel and Jordan. - Desalin. Water Treat. 41, 9. doi:-10.1080/19443994.2012.664674

Palenzuela, P., 2012. Coupling assessment of multi-effect distillation plants and solar thermal power plants. Universidad de Almería y Plataforma Solar de Almería, Almería.

Palenzuela, P., Zaragoza, G., Alarcón, D., Blanco, J., 2011. Simulation and evaluation of the coupling of desalination units to parabolic-trough solar power plants in the Mediterranean region. Desalination 281, 379–387. doi:10.1016/j.desal.2011.08.014

Shiklomanov, I.A., Rodda, J.C., 2003. World water resources at the beginning of the twenty-

first century. Cambridge University Press, Cambridge, UK; New York.

Tol, R.S.J., 2014. Quantifying the consensus on anthropogenic global warming in the literature: Rejoinder. Energy Policy 73, 709. doi:10.1016/j.enpol.2014.06.003

Unesco and World Water Assessment Programme, 2009. The 3rd United Nations World Water Development Report water in a changing world.

Veolia, 2016. Processes for Sea Water Desalination [WWW Document]. URL http://www.veoliawatertech.com/nawatersytems/ressources/documents/1/20581,MultiEffectDistillation.pdf (accessed 10.31.16).

Wellmann, J., Neuhäuser, K., Behrendt, F., Lehmann, M., 2015. Modeling an innovative low-temperature desalination system with integrated cogeneration in a concentrating solar power plant 55, 3163–3171. doi:10.1080/19443994.2014.940212

World Health Organization, 2011. Guidelines for drinking-water quality, 4th ed. ed. World Health Organization, Geneva.

Xu, X., Vignarooban, K., Xu, B., Hsu, K., Kannan, A.M., 2016. Prospects and problems of concentrating solar power technologies for power generation in the desert regions. Renew. Sustain. Energy Rev. 53, 1106–1131. doi:10.1016/j.rser.2015.09.015

Zak, G.M., Ghobeity, A., Sharqawy, M.H., Mitsos, A., 2013. A review of hybrid desalination systems for co-production of power and water: Analyses, methods, and considerations. Desalin. Water Treat. 51, 5381–5401.

Chapter 2. Seawater desalination integrated in solar thermal power plants based on parabolic trough collectors

Part of this chapter has been published as a scientific article in Desalination, 392, pp.102–117. doi:10.1016/j.desal.2016.03.016.

Title:

"Thermoeconomic comparison of integrating seawater desalination processes in a concentrating solar power plant of 5 MW_e"

Authors:

Bartolomé Ortega-Delgado. Affiliation: CIEMAT-Plataforma Solar de Almería, Ctra. de Senés s/n, 04200 Tabernas, Almería, Spain. E-mail: bartolome.ortega@psa.es

Lourdes García-Rodríguez. Department of Energy Engineering, University of Seville, ETSI, Camino de los Descubrimientos s/n, 41092 Sevilla, Spain. E-mail: mgarcia17@us.es

Diego-César Alarcón-Padilla. Affiliation: CIEMAT-Plataforma Solar de Almería, Ctra. de Senés s/n, 04200 Tabernas, Almería, Spain. E-mail: diego.alarcon@psa.es

Abstract

In this work a thermoeconomic analysis of the joint production of electricity and water for a simulated 5 MW_e Solar Thermal Power Plant (STPP) based on parabolic trough mirrors and Direct Steam Generation (DSG) is carried out. The location considered for this plant is Almería, in southeast of Spain. Two different seawater technologies have been selected to be coupled with the STPP: Multi-Effect Distillation (MED) and Reverse Osmosis (RO). The Power Block (PB) has been designed to maximize the thermal efficiency, including regeneration and reheating. Four coupling arrangements have been investigated: the MED replacing the condenser of the PB, the MED being fed by one steam extraction of the PB, the RO directly using the electricity generated by the PB and the RO connected to the local grid. Results show that the best coupling option is with the RO unit being connected to the local grid, which produces the lower Levelised Water Cost (LWC).

Keywords: solar desalination, multi-effect distillation, reverse osmosis, cogeneration, solar thermal power plants, Rankine cycle

Contents

List of figures

List of tables

Nomenclature

Variables

A_{SF}	Solar field aperture area, m^2
A_c	Solar collector aperture area, m^2
A	Levelised value of a quantity of money
b	Molality, mol/kg
c	Exergetic unit cost, €/kWh
$\dot{C}$	Cost rate, €/h
CRF	Capital recovery factor
ex	Specific exergy, kJ/kg
E_1	Annual energy or output type 1 produced, kWh
E_w	Yearly production of fresh water, m^3/y
$\dot{E}$	Exergy rate, kW
$\dot{E}_{rad}$	Exergy rate associated with the direct normal irradiance, kW
E_2V_{e2}	Discounted sum of other revenues, €
f	Conversion factor
h	Specific enthalpy, kJ/kg
HR	Heat rate of the power block, kJ/kWh
I_d	Direct normal irradiance at the design day, kw/m^2
k_n	Nominal discount rate or nominal cost of capital
L_e	Discounted sum of input energy expenses, €
M	Discounted sum of operating expenses, €
m_d	Daily production of freshwater, m^3/d
N	Lifetime project, y
N_c	Number of collectors
n_h	Hours of daily operation, h/d
p	Pressure, bar
P_I	Discounted investment costs, €
P_{OM}	Discounted O&M expenses, €
P_F	Discounted fuel expenses, €
P_0	Value of an expenditure at the beginning of the first year, €
Q_a	Heat per unit of mass added to the power cycle, kJ/kg
Q	Heat per unit of mass, kJ/kg
q	Mass flow rate, kg/s
$\dot{Q}_{MED}$	Heat rate added to the MED, MW
$\dot{Q}_{COND}$	Heat rate consumption in the condenser, MW

$\dot{Q}_{sun}$	Heat rate of the direct normal irradiance in the solar field, kW
R	Discounted sum of replacement costs, €
r_i	Annual inflation rate
r_n	Nominal escalation rate
s	Specific entropy, kJ/kg
S_c	Collector aperture area, m^2
T	Temperature, °C
T_{out}	Temperature of the heat transfer fluid in the outlet of the solar field, °C
V_{e2}	Value of energy type 2 produced in year zero
W_T	Specific total work extracted in the turbines, kJ/kg
W_P	Specific total work consumed by the pumps in the power cycle, kJ/kg
$\dot{W}_e$	Net electric power, MW
$W_{e,n}$	Net electric energy, kwh/y
W	Specific work, kJ/kg
W_{main}^{RO}	Specific energy consumption of the main pumps, kwh/m^3
W_{aux}^{RO}	Specific energy consumption of the booster pumps, kwh/m^3
x	Title of steam
Y	Specific cost
$\dot{Z}$	Cost rate associated to capital investment and O&M, €/h

Acronyms and abbreviations

CFD	Computational Fluid Dynamics
COND	Condenser
CP	Condensate Pump
CPV	Concentrator Photovoltaic
CSP	Concentrating Solar Power
CSPonD	Concentrating Solar Power on Demand
DCF	Discounted Cash Flow
ED	Electrodialysis
EERA	European Energy Research Alliance
EV	Evaporator
FF	Forward Feed
FP	Feeding Pump
G	Electric Generator
GOR	Gain Output Ratio
HP	High Pressure Turbine
HR	Heat Rate

HTF	Heat Transfer Fluid
I+P	Intake plus Pretreatment
ISCC	Integrated Solar Combined Cycle
LEC	Levelised Electricity Cost
LWC	Levelised Water Cost
LP	Low Pressure Turbine
LT-MED	Low Temperature Multi-Effect Distillation
LWC	Levelised Water Cost
MD	Membrane Distillation
MED	Multi-Effect Distillation
MENA	Middle East and North Africa
MEH	Multi-Effect Humidification
MIT	Massachusetts Institute of Technology
MSF	Multi-Stage Flash
MVC	Mechanical Vapour Compressor
O&M	Operation and Maintenance
ORC	Organic Rankine Cycle
OT	Once-Through
PB	Power Block
PCM	Phase Change Material
PF	Parallel Feed
PH	Preheater
POWERSOL	Mechanical POWER generation based on SOLar heat engines
PT	Parabolic Trough
PV	Photovoltaic
RH	Reheater
RO	Reverse Osmosis
SEC	Specific Energy Consumption
SF	Solar Field
SH	Superheater
STPP	Solar Thermal Power Plant
SWRO	Seawater Reverse Osmosis
TBT	Top Brine Temperature
TDS	Total Dissolved Solids
TES	Thermal Energy Storage
TVC	Thermal Vapour Compression

Subscripts

a	Heat added to the power block
amb	Ambient
ap	Apparent
aux	Auxiliary
c	Condensation
d	Daily production of fresh water
e	Electric
F	Fuel
g	Global
I	Investment
n	Net
p	Pump
P	Product
out	Outlet
t	Turbine
th	Thermal
u	Useful
v	Vapour
w	Water
0	First year
1	Energy type one
2	Energy type two

Superscripts

CI	Capital Investment
OM	Operation and Maintenance
RK	Rankine
RO	Reverse Osmosis

Greek

α_i	Mass fraction of steam extracted from the bleed *i*
η_g	Global efficiency
η_b^{RO}	Internal efficiency of the booster pumps in the RO plant
η_m	Mechanical efficiency
η_{HP}^{RO}	Internal efficiency of the high pressure pumps in the RO plant
η_{th}	Thermal efficiency

η_{sh}	Shaft efficiency
η_X	Exergetic efficiency
θ	Incidence angle of the solar rays
ρ	Density, kg/m^3
τ	Annual average availability of the plant, h/y

2.1 Literature review on CSP+D

The literature regarding desalination processes powered by concentrating solar power (Concentrated Solar Power and Desalination, CSP+D) is very limited, despite the great interest aroused in the last years. The different approaches and studies that have been presented regarding this concept during the last decade are briefly reviewed hereafter.

It is well known that seawater desalination is an energy-intensive consumer process, especially in the case of thermal methods. In this respect, solar irradiation may provide the energy necessary to drive such processes, particularly in arid regions of the world with high levels of annual solar irradiation, which normally lack from fresh water sources. Solar irradiation may be used in low temperature desalination processes without concentration, by means of flat plate collectors or evacuated tube collectors, up to 100 – 200 °C (Mekhilef et al., 2011). Also, solar energy can be concentrated in order to reach higher temperature levels, with single axis tracking collectors, such as linear Fresnel and Parabolic Trough (PT), obtaining temperatures of 300 °C and 400 °C, respectively (Suman et al., 2015). Further temperature levels may be attained with two axes tracking collectors, using central tower receivers or parabolic dish reflectors technologies, which achieves temperatures of 1500 and 2000 °C, respectively (Kalogirou, 2004). Within non-concentrating solar thermal technologies, some efficient methods for solar-driven desalination processes have been investigated. Garaway & Grossman (2006) developed a Multi-Effect Humidification (MEH) system for desalination purposes, using solar irradiation as the heat source of the system. They employed heat recovery from the condensed steam to preheat the seawater and used Computational Fluid Dynamics (CFD) to optimize the process and geometry of the facility. Results showed a low value for the distillate salinity (17 ppm) using saline feed water (23,000 ppm) and the operating efficiency (Gained Output Ratio, GOR) was comparable to that of ideal case in a MEH desalination device. Also, the possibilities of low temperature solar collectors for powering desalination systems were investigated by García-Rodríguez and Delgado-Torres (2007). They evaluated solar powered Rankine cycles providing shaft power to a Reverse Osmosis (RO) unit, for seawater or brackish water desalination. They concluded that desalination systems combined with solar-powered organic Rankine cycles had lower specific solar energy consumption compared to solar distillation and solar photovoltaic RO systems. This concept was later further exploited within the POWERSOL (mechanical POWER generation based on SOLar heat engines) Project (García-Rodríguez and Blanco-Gálvez, 2007), aimed to study and optimise solar thermal-driven mechanical power generation systems based on a solar-heated thermodynamic cycle, from low to medium temperature levels (80 – 250 °C). Different solar collectors were assessed: flat plate collectors, compound parabolic concentrators, linear Fresnel concentrators and parabolic trough collectors. Preliminary results showed that this technology could be more efficient and cost effective than photovoltaic systems.

There are a large number of studies considering the use of Photovoltaic (PV) solar panels for desalination processes, technology that has gained share in the solar power market during the last years. One of the main reasons for this is their ability to convert directly the solar energy into electricity, with laboratory cell efficiencies up to 46% using Concentrator Photovoltaic (CPV) multi-junction cells, and large modules with efficiencies up to 38.9%, although overall systems have practical efficiencies below 30% (Philipps et al., 2015). El-Sayed (2007) investigated the competitiveness of solar desalination systems based on PV solar panels and spiral-wound reverse osmosis modules. He modelled the RO subsystem using equations related to the separation process within the membranes by a dimensional analysis. The PV subsystem was modelled by means of cost-efficiency relationships for three different types of cells: amorphous silicon, crystal silicon and multi-junction concentrators. He concluded that solar desalination systems may displace those ones using fossil fuels as the energy source when high efficiency RO modules and PV cells are selected.

Werner & Schäfer (2007) analysed small-scale RO solar desalination facilities for remote areas in Australia, focusing on the social aspects related to the introduction of new desalination technologies in those areas. The facility included PV solar panels powering RO membrane modules and nanofiltration or ultrafiltration processes in order to remove the turbidity and microbiological organisms of the water. They evaluated the sustainability of the facility regarding social aspects such as water quality, availability of human resources able to operate and maintain the installation, and the personal involvement of the population. Results showed that the salinity of the permeate obtained was low but not of acceptance by local people, while the water production was higher than needed. They also noticed that it was needed high qualification staff for the operation and maintenance of the facility. Generally, the new technology was well accepted by the community although some recommendations about the design and management of the installation were proposed.

The economic viability of small-scale PV+RO solar desalination plants for low-salinity water in remote areas was also studied by De Munari et al. (2009). They evaluated the powering of a RO pilot plant in Coober Pedy (Australia) using PV panels (without batteries) instead the conventional energy source, and introducing ultrafiltration as the pre-treatment of the raw water. Results of tests carried out during three days showed that PV+RO produced water with good quality standards, and reached a Specific Energy Consumption (SEC) of 3.2 kWh/m^3 when dealing with low salinity water. Therefore, it could represent a promising option in order to reduce the high costs of the desalination process.

Ali et al. (2011) made an extensive techno-economic review of the main indirect solar desalination technologies, using PV panels and solar thermal collectors. In the first case, the power produced is used to feed membrane desalination methods, as RO and Electrodialysis (ED), while in the latter case the collected energy is used to drive thermal desalination

processes, such as Multi-Stage Flash (MSF), Multi-Effect Distillation (MED), Thermal Vapour Compression (TVC) and Membrane Distillation (MD). They concluded that membrane desalination technologies based on RO and ED were the most competitive regarding production costs (high recovery ratio and lower specific energy consumption). Nevertheless, for large-scale solar desalination systems the authors recommended the MED thermal desalination technology as it had the lower water costs.

The combination of power plants and thermal desalination processes has great interest because of the inherent synergy existing between both systems. The use of common facilities and further utilization of process heat available in conventional power plants makes this integration very attractive. Moreover, environmentally friendly technologies for power production based on renewable energy are preferred, instead of those using fossil fuels which are contributing to global warming and have harmful effects on human health and nature equilibrium. Among the different *green* technologies available, Concentrating Solar Power plants have been proven as a reliable and mature method for power production. Taking into account the difficulties for the market introduction of CSP plants and desalination processes as stand-alone power and water generation systems, combinations with conventional power plants could represent an opportunity to facilitate their accessibility. To this respect, several authors have analysed the combination of desalination and CSP plants.

The thermodynamic performance of cogeneration schemes using CSP and gas turbine plants coupled to hybrid Low Temperature Multi-Effect Distillation (LT-MED) and RO seawater desalination processes was studied by Alrobaei (2008), for the Middle East and North Africa (MENA) region. Two different configurations were proposed: combined solar power and seawater desalination plant, and Integrated Solar Combined Cycle (ISCC). In the first scheme, direct steam generation in the collectors and a flash steam separator vessel for feeding the back-pressure steam turbine of the power block were considered. The RO unit was connected directly to the grid, being fed by the rejected cooling seawater from the MED unit. In the second design a gas turbine unit was introduced, using the waste heat from the exhaust gases to generate additional steam for the steam turbine block. As a result of the study it was concluded that the ISCC design increased the thermal efficiency with respect the other configuration by 44.5%. In addition, this scheme would help to reduce the fossil fuel consumption of a conventional power plant and would permit to match the power and fresh water demand during 24 h per day.

Trieb & Müller-Steinhagen (2008) investigated the fresh water demand projected in the MENA region for long-term periods and how it could be satisfied by means of a better and sustainable management of the existing water resources, together with the utilization of seawater desalination processes powered by solar energy. Among the different options, CSP plants were identified as a good and sustainable alternative to plants based on fossil fuels. In this regard,

Trieb et al. (2009) analysed the state-of-the-art of CSP technology, including linear focusing concentrating collectors (Fresnel and parabolic trough) and point focusing concentrating systems (central receiver), which were suitable to feed Rankine and Brayton cycles, respectively, in the MENA region, concluding that CSP is not only an option but an affordable and unavoidable technology for meeting the power and water demand in such areas. Also, it was suggested that the market introduction of these new technologies should be encouraged by the local governments in order to deal with the increasingly water demand.

Gastli et al. (2010) evaluated the possibilities of coupling between CSP plants and desalination plants in Duqum (Oman), considering MED and RO as desalination processes. They used a Geographic Information System (GIS) solar radiation tool to select the best place for the plant location. They also highlighted the advantages of the MED coupling arrangement in comparison with the RO option: the reduction of primary energy consumption, better competitiveness for large consumers regarding the purchasing prices from external suppliers of power and water, smaller collector field requirements and lower fuel consumption due to the better technical performance. Moreover, although the initial investment costs could be higher for CSP+MED case, the more expensive maintenance of the RO unit (more sophisticated pretreatment, membrane replacements, etc.) during the lifetime of the plant leads to the CSP+MED option to be slightly cheaper than CSP+RO, in contrast with commonly accepted criteria. However, to the opinion of the authors, only a deep and detailed study of the economic and technical performance of the complete system could provide the best combination for CSP and desalination plants. Also, it was pointed out that although solar-powered desalination plants have some environmental impacts, mainly due to the concentrating brine discharge to the sea along with the chemical additives included in the pretreatment of the seawater, they are minimal compared to conventional desalination plants using fossil fuels. Furthermore, a site selection analysis in Duqum was performed for a hypothetical CSP+D plant. It was concluded that the best location for a CSP plant, in the particular case of Duqum, was near to the coast and close to an industrial park, which is a large energy consumer and could buy the power generated from the CSP+D plant at lower costs than that of the external sources (local grid).

One significant issue associated with the sustainability of CSP plants is the huge amount of water consumed by the power cycle when using evaporative cooling tower technology. This is particularly important in desert locations with water scarcity, where CSP plants have more potential due to the good solar irradiation levels. The use of dry cooling systems could be a solution but, in that case, the thermal performance of the power block is reduced. As an example, for a dry-cooled parabolic trough solar plant located in the Mojave Desert (EEUU) the annual electric production would be reduced in 5% and the generation costs would increase by 7% to 9%, according to a study performed by the (U.S. Department of Energy (DOE), 2009). The penalties may vary depending on the location considered and the air temperature,

though. Damerau et al. (2011) analysed the costs of reducing the water consumption in CSP plants located in North Africa. They indicated that a typical parabolic trough CSP plant located in Mojave Desert using wet cooling could consume about 3000 m^3/GWh of water, while if a dry cooling system was considered, this amount would be reduced to 300 – 340 m^3/GWh, of which near to 75 m^3/GWh would be dedicated to mirror cleaning. Results obtained also showed that parabolic trough technology consumes 40% more of water than central tower. Furthermore, cost penalties associated with the use of dry or hybrid cooling processes were relatively minor (6% and 9% of annual efficiency loss in the hottest site studied for the hybrid and dry cooling, respectively). Also, with the advance of the dry cooling technology, it could become more cost competitive compared to conventional cooling methods. For instance, dry-cooled plants may be improved with the pre-cooling of the inflow air to the air-cooled condenser, or PV panels could drive the cooling fans. Finally, they concluded that the sustainability of CSP plants is not dependent on the technical constraints or the decrease in the efficiency, but on political regulations that help to introduce new and environmental friendly technologies for power and water generation, according the specific needs of each location.

Ghobeity et al. (2011) presented the design, modelling and optimization of a Solar Thermal Power Plant (STPP), or CSP plant, combined with a desalination plant. The STPP consisted on a volumetric absorption molten salt receiver that also acts as thermal energy storage (salt tank), eliminating the need of a tower and the pumping of the salts. This concept is known as Concentrating Solar Power on Demand (CSPonD) and it was developed by the Massachusetts Institute of Technology (MIT) (Slocum et al., 2011). The receiver is heated by a heliostat field located on the top of a hill being the heat source of a regenerative Rankine cycle with steam extractions and a power capacity of 4 MW_e. A hybrid MED/RO desalination system was selected, being the MED unit fed by a steam extraction of the power block and the RO powered by the electricity generated by the cycle. Results obtained from the simulations showed that, for particular cases studies located in Cyprus during a summer day, and without any subsidy for power or water generation, the highest income was achieved using low pressure steam extraction for the MED unit. On the contrary, if a feed-in tariff is accounted, it is not recommended to extract any steam for the distillation unit. Moreover, in all the simulated cases, for the small-scale production MED unit considered to be combined with the 4 MW_e power plant, the RO energy consumption was lower than that of the MED.

A thermo-economic analysis of the coupling between a parabolic trough solar field and a Parallel Feed (PF) MED desalination plant driven by a thermocompressor and a Mechanical Vapour Compressor (MVC), namely MED-TVC and MED-MVC, was performed by Sharaf et al. (2011). Two different configurations were investigated: in the first one, the PT solar field fed a MED-TVC unit using a boiler heat exchanger. In the second, the vapour generated in the boiler was used to drive an Organic Rankine Cycle (ORC) and the power output to feed a

MED-MVC unit. From the analysis done they drew that the first case considered was more convenient than the second due to the lower Specific Energy Consumption (SEC), water price and product costs. Also, they recommended lowering the Top Brine Temperature (TBT) to 60 ~ 65 °C and to increase the number of MED effects by 16 ~ 20 because of the better efficiency achieved, lower SEC, less solar field area required and lower thermo-economic product costs.

Iaquaniello et al. (2014) presented a MED/RO hybridization scheme coupled to a parabolic trough CSP plant using molten salts as heat transfer fluid. Also, thermal storage and a back-up system using a gas turbine were considered. In this way, the natural intermittence of the solar irradiation in CSP plants could be partially addressed. Also, the hybridization of MED and RO processes permits to use the same intake and outfall installations with the subsequent benefit in pumping energy, compared with the standalone cases. In the integration scheme proposed, the feed of the RO system is comprised of cold seawater intake (79%), warm seawater rejected from the end condenser of the MED (14%), and from the brine blowdown (7%). It allows the feed to the RO to be warmed up and to increase the permeate production. The MED unit is fed by the exhaust steam of the back-pressure turbine at 0.24 bar and 69 °C. Results obtained showed that the presented configuration allows the continuous operation of the plant and the reduction of the water production costs below 1 €/m^3. Particularly, increasing the capacity of the desalination plant from 1224 to 3672 m^3/d led to a 25% of cost reduction (0.97 to 0.73 €/m^3).

Palenzuela et al. (2011a) carried out a thermodynamic evaluation in a design point for several coupling arrangements between parabolic trough solar thermal power plants and desalination plants in arid regions, based on RO and MED processes. From the simulations carried out, they proved that, under harsh climate conditions where there is not a water cooling source available and dry cooling is unavoidable, the integration of the MED replacing the condenser of the cycle is thermodynamically more efficient than the coupling of a RO (powered by the electricity generated by the power block). Moreover, a novel coupling arrangement was introduced using a LT-MED unit coupled with a thermocompressor, where the entrainment vapour is taken from the exhaust steam of the low pressure turbine, while the motive steam is obtained from the high pressure turbine or intermediate bleeds (design known as LT-MED-TVC). In the latter case, and for low values of the motive steam pressure, the results obtained were similar to the RO integration case, due to the lower cooling requirements. Therefore, coupling of this MED plant with a PT-CSP plant may represent a valid option in arid or semi-arid regions of the world.

Another study presented by Palenzuela et al. (2011b) accounted for the assessment and evaluation of the coupling of desalination plants (MED, MED-TVC and RO) and CSP plants in the Mediterranean region. Different integration schemes were proposed: MED taking vapour from an intermediate steam extraction of the low pressure turbine, MED-TVC fed by motive

steam from the outlet of the high pressure turbine and taking the entrainment vapour from an intermediate effect of the desalination plant, MED-TVC driven directly by steam generated by the solar field, and RO coupled to the power line at the outlet of the power plant. Results obtained showed that the best cycle efficiency was achieved for the RO integration, although not very far from the MED integration case that had the advantage of reducing the waste heat of the cooling system and therefore the cooling requirements. The MED-TVC case, although it presented higher desalination efficiencies in terms of GOR, it had lower cycle thermal efficiency. Moreover, in these plants the cooling requirements of the end condenser of the desalination unit are reduced or even nulled since vapour from the MED process is recovered through the thermocompressor. Therefore, it was concluded that the MED-TVC technology could be an alternative to RO and MED for the coupling with CSP plants.

The same authors presented an analysis of the different cooling processes in a power block and their impact on the efficiency of the cycle, for different combinations between CSP and desalination plants located in the Mediterranean area (Palenzuela et al., 2013). Two different MED arrangements were considered: LT-MED fed by exhaust steam of the steam turbine at 70 °C and LT-MED driven by compressed steam coming from a thermocompressor (LT-MED-TVC), which was fed by high pressure steam from the turbine and entrainment steam from the outlet of the turbine. These configurations were techno-economically compared with the integration of a RO plant using the power line of the CSP plant in which different cooling technologies were considered for the power cycle: once-trough, evaporative cooling tower and dry-cooling. Results obtained showed that the LT-MED coupling arrangement was thermodynamically more efficient than that of the LT-MED-TVC, and because of that it was selected for comparing with the RO case, considering the three proposed cooling methods. From this comparison it was concluded that the highest efficiency was reached using the RO unit for coupling with the CSP plant for all the cooling methods. Also, it was seen that the use of evaporative cooling tower was the most efficient and economic system with respect the power generation, although it required additional fresh water production from the desalination plant. Therefore, the cost of water was higher than in once-through and dry cooling methods. In the latter cases, the seawater pumping and power consumption from fans made the Levelised Electricity Cost (LEC) higher than the LT-MED-CSP option.

Further investigation about the feasibility of the integration of MED into CSP plants with respect the separate fresh water and electricity production by RO with CSP was carried out by Palenzuela et al. (2015b) by an extensive sensitivity analysis in which the SEC and exhaust steam temperature were varied. They proposed three different configurations for the integration between the MED process and the CSP plant: in the first case a LT-MED was fed by the exhaust steam of the power block, acting as the condenser of the cycle, the second case consisted in a LT-MED-TVC arrangement, and in the third arrangement a typical MED-TVC

unit was considered, being the thermocompressor fed with motive steam from the high pressure turbine and entrainment steam from an intermediate effect of the MED unit. In the two latter configurations and in the case of RO+CSP, the three cooling methods mentioned above were considered for the sensitivity analysis. They concluded that, under certain conditions, that is, high temperature of the exhaust steam and high electricity consumption of the RO unit, the integration of a LT-MED process was more efficient than the coupling of a RO unit to the CSP plant, for the three cooling systems considered. The MED-TVC integration case resulted worse than RO option in all cases, although the LT-MED+TVC scheme was more efficient than RO for conditions similar to those of the Arabian Gulf region: high ambient temperature and high RO SEC (above 4.5 kWh/m^3), using dry cooling or once-through cooling systems.

The same authors carried out a techno-economic analysis of the configurations mentioned above for two study cases: a representative location in the Mediterranean Sea and a representative location in the Arabian Gulf (Palenzuela et al., 2015a). It resulted that the recommended desalination technology for integrating with a CSP plant in the Arabian region was the LT-MED+TVC arrangement, which was not better in terms of efficiency (LT-MED resulted the optimal option) but had other advantages such as the possibility of de-coupling the water production from the power generation and also being able to regulate the amount of fresh water produced, meeting the daily and seasonal demand of the location. If a Mediterranean area was considered for the CSP plant, the LT-MED scheme had better efficiency than RO case but not with evaporative cooling as the refrigeration method of the power block. The LT-MED+TVC scheme was recommended only if dry-cooling was selected for the power cycle, although the differences with the RO option were not very large.

Blanco et al. (2013) carried out a techno-economic evaluation of the coupling between desalination plants, based on MED and RO processes and a PT-CSP plant, taking Port Safaga (Egypt) as location. Three different coupling configurations were considered: LT-MED, LT-MED-TVC, and RO, which were previously described. It was concluded that in cases in which the only feasible cooling option for the power block is done by means of dry condensers, which is the typical case in arid regions, the integration of a MED unit substituting the condenser of the cycle provided better thermal efficiency than the RO option, and production costs were similar. For such analysis, a high specific power consumption for the RO was selected (5.5 kWh/m^3), which is habitual in arid regions dealing with harsh seawater. The LT-MED-TVC option resulted had the lowest efficiency, although in this case the water production is de-coupled from the power generation, which is a major advantage.

A techno-economic study of a cogeneration CSP plant for the combined production of power and water in Cyprus was performed by Fylaktos et al. (2014). They considered three different arrangements: only power production, power and water using RO and power and water using MED process. The capacity of the power plant and desalination unit were 4 MW$_e$ and

5035 m^3/d, respectively. A Discounted Cash Flow (DCF) method was selected for the financial analysis in order to estimate the annual electricity and water yields. The uncertainty of the input economic parameters was accounted using Monte Carlo simulations and pre-assigning them distribution functions. Results showed that the only-electricity production was the best option from an economic point of view, followed by the coupling of the MED, which provided slightly better LCOE and LCW. Also, it was suggested that the integration of desalination processes in CSP plants could be economically feasible in all cases and may be competitive with stand-alone CSP power production if water desalination by means of renewable energy were financially supported in the same manner than the electricity generation. Moreover, it was revealed that the financial performance of the plant is highly dependent on the electricity tariff in the three arrangements proposed.

The accurate determination of the annual yield of power and water in CSP+D plants is important for performing thermo-economic and financial analyses, which are useful to predict the production costs and the feasibility of the project. In order to obtain the annual yield in CSP+D plants, time dependent analyses are required, due to the inherent variability and intermittence of the solar resource. Moreover, part load operation issues surged in MED units coupled to CSP plants is one of the reasons for the lack of real large-scale solar desalination plants in the market (Hassabou et al., 2013). Therefore, there is a necessity of further investigation in the part load operation in CSP+D plants and to develop mathematical models for predicting the performance of the system in such conditions.

In this respect, Casimiro et al. (2014) presented a model for simulating the operation of a CSP plant coupled with a Forward Feed (FF) MED desalination unit acting as the condenser of the Rankine cycle, and taking as location San Diego (EEUU). In addition, four different cooling options were analysed: both the MED unit and a Once-Through (OT) condenser acting together, dry cooling, evaporative wet cooling and once-through cooling alone. Different control strategies were implemented, taking into account the minimum load for the operation of the power block and the MED unit. From the annual simulations performed it was obtained that the use of MED+OT cooling in a CSP was feasible and produced a penalty in the performance of the system below 5%, compared to the use of wet cooling method. Also, with the MED-OT option, fresh water is produced along with power.

Also, Hassabou et al. (2013) analysed the transient operation of a 5000 m^3/d MSF seawater desalination plant conceptually coupled to a CSP plant, located within the MENA region. Particularly, they selected a parabolic trough solar field with latent heat thermal energy storage (Phase Change Material, PCM) and a natural gas boiler as back-up system. The use of thermal energy storage extends the daily operation of the plant and permits to continue the operation when there is not available solar irradiation. Simulations with variable operation and changing weather conditions were performed over a year. Results obtained showed that the cost of the

energy source greatly depends on the selected solar fraction, plant location and energy prices. In addition, a solar fraction of 96% may be attained with average solar collector area and thermal storage size. The fresh water production costs of the MSF unit were almost three times higher than conventional technologies based on fossil fuels and RO system operating in the Arabian Gulf region. However, other features of the solar energy such as being a free and sustainable energy source or environmentally friendly technology should be taken into account when comparing with traditional power and water production plants. The water cost using CSP+RO was found to be competitive with conventional systems, although this technology has to face other problems in the Gulf region associated with high salinity and turbidity of the seawater, among *red tides* phenomena or high marine life. Finally, other desalination methods as MED process were suggested to be coupled with the CSP plant as they are more efficient thermodynamically than MSF.

There are also studies on stand-alone solar desalination systems working out of design conditions. Fernández-Izquierdo et al. (2012) experimentally assessed the operation out of nominal conditions of the SOL-14 MED pilot plant located at Plataforma Solar de Almería solar research centre, in Almería (Spain). This vertically-stacked pilot plant consists of 14 effects with preheaters and a nominal capacity of 3 m^3/h. After the experimental campaign conducted, it was concluded that the effects of the part load operation of the plant were higher on the distillate production (which decreased a 37% for a 19% heating steam temperature reduction, from 70 to 57 °C) than on the performance ratio (only suffered 11% of reduction, from 10 to 8.9, for the same case). Also, it was observed that the operation over the nominal values did not provide higher distillate production.

Apart from parabolic trough, other CSP technologies could be considered for the solar thermoelectric production. Kalogirou (2013) investigated the optimal concentrating solar power technology for its implementation in Cyprus, among parabolic trough, central receiver and parabolic dishes. He obtained that the best option, in terms of the electricity production costs, was the central receiver. However, parabolic trough technology was preferred because of its maturity and proven operation in real plants. Moreover, PT plants have high global solar-to-electric efficiency and low area requirements per MWh. In opinion of the author, this plant should be located near to the sea, in order to use seawater as the cooling source of the condenser in the power block. Most conventional power stations are located in coastal areas for the same reason. In that case, it was recommended to combine the CSP plant with a desalination unit and produce fresh water as a second product.

Also, the Fresnel solar collector technology has become commercial recently with a 30 MW_e plant built in Puerto Herrado (Spain) in 2012 (Novatecsolar, 2016). In this regard, Hamed et al. (2016) studied the feasibility of the coupling between a Fresnel CSP plant and a MED-TVC desalination unit. A fossil back-up system was taken into account for supplying energy to the

desalination plant when solar irradiation was not available. The proposed scheme was compared with a MED-TVC unit using only fossil fuel. Results showed that both cases provided similar Levelized Water Cost (LWC) for a fuel cost of $92/bbl, with the climatic conditions considered of Saudi Arabia (yearly DNI of 1132 kWh/m^2). That means that up to this value, the scheme using only fossil fuel would provide lower LWC. If a location with higher annual DNI is selected (1937 kWh/m^2), such as Almería (Spain), the breakeven fuel cost would decrease up to $52/bbl. From this value above, the Fresnel CSP would be more convenient. Moreover, with the specified climatic conditions, the combination of a Fresnel CSP plant and a MED-TVC unit without thermal energy storage resulted more economic than including a TES system.

Kouta et al. (2016) investigated the coupling between a solar tower plant (central receiver) and a MED-TVC desalination unit for the co-production of power and water. In this case the power cycle selected was a supercritical CO_2 Brayton cycle, and a thermal energy storage comprised of two tanks of molten salts was included. The entropy analysis revealed that the maximum entropy generation was produced by the solar tower (80%), followed by the MED-TVC unit and the sCO2 power cycle. The steam ejector was the component that had more entropy contribution in the desalination plant, followed by the end condenser. It was also shown that the specific entropy generation in the MED-TVC unit decreased when increasing the number of effects. Finally, a techno-economic analysis was carried out for Saudi Arabia from which it was drawn that the lowest LEC and LWC were obtained in regions with the highest solar irradiation levels during the year.

2.2 Thermoeconomic comparison of integrating seawater desalination processes in a concentrating solar power plant of 5 MWe

This section deals with the case study of integrating seawater desalination processes in a specific CSP plant of 5 MW_e, based on direct steam generation within absorber tubes of parabolic trough collectors. Zarza et al. (2006) designed and thoroughly described in this reference a CSP plant with these features. Based on this plant, the authors evaluate the power cycle and propose the best design in order to compare four coupling arrangements. Firstly, the coupling of a multi-effect distillation plant is analysed, thus integrating the fresh water and electricity production. Two different configurations are studied: the maximum water production by means of replacing the condenser by the distillation plant and the use of an intermediate steam extraction from the steam turbine to feed the MED unit. Secondly, the reverse osmosis desalination process is considered. Two options are examined: the integrated production of water and electricity, in which the desalination plant only produce water when the CSP plant operates, and the independent production of water and electricity. In this case two different plants can be installed in near but different locations. Since the use of distillation processes only makes sense for seawater desalination, the comparison is restricted to Sea Water Reverse Osmosis (SWRO). Moreover, a MED plant requires steam below 70 °C (to avoid the appearance of scaling in the tubes), hence the influence of this requirement on the power cycle efficiency is thoroughly calculated in this section, in order to compare distillation and membrane desalination processes. The cost of the fresh water production is also comparatively analysed in the four coupling arrangements considered.

Although RO is currently the dominant technology in large-scale seawater desalination, some authors consider distillation as the only appropriate desalination process due to different reasons:

- The requirement of extremely high quality water - concentration around a few ppb - to compensate the power cycle leakages, makes the RO process useless. Nevertheless, this is not a barrier for the RO process since further treatment of its product can be performed by means of other processes as electro-deionization. Moreover, the human consumption does not require any additional treatment, and then only a part of the water production would need it in that case.

- The cooling requirement of the condenser is argued by some authors to be substituted by the distillation plant. Nevertheless, the seawater flow required by an MED plant is similar to the flow required by the corresponding once-trough cooled condenser. This is due to the need of cooling the end condenser in the distillation process. In addition, the hot brine disposal is an environmental problem similar to the once-through cooling of a

CSP plant. Moreover, if a SWRO is installed, the condenser of the power cycle could be cooled by the feed, product or blowdown of the SWRO plant.

- The self-consumption attributable to the electricity demand of the RO process, if it is integrated into the power production, is another drawback of RO process from the point of view of some authors. This is the case in which the electricity production has a direct subsidy. However, the coupling of a distillation process causes a decrease on the power cycle efficiency and needs a significant amount of energy for pumping, especially in the end condenser where the seawater is used as cooling stream. Furthermore, the temperature of the power cycle condenser in dry or evaporative cooling is higher than in once-trough cooling, in which an open circuit of water flows at ambient temperature and pass through the condenser. If a desalination process is considered together with the power generation, and a water stream is available at the CSP plant, then it can be used to partially or totally cool the power cycle condenser. Therefore, a realistic comparison should not consider the dry cooling as the only process to condense the power cycle steam.

Due to above-mentioned reasons, the design of both, the desalination process and the condenser cooling should be carried out as a whole, and based on a realistic assessment of the power cycle efficiency for a given fresh water demand. Other key issue is related to the existence of conventional power backup for the electricity production, since in case of discontinuous operation distillation plants exhibit meaningful additional risk of scaling. Finally, in case of discontinuous operation, the nominal capacity of the desalination plant to supply a given fresh water demand should be significant higher. This does not make sense in case the water production is not only attributable to the self-consumption of the CSP plant.

In addition, the interest in desalination coupled to solar power plants has been pointed out within the framework of the European Energy Research Alliance (EERA, 2015), by establishing a sub-programme on “Concentrated Solar Power plus Desalination” within the Joint Programme on CSP. Both, distillation and reverse osmosis, may be considered as the desalination process to be coupled to a solar power plant.

This section is focused on the thermoeconomic comparison between distillation and reverse osmosis desalination technologies integrated in a parabolic trough solar thermal power plant, based on direct steam generation within the solar field. Since the comparison between heat or electricity consumptions is complex, the well-known thermoeconomic methodology is selected in order to assess the actual cost of the steam consumption of the distillation process.

2.2.1 Concentrating Solar Power and Seawater Reverse Osmosis plants

2.2.1.1 Concentrating Solar Power (CSP) plant

The first step of considering the coupling between CSP and desalination is to estimate realistic performances of both processes. Table 2.1 shows a record of representative PT-CSP plants, specifically those installed in the Mojave Desert, with the thermal efficiencies of the Rankine cycle.

Table 2.1. Some representative PT-CSP plants (NREL, 2016).

Plant	Location	Year	$\dot{W}_e$ (MW_e)	T_{out} (°C)	A_{SF} (m^2)	η_{th} %	Power block	Back-up
Solana	Arizona, US	2013	250	390	2,200,000	-	100 bar, reheat	Molten salts
Andasol I	Granada, Spain	2008	49.9	393	510,120	37.5	100 bar, reheat	Molten salts
Nevada Solar I	Boulder City, NV	2007	64	390	357,200	37.6	100 bar, reheat	None
APS Saguaro	Tucson, AZ	2006	1	300	10,340	20.7	ORC	None
SEGS IX	Harper Lake, CA	1991	80	390	483,960	37.6	100 bar, reheat	HTF heater
SEGS VIII	Harper Lake, CA	1990	80	390	464,340	37.6	100 bar, reheat	HTF heater
SEGS VI	Kramer Junction, CA	1989	30	390	188,000	37.5	100 bar, reheat	Gas boiler
SEGS VII	Kramer Junction, CA	1989	30	390	194,280	37.5	100 bar, reheat	Gas boiler
SEGS V	Kramer Junction, CA	1988	30	349	250,500	30.6	40 bar, steam	Gas boiler
SEGS III	Kramer Junction, CA	1987	30	349	230,300	30.6	40 bar, steam	Gas boiler
SEGS IV	Kramer Junction, CA	1987	30	349	230,300	30.6	40 bar, steam	Gas boiler
SEGS II	Daggett, CA	1986	30	316	190,338	29.4	40 bar, steam	Gas boiler
SEGS I	Daggett, CA	1985	13.8	307	82,960	31.5	40 bar, steam	3-hrs TES

$\dot{W}_e$ is the nominal electric power generated, T_{out} is the heat transfer fluid outlet temperature in the solar field, A_{SF} is the solar field aperture area and η_{th} is the thermal efficiency of the power block.

The power block is analysed considering limits in temperature and pressure of the solar field described in Zarza et al. (2006). The sizing of the solar field is consistent with this reference. It has been assumed the same heat–area ratio than that one of the mentioned work. Therefore, the area of the solar field is function of the power generated in the plant, the thermal efficiency of the Rankine cycle and the solar field area and heat rate provided by the collectors in Zarza et al. (2006).

$$\frac{\dot{Q}_a^*}{A_{SF}^*} = \frac{\dot{Q}_a}{A_{SF}} \Rightarrow A_{SF} = \frac{\dot{Q}_a}{\dot{Q}_a^*} A_{SF}^* = \frac{\dot{W}_e/\eta_{th}}{\dot{W}_{e,n}^* HR_n^*} A_{SF}^* \quad \text{(Eq. 2.1)}$$

where $\dot{Q}_a$ is the heat rate added by the solar field, A_{SF} is the solar field area, $\dot{W}_e$ is the electric power produced in the generator, η_{th} is the thermal efficiency of the cycle, HR is the heat rate of the cycle, the subscript n represents the net value and the superscript * is related to that variable in Zarza et al. (2006).

The thermal and economic analysis have been carried out using Engineering Equation Solver (EES) (Klein, 2013) as the main software environment for the calculations. This software is intended for solving non-linear equation systems simultaneously by the Newton-Raphson method. Moreover, it contains libraries to obtain the thermophysical properties of the pure water/steam, using the "IAPWS Formulation 1995 for the Thermodynamic Properties of Ordinary Water Substance for General and Scientific Use" (Wagner and Pruß, 2002), and seawater, using the formulation by Sharqawy et al. (2010).

Table 2.2 shows the main parameters used in the design of the solar field and power block, which has been carried out at solar noon on 21st June. The solar field comprises 70 parabolic trough collectors, which generate steam at 400 °C and 60 bar for the turbines of the power block. The condensation of the cycle by means of evaporative cooling occurs at 30 °C with a temperature increase of 10 °C. Pressure loses in the solar field and main valves at the inlet of the high pressure turbine are considered to be of 5%. Besides that, the selected configuration of the power cycle, in which a deaerator and three closed preheaters are included, is shown in Figure 2.1. Each point of the cycle has been thermodynamically characterized and the equations used for solving the model are presented in Appendix 2-A. Performances of main items (turbines, pumps, etc.) are given in Table 2.3. Notice that the solar field efficiency, which varies with the change in the operation conditions of the cycle, has been calculated using the Eq. (2-A.8) in Appendix 2-A.

Table 2.2. Design parameters (Zarza et al., 2006).

Parameter	Value
Solar field	
Parabolic trough collector model	ET-100
Number of parallel rows	7
Number of collectors per row	10
Overall length of a single collector, m	98.5
Parabola width, m	5.76
Net collector aperture per collector, m^2	548.35
Design point: solar noon on 21st June	
Direct solar irradiance, W/m^2	875
Longitude of the location	5°58′ W
Latitude of the location	37°24′ N
Air temperature, °C	20
Incident angle	13.7°
Power block	
Live steam temperature, °C	400
Live steam pressure, bar	60
Condensation temperature, °C	30
Net power, kW_e	5175
Net heat rate, kJ/kWh	14,460

Table 2.3. Performance of individual items in which is based the configuration given in Figure 2.1 (Blanco-Marigorta et al., 2011).

Parameter	η	η_m
High pressure turbine	0.85	0.98
Low pressure turbine	0.85	0.98
Condensate pump	0.8	0.85
Feeding pump	0.8	0.85
Generator	0.97	-
Turbine shaft	-	0.98
Solar field	0.443*	-

*Calculated in the base case

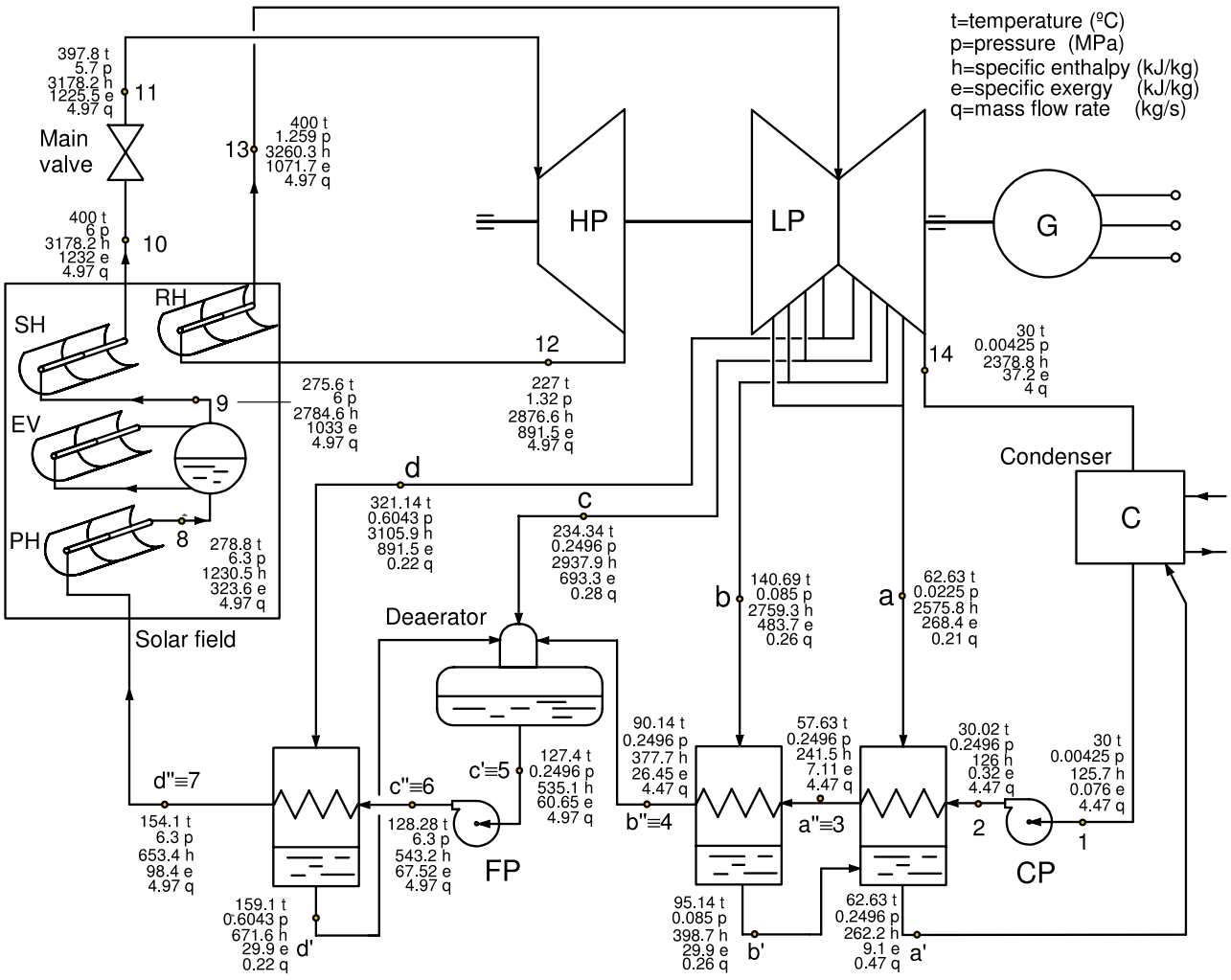

Figure 2.1. Layout of the power cycle and thermodynamic properties of mass flows.
HP=high pressure turbine; LP=low pressure turbine; FP=feeding pump; CP=condensate pump; G=electric generator; PH=preheater; EV=evaporator; SH=super-heater; RH=reheater

The key parameters of the power cycle are summarized in Table 2.4, showing the specific work extracted by the turbines, the specific work consumed by the pumps, the specific heat provided by the solar field and the thermal efficiency of the cycle, among others. In addition, in order to facilitate the comparison and permit the adaptation of results from this section to other configurations, Table 2.5 compares the principal parameters of the selected cycle with a simple Rankine cycle and the cycle with reheating. It is also worth mentioning that the reheating pressure has been optimized in order to achieve the maximum thermal efficiency of the power block.

Table 2.4. Main parameters of configuration given in Figure 2.1.

Parameter	Value
Specific work extracted by the HP turbine (W_{HP}), kJ/kg	301.6
Specific work extracted by the LP turbine (W_{LP}), kJ/kg	789.1
Total specific work extracted (W_T), kJ/kg	1090.7
Specific work consumed by the condensate pump (W_{CP}), kJ/kg	0.28
Specific work consumed by the feeding pump (W_{FP}), kJ/kg	8.07
Total specific work consumed by the pumps (W_P), kJ/kg	8.35
Specific heat provided by the solar field (Q_a), kJ/kg	2908.5
Useful net specific work (W_u), kJ/kg	1059.1
Net electricity power ($\dot{W}_e$), kW	5000
Steam mass flow rate (q_v^{RK}), kg/s	4.97
Heat rate (HR), kJ/kWh	9674
Thermal efficiency (η_{th})	0.37
Global efficiency (η_g)	0.16

Table 2.5. Comparison of selected configuration (regenerative Rankine cycle with reheating) with more simple Rankine cycles with the same maximum and minimum temperature and pressure values.

Parameter	Simple cycle	Reheating cycle	Reheating and regenerative cycle
W_T (kJ/kg)	1015.6	1183.1	1090.7
W_P (kJ/kg)	7.89	7.89	8.35
Q_a (kJ/kg)	3044.6	3428.3	2908.5
η_{th}	0.33	0.34	0.37
η_X	0.59	0.62	0.67
x	0.84	0.93	0.93

η_X is the exergetic efficiency of the cycle and x the vapor quality.

2.2.1.2 Seawater reverse osmosis (SWRO) plant

The use of SWRO desalination process is appropriate to achieve fresh water with enough quality to human consumption in all coastal areas. The complexity of the design could be quite different, depending on feed water quality. The simplest design consists in only a series of seven conventional SWRO membrane elements together with other main components of a desalination plant (physical and chemical pretreatment, pumping of the seawater, post-treatment, etc.) – see Figs. 2.2 and 2.3. Canary Islands are an example of this simple design. Nevertheless, in Middle East a second membrane series (second pass) is required to treat this product obtained from the first membrane series (first pass). Designs adopted in SWRO plants are shown in the literature (Wilf and Awerbuch, 2007).

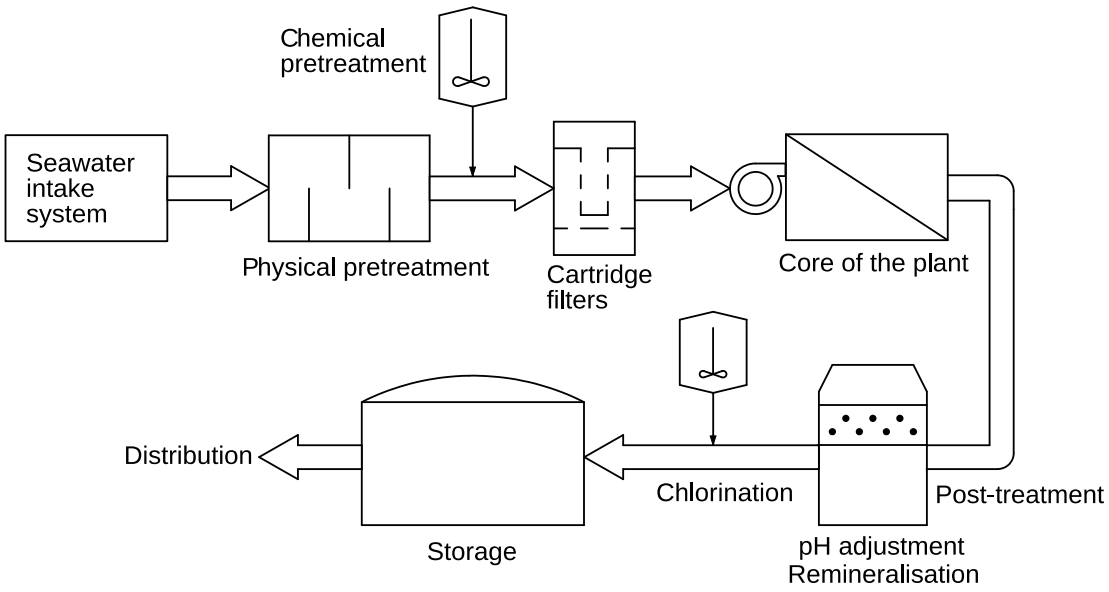

Figure 2.2. Basic scheme of a SWRO plant.

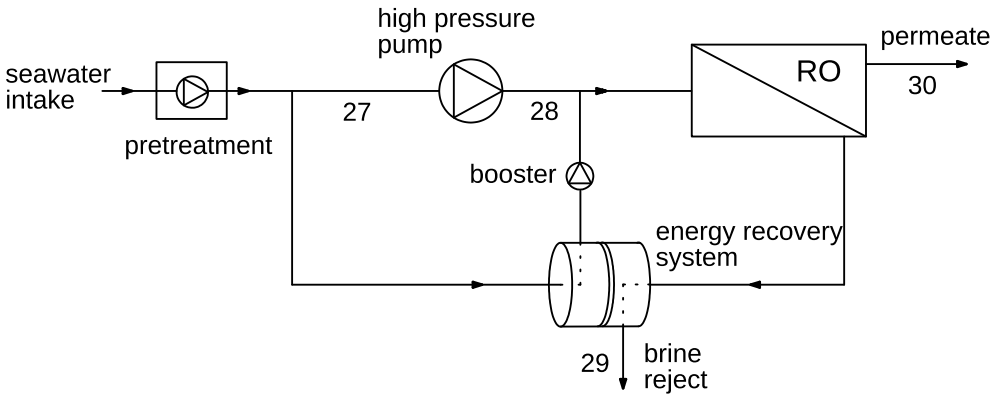

Figure 2.3. Basic layout of the productive core of a SWRO plant.

Higher quality water could be required in the CSP plant for other uses, such as demineralised water required by the steam turbine, or other water requirements necessary to wash the mirror reflective area of the solar field. Salt concentration as low as demineralised water could be obtained with a suitable design of the SWRO plants followed by other process as ionic exchanger, electro-deionization or electro-dialysis.

Considering a plant location similar to Canary Islands (Spain) (Figure 2.3), the thermodynamic properties of the streams and design data are shown in Table 2.6. It is assumed a specific energy consumption of the SWRO plant of 2.99 kWh/ m^3, corresponding to the high pressure pump and booster pump, 2.14 kWh/m^3, plus 0.85 kWh/m^3 of auxiliaries (Peñate and García-Rodríguez, 2012). Moreover, the solar thermal power plant water consumption for the cooling of the power block, cleaning of mirrors, purges and other uses is assumed to be 30 m^3/h (Palenzuela et al., 2015b).

Table 2.6. Thermodynamic properties of the streams and design data for SWRO plant (Peñate and García-Rodríguez, 2012).

Thermodynamic properties[*]

Stream	T (ºC)	p (bar)	b (mol/kg)	h (kJ/kg)	s (kJ/kg-K)	ex (kJ/kg)
Process feed (27)	20	1	0.632	-2,189E-03	-1.602E-05	2.507E-03
Membranes feed (28)	20	52.75	0.632	4.667	-1.288E-03	5.044
Rejected brine (29)	21	50.78	1.078	10.952	0.029	2.393
Permeate (30)	20	1.7	4.436E-03	-2.807	-0.033	6.733

Design data

Feed seawater salinity (TDS), mg/l	38,170
Conversion factor (f)	0.40
High pressure pump efficiency (η_{HP}^{RO})	0.74
Booster pump efficiency (η_{b}^{RO})	0.77
Hours of daily operation (η_h), h	5.726
Number of years of useful life (N)	20
Specific energy consumption of the main pumps (W_{main}^{RO}), kWh/m^3	2.14
Specific energy consumption of the auxiliaries (W_{aux}^{RO}), kWh/m^3	0.85

[*]Reference state: T_{amb}=293.15 K; b_{amb}=0.632 mol/kg; p_{amb}= 1 bar

In order to carry out the general study of the fresh water production coupled to the power production (RO1 case, with the desalination plant using electricity from the CSP plant), the steam flow through the turbines remains constant while different fresh water demands are considered. Other constant parameters are the following: thermal efficiency of the power block and solar field, global efficiency of the entire system and electric power consumed by the pumps in the power block. Table 2.7 gives a summary of results: first and last columns show the fresh water production expressed in different units – m^3/h and m^3/d under the assumption of 6 h/d of CSP plant operation; the fifth column provides the net electricity production sent to the grid after subtracting the power consumption for pumping in the Rankine cycle (41.3 kW) and the RO unit (as the sum of the main process plus the intake and pretreatment). It has also been represented the exergetic power of the different streams along with the mass flow rate of the feeding to the main pump and the rejected brine. This study should be adapted for other locations to the specific feed quality by designing the SWRO and calculate the specific energy consumption. In addition, demineralised water flow, if any, would require the adequate selection of the SWRO product treatment. The two last values of the fresh water demand have been considered for comparison purposes with the case of the MED integration and it will be explained in the next section.

Table 2.7. Exergetic power and mass flow rates corresponding to different SWRO plant productions in the RO1 case.

q_{30}^{RO} (m^3/h)	$\dot{W}_{main}^{RO}$ (kW)	$\dot{W}_{aux}^{RO}$ (kW)	$\dot{W}_{T}^{RO}$ (kW)	$\dot{W}_{grid}^{RO}$ (kW)	$\dot{E}_{27}^{RO}$ (kW)	$\dot{E}_{28}^{RO}$ (kW)	$\dot{E}_{29}^{RO}$ (kW)	$\dot{E}_{30}^{RO}$ (kW)	q_{27}^{RO} (m^3/h)	q_{29}^{RO} (m^3/h)	$q_{w,6h}$ (m^3/d)
15	32.1	12.8	44.9	4913.8	0.026	52.34	14.9	-56.02	37.4	22.5	90
50	107	42.5	149.5	4809.2	0.087	174.5	49.7	-28.07	124.7	75.1	300
85	181.9	72.3	254.2	4704.5	0.147	296.6	84.4	37.14	212.0	127.6	510
120	256.8	102	358.8	4599.9	0.208	418.7	119.2	102.3	299.3	180.1	720
150	321	127.5	448.5	4510.2	0.260	523.4	149	167.6	374.2	225.2	900
158.6	339.4	134.8	474.2	4484.5	0.275	553.4	157.5	223.5	395.6	238.1	951.6
186.4	398.9	158.4	557.3	4401.3	0.323	650.4	185.2	239.5	465.0	279.8	1118

27=pretreated seawater; 28=feed seawater to RO process; 29=rejected brine; 30=permeate

As a comparative study, let us consider that the SWRO plant is not integrated in the CSP plant (RO2 case). Therefore, the SWRO operate continuously and consumes electricity from the grid. In this case, the CSP production is not affected by the fresh water demand. Table 2.8 shows the SWRO process consumption for different nominal capacities installed.

Table 2.8. Power and mass flow rates corresponding to different SWRO plant productions in the RO2 case.

q_{30}^{RO} (m^3/h)	$\dot{W}_T^{RO}$ (kW)	$\dot{W}_{grid}^{RO}$ (kW)	$q_{w,24h}^{*}$ (m^3/d)
15	44.9	4958.7	360
50	149.5	4958.7	1200
85	254.2	4958.7	2040
120	358.8	4958.7	2880
150	448.5	4958.7	3600
158.6	474.2	4958.7	4080
186.4	557.3	4958.7	4474

* Operating 24 h/d

2.2.2 Integration of a MED plant into the power production

Two different configurations are analysed in this section, referred to as MED1 and MED2 respectively:

- **MED1**. The MED plant substitutes the condenser of the CSP plant in this option (see Figure 2.4). This is only an operational replacement, since the end condenser should be implemented in order to permit maintenance in the desalination plant. Once selected the best configuration of the power cycle, the fresh water production is estimated and is considered as a fixed parameter (186.4 m^3/h). The condensation temperature is raised up to 70 °C, which is the temperature of the vapour feeding the first effect of the MED. Because of that, the first extraction of the power block at 63 °C in the base case (Figure 2.1) is eliminated.

- **MED2**. A more general case in which the MED plant consumes steam from an intermediate turbine extraction at 63 °C is studied. Power cycle efficiency and other parameters are calculated depending on the fresh water production. Figure 2.5 shows the plant layout. The effect of different plant capacities on operational parameters of the power cycle is calculated. Results are summarized as follows: Figure 2.6 depicts the effect of the fresh water demand (q_{33}) on the steam mass flow in the condenser of the power cycle (q_{28}), the thermal power consumption of the MED plant ($\dot{Q}_{MED}$), and the condensing thermal power ($\dot{Q}_{COND}$), considered an energy consumption of 230 kJ/kg (Al-Karaghouli and Kazmerski, 2013) and a conversion factor of 45%. Notice how in this case the maximum fresh water production is limited to 158.6 m^3/h, which corresponds to a null

value of the condensing thermal power in the PB. The effect of water production on thermal performance of the power cycle and other parameters are shown in Figure 2.7, and finally, mass fraction of successive steam extractions is presented in Figure 2.8. Calculation procedure is reported in Appendix 2-A.

Table 2.9 shows a comparison of the MED1 and MED2 arrangements on the main operation variables along with the base case, where no water is produced.

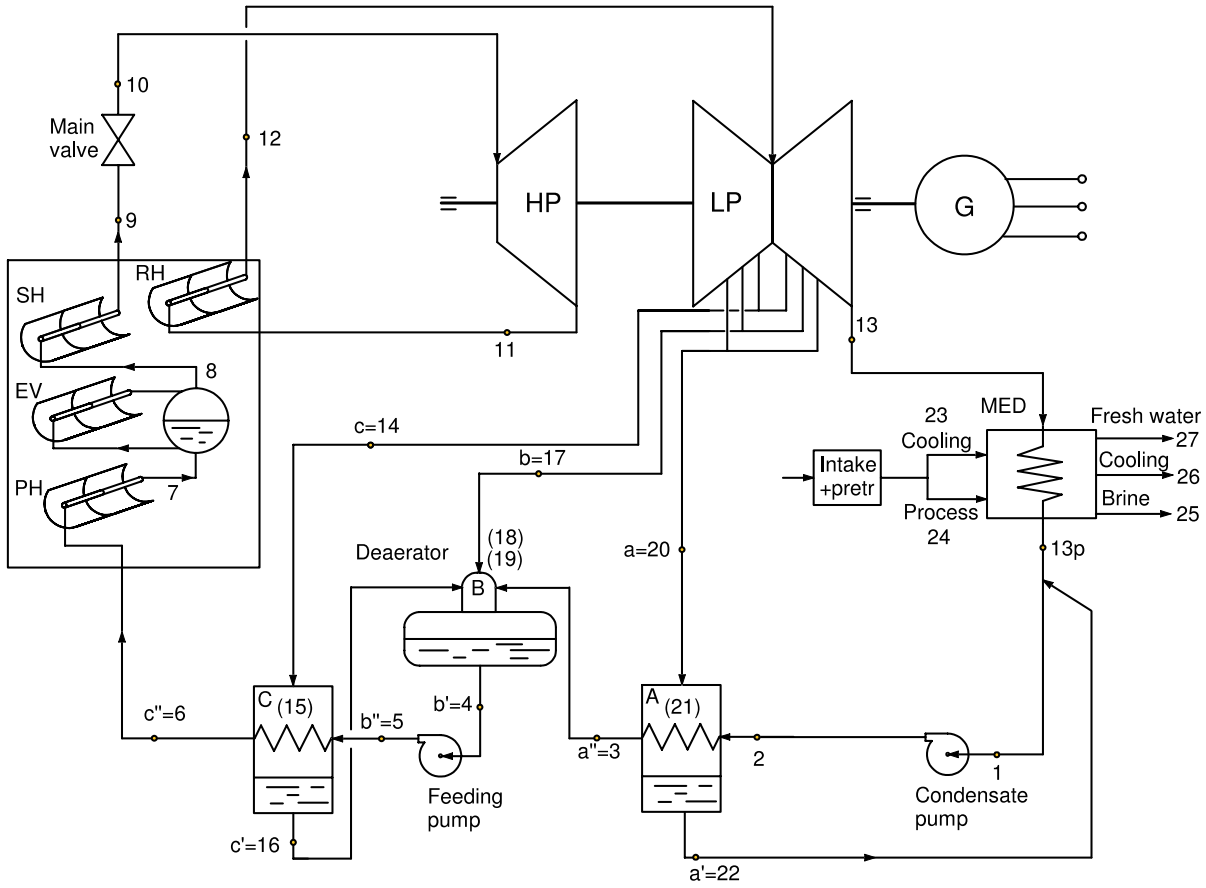

Figure 2.4. Layout of the MED1 configuration: a MED plant replacing the CSP plant cooling system (only functionally).

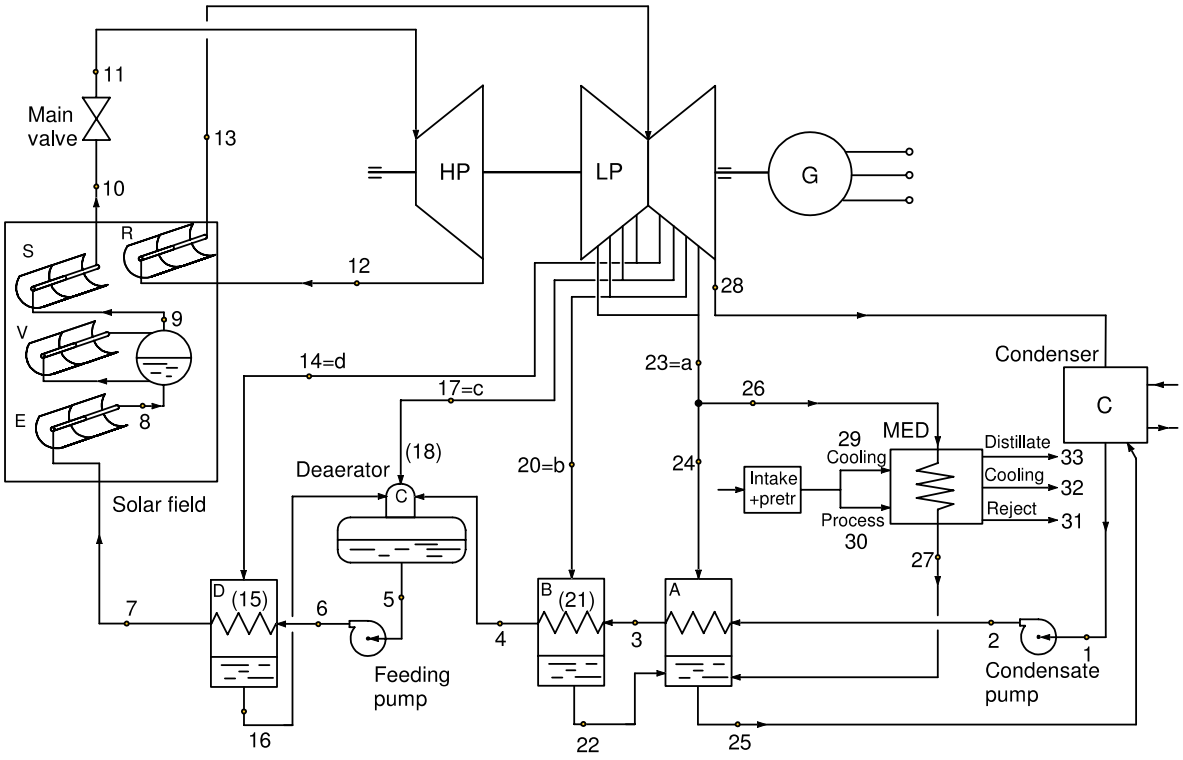

Figure 2.5. Basic layout of the MED2 configuration: a MED plant integrated within the CSP plant fed by an extraction.

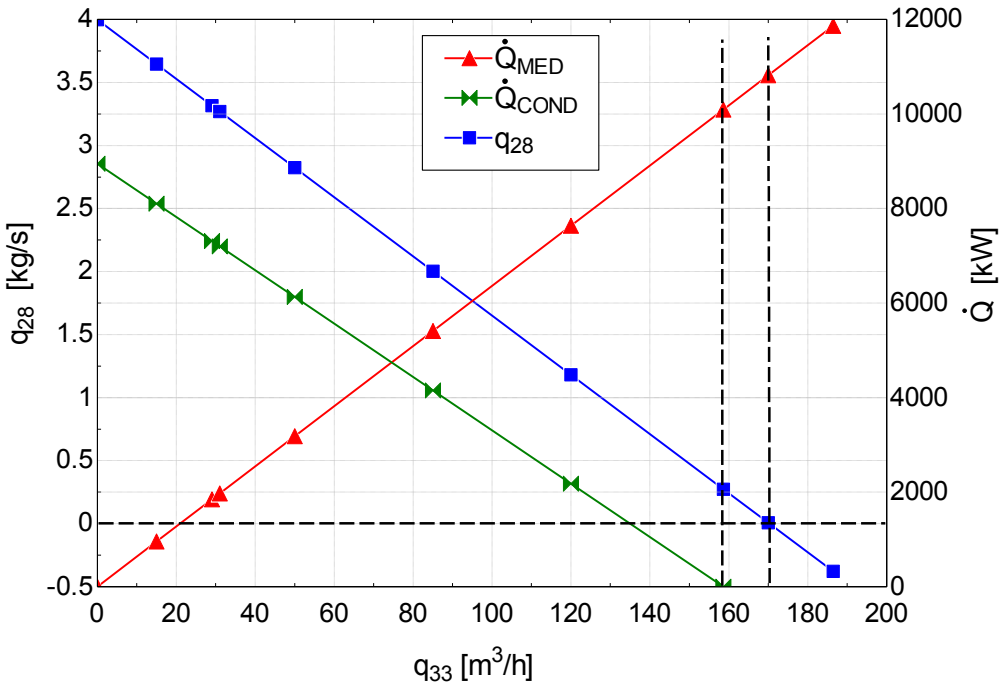

Figure 2.6. Analysis of the condensing thermal power of the Rankine cycle ($\dot{Q}_{cond}$), thermal power consumption in the MED ($\dot{Q}_{MED}$) and mass flow rate of exhaust steam (q_{28}) as function of the fresh water production (q_{33}) for MED2 configuration.

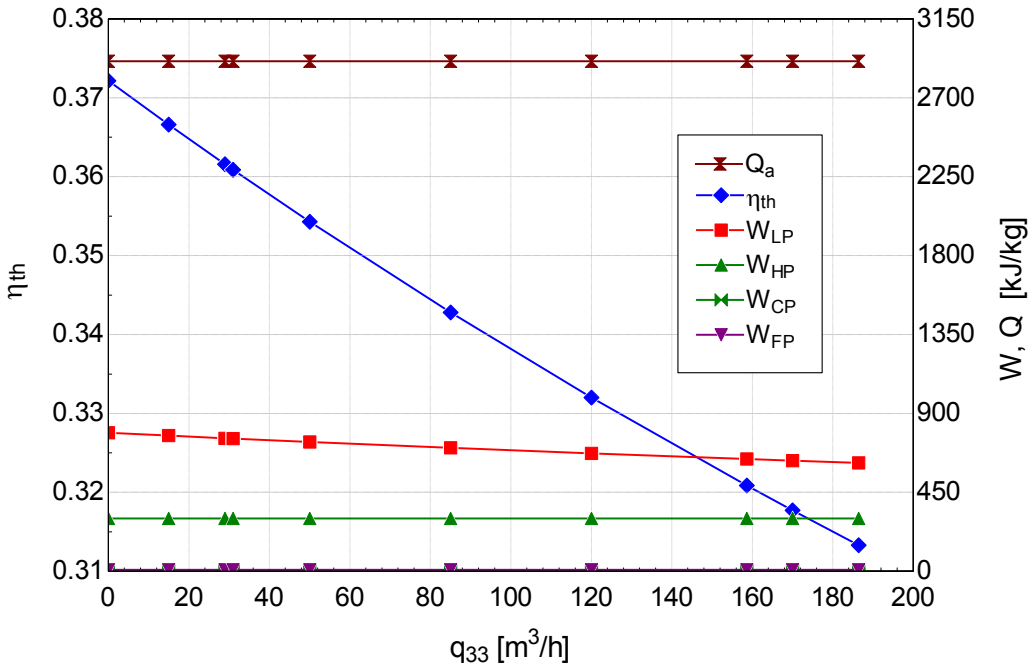

Figure 2.7. Effect of the fresh water production (q_{33}) on the thermal performance of the power cycle (η_{th}), specific thermal energy added by the solar field (Q_a), specific work extracted in the low and high pressure turbines, (W_{LP} and W_{HP}, respectively) and specific work consumed by the condensing and feeding pumps (W_{CP} and W_{FP}, respectively) for MED2 configuration.

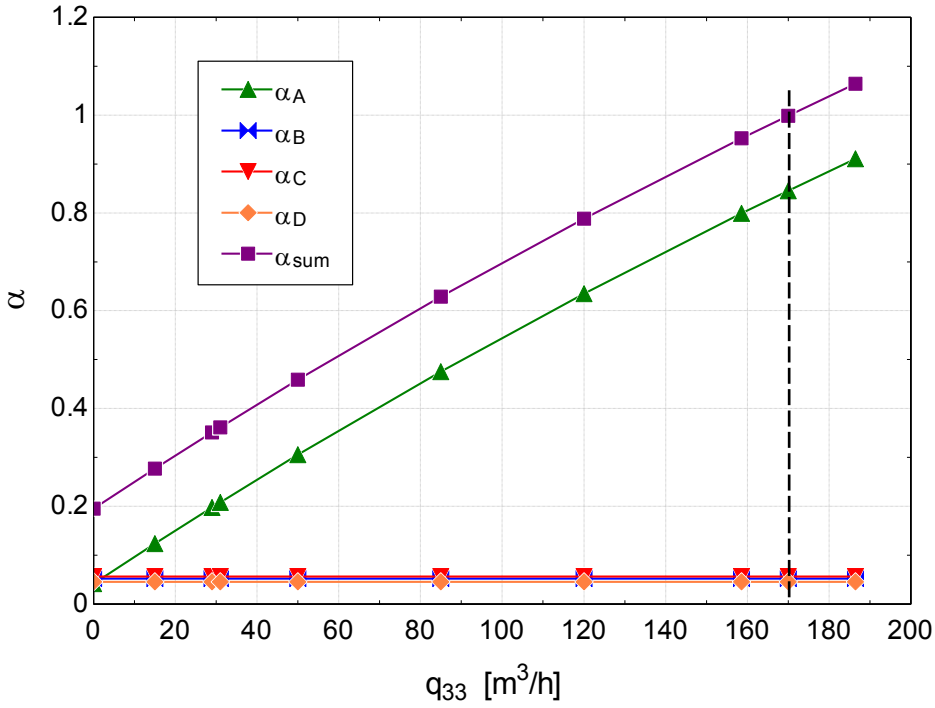

Figure 2.8. Analysis of the extractions from the low pressure steam turbine ($\alpha_A, \alpha_B, \alpha_C, \alpha_D$ and total α_{sum}) for different fresh water productions (q_{33}) in MED2 configuration.

Table 2.9. Main operational parameters in MED1 and MED2 configurations respect to the base case.

Parameter	Unit	Base case	MED1	MED2
q_w	m^3/h	-	186.4	158.6
T_c	ºC	30	70	30
W_T	kJ/kg	1090.7	908.2	941.6
W_P	kJ/kg	8.35	8.35	8.35
Q_a	kJ/kg	2908.5	2891.1	2908.5
η_{th}	-	0.372	0.311	0.321
η_X	-	0.668	0.566	0.576
A_{SF}	m^2	248,110	296,640	287,750
x	-	0.927	0.99	0.927
$\dot{Q}_{MED}$	kW	0	11,865	10,094

2.2.3 Comparative analysis of efficiency and production

Table 2.10 summarizes the four cases considered for water and electricity production based on different configurations. In the MED1 arrangement the distillate produced cannot be regulated because it depends on the power block condensation. The quantity of water obtained is then fixed by the exhaust steam coming from the low pressure turbine. Besides, the daily fresh water production is limited to an average of 5.73 hours in the MED1, MED2 and RO1 cases due to the dependence on the solar resource, while the RO2 case may produce 24 hours per day, which is a major advantage. Notice how, in the RO1 configuration, the fresh water production can be chosen based on the quantity of electric energy consumed from the generator. As an example, there has been taken two values, corresponding to the fixed production in the MED1 case and the maximum production (when all the electric power generated has been consumed), respectively.

Table 2.10. Summary of results related to the four configurations analysed.

Parameter	Unit	MED1	MED2	RO1		RO2
Product flow regulation		No	Yes	Yes		Yes
Average daily operation	h/d	5.73	5.73	5.73		24
Fresh water production	m^3/h	186.4	158.6	186.4	1,658	186.4
Plant capacity	m^3/d	1067.3	908.8	1067.3	9500.3	4473.6
Net electric power	kW	4577.5	4635	4401.3	0	4958.7
Thermal power consumption	kW	11,865	10,094	0	0	0
Electric power consumption	kW	372.8	317.2	557.3	4958.7	557.3
Pump power of the cycle	kW	49.7	47.9	41.3	41.3	41.3
Specific consumption of auxiliaries	kWh/m^3	2♠	2	0.85♣	0.85	0.85
Specific consumption of the process						
Thermal energy	kWh/m^3	63.6	62.7	-	-	-
Electric energy	kWh/m^3	-	-	2.14♣	2.14	2.14

♠ Palenzuela et al. (2015b)

♣ Peñate and García-Rodríguez (2012)

2.2.4 Cost analysis

2.2.4.1 Thermoeconomic analysis

Thermoeconomy combines the exergetic analysis alongside the economic principles to provide the designer of thermal systems information not available by means of classic thermal and economic analysis (Bejan et al., 1996). This helps them to identify possible improvements to the system and production costs. The exergetic balance gives the inefficiency associated to each element of the system considered: exergy destructions, which are internal and inherent to the component due to irreversibilities, and exergy losses, which are related to material and energy streams exiting the system without any further technical utilization. In systems with two products, like in this case, electricity and water, it is of great interest to know the cost of production for each asset and the services used to generate them so that these costs can be properly charged.

2.2.4.2 Assumptions

The well-known thermoeconomic analysis (Bejan et al., 1996) is applied to compare the four configurations described in sections 2-3. Main hypothesis applied are the following:

- Steady-state operation.
- The useful life of the CSP and desalination plants is 20 years.
- Input data are referred to their values in the base year and updated for the following years according to the annual inflation rate r_i (which is assumed constant and equal to 2%) and the nominal discount rate or nominal cost of capital k_n, established to 6% (real discount rates for technology comparison analysis are in the 5-10 percent range (International Energy Agency, 1991)).
- The economic analysis is performed in current value because it includes the effect of inflation in the general interest definition.
- The total capital investment is done by means of a bank loan at a given interest.
- The depreciation and production taxes are not considered.
- All the costs are levelized, i.e., converted to a series of different money quantities paid or collected to a constant annuity affected by the effective annual discount rate and the nominal escalation rate.

2.2.4.3 Exergy costing

The exergy costing study allows quantifying the energy quality of the different flows considered entering and exiting the system, as well as the degree of inefficiency of the process or component. In this method, a unitary cost is associated to every exergetic power stream. The thermoeconomic analysis is done by means of the economic balance:

$$\sum_{\forall e} \dot{C}_e = \sum_{\forall i} \dot{C}_i + \dot{Z} \qquad \text{(Eq. 2.2)}$$

where $\dot{C}_e$ and $\dot{C}_i$ are the cost rate associated with outlet and inlet streams respectively, both energetic and matter, in €/h, while $\dot{Z}$ is the cost rate of the capital investment and the operation and maintenance of each component, in €/h, also referred to as *carrying charges*.

The cost rate is defined by:

$$\dot{C}_J = c_j \dot{E}_J \quad \text{(Eq. 2.3)}$$

being c_j the exergetic unit cost, in €/kWh, and $\dot{E}_J$ is the exergetic power of the stream j, in kW. Assuming known the exergetic unit cost of all inlet flows, the exergetic power of the matter and energy streams, the cost rates associated with the capital investment and O&M, $n_e - 1$ additional equations are needed to close the problem involving the levelized costs per unit of exergy c_i, where n_e is the the number of outlet streams.

The investment and operation costs of a system or component are written as follows:

$$\dot{Z} = \dot{Z}^{CI} + \dot{Z}^{OM} \quad \text{(Eq. 2.4)}$$

where $\dot{Z}^{CI}$ is the cost rate associated with capital investment and $\dot{Z}^{OM}$ the cost rate related to the operation and maintenance, in €/h. It accounts for the expenditures associated with the purchase and operation and maintenance of the component. It is calculated as the levelized cost divided per the number of hours of annual operation.

2.2.4.4 Economic balances

It is useful to make a diagram numbering all the matter and energy streams in the system. In this way the data is ordered and the streams can be defined as fuels or products. *Fuel* (F) is the resource used to generate the desired utility, whether it is one or several simple or compound streams, of matter or energy. *Product* (P) is defined as the flow or flows of interest, which can be simple or compound as well, of matter or energy. It is the purpose for which the component or system is planned and designed. The definition of fuel and product for every component of the system in study is presented in Table 2.11.

The following considerations have been taken into account when performing the cost assignments to the streams of exergy:

- It is assumed that the unitary exergy costs of inlet streams are known.
- The direct normal irradiance and the seawater intake have null costs due to they are a free source of energy and matter, respectively.
- The unitary exergy costs related to the waste streams are assumed to be zero as its dispersion cost to the environment is considered to be null.

- The cost per unit of exergy related with the electricity production does not vary both in condensing and cogeneration mode due to the penalty caused by the water production is charged to the solar field, which will have to be bigger enough in order to maintain the 5 MW_e of electric power in the generator.
- The electricity for pumping is taken from the self-production in the MED1, MED2 and RO1 cases, thus the unitary exergy cost associated is the same that the one from the electricity generated. In the fourth case, RO2, with the desalination plant connected to the grid, the electricity is purchased according to the high-voltage power access tariffs established by the liberalized energy market.

The exergy rates of the pumping, extracted steam, condensate water and electricity were determined in Section 3. The exergy rate associated with the direct normal irradiance is obtained using the following equation:

$$\dot{E}_{rad}(Q_{sun}) = \dot{Q}_{sun}\left(1 - \frac{T_{amb}}{T_{ap,sun}}\right) \quad \text{(Eq. 2.5)}$$

being $\dot{Q}_{sun}$ the heat rate of the direct normal irradiance in the solar field, in kW, T_{amb} the temperature of the environment, in K, and $T_{ap,sun}$ the apparent temperature of the Sun, taken as 5770 K. The term $\dot{Q}_{sun}$ is determined with:

$$\dot{Q}_{sun} = S_c \cdot N_c \cdot I_d \cdot cos(\theta) \quad \text{(Eq. 2.6)}$$

where S_c is the collector aperture area, in m^2, N_c is the number of collectors, I_d the direct normal irradiance at the design day (June 21st at solar noon) and θ the incidence angle of the solar rays.

The cost rate of capital investment and O&M are determined using the methodology described in Appendix 2-B. The levelised cost of energy, LC, for both electricity and water, is defined by the International Energy Agency (1991) as:

$$LC = \frac{P_I + L_e + M + R - E_2 V_{e2}}{E_1 \sum_{t=1}^{n} \frac{1}{(1+k_n)^t}} \quad \text{(Eq. 2.7)}$$

where P_I is the discounted investment cost, L_e the discounted sum of input energy expenses, M is the discounted sum of operating expenses, R is the discounted sum of replacement costs, E_1

is the annual energy or output produced and E_2V_{e2} is the discounted sum of other revenues. This factor is equal to the unitary exergy costs of the electricity and freshwater streams in the thermoeconomic diagram. Figs. 2.9 and 2.10 along with Table 2.11 present the diagrams of main components and input parameters.

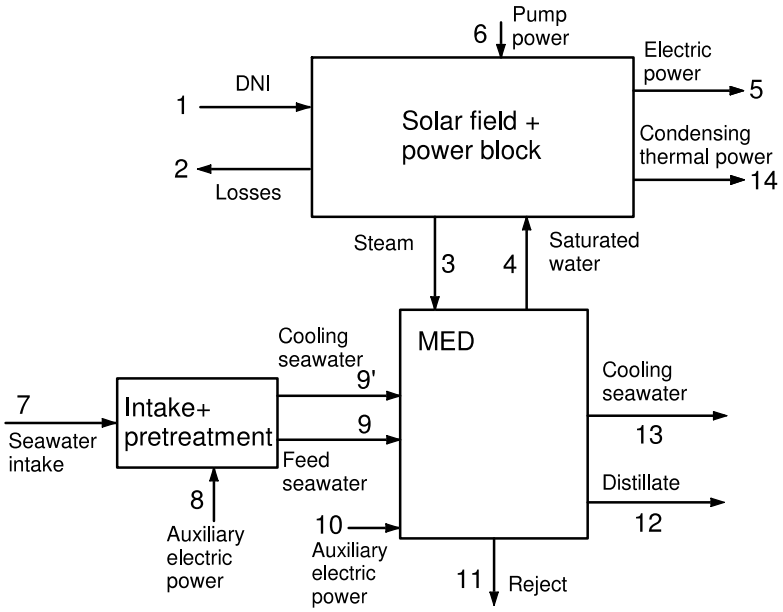

Figure 2.9. Block diagram of the material, thermal and mechanical interactions between the different subsystems in the MED1 and MED2 cases.

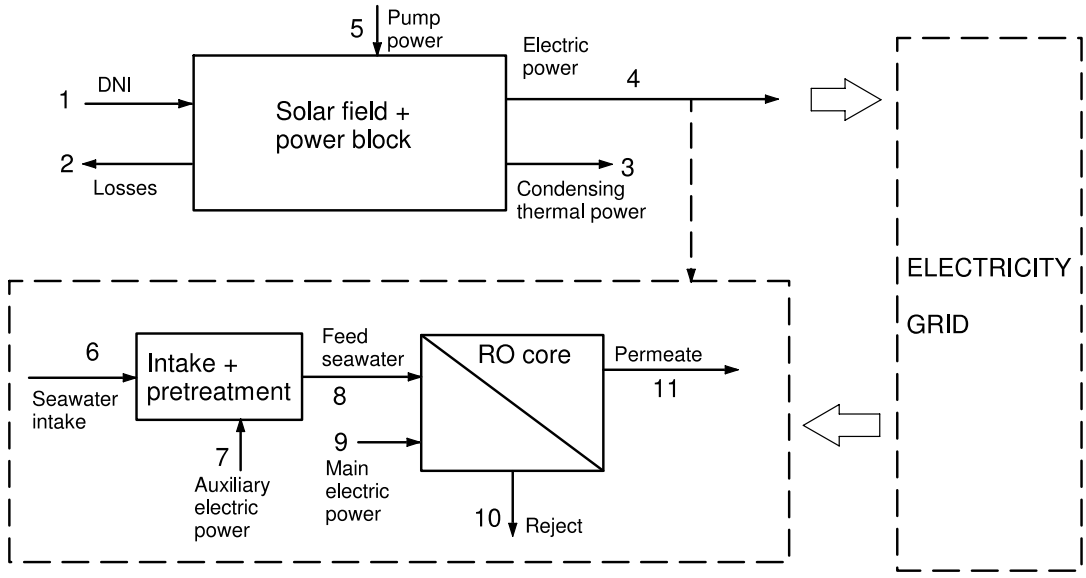

Figure 2.10. Block diagram of the material, thermal and mechanical interactions between the different subsystems in the RO1 and RO2 cases.

Table 2.11. Economic balances.

STPP=Solar Thermal Power Plant; I=Intake; P=pretreatment; A.e.=Auxiliary equations

	Subsystem	Fuel	Product	Economic balance	A. e.
MED1	STPP	(1-2)+6	5+(3-4)	$c_2\dot{E}_2 + c_3\dot{E}_3 + c_5\dot{E}_5 = c_1\dot{E}_1 + c_4\dot{E}_4 + c_6\dot{E}_6 + \dot{Z}_{PP}$	$c_3 = c_4$ $c_2 = 0$
	I+P	8	(9+9')-7	$c_9\dot{E}_9 + c_{9'}\dot{E}_{9'} = c_7\dot{E}_7 + c_8\dot{E}_8 + \dot{Z}_{PRE}$	$c_9 = c_{9'}$
	MED	(3-4)+10 +(9'-13) +(9-11)	12	$c_{11}\dot{E}_{11} + c_{12}\dot{E}_{12} + c_{13}\dot{E}_{13} + c_4\dot{E}_4 = c_3\dot{E}_3 + c_9\dot{E}_9 + c_{9'}\dot{E}_{9'} + c_{10}\dot{E}_{10} + \dot{Z}_{MED}$	$c_{13} = 0$ $c_{11} = 0$
MED2	STPP	(1-2)+6-14	5+(3-4)	$c_2\dot{E}_2 + c_3\dot{E}_3 + c_5\dot{E}_5 + c_{14}\dot{E}_{14} = c_1\dot{E}_1 + c_4\dot{E}_4 + c_6\dot{E}_6 + \dot{Z}_{PP}$	$c_3 = c_4$ $c_2 = c_{14} = 0$
	I+P	8	(9+9')-7	$c_9\dot{E}_9 + c_{9'}\dot{E}_{9'} = c_7\dot{E}_7 + c_8\dot{E}_8 + \dot{Z}_{PRE}$	$c_9 = c_{9'}$
	MED	(3-4)+10 +(9'-13) +(9-11)	12	$c_{11}\dot{E}_{11} + c_{12}\dot{E}_{12} + c_{13}\dot{E}_{13} + c_4\dot{E}_4 = c_3\dot{E}_3 + c_9\dot{E}_9 + c_{9'}\dot{E}_{9'} + c_{10}\dot{E}_{10} + \dot{Z}_{MED}$	$c_{11} = 0$ $c_{13} = 0$
RO1 & RO2	STPP	(1-2)-3+5	4	$c_2\dot{E}_2 + c_3\dot{E}_3 + c_4\dot{E}_4 = c_1\dot{E}_1 + c_5\dot{E}_5 + \dot{Z}_{PP}$	$c_2 = 0$ $c_3 = 0$
	I+P	7	8-6	$c_8\dot{E}_8 = c_6\dot{E}_6 + c_7\dot{E}_7 + \dot{Z}_{PRE}$	-
	RO	9-10	11-8	$c_{10}\dot{E}_{10} + c_{11}\dot{E}_{11} = c_8\dot{E}_8 + c_9\dot{E}_9 + \dot{Z}_{RO}$	$c_{10} = 0$

2.2.5 Comparative results

The levelised electricity and water costs for the four cases considered, MED1, MED2, RO1 and RO2 are depicted in Figure 2.11. It is observed that the lowest water cost (0.76 €/kWh) is achieved in the RO2 arrangement, where the desalination plant is connected to the grid operating 24 hours per day. The main reason is because of the larger value corresponding to the net electricity produced in the power block, compared with the other cases analysed, as the only internal electricity consumption is due to the pumping in the cycle. Besides that, the total cost (capital investment and O&M) is lower in the RO case.

The LWC obtained in the multi-effect distillation cases is higher than those achieved with the reverse osmosis technology, both directly coupled (RO1) and with the indirect integration (RO2, connected to the grid). The values obtained are 1.239 and 1.265 €/kWh for the MED1 and MED2 configurations, respectively. The LEC is constant and equal to 0.1308 €/kWh as it has been assumed that this cost, calculated in the only-electricity mode, does not change when operating in cogeneration mode.

Comparing the two cases proposed in the distillation technology, there are no significant differences in the water production cost when choosing to substitute the condenser of the cycle by the MED plant or to feed the MED in parallel to the first feedwater heater at 63 °C. A more detailed description of the different terms used to calculate the LEC and LWC is showed in Appendix 2-B. Similar values are obtained using conventional power generation plants (Al-Hengari et al., 2014; Mahbub et al., 2012) and solar thermal power plants (Palenzuela et al., 2013). Additionally, it has been analysed the case of a feed-in tariff on the electricity production, with a constant value of 28.5 c€/kWh during the project lifetime. Results indicate that if grants are offered for this kind of plants, there are no costs associated with the water production.

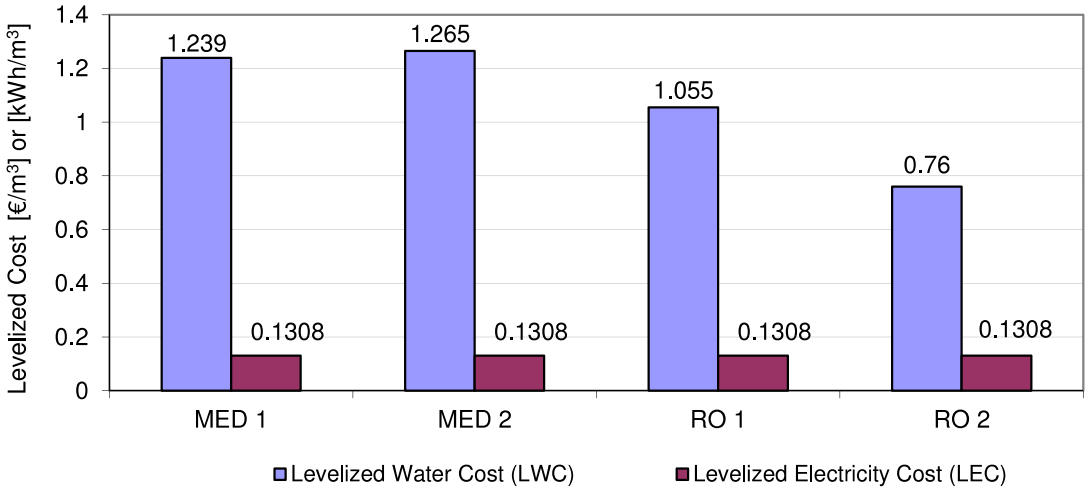

Figure 2.11. Levelised electricity and water costs in the four cases considered.

Actual prices of water in Almería for industrial use are 0.463 €/m^3 for a consumption lower than 50 m^3 and 1.163 €/m^3 for more than 50 m^3 ("Aqualia - Almería," 2014). The average electricity prices for industrial use, according to the annual statistics report of the year 2012 from the Spain's Ministry of Industry, Energy and Tourism, are 0.13 and 0.097 €/kWh for high tension tariffs 3.1A (<450 kW) and 6.1 (>450 kW), respectively (MINECO, 2014). Comparing with the LWC and LEC obtained, slight difference is found between production and purchasing costs.

It is interesting to study the influence of the water flow rate in the LWC, for the three cases where the flow can be regulated (MED2, RO1 and RO2). For comparison purposes, 186.4 m^3/h was established in all cases except in the MED2 configuration due to the top limit was 158.6 m^3/h (all the steam condensed in the feedwater heaters). Figure 2.12 shows that increasing the water production causes a decrease in the LWC, which is more accused in the MED2 and RO1 cases, tending to a constant value. In the RO2 arrangement that abrupt reduction does not exists because the daily fresh water production covers the self-consumption. For water flow rates below 30 m^3/h do not make sense to analyse the influence in the LWC as it is lower than the water required for the mirrors cleaning, steam purges and other uses. The higher costs observed for low flow rates are due to the larger installation costs charged to a low net fresh water production.

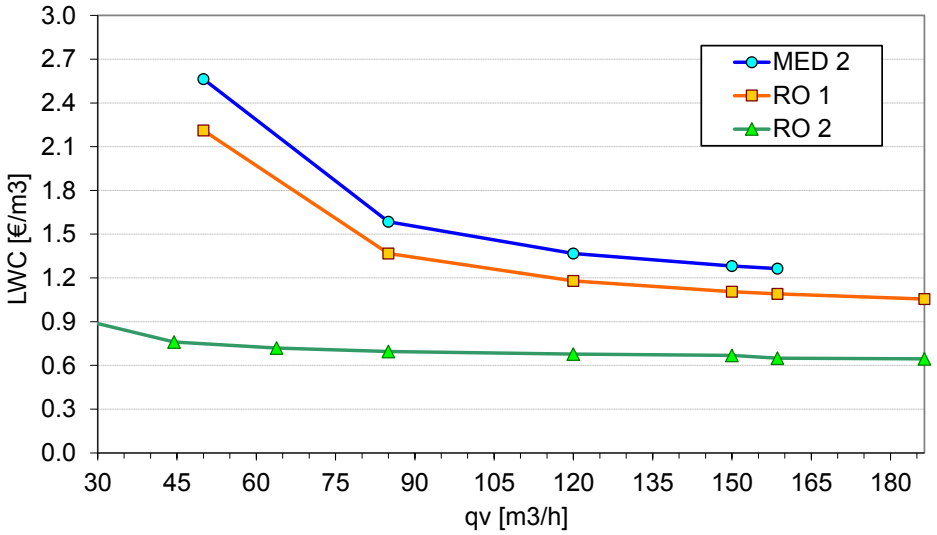

Figure 2.12. Levelized water cost as function of the water flow rate.

The LWC depends on the price of the electricity purchased from the grid in the RO2 case. The value selected, 0.0481 €/kWh, has been calculated according to the basic billing terms and high tension tariffs of the electricity market in Spain, for 44.47 m^3/h of freshwater production.

The LEC and LWC depend on the economic parameter estimations and assumptions made. In order to analyse the influence of the different key variables, several studies have been carried out, varying the solar field, MED and RO specific costs, the nominal discount rate and the annual capacity factor and maintaining constant the rest of variables. Results are showed in Figure 2.13, where the most significant change in the LWC value is due to the variation of the capacity factor and the discount rate.

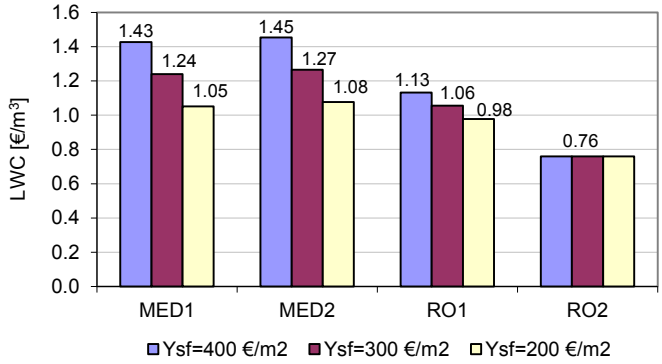
LWC [€/m³]
1.43
1.24
1.05
1.45
1.27
1.08
1.13
1.06
0.98
0.76
MED1
MED2
RO1
RO2
Ysf=400 €/m2
Ysf=300 €/m2
Ysf=200 €/m2

(a)

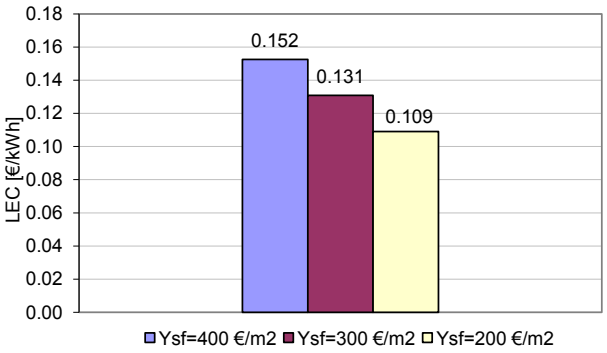
LEC [€/kWh]
0.152
0.131
0.109
Ysf=400 €/m2
Ysf=300 €/m2
Ysf=200 €/m2

(b)

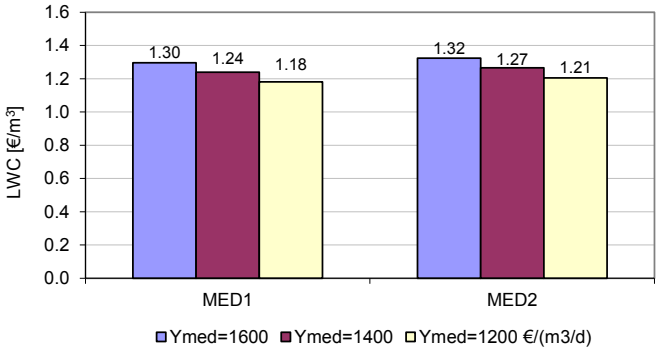
LWC [€/m³]
1.30
1.24
1.18
1.32
1.27
1.21
MED1
MED2
Ymed=1600
Ymed=1400
Ymed=1200 €/(m3/d)

(c)

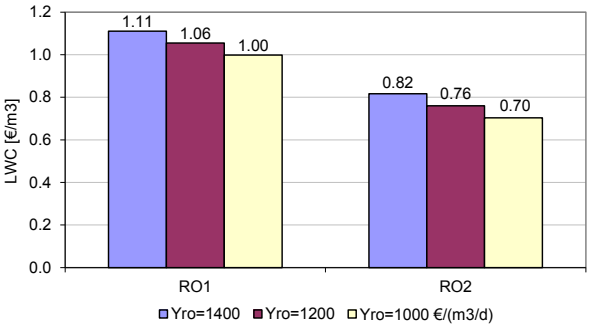
LWC [€/m3]
1.11
1.06
1.00
0.82
0.76
0.70
RO1
RO2
Yro=1400
Yro=1200
Yro=1000 €/(m3/d)

(d)

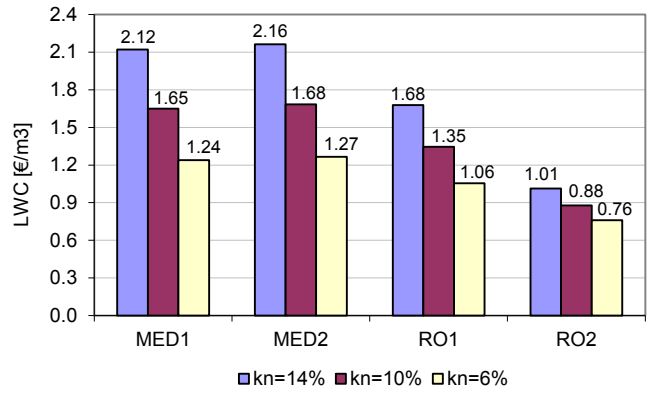
LWC [€/m3]
2.12
1.65
1.24
2.16
1.68
1.27
1.68
1.35
1.06
1.01
0.88
0.76
MED1
MED2
RO1
RO2
kn=14%
kn=10%
kn=6%

(e)

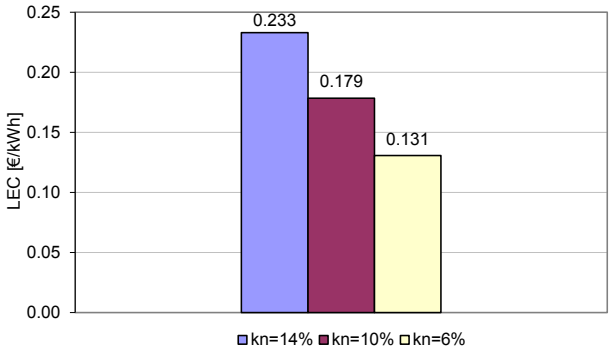
LEC [€/kWh]
0.233
0.179
0.131
kn=14%
kn=10%
kn=6%

(f)

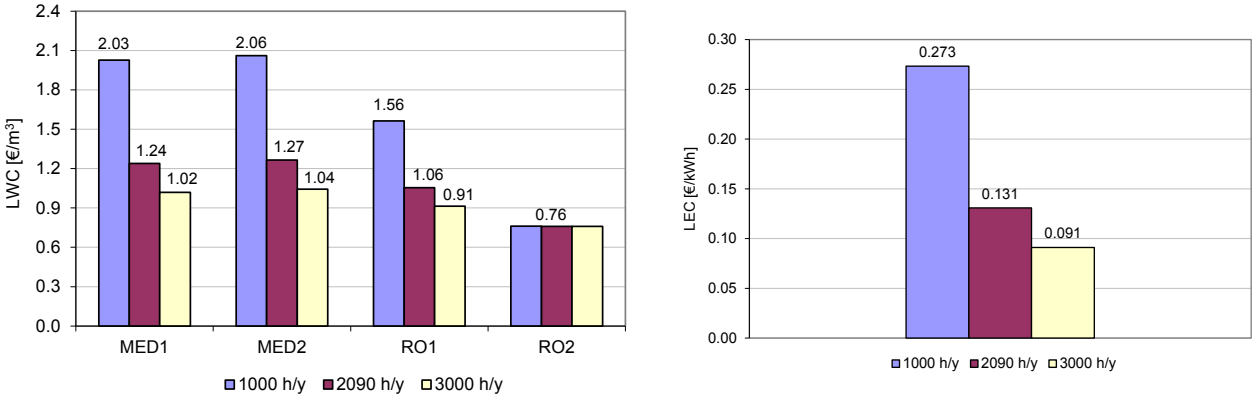

(g) (h)

Figure 2.13. Sensitivity analysis of the LWC and LEC with the specific costs of solar field (a,b), MED (c), RO (d), the discount rate (e,f) and the capacity factor (g,h).

2.2.6 Conclusions of the thermoeconomic analysis

In this section a thermoeconomic comparison between MED and RO desalination technologies has been carried out in order to find the best arrangement of coupling with a simulated 5 MW_e solar thermal power plant based on parabolic trough collectors and direct steam generation, located in Almería. The main conclusions reached by this research are as follows:

- The respective costs of the low pressure steam consumed by the MED unit obtained in case MED1 and MED 2 are 0.041 €/kWh and 0.046 €/kWh (see Table 2-B.2, Appendix 2-B). These results are useful in future comparison of distillation processes driven by solar power plants based on other technologies or driven by other energy sources.
- Results obtained show that the SWRO option produces fresh water at the lower cost, both in the case where the unit is fed by the electricity generated in the power block, as in the case where the RO plant takes the electricity directly from the grid. Between these two options, decoupling the SWRO plant from the power plant is found as the best configuration, reaching the levelised water cost a value of 0.76 €/m^3, against the 1.055 €/m^3 in the RO1 case. The MED1 and MED2 configurations provide 1.239 and 1.265 €/m^3, respectively, being significantly higher that the RO cases.
- The results derived from the economic analysis rely on the choice of the economic factors, as the discount rate, the specific capital cost of the desalination unit or the electricity price purchased from the grid. If there are feed-in tariffs associated with the sale of electricity, the LWC is negative, which means that there are not costs associated

with the water production, as the revenues for the selling electricity are higher than the expenses.

- The capacity factor and the discount rate have great influence on the LEC and LWC. The more hours the CSP is operating during the year, the lower is the cost of production. The discount factor is estimated based on the time value of money and the risk of future cash flows. It depends on the company's financing method, as function of the debt and equity. Large values of this parameter generate a rise in the LEC and LWC, because of the uncertainty of the investment. Furthermore, the increase on the fresh water production causes a reduction on the LWC.
- Summarizing, the best option of coupling between the desalination unit and the CSP plant, taking into account all the assumptions made and for the specified values of the economic parameters, would be to use a reverse osmosis plant which makes use of the electricity generated in the CSP plant. However, the low annual capacity factor penalizes the LWC, thus it is recommended the direct connection of the RO to the grid 24 h per day and sell all produced electricity in the CSP plant with a feed-in tariff.

2.3 Conclusions

After the analysis performed in this chapter regarding the best desalination technology to be coupled with a CSP plant, from both thermal and economic point of views, and taking into account the extensive literature revision conducted, where the most relevant scientific articles published in the last decade has been accounted, it can be concluded that there is no a clear agreement among scientific community about the selection of the desalination technology.

Many factors affect to the suitability of using one technology or another, like the selected location, environmental conditions, the energy source availability, the variable fuel prices, socio-economic issues, political decisions, etc. The diverse analyses carried out give different results, depending on the assumptions and boundary conditions selected for the assessments. Therefore, further investigation on the performance and technical opportunities of CSP plants and desalination processes need to be accomplished.

Acknowledgements

The authors wish to thank the European Commission (DG for Research & Innovation) for its financial assistance within the Integrated Research Programme in the field of Concentrated Solar Power (CSP) (STAGE-STE Project; Grant Agreement No. 609837).

Appendix 2-A

The electric power produced by the power cycle is given by product of the rate of useful work available and the mechanical coupling efficiency of the turbines with the shaft and the electric generator efficiency:

$$\dot{W}_e = \dot{W}_u \cdot \eta_{sh} \cdot \eta_{gen} = W_u \cdot q_v^{RK} \cdot \eta_{sh} \cdot \eta_{gen} = \left(W_{HP} \cdot \eta_{HPm} + W_{LP} \cdot \eta_{LPm} - \frac{W_{CP}}{\eta_{CPm}} - \frac{W_{FP}}{\eta_{FPm}} \right) \cdot q_v^{RK} \cdot \eta_{sh} \cdot \eta_{gen} \quad (2\text{-A.1})$$

where $\dot{W}_u$ is the rate of useful work, in kW, η_{sh} the mechanical efficiency in the shaft, η_{gen} is the electric generator efficiency, W_u is the specific useful work, in kJ/kg, q_v^{RK} is the mass flow rate of steam in the cycle, in kg/s, W_{HP} and W_{LP} are the specific enthalpy extracted in the high pressure and low pressure turbines, respectively, in kJ/kg, η_{HPm} and η_{LPm} are the mechanical efficiency of the high pressure and low pressure turbines, respectively, W_{CP} and W_{FP} are the specific enthalpy consumed by the condensate and feeding pumps, respectively, in kJ/kg, and finally η_{CPm} and η_{FPm} are the mechanical efficiency of the condensate and feeding pumps.

The thermal efficiency of the power block cycle, η_{th}, is calculated using the following expression:

$$\eta_{th} = \frac{W_T - W_P}{Q_a} = \frac{W_{HP} + W_{LP} - W_{CP} - W_{FP}}{Q_a} \quad (2\text{-A.2})$$

$$W_{HP} = h_{11} - h_{12} \quad (2\text{-A.3})$$

$$W_{LP} = h_{13} - [\alpha_D h_D + \alpha_C h_C + \alpha_B h_B + \alpha_A h_A + (1 - \alpha_D h_D + \alpha_C h_C + \alpha_B h_B + \alpha_A h_A) h_{28}] \quad (2\text{-A.4})$$

$$W_{CP} = (1 - \alpha_C + \alpha_D) \frac{p_c - p_1}{\rho_1 \eta_{CP}} \quad (2\text{-A.5})$$

$$W_{FP} = \frac{p_8 - p_C}{\rho_5 \eta_{FP}} \quad (2\text{-A.6})$$

$$Q_a = h_{10} - h_7 + h_{13} - h_{12} \quad (2\text{-A.7})$$

where h_i is the specific enthalpy of the steam/water, in kJ/kg, α_i is the mass fraction of steam extracted, p_i is the pressure, in MPa, and ρ_i is the density of the steam/water, in kg/m^3, referred to the point i of the Figure 2.1.

The thermal energy consumed by the MED process is calculated applying the energy balance in the MED block, taking into account the specific energy consumption, the conversion factor and a temperature increase of 10 °C in the seawater.

The solar field efficiency is calculated with the following expression (referred to Figure 2.1):

$$\eta_{sf} = \frac{q_v \Delta h}{N_c \cdot A_c \cdot I_d \cdot cos\phi} = \frac{q_v (h_{10} - h_7 + h_{13} - h_{12})}{N_c \cdot A_c \cdot I_d \cdot cos\phi} \quad \text{(2-A.8)}$$

where q_v is the mass flow rate of steam entering the high pressure turbine, N_c is the number of solar collectors, A_c is the mirror aperture area of the collector, I_d is the direct normal irradiance and ϕ is the angle of incidence of the solar radiation. Notice that the solar field efficiency varies with the fresh water production in the MED cases due to the change in the total vapour flowing in the Rankine cycle. In the RO cases the vapour in the Rankine cycle is kept constant and consequently the solar field efficiency does not vary with the fresh water production.

Appendix 2-B

The cost rate associated with the capital investment and the operation and maintenance of a component or system is defined as follows:

$$\dot{Z} = \dot{Z}^{CI} + \dot{Z}^{OM} = \frac{P_I + P_{OM}}{\tau \cdot \sum_{t=1}^{N} \frac{1}{(1+k_n)^t}} \tag{2-B.1}$$

where P_I are the discounted investment costs, in €, P_{OM} are the discounted O&M expenses, in €, τ is the annual average availability of the plant, in h/y, N is the project lifetime, in years and k_n is the discount factor or cost of capital.

All the costs considered are levelized, that is the conversion of different payments or charges to a financially equivalent constant quantity over a particular time period (usually a year), affected by the inflation rate and the discount rate. The levelization of a quantity of money P_0 paid in the base year is done as stated below:

$$\begin{aligned} A = P_0 \cdot \frac{\sum_{t=1}^{N} \left(\frac{1+r_n}{1+k_n}\right)^t}{\sum_{t=1}^{N} \frac{1}{(1+k_n)^t}} &= P_0 \cdot \frac{k \cdot (1-k^N)}{1-k} \cdot \frac{k_n \cdot (1+k_n)^N}{(1+k_n)^N - 1} \\ &= P_0 \cdot \frac{k \cdot (1-k^N)}{1-k} \cdot CRF \end{aligned} \tag{2-B.2}$$

$$k = \frac{1+r_n}{1+k_n} \tag{2-B.3}$$

$$CRF = \frac{k_n \cdot (1+k_n)^N}{(1+k_n)^N - 1} \tag{2-B.4}$$

with r_n the nominal escalation rate, k_n the nominal discount rate and CRF the capital recovery factor.

Besides that, Table 2-B.1 shows input data required for the economic analysis. Regarding the capital costs of desalination technologies, Palenzuela et al. (2015) estimated a specific investment cost of 1207 \$/(m^3/d) for a SWRO plant. Also, capital costs of 1054 €/(m^3/d) and 875 €/(m^3/d) were reported for the "Alicante 2" and Barcelona-Llobregat SWRO plants (Pankratz, 2011), while 1562-1181 \$/(m^3/d) were presented for distillation plants in the same reference. Previous values of capital costs reported (Wangnick, 2002) for distillation plants with capacities below 10,000 m^3/d are above 2000 \$/(m^3/d). RO plants are modular, unlike

distillation plants, therefore the capital cost increases significantly in distillation plants as plant capacity decreases.

Table 2-B.1. Input data to the economic analysis.

Concept	Value	Ref
Solar thermal power plant		
Project lifetime, years	20	Assumption
Full operation hours, h/y	2090	(Zarza et al., 2006)
Average daily operation hours, h	5.726	Calculated
Plant construction period, years	2	Assumption
Electric power in the generator, kW	5000	(Zarza et al., 2006)
Specific cost of the power block, €/kW	1500	(Balsa Escalante, 1999)
Water consumption in the STPP, m^3/h	30	Assumption
Solar field		
Specific cost, €/m^2	300	Assumption
Heat rate, kJ/kWh	14,460	(Zarza et al., 2006)
Unitary heat rate	4.02	(Zarza et al., 2006)
Net electricity power, kW	5175	(Zarza et al., 2006)
Heat rate provided by the solar field, kW	20,786.3	(Zarza et al., 2006)
Collector area of the solar field, m^2	38,385	(Zarza et al., 2006)
MED plant		
Specific cost, €/(m^3/d)	1400	Assumption
Average daily operation hours, h	5.726	Calculated
O&M man power, €/m^3	0.04	(Perera, 1999)
O&M pretreatment, €/m^3	0.04	(Perera, 1999)
Pretreatment cost, % of total cost	10	Assumption
RO plant		
Specific cost, €/(m^3/d)	1200	(Palenzuela et al., 2015a)
Average daily operation hours, h	5.726/24	Calculated
O&M man power, €/m^3	0.086	(Medina, 2004)
O&M membrane replacement, €/m^3	0.036	(Medina, 2004)
O&M pretreatment, €/m^3	0.054	(Medina, 2004)
Pretreatment cost, % of total cost	0.17	(Sanchez, 2008)

Table 2-B.2 presents the exergy rate and exergetic unit cost associated with the streams of the MED1 and MED2 cases, and Table 2-B.3 shows the same for the RO1 and RO2 configurations. Notice how the negative exergy rate of the brine reject and condensing thermal power means that these streams would produce work if there were a machine able of taking them to the zero state. A detailed description of the different terms used to calculate the LEC and LWC is showed in Table 2-B.4.

Table 2-B.2. Summary of results related to the MED1 and MED2 configurations analysed in section 2.2.2.

		MED1		**MED2**	
Stream	**Description**	$\dot{E}$ (kW)	c (€/kWh)	$\dot{E}$ (kW)	c (€/kWh)
1	Direct normal irradiance	30,945	0	30,945	0
2	Global thermal losses in solar field	0	0	0	0
3	Heating steam from PB to MED	1636	0.041	1171	0.046
4	Condensed heating steam from MED	65.96	0.041	39.7	0.046
5	Electric power in generator	5000	0.131	5000	0.131
6	Pump power	49.69	0.131	47.9	0.131
7	Seawater intake	0	0	0	0
8	Aux. electric power intake+pretreat.	372.8	0.131	317.2	0.131
9	Feed seawater to MED	0	0	0	0
9’	Seawater entering the condenser	0	0	0	0
10	Auxiliary electric power for cooling	0	0	0	0
11	Brine reject	-124.7	0	-106.1	0
12	Distillate water	297.8	1.239*	244.8	1.265*
13	Cooling seawater rejected to the sea	126.2	0	107.3	0
14	Condensing thermal power of the PB	-	-	0	0

* In €/m^3

Table 2-B.3. Summary of results related to the RO1 and RO2 configurations analysed in section 2.2.1.

Stream	Description	RO1		RO2	
		$\dot{E}$ (kW)	c (€/kWh)	$\dot{E}$ (kW)	c (€/kWh)
1	Direct normal irradiance	30,945	0	30,945	0
2	Global thermal losses in solar field	0	0	0	0
3	Condensing thermal power of the PB	-310.7	0	-310.7	0
4	Electric power in generator	5000	0.131	5000	0.131
5	Pump power in the power block	41.32	0.131	41.32	0.131
6	Seawater intake	0.323	0	0	0
7	Aux. electric power intake+pretreat.	158.4	0.131	37.8	0.048
8	Seawater feed to RO process	0	0	0	0
9	Main electric power RO process	398.9	0.131	95.17	0.048
10	Brine reject	185.2	0	44.17	0
11	Permeate	292	1.054*	69.67	0.76*

* In €/m^3

Table 2-B.4. LEC and LWC for the four cases considered.

	q_w (m^3/h)	n_h (h/d)	q_d (m^3/d)	P_I (€)	P_{OM} (€)	P_F (€)	$W_{e,n}$ (kWh/y)	$E_{w,n}$ (m^3/y)	LEC (€/kWh)	LWC (€/m^3)	LWC^* (€/m^3)
STPP	0	5.726	0	15,236,313	306,753	0	10,363,641	0	0.131	-	-
MED1	186.4	5.726	1067.3	18,229,070	763,153	0	9,566,912	326,876	=	1.239	-4.099
MED2	158.6	5.726	908.1	17,732,279	694,070	0	9,686,878	268,774	=	1.265	-6.278
RO1	186.4	5.726	1067.3	16,504,665	1,245,088	0	9,198,809	326,876	=	1.055	-4.835
RO2	44.5	24	1067.3	16,504,604	1,245,043	642,991	10,363,641	326,876	=	0.76	-5.875

LWC^*= levelized water cost with feed-in tariff for the electricity production

References

Al-Hengari, S., ElMoudir, W., El-Bousiffi, M.A., 2014. Economic assessment of thermal desalination processes. Desalin. Water Treat. 1–14. doi:10.1080/19443994.2014.957982

Al-Karaghouli, A., Kazmerski, L.L., 2013. Energy consumption and water production cost of conventional and renewable-energy-powered desalination processes. Renew. Sustain. Energy Rev. 24, 343–356. doi:10.1016/j.rser.2012.12.064

Ali, M.T., Fath, H.E.S., Armstrong, P.R., 2011. A comprehensive techno-economical review of indirect solar desalination. Renew. Sustain. Energy Rev. 15, 4187–4199. doi:10.1016/j.rser.2011.05.012

Alrobaei, H., 2008. Novel integrated gas turbine solar cogeneration power plant. Desalination 220, 574–587. doi:10.1016/j.desal.2007.01.058

Aqualia - Almería [WWW Document], 2014. URL http://test.aqualia.es/almeria/gestion_clientes/t_vigente.asp (accessed 12.3.14).

Balsa Escalante, P., 1999. Operation of Parabolic Trough Solar Collectors. Sol. Therm. Electr. Gener. Train. Mobil. Res. Program. CIEMAT.

Bejan, A., Tsatsaronis, G., Moran, M.J., 1996. Thermal Design and Optimization. John Wiley and Sons, New York etc.

Blanco-Marigorta, A.M., Victoria Sanchez-Henríquez, M., Peña-Quintana, J.A., 2011. Exergetic comparison of two different cooling technologies for the power cycle of a thermal power plant. 5th Dubrovnik Conf. Sustain. Dev. Energy, Water Environ. Syst. 36, 1966–1972. doi:10.1016/j.energy.2010.09.033

Blanco, J., Palenzuela, P., Alarcón-Padilla, D., Zaragoza, G., Ibarra, M., 2013. Preliminary thermoeconomic analysis of combined parabolic trough solar power and desalination plant in Port Safaga (Egypt). Desalin. Water Treat. 51, 1887–1899.

Casimiro, S., Cardoso, J., Alarcón-Padilla, D.-C., Turchi, C., Ioakimidis, C., Mendes, J.F., 2014. Modeling Multi Effect Distillation Powered by CSP in TRNSYS. Energy Procedia 49, 2241–2250. doi:10.1016/j.egypro.2014.03.237

Damerau, K., Williges, K., Patt, A.G., Gauché, P., 2011. Costs of reducing water use of concentrating solar power to sustainable levels: Scenarios for North Africa. Energy Policy 39, 4391–4398. doi:10.1016/j.enpol.2011.04.059

De Munari, A., Capão, D.P.S., Richards, B.S., Schäfer, A.I., 2009. Application of solar-powered desalination in a remote town in South Australia 248, 72–82. doi:10.1016/j.desal.2008.05.040

EERA, 2015. Concentrated Solar Power (CSP) | EERA [WWW Document]. URL http://www.eera-set.eu/eera-joint-programmes-jps/concentrated-solar-power-csp/ (accessed 2.8.16).

El-Sayed, Y.M., 2007. The rising potential of competitive solar desalination. Desalination 216,

314–324. doi:10.1016/j.desal.2007.01.009

Fernández-Izquierdo, P., García-Rodríguez, L., Alarcón-Padilla, D.C., Palenzuela, P., Martín-Mateos, I., 2012. Experimental analysis of a multi-effect distillation unit operated out of nominal conditions. Desalination 284, 233–237. doi:10.1016/j.desal.2011.09.004

Fylaktos, N., Mitra, I., Tzamtzis, G., Papanicolas, C.N., 2014. Economic analysis of an electricity and desalinated water cogeneration plant in Cyprus. Desalin. Water Treat. 1–18. doi:10.1080/19443994.2014.940219

Garaway, I., Grossman, G., 2006. Investigation of a solar-powered desalination system employing regeneration. Desalination 197, 63–74. doi:http://dx.doi.org/10.1016/j.desal.2005.12.016

García-Rodríguez, L., Blanco-Gálvez, J., 2007. Solar-heated Rankine cycles for water and electricity production: POWERSOL project. Desalination 212, 311–318. doi:10.1016/j.desal.2006.08.015

García-Rodríguez, L., Delgado-Torres, A.M., 2007. Solar-powered Rankine cycles for fresh water production. Desalination 212, 319–327. doi:10.1016/j.desal.2006.10.016

Gastli, A., Charabi, Y., Zekri, S., 2010. GIS-based assessment of combined CSP electric power and seawater desalination plant for Duqum-Oman. doi:10.1016/j.rser.2009.08.020

Ghobeity, A., Noone, C.J., Papanicolas, C.N., Mitsos, A., 2011. Optimal time-invariant operation of a power and water cogeneration solar-thermal plant. Sol. Energy 85, 2295–2320. doi:10.1016/j.solener.2011.06.023

Hamed, O.A., Kosaka, H., Bamardouf, K.H., Al-Shail, K., Al-Ghamdi, A.S., 2016. Concentrating solar power for seawater thermal desalination. Desalination 396, 70–78. doi:10.1016/j.desal.2016.06.008

Hassabou, A.H., Spinnler, M., Polifke, W., 2013. Tecnoeconomic Analysis of Medium and Large-sacle Desalination Plants Driven by Concentrated Solar Systems in the Mena Region. Energy Procedia 42, 735–744. doi:10.1016/j.egypro.2013.11.076

Iaquaniello, G., Salladini, A., Mari, A., Mabrouk, A.A., Fath, H.E.S., 2014. Concentrating solar power (CSP) system integrated with MED–RO hybrid desalination. Desalination 336, 121–128. doi:10.1016/j.desal.2013.12.030

International Energy Agency, 1991. Guidelines for the economic analysis of renewable energy technology applications. International Energy Agency, Chateau Montebello, Quebec, Canada.

Kalogirou, S.A., 2013. Solar thermoelectric power generation in Cyprus: Selection of the best system. Renew. Energy 49, 278–281. doi:10.1016/j.renene.2012.01.014

Kalogirou, S.A., 2004. Solar thermal collectors and applications. Prog. Energy Combust. Sci. 30, 231–295. doi:10.1016/j.pecs.2004.02.001

Klein, S.A., 2013. Engineering Equation Solver Software (EES).

Kouta, A., Al-Sulaiman, F., Atif, M., Marshad, S. Bin, 2016. Entropy, exergy, and cost analyses of solar driven cogeneration systems using supercritical CO2 Brayton cycles and MEE-TVC desalination system. Energy Convers. Manag. 115, 253–264. doi:10.1016/j.enconman.2016.02.021

Mahbub, F., Hawlader, M.N.A., Mujumdar, A.S., 2012. Combined water and power plant (CWPP) — a novel desalination technology. Desalin. Water Treat. 5, 172–177. doi:10.5004/dwt.2009.581

Medina, J.A., 2004. 20 years evolution of desalination costs in Spain, in: Proceedings of International Conference on Desalination Costing. Limassol, Cyprus.

Mekhilef, S., Saidur, R., Safari, A., 2011. A review on solar energy use in industries. Renew. Sustain. Energy Rev. 15, 1777–1790. doi:10.1016/j.rser.2010.12.018

MINECO, 2014. Estadísticas eléctricas anuales - Estadísticas y Balances Energéticos - Energía - Ministry of Industry, Energy and Tourism [WWW Document]. URL http://www.minetur.gob.es/energia/balances/Publicaciones/ElectricasAnuales/Paginas/ElectricasAnuales.aspx (accessed 12.3.14).

Novatecsolar, 2016. NOVATEC SOLAR · Concentrating Solar Power [WWW Document]. URL http://www.novatecsolar.com/56-1-PE-2.html (accessed 9.1.16).

NREL, 2016. NREL: Concentrating Solar Power Projects - Concentrating Solar Power Projects with Operational Plants [WWW Document]. URL http://www.nrel.gov/csp/solarpaces/projects_by_status.cfm?status=Operational (accessed 4.25.16).

Palenzuela, P., Alarcón-Padilla, D.-C., Zaragoza, G., Blanco, J., 2015a. Comparison between CSP+MED and CSP+RO in Mediterranean Area and MENA Region: Techno-economic Analysis. Energy Procedia 69, 1938–1947. doi:10.1016/j.egypro.2015.03.192

Palenzuela, P., Zaragoza, G., Alarcón-Padilla, D.C., 2015b. Characterisation of the coupling of multi-effect distillation plants toconcentrating solar power plants. Energy 82, 986–995. doi:10.1016/j.energy.2015.01.109

Palenzuela, P., Zaragoza, G., Alarcón-Padilla, D.C., Blanco, J., 2013. Evaluation of cooling technologies of concentrated solar power plants and their combination with desalination in the mediterranean area. Appl. Therm. Eng. 50, 1514–1521. doi:10.1016/j.applthermaleng.2011.11.005

Palenzuela, P., Zaragoza, G., Alarcón-Padilla, D.C., Guillén, E., Ibarra, M., Blanco, J., 2011a. Assessment of different configurations for combined parabolic-trough (PT) solar power and desalination plants in arid regions. Energy 36, 4950–4958. doi:10.1016/j.energy.2011.05.039

Palenzuela, P., Zaragoza, G., Alarcón, D., Blanco, J., 2011b. Simulation and evaluation of the coupling of desalination units to parabolic-trough solar power plants in the Mediterranean region. Desalination 281, 379–387. doi:10.1016/j.desal.2011.08.014

Pankratz, T., 2011. IDA Desalination Yearbook (2009-2010). Media Analytics Ltd, UK.

Peñate, B., García-Rodríguez, L., 2012. Seawater reverse osmosis desalination driven by a solar Organic Rankine Cycle: Design and technology assessment for medium capacity range. Desalination 284, 86–91. doi:10.1016/j.desal.2011.08.040

Perera, J.C.I., 1999. Desalación de aguas. Colegio de Ingenieros de Caminos Canales y Puertos, Madrid.

Philipps, S., Bett, A.W., Horowitz, K., Kurtz, S., 2015. Current Status of Concentrator Photovoltaic (CPV) Technology. United States. Dept. of Energy. Office of Solar Electric Technology, Washington, D.C.

Sanchez, J., 2008. Estado del arte en el diseño del proceso de plantas desaladoras de agua de mar de gran capacidad. Tecnol. del Agua 28, 64–69.

Sharaf, M.A., Nafey, A.S., García-Rodríguez, L., 2011. Thermo-economic analysis of solar thermal power cycles assisted MED-VC (multi effect distillation-vapor compression) desalination processes. Energy 36, 2753–2764.

Sharqawy, M.H., Lienhard V, J.H., Zubair, S.M., 2010. Thermophysical properties of seawater: A review of existing correlations and data. Desalin. Water Treat. 16, 354–380. doi:http://dx.doi.org/10.5004/dwt.2010.1079

Slocum, A.H., Codd, D.S., Buongiorno, J., Forsberg, C., McKrell, T., Nave, J.-C., Papanicolas, C.N., Ghobeity, A., Noone, C.J., Passerini, S., Rojas, F., Mitsos, A., 2011. Concentrated solar power on demand. Sol. Energy 85, 1519–1529. doi:10.1016/j.solener.2011.04.010

Suman, S., Khan, M.K., Pathak, M., 2015. Performance enhancement of solar collectors—A review. Renew. Sustain. Energy Rev. 49, 192–210. doi:10.1016/j.rser.2015.04.087

Trieb, F., Müller-Steinhagen, H., 2008. Concentrating solar power for seawater desalination in the Middle East and North Africa 220, 165–183. doi:10.1016/j.desal.2007.01.030

Trieb, F., Müller-Steinhagen, H., Kern, J., Scharfe, J., Kabariti, M., Al Taher, A., 2009. Technologies for large scale seawater desalination using concentrated solar radiation. Desalination 235, 33–43. doi:10.1016/j.desal.2007.04.098

U.S. Department of Energy (DOE), 2009. Concentrating Solar Power Commercial Application Study. United States. doi:10.2172/1218186

Wagner, W., Pruß, A., 2002. The IAPWS formulation 1995 for the thermodynamic properties of ordinary water substance for general and scientific use. J. Phys. Chem. Ref. Data 31, 387–535.

Wangnick, K., 2002. 2002 IDA Worldwide Desalting Plants Inventory. Report No. 17. IDA (International Desalination Association).

Werner, M., Schäfer, A.I., 2007. Social aspects of a solar-powered desalination unit for remote Australian communities. Desalination 203, 375–393. doi:10.1016/j.desal.2006.05.008

Wilf, M., Awerbuch, L., 2007. The guidebook to membrane desalination technology : reverse osmosis, nanofiltration and hybrid systems : process, design, applications and economics. Balaban Desalination Publications, L'Aquila, Italy.

Zarza, E., Rojas, M.E., González, L., Caballero, J.M., Rueda, F., 2006. INDITEP: The first pre-commercial DSG solar power plant. Sol. Power Chem. Energy Syst. 80, 1270–1276. doi:10.1016/j.solener.2005.04.019

Chapter 3. Opportunities of improvement of the MED seawater desalination process by pretreatments allowing high temperature operation

Contents

List of figures

List of tables

Nomenclature

Variables

A	Heat transfer area, m^2
$\bar{c}_p$	Specific heat at constant pressure and mean temperature
h	Specific enthalpy, kJ/kg
q	Mass flow rate, kg/s
Q	Heat rate, kW
sA	Specific heat transfer area
sE	Specific energy consumption
T	Temperature, °C
X	Salinity, ppm
U	Overall heat transfer coefficient

Acronyms and abbreviations

BPE	Boiling Point Elevation
FF	Forward-Feed
GOR	Gain Output Ratio
LMTD	Logarithmic Mean Temperature Difference
MED	Multi-Effect Distillation
MSF	Multi-Stage Flash
NEA	Non-Equilibrium Allowance
NF	Nanofiltration
RO	Reverse Osmosis
TBT	Top Brine Temperature
TDS	Total Dissolved Solids
TTD	Terminal Temperature Difference

Subscripts

B	Brine
c	Condenser or condensation
cw	Cooling seawater
C	Condensate

D	Distillate
e	Evaporator
F	Feed
FB	Flash box
FE	Flash in the effect
in	Intake
N	Last effect
preh	Preheater
s	Steam
sat	Saturated conditions
T	Total
V	Vapour

Superscripts

$'$	Vapour conditions after the demister
$''$	Vapour conditions in the flash box

Greek

α	Fraction of vapour condensed
λ	Specific enthalpy of phase change, kJ/kg

3.1 Introduction

Despite of the current dominance of the Reverse Osmosis (RO) technology in the seawater desalination market, thermal processes such as Multi-Effect Distillation (MED) still have room for improvement, particularly in applications dealing with harsh waters or high fresh water purity requirements. However, the higher energy consumption of the MED process in comparison with the RO option constitutes one of the main drawbacks of this technology. Nevertheless, the thermal efficiency of this system can be increased by elevating the Top Brine Temperature (TBT), which is typically limited by the salts precipitation (scale formation) in the surface of the heat exchangers, mainly calcium carbonate, magnesium hydroxide and calcium sulphate (Al-Hamzah and Fellows, 2015). On the other hand, the use of membrane processes such as RO also present problems of scaling and fouling in the membranes, associated with high levels of Total Dissolved Solids (TDS) in the intake seawater, which reduces the permeate production (Hassan et al., 1998). Hence, different pretreatment processes have been proposed in order to permit reduction in the energy consumption, limit the scale formation and eliminate the technical constraints intrinsically related to those technologies. One method already tested in commercial desalination plants is the Nanofiltration (NF) pretreatment of the raw seawater entering a RO, MSF, or MED process, which can retain bivalent cations Ca^{+2} and Mg^{+2} and as consequence to increase the heating steam temperature in the case of MED and MSF processes (and so the number of effects) without risk of scaling. This integration helps to remove the main commented limitations associated with the low recovery ratio, the maximum temperature of operation or high TDS levels.

Studies found in the literature including nanofiltration pretreatment for seawater desalination processes are scarce, despite its potential for reducing the energy consumption and therefore improving the thermal efficiency. Those benefits were first verified in a project developed by the Saline Water Conversion Corporation (SWCC) and Hassan et al. (1998), where a NF unit was integrated into a RO and MSF pilot plants. The same author patented the use of NF membranes in combination with MSF, RO and MED desalination processes and proposed different integration and hybridization arrangements (Hassan, 1999). As a result, it was observed that the use of NF pretreatment reduced the turbidity, microorganisms, scale forming ions (Ca^{2+}, Mg^{2+}, $SO_4^{=}$, etc.) and total dissolved solids from the intake seawater, which allowed to increase the recovery ratio up to 70 – 80%, rise the top brine temperature to 120 °C and reduce the energy consumption between 25 – 30%. At commercial scale, the first NF system integrated into a MSF plant was proved to increase the capacity over 40% from the nominal value (22,700 m^3/d), at Sharjah Electricity and Water Authority (UAE) (Wilf and Awerbuch, 2007). The TBT was raised from 105 to 120 °C approximately, with the respective increase in the capacity of the plant. In addition, the capital and operation costs were reduced, compared with the standalone systems. Hamed (2005) reviewed hybrid desalination systems including

membrane and thermal processes coupled to power plants. He highlighted the promising concept of NF pretreatment for the removal of the ions responsible for alkaline and non-alkaline scale on the tubes of the evaporators. Tests carried out on a MSF pilot plant operating at a TBT of 130 °C resulted successful, increasing the product recovery up to 70% with respect 35% of conventional MSF plants. Also, Zhou et al. (2015) pointed out the benefits of introducing nanofiltration pretreatment into diverse seawater desalination technologies in order to reduce the costs associated with the scale formation. Particularly, if MED process is considered, the top brine temperature could be raised up to 125 °C without the risk of scaling. Moreover, the recovery ratio and water production could be improved.

Accordingly, the introduction of pretreatment processes for eliminating the risk of scaling in MED desalination technology and increase the TBT would result in a significant improvement of the thermal efficiency and reduction of the overall energy consumption. Particularly, the detailed analysis of the increment of the TBT in MED units and the influence on the main design and performance parameters is of great interest and suggested by the above-mentioned authors. Notice that, among the different MED configurations, the forward feed is the most suitable one to investigate the augmentation of the maximum temperature of operation due to the lower risk of scaling (the maximum brine concentration is reached in the effect of lowest temperature) (El-Dessouky and Ettouney, 2002).

One of the first steady-state mathematical models found for MED process with Forward Feed (MED-FF) arrangement was developed by El-Sayed and Silver (1980), relying on simplified assumptions such as constant thermophysical properties of the seawater or equal heat rates on the evaporators. The effect of the vapour pressure losses caused by friction was accounted by augmenting the BPE. They obtained useful analytical expressions to calculate the performance ratio, the thermal loads and heat transfer surface areas. In addition, they considered preheaters and flash boxes in the system analysis. El-Dessouky et al. (1998) developed a detailed mathematical model for MED-FF units, including preheaters and flash boxes. They assumed constant heat transfer areas in evaporators and preheaters, the influence of vapour leaks on the venting system and the effect of thermodynamic losses due to the BPE, Non-Equilibrium Allowance (NEA) and vapour pressure drops through the demisters, connecting lines and during the condensation inside the tubes of the evaporators. Moreover, the thermophysical properties of the seawater were calculated as function of the temperature and salinity, and the effect of the non-condensable gases on the condensation heat transfer coefficients was accounted. They concluded that the thermal performance of the unit is nearly independent of the top brine temperature (for a fixed number of effects) and significantly affected by the number of effects. Also, the overall heat transfer coefficients in evaporators and preheaters increased with the temperature, being higher for evaporators than for the preheaters (2.3–2.7 and

1.9–2.1 kW/(m^2-°C), respectively). Other steady-state mathematical model for MED-FF plants, based on mass and energy balances applied on the different components of the system, was presented by Mistry et al. (2013). They used a simultaneous equation solver, which provides more flexibility to the model as it does not require developing any algorithm to reach the convergence and at the same time reduces the number of assumptions. The model was compared with others found in the literature by simulating the Gain Output Ratio (GOR) and specific heat transfer area (sA) as function of different operational variables. The results showed that the model agreed quite well with the one from El-Sayed and Silver (1980), providing more details about the temperature profiles in the MED plant. Moreover, it had much simpler implementation and less assumptions that the model from El-Dessouky et al. (1998). However, only the BPE was considered in the calculation of the thermodynamic losses, ignoring the saturation temperature losses due to the pressure drops in the demisters, connecting lines and during the condensation inside the evaporators. Due to the fact that the specific heat transfer area is greatly affected by the saturation temperature losses of the generated vapour, from its generation in one effect to the condensation inside the evaporator of the following effect, they should be properly accounted while modelling MED plants. In addition, some approximations were done, such as neglecting the effect of the non-equilibrium allowance as a result of the flashing processes of the brine in the effects and the distillate in the flash boxes. The present model for MED-FF units takes advantage of the flexibility of a simultaneous equation solver while calculating in detail the thermodynamic losses, including boiling point elevation, non-equilibrium allowance and saturation temperature reduction of the vapour as consequence of the pressure drop in the demister, connecting lines and during the condensation inside the tubes of the evaporator.

The objective of this chapter is to investigate the effect of augmenting the top brine temperature and number of effects in MED-FF units on the main design and operation parameters (GOR, specific heat transfer area and specific energy consumption) and further improve the existing FF-MED models in the literature. Seawater pretreatment like nanofiltration would permit to increase the TBT without the risk of scaling and fouling, by retaining the bivalent ions and rejecting the microorganisms. For that purpose, a detailed mathematical steady-state model of a MED with Forward Feed (MED-FF) arrangement has been developed and validated against data found in the literature. This model includes some improvements with respect others previously published, like the detailed calculation of the thermodynamic losses. Also, a sensibility analysis regarding different design and operational parameters of the MED process (number of effects, terminal temperature difference in the first effect, brine salinity of the intake seawater, etc.) has been carried out.

3.2 Forward feed MED model

3.2.1 Process description

A multi-effect distillation unit for seawater desalination consists basically on a sequence of evaporation and condensation processes taking place inside a train of connected vessels, called effects, each one at lower pressure and temperature than the previous. In essence, this system takes advantage of the enthalpy of condensation of the generated vapour in one effect for promoting a new evaporation process in the following effect, repeating the sequence up to the last effect.

Among the different feed arrangements of the MED system, the forward feed configuration is characterized by the equal direction of the vapour and feed flows in the system. Furthermore, the lowest salinity of the brine is reached in the first effect and is progressively increasing up to the last effect. Hence, this configuration is specially indicated for higher temperatures of the external heating steam as the risk of scale formation is minimized.

In this system, each effect is comprised of a horizontal tube falling film evaporator, a demister and a preheater, except the last one which does not have a preheater but a condenser, called end condenser (see Figure 3.1). The external thermal energy, usually saturated steam (heating steam) below 70 °C to avoid the appearance of scaling in the tubes, is introduced exclusively in the evaporator of the first effect and represents the primary energy source which drives the entire distillation process. Firstly, the seawater enters the system from intake beach wells or submarine pipelines. It is directed to the end condenser where is used to condensate the vapour generated in the last effect. At the outlet of the end condenser, the seawater is divided in two streams: the feed seawater, which goes to the first effect passing through the preheaters of each effect, and the cooling seawater, which rejects the waste heat back to the sea. The preheating of the seawater permits to reduce the energy requirements of the process thanks to the condensation of a fraction of the total vapour generated in each effect. The feed seawater (feedwater), after being preheated, is sprayed over the tube bundle of the first evaporator where is partially evaporated due to the heat released by the condensation of the external vapour, which returns as saturated liquid to the steam generation source. From one side, vapour is produced, while the unevaporated brine remains at the bottom of the effect and constitutes the feedwater for the next effect. The vapour produced, considered free of salts, passes through a demister in order to retain the brine droplets, and is directed to a preheater where part of it condenses. The rest of the vapour is brought to the evaporator of the second effect and constitutes the driven force of the new evaporation process, at lower pressure and temperature. In this effect, the feedwater is the brine generated in the previous, which undergoes a flash process and produces additional vapour. Both the distillate produced in the preheater and inside

the evaporator are collected in a flash box, producing additional flash vapour which is introduced in the vapour space of the effect. This process is repeated sequentially up to the last effect.

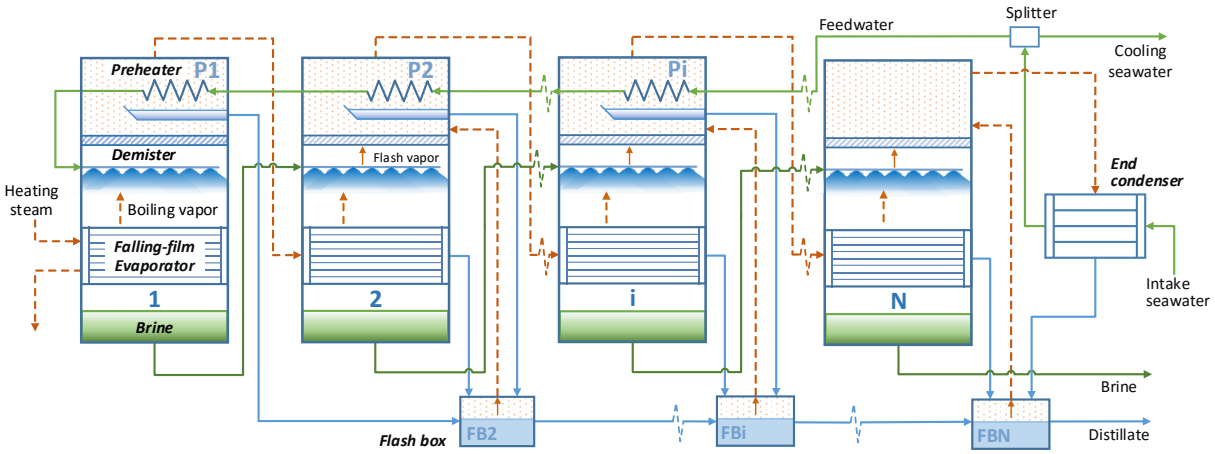

Figure 3.1. Scheme of the FF-MED plant.

3.2.2 Mathematical model

A steady-state mathematical model for a FF-MED process is developed by applying the mass and energy balance equations over the different components of the plant, along with the heat transfer equations associated with the heat exchangers (evaporators, preheaters and end condenser). The generic FF-MED system includes N effects, $N-1$ preheaters and $N-1$ distillate flashing boxes (see Figure 3.1). By default, the input variables needed to solve the model are the following: the temperature of the heating steam, T_s, the temperature and salinity of the seawater intake, T_{in} and X_{in}, respectively, the temperature and salinity of the brine in the last effect, T_N and X_N, respectively, the temperature of the cooling seawater, T_F, the minimum temperature difference in the end condenser, DTT_c, and last preheater, DTT_1, and the geometric and physical characteristics of the demister, connecting lines, and evaporator tubes.

The model has been implemented in Engineering Equation Solver (EES) software environment (Klein, 2013), which solves simultaneously all the nonlinear equations set in the system (using the Newton-Raphson method) after a proper initialization of the variables. This software is useful for the characterization of thermal systems like the one studied here because it includes libraries for the thermophysical properties of numerous substances, particularly, pure water, using the IAPWS Formulation 1995 (Wagner and Pruß, 2002), and seawater (Sharqawy et al., 2010). Moreover, it does not need to create an algorithm to sequentially solve the equations, providing more degrees of freedom. On the other hand, the convergence is strongly subject to proper initial guesses and a reasonable range of variation of the variables.

In the development of the model, the following assumptions and approximations have been taken into account:

- Constant and equal heat transfer areas in evaporators and preheaters. This is a common practice in the real thermal desalination industry due to economic reasons.
- The thermophysical properties of the seawater are function of the temperature and salinity.
- The distillate produced is considered salt-free.
- The thermal losses to the environment are neglected as the equipment is supposed to be well insulated and the operation temperatures are relatively low (40–120°C).
- The temperature of the vapour is considered equal to the brine temperature in each effect. That means that the vapour is slightly superheated by the boiling point elevation.
- In each evaporator both the inlet steam and the exiting condensed liquid are supposed to be in saturation conditions.
- The thermodynamic losses have been taking into account: the boiling point elevation, the non-equilibrium allowance in the effects and flashing boxes, and the saturation temperature decrease of the vapour due to the pressure losses in the demister, connecting lines and during the condensation inside the evaporators.
- The vapour suffers an isenthalpic process while passing through the demister.
- The temperature of the flashing vapour in the flash box is equal to the temperature in the vapour space of the effect.
- Due to the utilization of a vacuum system, no vapour leaks have been considered.

3.2.2.1 Global mass and salt balances

The global mass and salinity balance applied to the complete system leads to:

$$q_F = q_D + q_B \quad \text{(Eq. 3.1)}$$

$$q_F X_F = q_B X_N \quad \text{(Eq. 3.2)}$$

where q_F is the mass flow rate of feed seawater entering the first effect, q_D is the total mass flow rate of distillate produced, q_B is the mass flow rate of brine exiting the last effect, X_F is the salinity of the feed seawater and X_N the salinity of the brine in the last effect. Notice that as local mass balances have been applied in the effects, the global mass balance is only for

verification purposes. Similarly, the global salinity balance is equivalent to the salinity balance in the last effect.

The total mass flow rate of distillate generated in the plant is the sum of the mass flow rate of vapour produced by boiling in each effect q_{Di} plus the vapour produced by flashing q_{FEi} (except in the first effect where there is not flashing phenomena):

$$q_D = \sum_{i=1}^{N} q_{Di} + \sum_{i=2}^{N} q_{FEi} \quad \text{(Eq. 3.3)}$$

3.2.2.2 Temperature profiles

The temperature of the brine in a generic effect i is equal to the saturation temperature of the vapour formed by boiling plus the boiling point elevation, which takes into account the presence of salts in the water:

$$T_i = T_{Vsat,i} + BPE_i \quad \text{(Eq. 3.4)}$$

The boiling point elevation is obtained with the correlation proposed by Sharqawy et al. (2010), which is function of the temperature and salinity of the brine.

Also the temperature of the brine and the temperature of the vapour in each effect are considered equal:

$$T_i = T_{V_i} \quad \text{(Eq. 3.5)}$$

It is supposed that the vapour suffers an isenthalpic process through the demisters, reaching a temperature T'_{Vi} in the vapour space, with the respective pressure drop. The saturation temperature of the generated vapour decreases in the path to the next evaporator, because of the pressure drop in the demister, the connecting lines and the condensation inside the tubes. This temperature drop causes a reduction in the temperature difference between effects, which is the driven force of the process. Therefore, the condensation temperature of the vapour generated in the effect i, which takes place inside the evaporator of the effect $i+1$, from $i = 1..N-1$, is obtained with:

$$T_{c,i} = T_{Vi} - BPE_i - \left(\Delta T_{m,i} + \Delta T_{l,i} + \Delta T_{c,i}\right) \quad \text{(Eq. 3.6)}$$

where $\Delta T_{m,i}$, $\Delta T_{l,i}$ and $\Delta T_{c,i}$ are the saturation temperature drops in the demister, connecting lines and condensation process, all referred to the effect i and starting from the second effect. Notice that the condensation temperature in the first evaporator is the saturation temperature of the heating steam and the corresponding condensation temperature of the effect $i+1$ is $T_{c,i}$, from $i = 1..N-1$.

The decrease in the saturation temperature of the vapour after passing through the demister of a generic effect i is the difference between the saturation temperature of the vapour generated before the demister ($T_{Vsat,i}$) and that one after the demister ($T'_{Vsat,i}$). Similarly, the saturation temperature drop occurring in the connecting lines between the effect i and effect $i+1$ is equal to $T'_{Vsat,i}$ minus the saturation temperature of the vapour at the inlet of the following evaporator ($T'_{c,i}$). Finally, the saturation temperature losses of the vapour during the condensation in the tube bundle are defined as the difference between $T'_{c,i}$ and the condensation temperature ($T_{c,i}$).

$$\Delta T_{m,i} = T_{Vsat,i} - T'_{Vsat,i} \quad \text{(Eq. 3.7)}$$

$$\Delta T_{l,i} = T'_{Vsat,i} - T'_{c,i} \quad \text{(Eq. 3.8)}$$

$$\Delta T_{c,i} = T'_{c,i} - T_{c,i} \quad \text{(Eq. 3.9)}$$

The above mentioned temperatures are calculated with the pressure drops of the formed vapour while flowing to the tubes of the next evaporator. Particularly, the pressure decrease in the demister is obtained with the correlation proposed by El-Dessouky and Ettouney (2002). For the pressure drop in the connecting lines, due to the friction with the walls, the Unwin's formula (Nayyar, 2006) has been used. Finally, the pressure drop due to the condensation of the vapour inside the tubes of the evaporator has been determined by means of the methodology described in ESDU (1993), which relies on the Friedel's correlation (Friedel, 1979).

3.2.2.3 First effect

The first effect is different from the rest of the MED unit as is the place where the external energy is introduced (see Figure 3.2). The mass balance applied to a Control Volume (CV) containing the first effect establishes:

$$q_F = q_{B1} + q_{T1} \quad \text{(Eq. 3.10)}$$

where q_{B1} is the mass flow rate of brine exiting the first effect and q_{T1} the total mass flow rate of vapour generated within the first effect, which in this case is only the one produced by boiling (q_{D1}). Notice that in this effect the seawater introduced does not suffer a flash process because its temperature is below the saturation temperature at the existing pressure inside the effect.

The salinity balance applied to the same CV is shown below, where it has been assumed that the vapour generated is free of salts:

$$q_F X_F = q_{B1} X_1 \qquad \text{(Eq. 3.11)}$$

with q_{B1} and X_1 the mass flow rate and salinity of the brine in the effect 1, respectively.

Finally, the energy balance in this first effect, considering all the streams entering and exiting the CV, is as follows:

$$q_s \lambda_s + q_F h_{preh2} = (1-\alpha_1) q_{T1} h'_{V1} + \alpha_1 q_{T1} h'_{C1} + q_{B1} h_{B1} \qquad \text{(Eq. 3.12)}$$

where q_s is the mass flow rate of heating steam, λ_s is the specific enthalpy of condensation of the heating steam at T_s, h_{preh2} is the specific enthalpy of the feed seawater before entering the first preheater, at t_{preh2}, α_1 is the fraction of the total steam that condenses in the first preheater, h'_{V1} is the specific enthalpy of the steam in the vapour space at T'_{V1}, after passing through the demister, h'_{C1} is the specific enthalpy of the condensate in the preheater at T'_{V1}, and h_{B1} is the specific enthalpy of the brine at the bottom of the effect at T_1.

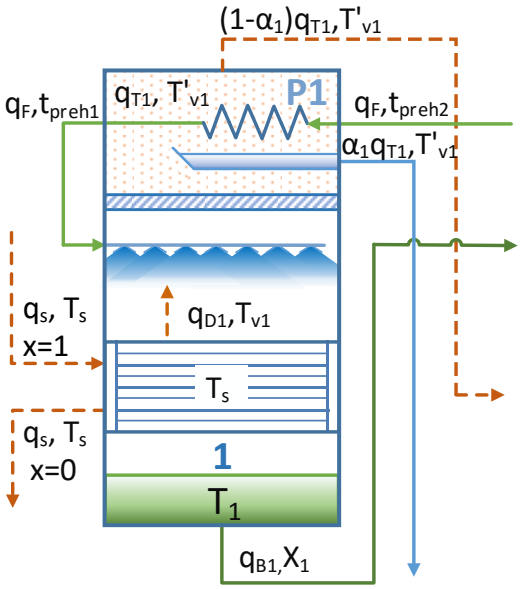

Figure 3.2. Schematic diagram of the first effect.

The area of the evaporator is obtained by applying the heat transfer equation in this component. The rate of heat transfer (Q_1) that takes place between the condensing steam and the sprayed seawater in this first evaporator accounts both for the sensible and latent heat added:

$$Q_1 = q_F \bar{c}_{p1}\left(T_1 - t_{preh1}\right) + q_{D1}\lambda_{V1} = A_1 U_{e1}(T_s - T_1) \qquad \text{(Eq. 3.13)}$$

where $\bar{c}_{p1}$ is the specific heat at constant pressure of the feedwater between T_1 and t_{preh1}, t_{preh1} is the temperature of the feedwater after passing through the preheater associated with the first effect, q_{D1} is the mass flow rate of vapour produced by boiling in the first effect, λ_{V1} is the specific enthalpy of evaporation of the water at $T_{Vsat,1}$, A_1 is the heat transfer area of the evaporator and U_{e1} is the overall heat transfer coefficient of the evaporator, which is calculated using the correlation proposed by El-Dessouky and Ettouney (2002) as function of the temperature:

$$U_{e1} = 1.9695 + 1.2057 \cdot 10^{-2} T_1 - 8.5989 \cdot 10^{-5} T_1^2 + 2.5651 \cdot 10^{-7} T_1^3 \qquad \text{(Eq. 3.14)}$$

3.2.2.4 Effects from 2 to N-1

The mass balance applied to the CV defined by the generic effect i (see Figure 3.3) is as follows:

$$q_{Bi} = q_{B,i-1} - q_{Di} - q_{FEi} \qquad \text{(Eq. 3.15)}$$

being q_{Bi} and $q_{B,i-1}$ the mass flow rates of the brine exiting and entering the effect i, repectively.

Similarly, the salt balance in the CV establishes that:

$$q_F X_F = q_{Bi} X_i \qquad \text{(Eq. 3.16)}$$

where q_{Bi} and X_i are the mass flow rate and salinity of the brine in the effect i.

The energy balance applied to the same CV gives:

$$\begin{aligned}(1-\alpha_{i-1}) q_{T,i-1}\lambda_{c,i-1} + q_{FBi} h''_{Vi} + q_{B,i-1} h_{B,i-1} \\ = (1-\alpha_i) q_{Ti} h'_{Vi} + \alpha_i q_{Ti} h'_{ci} + q_F \bar{c}_{p,preh,i}\left(t_{preh,i} - t_{preh,i+1}\right) + q_{Bi} h_{Bi}\end{aligned} \qquad \text{(Eq. 3.17)}$$

where α_i is the fraction of vapour condensed in the preheater i, $\lambda_{c,i-1}$ is the specific enthalpy of condensation of the vapour inside the evaporator of the effect i, at $T_{c,i-1}$, q_{FBi} is the mass

flow rate of vapour produced by flash in the flash box i, h''_{Vi} is the specific enthalpy of the flashing vapour at T''_{Vi}, $\bar{c}_{p,preh,i}$ is the specific heat of the feedwater at constant pressure and mean temperature between $t_{preh,i}$ and $t_{preh,i+1}$ and q_{Ti} is the total mass flow rate of vapour produced by boiling within the effect (q_{Di}), by flashing of the brine (q_{FEi}) and by flashing of the distillate (q_{FBi}):

$$q_{Ti} = q_{Di} + q_{FEi} + q_{FBi} \qquad \text{(Eq. 3.18)}$$

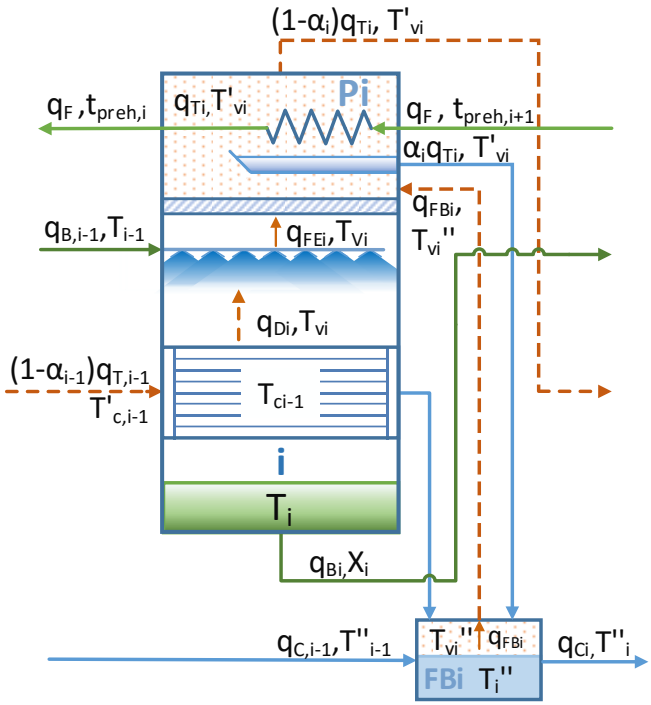

Figure 3.3. Schematic diagram of the generic effect i.

In the effects from 2 to N, the brine entering the effect suffers a flashing process because of being slightly superheated and discharged into a lower pressure effect. This process is described with the following balance:

$$q_{FEi}\lambda_{FEi} = q_{B,i-1}\bar{c}_{p,FEi}\left(T_{i-1} - T_{B,FEi}\right) \qquad \text{(Eq. 3.19)}$$

where λ_{FEi} is the specific enthalpy of evaporation of the seawater at T_i, $\bar{c}_{p,FEi}$ is the specific heat at constant pressure and mean temperature between T_{i-1} and $T_{B,FEi}$, with $T_{B,FEi}$ the temperature of the unevaporated brine in the effect i after the flashing process. The temperature of the brine is higher than the boiling temperature T_i by the non-equilibrium allowance, which represents the deviation of the real process respect to the ideal one in equilibrium. This variation is mainly caused by the finite time period in which the flash process occurs (Fiorini et al., 2001). For that reason, the equilibrium conditions between the liquid and the vapour cannot

be reached and the temperature of the resulting brine is higher than the temperature in the equilibrium.

$$T_{B,FEi} = T_i + NEA_i \quad \text{(Eq. 3.20)}$$

where the NEA_i is calculated by means of the correlation proposed by Miyatake et al. (1973) as function of the temperature difference (ΔT_i) of the boiling brine in the effects $i-1$ and i:

$$NEA_i = \frac{33(\Delta T_i)^{0.55}}{T_{Vi}} \quad \text{(Eq. 3.21)}$$

The validity of this correlation is somehow limited to the experimental conditions considered in the work of these authors. Particularly, they obtained data from flash evaporation experiments carried out in a pool of pure water, inside a chamber of 40 cm high and a diameter of 8 cm.

The heat transfer areas of the evaporators (from 2 to $N-1$) are obtained with the heat transfer equations related to the condensation–evaporation process that takes place in the tube bundle at constant temperature:

$$Q_i = (1-\alpha_{i-1}) q_{Ti} \lambda_{c,i-1} = A_i U_{ei} (T_{c,i-1} - T_i) \quad \text{(Eq. 3.22)}$$

where Q_i is the rate of heat transfer and U_{ei} the overall heat transfer coefficient in the evaporator i.

3.2.2.5 Last effect

The mass balance in the last effect (see Figure 3.4) establishes that the brine coming from the previous effect $(q_{B,N-1})$ is equal to the mass flow rate of vapour generated by flash $(q_{FE,N})$ plus the mass flow rate of vapour generated by boiling (q_{DN}) and the unevaporated brine remaining at the bottom of the effect (q_{BN}). This equation is expressed as follows:

$$q_{B,N-1} = q_{FE,N} + q_{DN} + q_{BN} \quad \text{(Eq. 3.23)}$$

The energy balance in this effect is different from the rest because of its particular configuration. There is not preheater associated with this effect and all the vapour generated is driven to the end condenser where it releases its latent heat to the intake seawater. The condensate generated here is collected in the last flash box.

$$(1-\alpha_{N-1})q_{T,N-1}\lambda_{c,N-1} + q_{FB,N}h''_{VN} + q_{B,N-1}h_{B,N-1} = q_{TN}h'_{VN} + q_{BN}h_{BN} \qquad \text{(Eq. 3.24)}$$

In addition, part of the vapour is produced by flash of the incoming brine:

$$q_{FE,N}\lambda_{FE,N} = q_{B,N-1}\bar{c}_{p,FEN}(T_{N-1} - T_{B,FEN}) \qquad \text{(Eq. 3.25)}$$

The temperature of the unevaporated brine, $T_{B,FEN}$, is obtained with the NEA_N:

$$T_{B,FEN} = T_N + NEA_N \qquad \text{(Eq. 3.26)}$$

Finally, the heat transfer equation associated with the evaporator of this last effect is as follows:

$$Q_N = (1-\alpha_{N-1})q_{T,N-1}\lambda_{c,N-1} \qquad \text{(Eq. 3.27)}$$

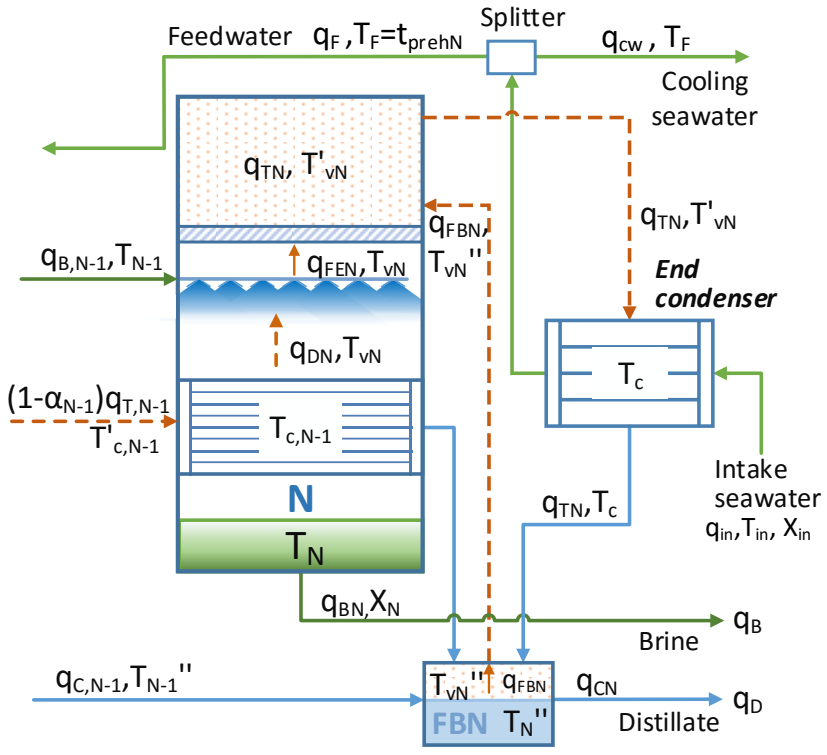

Figure 3.4. Schematic diagram of the last effect and end condenser.

3.2.2.6 End condenser

In the end condenser, the vapour generated in the last effect condenses and warms up the intake seawater (Figure 3.4). Part of the seawater at the outlet of the end condenser (rejected cooling seawater) is sent back to the sea in order to reject the excess of heat not used in the process.

The mass balance in the splitter and the energy balance applied in the end condenser are expressed, respectively, by:

$$q_{in} = q_F + q_{cw} \quad \text{(Eq. 3.28)}$$

$$q_{in}(h_F - h_{in}) = q_{TN}\lambda_c \quad \text{(Eq. 3.29)}$$

where q_{in} is the mass flow rate of intake seawater entering the end condenser, q_{cw} is the mass flow rate of cooling seawater, h_F is the specific enthalpy of the seawater at T_F after passing through the end condenser, h_{in} is the specific enthalpy of the intake seawater at T_{in} and λ_c is the specific enthalpy of condensation of the vapour coming from the last effect, at T_c.

The heat transfer equation applied to the end condenser, which is a shell and tube heat exchanger that can be assumed as counter-flow, is defined below:

$$Q_c = A_c U_c LMTD_c = U_c A_c \frac{\Delta T_{in}^c - \Delta T_{out}^c}{\ln\left(\frac{\Delta T_{in}^c}{\Delta T_{out}^c}\right)} = U_c A_c \frac{T_F - T_{in}}{\ln\left(\frac{T_c - T_{in}}{T_c - T_F}\right)} \quad \text{(Eq. 3.30)}$$

where A_c is the heat transfer area of the condenser, U_c is the overall heat transfer coefficient related to the end condenser and obtained using the correlation proposed by El-Dessouky and Ettouney (2002):

$$U_c = 1.7194 + 3.2063 \cdot 10^{-3} T_c + 1.5971 \cdot 10^{-5} T_c^2 - 1.9918 \cdot 10^{-7} T_c^3 \quad \text{(Eq. 3.31)}$$

and $LMTD_c$ is the log mean temperature difference of the condenser, defined as function of the temperatures differences at the inlet ($\Delta T_{in}^c = T_c - T_{in}$) and at the outlet of the condenser ($\Delta T_{out}^c = T_c - T_F$).

3.2.2.7 Preheaters

Each of the $N-1$ preheaters is thermodynamically defined by applying an energy balance over a CV containing them and with the heat transfer equation associated to the heat transfer process. It is assumed that the BPE of the generated vapour is released in the preheaters. Thus, the energy balance considers both latent and sensible heat transfer, and is established as follows:

$$q_F \bar{c}_{p,preh,i}\left(t_{preh,i} - t_{preh,i+1}\right) = \alpha_i q_{Ti} \lambda'_{Vi} + \alpha_i q_{Ti} \bar{c}_{p,BPEi}(T'_{Vi} - T'_{Vsat,i}) \quad \text{(Eq. 3.32)}$$

where $\bar{c}_{p,preh,i}$ is the specific heat of the seawater at constant pressure and mean temperature between $t_{preh,i}$ and $t_{preh,i+1}$, $t_{preh,i}$ and $t_{preh,i+1}$ are the temperatures of the seawater at the outlet and the inlet of the preheater i, respectively, and $\bar{c}_{p,BPEi}$ is the specific heat of the vapour at constant pressure and mean temperature between T'_{Vi} and $T'_{Vsat,i}$.

The heat transfer equations associated with the preheaters are defined below, formed similarly to the case of end condenser:

$$Q_{preh,i} = A_{preh,i} U_{preh,i} LMTD_{preh,i} = U_{preh,i} A_{preh,i} \frac{t_{preh,i} - t_{preh,i+1}}{ln\left(\frac{T'_{Vi} - t_{preh,i+1}}{T'_{Vi} - t_{preh,i}}\right)} \qquad \text{(Eq. 3.33)}$$

where $A_{preh,i}$ is the heat exchanger area, $U_{preh,i}$ is the overall heat transfer coefficient, and $LMTD_{preh,i}$ is the log mean temperature difference, referred to a generic preheater i, from $i = 1$ to $N - 1$. Notice that in Eq. (3.33) the effect of the sensible heat of the vapour (superheated by the BPE) has been neglected, when compared to the specific heat of condensation, for simplicity. Moreover, the overall heat transfer coefficient has been calculated using the same expression that for the end condenser case.

3.2.2.8 Flash boxes

The flash boxes are used to collect the distillate generated in the preheaters and evaporators and to generate additional flash vapour (see Figure 3.3). In this work it has been assumed that the vapour temperatures inside the flash boxes (T''_{Vi}) are equal to those of the vapour space in the effects, after the demisters (T'_{Vi}), as they are interconnected. Therefore, the condensate suffers a sudden flash process due to its saturated condition and the decrease in the pressure. The temperature of the distillate (T''_i) is then higher than the temperature of the vapour in the flash box by the non-equilibrium allowance (NEA''):

$$T''_i = T''_{Vi} + NEA''_i \quad \text{with} \quad i = 2..N \qquad \text{(Eq. 3.34)}$$

where the NEA''_i are obtained with the correlation of Eq. (3.21) adapted to the flash boxes:

$$NEA''_i = \frac{33\left(T_{c,i-1} - T''_i\right)^{0.55}}{T''_{Vi}} \qquad \text{(Eq. 3.35)}$$

There are $N - 1$ flash boxes, which has been numbered starting from the second. The mass balances applied in the flash boxes are as follows, where for $i = 1$ the equation provides the definition of q_{C1}:

$$q_{Ci} = \sum_{k=1}^{i-1} q_{T,k} + \alpha_i q_{Ti} - \sum_{j=2}^{i} q_{FB,j} \quad \text{with} \quad i = 1..N-1 \qquad \text{(Eq. 3.36)}$$

where q_{Ci} is the mass flow rate of the distillate collected in the flash box i at T_i''. In the last flash box the mass balance is:

$$q_{CN} = q_{C,N-1} + (1-\alpha_{N-1}) q_{T,N-1} + q_{TN} - q_{FB,N} \qquad \text{(Eq. 3.37)}$$

The energy balances in the flash boxes for are presented below, from $i = 2..N-1$:

$$q_{C,i-1} h''_{c,i-1} + (1-\alpha_{i-1}) q_{T,i-1} h_{c,i-1} + \alpha_i q_{Ti} h'_{ci} = q_{FBi} h''_{Vi} + q_{Ci} h''_{ci} \qquad \text{(Eq. 3.38)}$$

where $h''_{c1} = h'_{c1}$. Finally, the energy balance applied in the last flash box gives:

$$q_{C,N-1} h''_{c,N-1} + (1-\alpha_{N-1}) q_{T,N-1} h_{c,N-1} + q_{TN} h_{cN} = q_{FBN} h''_{VN} + q_{CN} h''_{cN} \qquad \text{(Eq. 3.39)}$$

3.2.3 Plant performance

The variable that measures the thermal efficiency of a MED process is the gain output ratio, defined as the ratio of distillate mass flow rate (q_D) produced to the heating steam mass flow rate (q_s) introduced in the first evaporator:

$$GOR = \frac{q_D}{q_s} \qquad \text{(Eq. 3.40)}$$

Other significant parameter related to the total cost of the MED plant is the specific heat transfer area (sA), which is defined as the sum of all the heat exchanger surface areas (evaporators, preheaters and end condenser) divided by the distillate mass flow rate:

$$sA = \frac{\sum_{i=1}^{N} A_i + \sum_{i=1}^{N-1} A_{preh,i} + A_c}{q_D} \qquad \text{(Eq. 3.41)}$$

The specific thermal energy consumption (sE) is also used to quantify the thermal efficiency of a MED, which is defined as the input energy added to the system (without accounting the work by pumps) per unit of distillate mass flow rate produced, that is, the mass flow rate of heating steam times the specific enthalpy of condensation of the steam divided by the mass flow rate of distillate produced, with the corresponding conversion factors, in kWh/m^3.

$$sE = \frac{q_s \lambda_s}{q_D/\rho_D} \cdot \frac{1}{3600} \qquad \text{(Eq. 3.42)}$$

3.3 Validation of the FF-MED model and sensitivity analysis

3.3.1 Validation of the model

The developed model is compared with others obtained from the literature in order to validate it. In general, the present model is similar to the one described by El-Dessouky et al. (1998) and shares some of its features. However, some differences can be observed. The most important difference is the programming method chosen for the implementation of the model, from which derives a simpler coding and higher flexibility in the simulations. As commented before, a simultaneous equation solver system was selected, contrary to the sequential solving taken by El-Dessouky et al. (1998), just as the model presented by Mistry et al. (2013). Also, the present model considers a preheater associated with the first effect, which is not accounted in El-Dessouky et al. (1998). In addition, in this model the amount of vapour condensed in the preheaters is a fraction α of the total vapour produced by boiling and flash, while in the latter only the flash vapour is considered to be condensed in the preheaters. On the contrary, the model developed by El-Dessouky et al. (1998) accounts for the presence of non-condensable gases and vapour leakages, which is not considered here. A list with the differences with other models presented in the selected literature is shown in Table 3.1.

Table 3.1. Comparison between the assumptions of the selected forward-feed MED models.

Parameter	**El-Dessouky et al. (1998)**	**Mistry et al. (2013)**	**Present**
Programming method	Sequential	Simultaneous	Simultaneous
Heat transfer area of evaporators	Constant	Constant	Constant
Heat transfer area of preheaters	Constant	Constant	Constant
BPE	Variable	Constant	Variable
NEA	Variable	Neglected	Variable
Non-condensable gases effect	Yes	No	No
Pressure losses	Yes	No	Yes
Tube bundle geometry	Yes	No	No
Thermophysical properties of seawater	Variable	Variable	Variable
Temp. difference between effects	Variable	Variable	Variable
Number of preheaters	$N-2$	$N-1$	$N-1$
Overall heat transfer coefficient	$f(R,h)$	$f(T)$	$f(T)$
Flow rate of vapour condensed in the preheaters	Only flash	Fraction of total vapour	Fraction of total vapour

For the validation of the MED-FF model, results from Mistry et al. (2013) have been taken. Particularly, the variation of the GOR and sA with the number of effects and heating steam temperature was considered. To perform the comparison, the same specifications for the MED were selected and presented in Table 3.2. The model has been calibrated by minimizing the thermodynamic losses: only the demister of the first effect has been taken into account and the diameters of the connecting lines and the tubes of the evaporators has been selected large enough in order to decrease the friction losses.

Table 3.2. Inputs taken for the validation of the model.

Parameter	**Value**
Number of effects	3–19
Fresh water production, kg/s	1
Heating steam temperature, °C	70
Intake seawater temperature, °C	25
Intake seawater salinity, ppm	42,000
Brine blow down temperature, °C	40
Brine blow down salinity, ppm	70,000
Minimum TTD in preheaters, °C	5
Temperature rise in the end condenser, °C	10

Figure 3.5 shows the GOR and sA as function of the number of effects, along with the results obtained by Mistry et al. (2013). It can be seen how the relative error made is lower than 2% for the GOR and 7% for the sA, following the same trend in both cases. It is observed that when the number of effects is increased, the efficiency grows but progressively decreases because of the elevation of the thermodynamic losses and the increase of the specific heat of evaporation. Also, the overall heat transfer coefficient associated with the heat exchangers decreases along the effects of the MED plant, which degrades the heat transfer process and reduces the freshwater production. Regarding the sA, a good agreement with Mistry et al. (2013) is also found. As shown, the sA increases considerably with the number of effects due to the difference of temperature between effects become smaller.

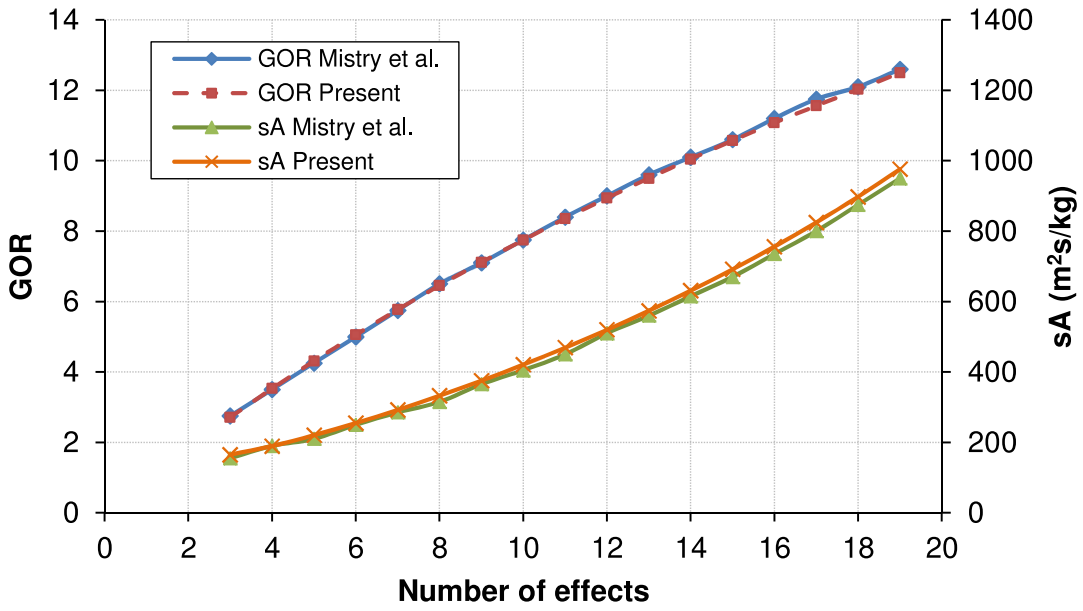

Figure 3.5. Comparison of the GOR and sA as function of the number of effects using the model from Mistry et al. (2013) and the present one.

Other significant variable for the assessment of the MED design is the maximum temperature reached by the brine (top brine temperature), which in the case of FF arrangement takes place in the first effect. There is a practical limit for this parameter at nearly 70 °C due to the appearance of scaling (salts precipitation) on the tubes of the evaporators, which is favoured by the increase of the seawater temperature. Both models are also compared with respect the GOR and sA by varying the heating steam temperature, with the number of effects fixed to 8 (see Figure 3.6). As it can be seen, the curves for both parameters present a good agreement with the results obtained by Mistry et al. (2013). The maximum relative errors found are lower than 2 and 8% for the GOR and sA, respectively. It is also observed that the thermal efficiency decreases only slightly (9.5%) when the heating steam temperature is elevated from 60 to 100 °C (40%). The decrease on the specific heat transfer area is more considerable, on the contrary.

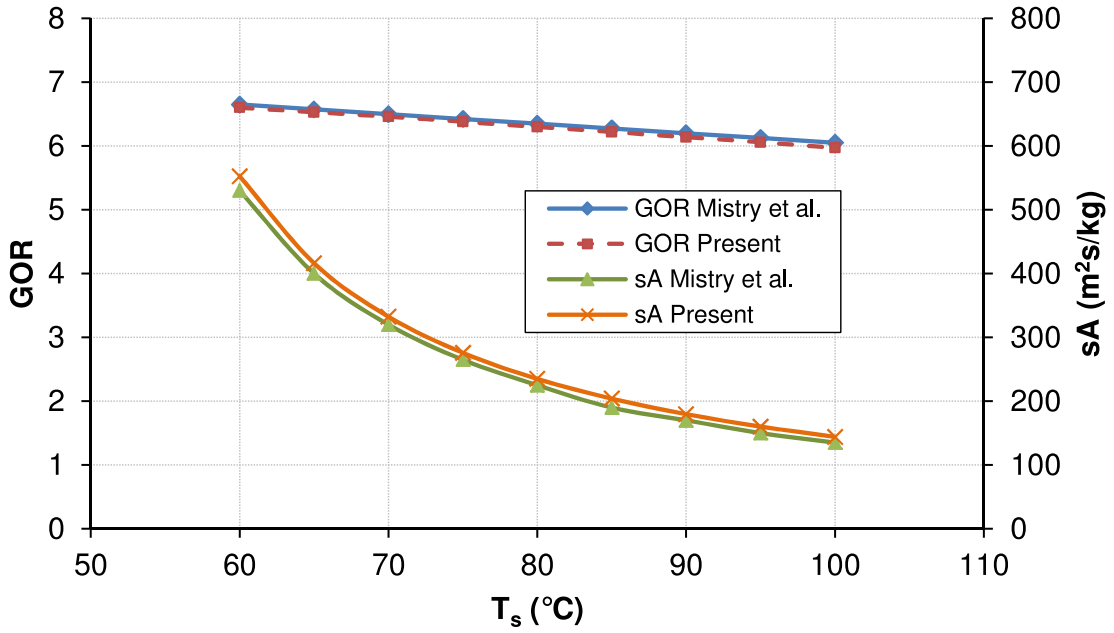

Figure 3.6. Comparison of the GOR and specific heat transfer area (sA) as function of the heating steam temperature (T_s) using the model from Mistry et al. (2013) and the present one.

3.3.2 Sensitivity analysis

In this section several key parameters for the design and operation of MED-FF systems, such as number of effects, temperature difference between effects, fraction of steam condensed in the preheaters, mass flow rate of distillate produced in each effect, etc. are analysed using the developed model. The base case selected for the sensitivity analysis is the one described in Mistry et al. (2013), previously defined in Section 3.3.1, but changing the last effect temperature for the TTD in the end condenser, which is chosen as 5 °C. As the temperature increase of the seawater at the end condenser is fixed (10 °C), the condensation temperature is also specified to 40 °C. Also, the thermodynamic losses have been minimized by removing all the demisters except the first one and increasing the diameters of the connecting lines and evaporator tubes.

3.3.2.1 Temperature difference between effects and preheaters

The difference of temperature between effects is an important parameter for the design of MED units and represents the driven force of the evaporation process in each effect. An increase of the number of effects, maintaining the total temperature difference constant, produces a decrease of the temperature drop between effects, as depicted in Figure 3.7, and consequently, a significant growth of the specific heat transfer area. Therefore, there is a practical limit in the maximum number of effects in MED plants related to an allowable temperature difference

between effects, which usually lies between 2 and 3 °C (Cipollina et al., 2005). Noteworthy, the effective temperature difference should discount the thermodynamic losses which further limit the practical number of effects. Moreover, the temperature drop profile along effects show only a slightly variation for each case. Similar trends are observed for the temperature difference between preheaters, as shown in Figure 3.8. It can be seen how the temperature variation decreases with the elevation of the number of effects, ant their values are approximately equal to those of the temperature differences between effects. In the particular case simulated, if 3 °C is selected as a reasonable value for the temperature difference, the number of effects should be below 10.

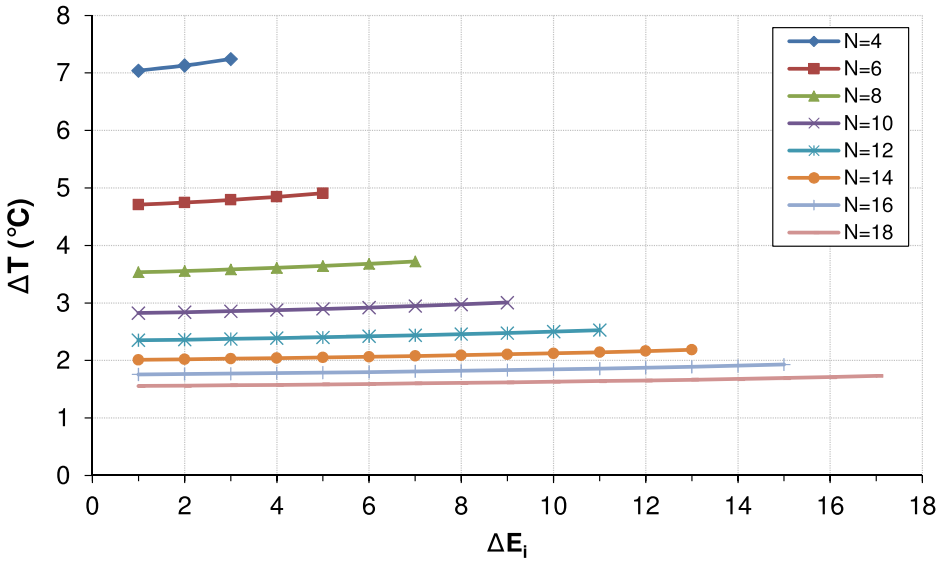

Figure 3.7. Difference of temperature between effects for different number of effects, from $N = 4$ to 18.

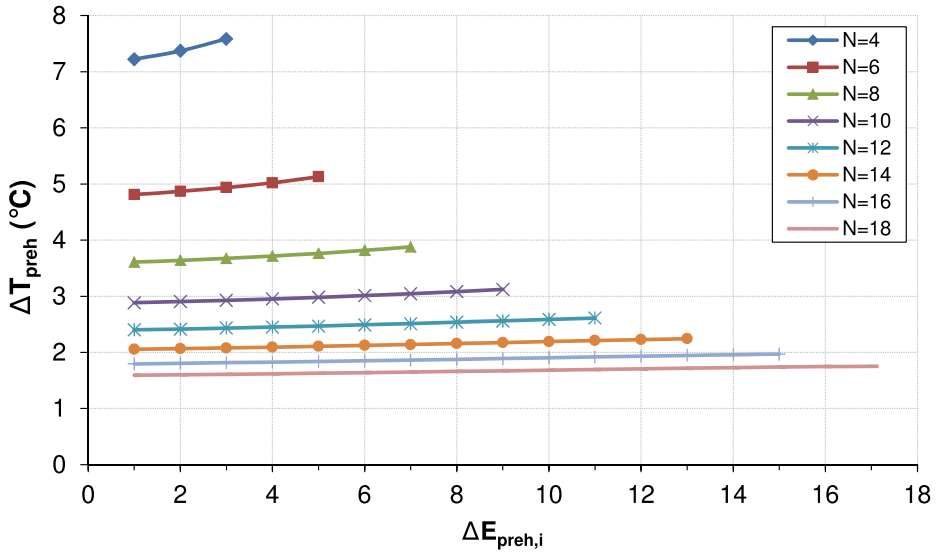

Figure 3.8. Difference of temperature between preheaters for different number of effects, from $N = 4$ to 18.

3.3.2.2 Mass fraction of vapour condensed in the preheaters

In this model it has been assumed that a fraction of the total vapour generated in each effect (by boiling in the evaporator, flash of the sprayed brine, and flash of the distillate collected in the flash box), denoted by α, condenses in the outer surface of the tubes in the preheater. The amount of condensed steam is directly associated with the boundary conditions imposed for solving the model, specifically the level of preheating of the feedwater. In this case the TTD of the preheater associated with the first effect is fixed to 5 °C, which is the difference of temperature between the TBT and the seawater entering the first effect, while for the rest there are not restrictions imposed. Figure 3.9 shows how the mass of vapour condensed is higher within the first preheaters and decreases gradually up to the last, possibly due to the lower temperature level of the vapour from the last effects.

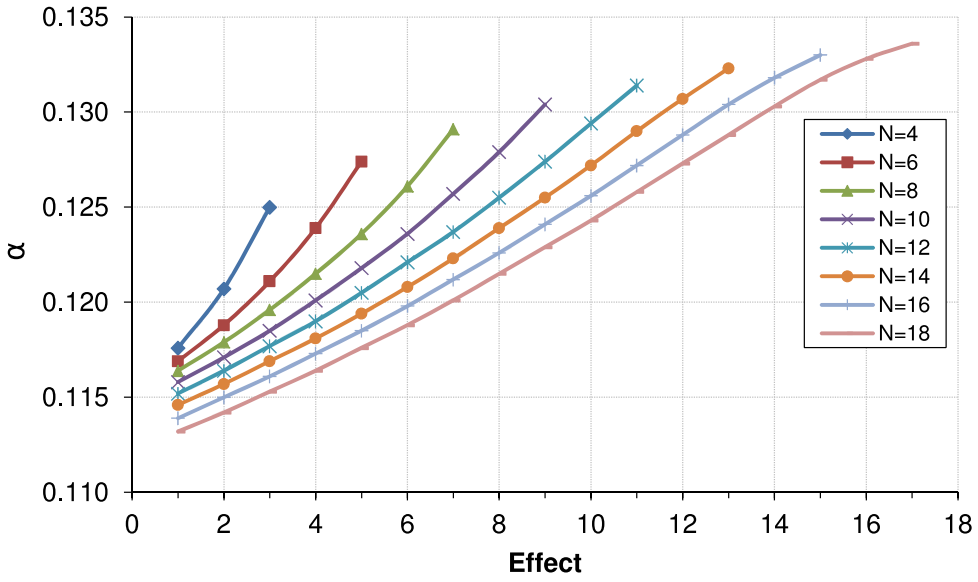

Figure 3.9. Fraction of vapour condensed in each preheater as function of the number of effects, from $N = 4$ to 18.

3.3.2.3 Terminal temperature difference of the preheaters

The terminal temperature difference of the preheaters for different number of effects is depicted in Figure 3.10, tending to increase along the plant from the minimum value, 5 °C, which is reached in the preheater associated with the first effect. These parameters are important because they have a great influence on the temperature of the seawater entering the first effect. The higher this temperature is, the lower thermal consumption needed, due to the less thermal energy required to preheat the seawater up to the saturation temperature. However, the area needed in the heat exchangers increases significantly, so the selection of this parameter should account for this trade-off.

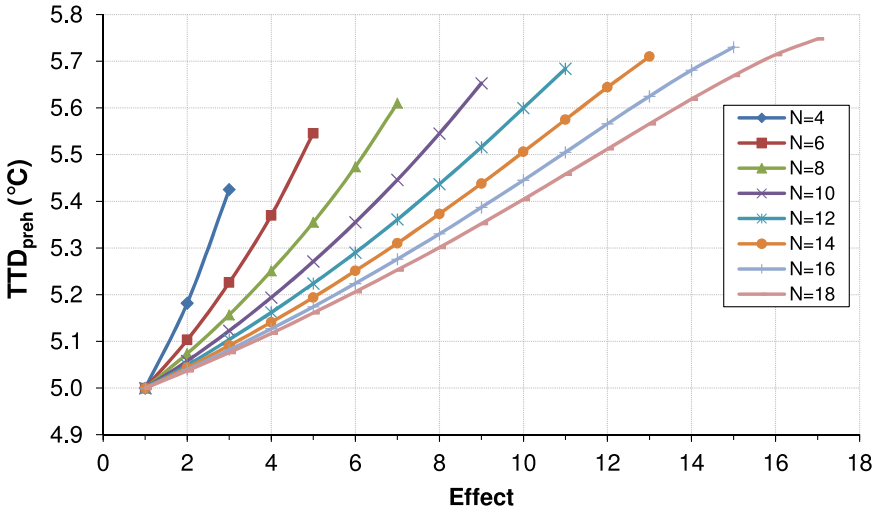

Figure 3.10. Terminal temperature difference in the preheaters as function of the number of effects, from N=4 to 18.

In the base case of study, the terminal temperature difference of the preheater associated with the first effect was set to 5 °C, as a conservative value (typically ranges from 3 – 5 °C). The effect of the variation of this parameter on the GOR and sA is presented in Figure 3.11. As mentioned above, a decrease in TTD_{preh1} improves the GOR but also increases the specific heat transfer area. It is needed a compromise solution between the size of the heat exchanger (and therefore its cost) and the thermal efficiency of the plant. For values lower than 4 – 3 °C, the specific heat transfer area grows markedly.

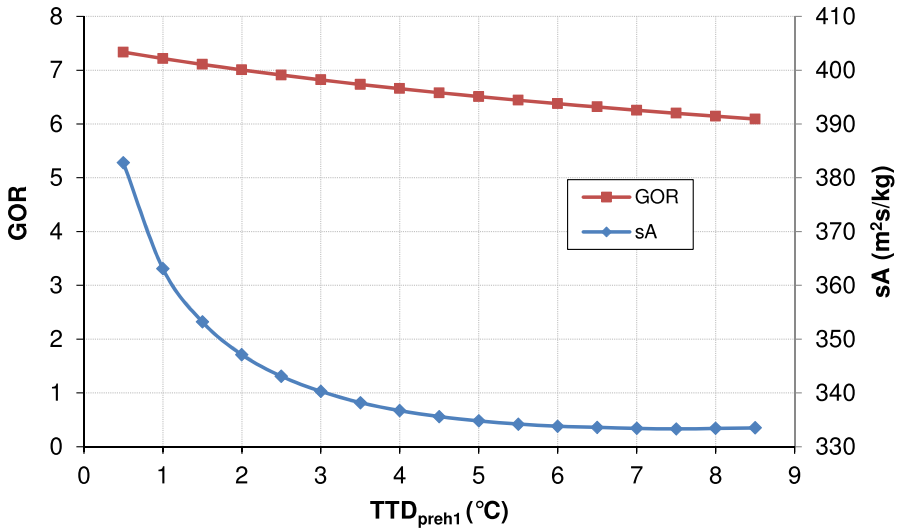

Figure 3.11. Gain output ratio and specific heat transfer area as function of the terminal temperature difference at the preheater of the first effect.

3.3.2.4 Vapour produced by boiling in each effect

The distribution of the vapour produced by boiling in each effect, for different number of effects, is depicted in Figure 3.12. The vapour produced slightly decreases in each effect, starting from the first. As a first approximation and in the case of high number of effects, the vapour produced in each effect may be considered constant as its variation is small. However, the small decrease could be caused by the increase on the specific enthalpy of evaporation of the seawater and the thermodynamic losses along the effects.

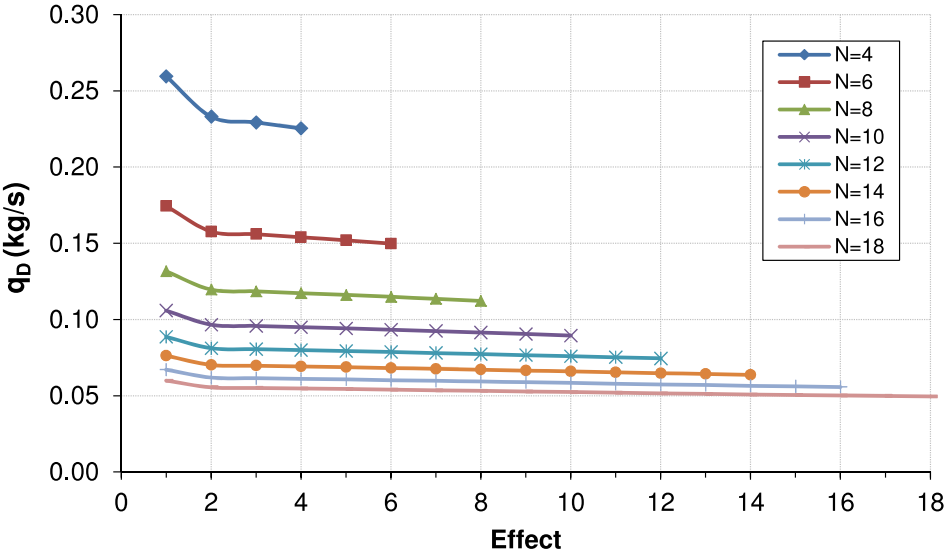

Figure 3.12. Mass flow rate of vapour produced by boiling in each effect, as function of the number of effects.

3.3.2.5 Internal diameter of the pipes connecting the effects

In the base case considered the distillate production has been fixed as 1 kg/s, which is a typical value used in the literature for the analysis of MED models. Nevertheless, it is interesting to investigate the influence of this parameter on the pressure losses of the vapour in the connecting lines between effects, which will eventually affect to the efficiency and heat transfer area of evaporators. For this purpose, different internal diameter of the pipes between effects have been considered, from 1000 mm to 200 mm, and the distillate production has been varied from 1 kg/s to 35 kg/s (nearly 86 and 3024 m^3/d, respectively), as shown in Figure 3.13. As the larger pressure loss inside the pipes of the connecting lines takes place on the last effect, where the vapour is driven to the end condenser, it has been selected for the simulation as the key design parameter. In addition, same features of the base case have been used along with the data presented in Table 3.3. Also, for this analysis, the presence of all the demisters has been considered and the thermodynamic losses have been accounted.

Table 3.3. Features of demisters, pipes connecting lines and evaporators.

Parameter	Value
Length of connecting lines, m	2
Length of evaporator tubes, m	5
External diameter of evaporator tubes, m	0.030
External diameter of evaporator tubes, m	0.029
Wire diameter of demisters, mm	0.28
Density of demisters, kg/m^3	280
Mesh pad thickness of demisters, m	0.15
Diameter of the vessel, m	4.8

From Figure 3.13 it is concluded that the pressure losses greatly increase with the distillate production when the internal diameter of the connecting lines is lower than 400 mm. In fact, for an internal diameter of 300 mm and a daily production of 3000 m^3/d, the pressure losses due to friction inside the pipe connecting the last effect and the end condenser are of 2145 Pa, which results in a saturation temperature drop of the vapour of almost 5 °C, as it can be seen in Figure 3.14. These are unfeasible conditions because the value of the thermodynamic losses in that case would rapidly increase the specific heat transfer area (see Figure 3.15), due to the decrease on the temperature difference between the condensing vapour inside the evaporator and the boiling brine in the corresponding effect. Typically, the total thermodynamic losses may vary in the range of 0.5 – 3 °C (El-Dessouky and Ettouney, 2002), so the minimum diameter of the pipes connecting the effects should be of 400 mm in this particular case.

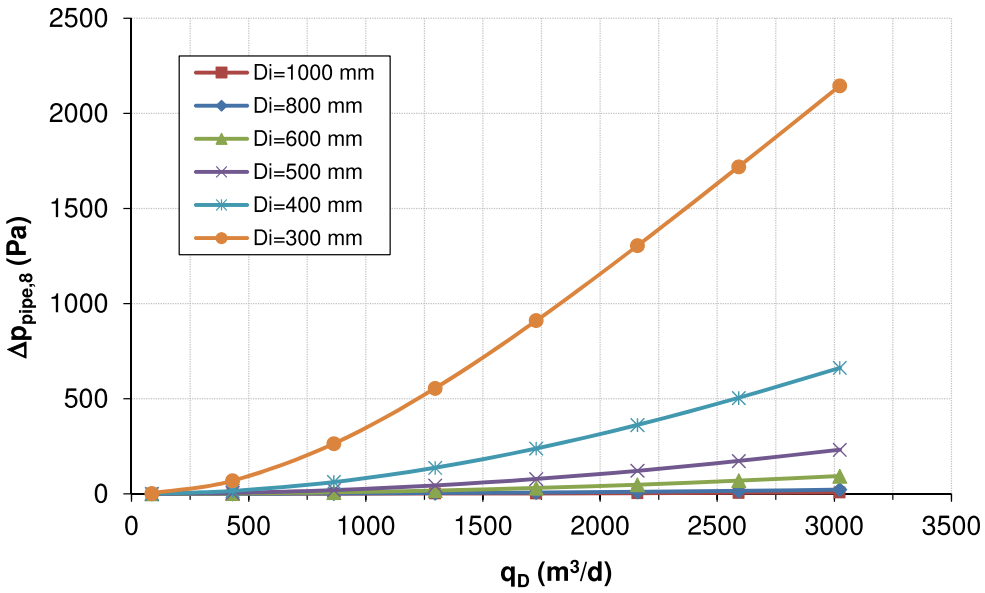

Figure 3.13. Pressure drop in the pipe connecting effect 8 and end condenser as function of the distillate production and for different internal diameters.

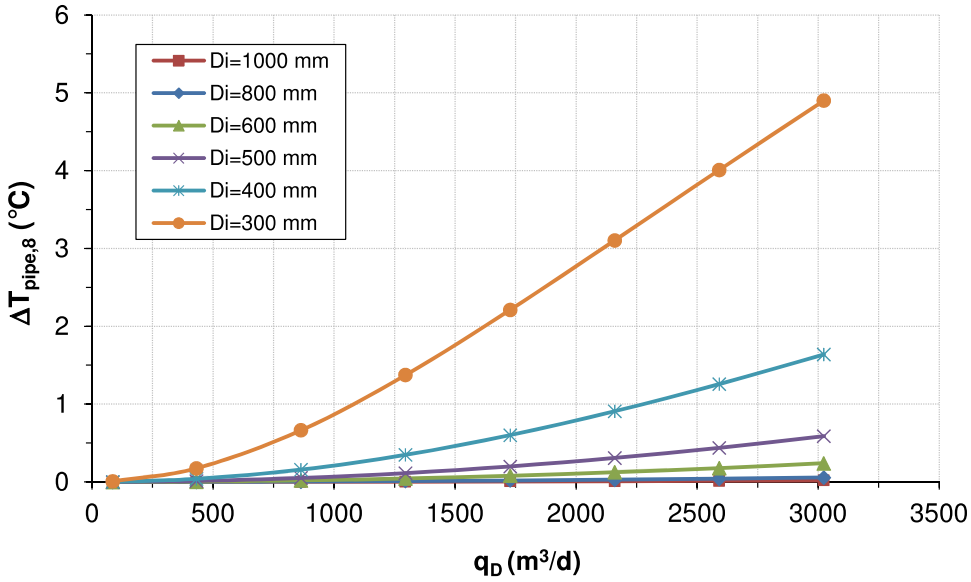

Figure 3.14. Saturation temperature decrease of the vapour in the pipe connecting effect 8 and end condenser as function of the distillate production and for different internal diameters of the pipes.

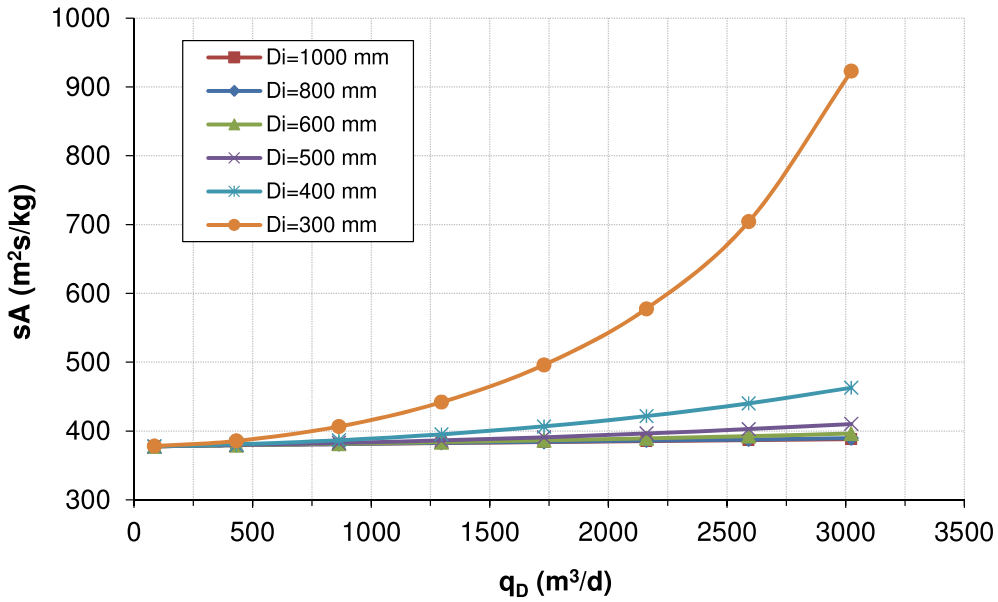

Figure 3.15. Specific heat transfer area as function of the distillate production and for different internal diameters of the pipes connecting the effects.

3.3.2.6 Intake seawater salinity

The salinity of the intake seawater is an important design parameter which depends on the location of the plant. Although the mean salinity of the seawater is typically considered as 35 g/L (South Atlantic ocean), some areas of the world present higher salinity values, like the Red Sea and Arabian Gulf region, with seawater salinity of around 40 and 50 g/L, respectively (Bower et al., 2000). Therefore, the influence of this parameter on the GOR, sA and specific flow rate of cooling seawater (sq_{cw}), defined as the mass flow rate of cooling seawater per unit of distillate produced, has been analyzed and the results are presented on Figure 3.16. It can be seen how the GOR and the sq_{cw} decrease with the increase in the intake seawater salinity, while the sA varies slightly reaching a maximum for a specific value of the salinity. The raise of the intake seawater salinity reduces the recovery ratio, all other variables maintained constant, and therefore increases the feedwater flow rate. Moreover, it decreases the rejected cooling seawater as the distillate production does not vary and the amount of total vapour to be condensed at the end condenser is almost the same. Hence, the intake seawater entering the end condenser does not change significantly. The reduction of the GOR may be explained by lower preheating of the feedwater flow rate, which is greatly reduced due to the increase of the feedwater flow rate. Because of that, the heat added in the first effect must be higher and more heating steam flow rate is consumed.

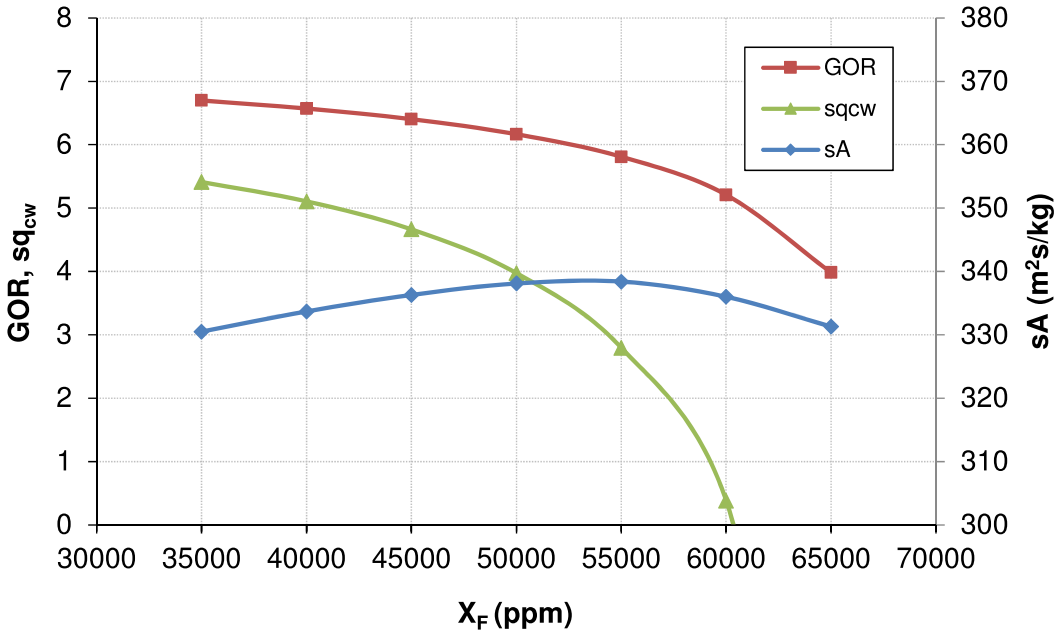

Figure 3.16. Gain output ratio, specific heat transfer area and specific flow rate of cooling seawater as function of the feed salinity.

3.4 Analysis of the MED process with high heating steam temperature

In this section it is analysed the increase of the heating steam temperature in order to reach higher thermal efficiency on the MED process, which permits to rise the number of effects up to a limit imposed by the minimum temperature difference between effects. The simulations have been done with the same inputs that the base case but changing the last effect temperature from 40 °C to 35 °C and a temperature increase of the seawater in the end condenser from 10 °C to 7 °C. The analysis has been carried out taken into account temperature differences between effects in the range of 2 – 4 °C.

The influence of the minimum temperature difference between effects on the GOR is analysed in Figure 3.17, for different number of effects and for three different heating steam temperatures: 70 °C, 100 °C and 120 °C. It is observed that a decrease in the temperature difference between effects increases the GOR significantly in all the cases, and the elevation of the heating steam temperature has also a great influence on the GOR. As an example, for a mean temperature difference of 2.5 °C, the maximum number of effects for heating steam temperatures of 70, 100 and 120 °C are 14, 26 and 34, with GOR of 10.38, 15.34 and 17.6, respectively.

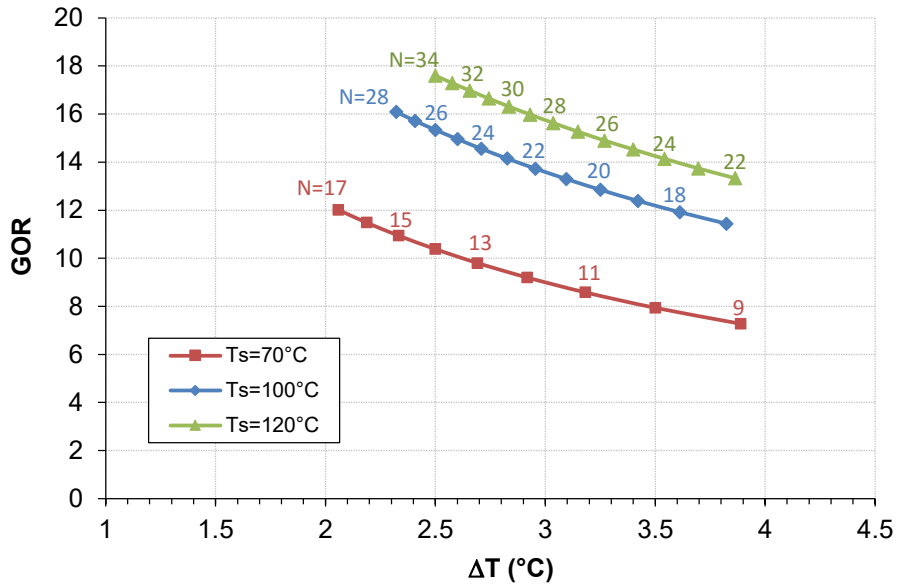

Figure 3.17. Gain output ratio as function of the mean temperature difference between effects and the number of effects, for each heating steam temperature.

As commented before, when the temperature difference between effects is reduced, for a given heating steam temperature, the specific heat transfer area rapidly increases. This can be clearly seen in Figure 3.18. But if at the same time the heating steam temperature is increased, more effects can be considered with a similar temperature drop, and the corresponding specific heat

transfer area is reduced. Particularly, for a temperature difference of 2.5 °C, and heating steam temperatures of 70, 100 and 120 °C, the resulting number of effects are 14, 26 and 34, with sA of 518.2, 483.1 and 463.9 $m^2/(kg/s)$. The reduction of the specific heat transfer area with the rise of the heating steam temperature, all other variables maintained constant, may be attributed to the improvement in the heat transfer process, specifically higher values of the overall heat transfer coefficients in the evaporators.

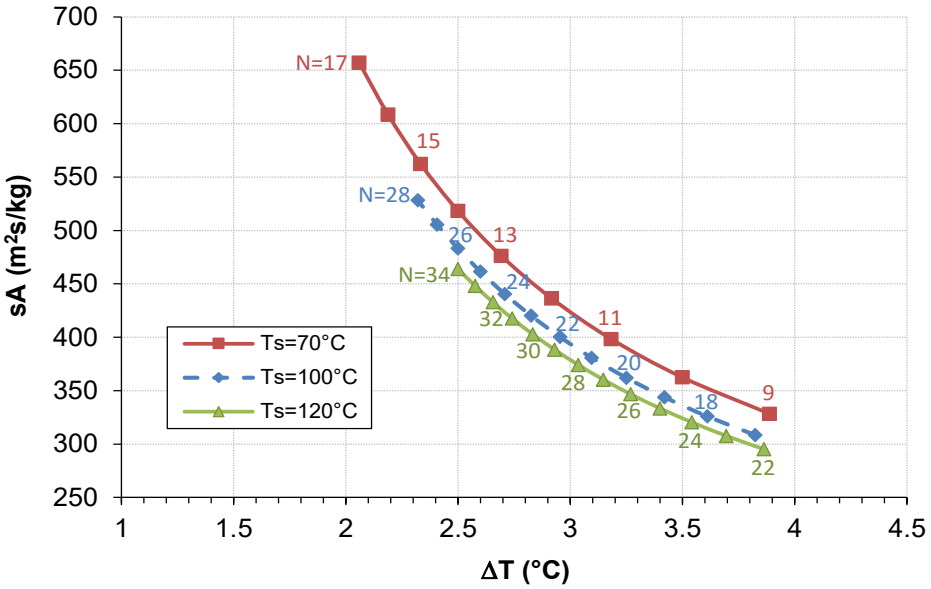

Figure 3.18. Specific heat transfer area as function of the mean temperature difference between effects and the number of effects, for each heating steam temperature.

Also, for a given freshwater production and heating steam temperature, further increase of the number of effects exploits the thermal energy introduced in the system and reduces the specific thermal energy consumption, sE, as it is depicted in Figure 3.19. In addition, if the temperature difference between effects is kept constant, increasing the heating steam temperature also decreases the specific energy consumption because more effects can be introduced, which permits additional reuses of the thermal energy contained in the vapour. For the particular case considered of a difference of temperature of 2.5 °C, the sE is 61.98, 40.54 and 34.49 kWh/m^3 for 70, 100 and 120 °C, respectively.

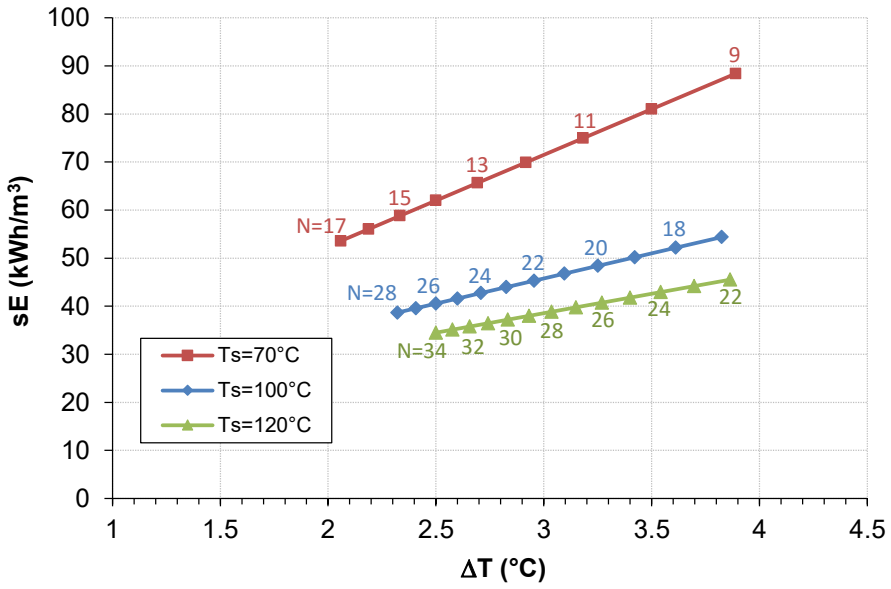

Figure 3.19. Specific thermal energy consumption as function of the mean temperature difference between effects and the number of effects, for each heating steam temperature.

3.5 Conclusions

In this work the improvement possibilities of the MED process have been investigated by rising the top brine temperature up to 120 °C, based on seawater pretreatments such as nanofiltration membranes. Particularly, an analysis of the thermal efficiency, specific heat transfer area and specific energy consumption as function of the number of effects and temperature difference between effects has been fully addressed. For this purpose a detailed MED-FF mathematical model has been developed including the thermodynamic losses of the vapour, and different key design parameters have been also evaluated. From the results obtained, the main conclusions reached are presented.

- Increasing the number of effects in a MED-FF process by elevating the top brine temperature, using seawater pretreatments such as nanofiltration membranes, that removes the bivalent ions (Ca^{2+}, Mg^{2+}, $SO_4^{=}$, etc.), significantly improves the GOR, decreases the specific heat transfer area and reduces the specific energy consumption. Particularly, for a difference of temperature between effects of 2.5 °C, if the heating steam temperature increases from 70 to 120 °C, the number of effects can be raised from 14 to 34, the GOR improves about 70% (from 10.38 to 17.6), the specific heat transfer area reduces a 11% (from 518.2 to 463.9 m^2/ (kg/s)) and the specific energy consumption a 45% (from 61.98 to 34.49 kWh/m^3).
- For a fixed heating steam temperature, the decrease of the temperature difference between effects permits to increase the number of effects, which elevates the GOR

but at the expense of greatly increase the specific heat transfer area. For instance, a reduction in the temperature difference from 3.5 to 2.5 °C with a heating steam temperature of 70 °C allows to increase the number of effects from 10 to 14. In this case the GOR increases nearly 31% (from 7.9 to 10.4), the sA grows a 143% (from 362.4 to 518.2 m^2s/kg) and the sE is reduced a 24% (from 81 to 62 kWh/m^3).

- From the sensitivity analysis carried out, it has been observed that the terminal temperature difference of the vapour in the preheater associated with the first effect has a great influence on the thermal efficiency of the process because determines the preheating degree of the seawater. However, augmentation of the specific heat transfer area limits the minimum value of this design parameter.
- Effects known in the literature as thermodynamic losses, namely BPE, NEA and saturation temperature losses due to pressure drop in demister, connecting lines and inside the evaporator tubes, considerably increase the specific heat transfer area as they reduce the effective temperature difference between effects. Geometrical features such as internal diameters of the tubes connecting the effects or the length of the tube-bundle of the evaporators are critical. Also, the specific heat transfer area increases with the distillate production because of the augmentation of the pressure losses.

Acknowledgement

The authors wish to thank the European Commission (DG for Research & Innovation) for its financial assistance within the Integrated Research Programme in the field of Concentrated Solar Power (CSP) (STAGE-STE Project; Grant Agreement No. 609837).

References

Al-Hamzah, A.A., Fellows, C.M., 2015. A comparative study of novel scale inhibitors with commercial scale inhibitors used in seawater desalination. Desalination 359, 22–25. doi:10.1016/j.desal.2014.12.027

Bower, A.S., Hunt, H.D., Price, J.F., 2000. Character and dynamics of the Red Sea and Persian Gulf outflows. J. Geophys. Res. Ocean. 105, 6387–6414. doi:10.1029/1999JC900297

Cipollina, A., Micale, G., Rizzuti, L., 2005. A critical assessment of desalination operations in Sicily. Desalination 182, 1–12. doi:10.1016/j.desal.2005.03.004

El-Dessouky, H., Alatiqi, I., Bingulac, S., Ettouney, H., 1998. Steady-state analysis of the multiple effect evaporation desalination process. Chem. Eng. Technol. 21, 437–451. doi:10.1002/(SICI)1521-4125(199805)21:5<437::AID-CEAT437>3.0.CO;2-D

El-Dessouky, H.T., Ettouney, H.M., 2002. Fundamentals of Salt Water Desalination. Elsevier.

El-Sayed, Y.M., Silver, R.S., 1980. Chapter 2 – Fundamentals of Distillation, in: Spiegler, K.S., Laird, A.D.K. (Eds.), Principles of Desalination. Academic Press, pp. 55–109. doi:10.1016/B978-0-12-656701-4.50008-5

ESDU, 1993. Condensation inside tubes: pressure drop in straight horizontal tubes. ESDU Heat Transf. Ser. Sect. 10 Condens.

Fiorini, P., Sciubba, E., Sommariva, C., 2001. A new formulation for the non-equilibrium allowance in MSF processes. Desalination 136, 177–188. doi:10.1016/S0011-9164(01)00180-1

Friedel, L., 1979. Improved friction pressure drop correlations for horizontal and vertical two-phase pipe flow. Eur. Two-Phase Flow Gr. Meet.

Hamed, O.A., 2005. Overview of hybrid desalination systems — current status and future prospects. Desalination 186, 207–214. doi:10.1016/j.desal.2005.03.095

Hassan, A.M., 1999. Process for desalination of saline water, especially sea water, having increased product yield and quality. WO/1999/016714.

Hassan, A.M., Al-Sofi, M.A.K., Al-Amoudi, A.S., Jamaluddin, A.T.M., Farooque, A.M., Rowaili, A., Dalvi, A.G.I., Kither, N.M., Mustafa, G.M., Al-Tisan, I.A.R., 1998. A new approach to membrane and thermal seawater desalination processes using nanofiltration membranes (Part 1). Desalination 118, 35–51. doi:10.1016/S0011-9164(98)00079-4

Klein, S.A., 2013. Engineering Equation Solver Software (EES).

Mistry, K.H., Antar, M.A., Lienhard, J.H., 2013. An improved model for multiple effect distillation. Desalin. Water Treat. 51, 807–821. doi:10.1080/19443994.2012.703383

Miyatake, O., Murakami, K., Kawata, Y., Fujii, T., 1973. Fundamental experiments with flash evaporation. Heat Transf. Jpn. Res. 2, 89–100.

Nayyar, M.L., 2006. Piping handbook [WWW Document]. URL

http://site.ebrary.com/id/10226666

Sharqawy, M.H., Lienhard V, J.H., Zubair, S.M., 2010. Thermophysical properties of seawater: A review of existing correlations and data. Desalin. Water Treat. 16, 354–380. doi:http://dx.doi.org/10.5004/dwt.2010.1079

Wagner, W., Pruß, A., 2002. The IAPWS formulation 1995 for the thermodynamic properties of ordinary water substance for general and scientific use. J. Phys. Chem. Ref. Data 31, 387–535.

Wilf, M., Awerbuch, L., 2007. The guidebook to membrane desalination technology : reverse osmosis, nanofiltration and hybrid systems : process, design, applications and economics. Balaban Desalination Publications, L'Aquila, Italy.

Zhou, D., Zhu, L., Fu, Y., Zhu, M., Xue, L., 2015. Development of lower cost seawater desalination processes using nanofiltration technologies — A review. Desalination 376, 109–116. doi:10.1016/j.desal.2015.08.020

Chapter 4. Preliminary model of TVC-MED plants coupled to parabolic trough concentrating solar power plants

Part of this chapter has been published as a scientific article in *Desalination and Water Treatment*, 2016. pp. 1-12. Article in Press. doi:10.1080/19443994.2016.1173377

Title:

"Quasi-steady state simulations of thermal vapour compression multi-effect distillation plants coupled to parabolic trough solar thermal power plants"

Authors:

Bartolomé Ortega-Delgado. Affiliation: CIEMAT-Plataforma Solar de Almería, Ctra. de Senés s/n, 04200 Tabernas, Almería, Spain. E-mail: bartolome.ortega@psa.es

Patricia Palenzuela. Affiliation: CIEMAT-Plataforma Solar de Almería, Ctra. de Senés s/n, 04200 Tabernas, Almería, Spain. E-mail: patricia.palenzuela@psa.es. Corresponding author.

Diego-César Alarcón-Padilla. Affiliation: CIEMAT-Plataforma Solar de Almería, Ctra. de Senés s/n, 04200 Tabernas, Almería, Spain. E-mail: diego.alarcon@psa.es

Lourdes García-Rodríguez. Department of Energetic Engineering, Seville University, ETSI, Camino de los Descubrimientos s/n, 41092 Sevilla, Spain. E-mail: mgarcia17@us.es

Abstract

The evaluation of the coupling of a 50 MW_e Parabolic Trough Concentrating Solar Power plant (PT-CSP) and a 10,000 m^3/d Multi-Effect Distillation plant with Thermal Vapour Compression (MED-TVC) was performed. To that end, a model for the entire system has been developed and implemented within Engineering Equation Solver and Matlab software environments. Two coupling arrangements between the PT-CSP plant and the MED-TVC unit were selected: one taking low pressure steam (at 1.224 bar) from the power block to feed the MED-TVC and the other one taking high pressure steam (at 20.6 bar), and the simulations of the electricity and fresh water production of the PT-CSP+MED-TVC plant to be located in Almería (Spain) were carried out during three days in summer (21st–23rd June) and three days in winter (21st–23rd December). Results obtained showed that the use of the low pressure steam to feed the MED-

TVC plant reduces the electricity penalization compared with the use of high pressure steam but also decreases the fresh water production. Since in Spain the electricity demand is lower in summer than in winter, and the contrary occurs with the fresh water demand, the optimum coupling arrangement in summer was using high pressure steam to feed the MED-TVC (enough steam available in the turbines) and that one in winter was to feed the MED-TVC with low pressure steam having the lower electricity penalization at the cost of the decrease of the fresh water production.

Keywords: concentrating solar power, desalination, modelling, multi-effect distillation, parabolic trough

Contents

List of figures

Appendix 4-B

List of tables

Nomenclature

Variables

p	Pressure, bar
E	Thermal energy, kWh
E_b	Direct normal irradiance, W/m^2
h	Specific enthalpy, kJ/kg
P	Thermal power, kW or MW
q	Mass flow rate, kg/s
T	Temperature, °C
UA	Heat exchanger constant, kW/m^2°C
W	Specific energy, kJ/kg

Acronyms and abbreviations

AF	Anti-Freeze System
BRICS	Brazil, Russia, India, China and South Africa
C	Cold Tank
CP	Condensate Pump
CSP	Concentrating Solar Power
CSP+D	Concentrating Solar Power and Desalination
CTP	Cooling Tower Pump
DSH	Desuperheater
EES	Engineering Equation Solver
EV	Expansion Vessel
FWH	Feedwater Heater
G	Electric Generator
GOR	Gain Output Ratio
H	Hot Tank
HCE	Heat Collection Elements
HP	High Pressure Turbine
HTF	Heat Transfer Fluid
HX	Heat Exchanger
LP	Low Pressure Turbine
MED	Multi-Effect Distillation
PB	Power Block

PC	Parallel-Cross
PH	Preheater
PT	Parabolic Trough
RH	Reheater
SCA	Solar Collector Assembly
SCE	Solar Collector Element
SF	Solar Field
SG	Steam Generator
SH	Superheater
CSP	Concentrating Solar Power
TES	Thermal Energy Storage
TMY	Typical Meteorological Year
TVC	Thermal Vapour Compression
UT	Universal Time

Subscripts

b	Direct normal
D	Distillate
gen	Generator
m	Motive
opt	Optical
ref	Reference
s	Isentropic
T	Total
t	Turbine
th	Thermal
u	Useful
v	Vapour

Greek symbols

α	Fraction of the total mass flow rate used in each extraction
β	Reduction of evaporator areas after the thermo-compressor extraction
η	Efficiency
τ	Receiver glass transmissivity

4.1 Introduction

The increase of the global population and the rise in the agrarian and industrial activities is leading to a continuous growth of the electricity and water demands. This has become a significant issue in developing countries with emerging economies, like those within the BRICS (Brazil, Russia, India, China and South Africa) group or those located in the Middle East, which will represent a major share of the worldwide population raise in the next decades.

Conventional power production systems based on fossil fuels are known to cause the global warming, mainly due to the CO_2 emissions to the atmosphere. Moreover, these systems rely on a limited source of energy (coal, oil, etc.) that will eventually run out. In this context, it is necessary the use of a mix of energy sources (conventional and renewable) to produce the power supply in the near future. Concentrating Solar Power plants (CSP) have been proved as reliable systems to produce electricity using solar irradiation as the energy source (NREL, 2015; Torresol Energy, 2015). Their use has sense in regions of the world with high direct normal solar irradiation levels. Sometimes these zones also suffer from severe water stress (caused by the physical scarcity of fresh water or by the absence of facilities to extract the water from the natural sources) and they are located close to the sea. In these scenarios, the integration of CSP and Desalination plants, concept known as CSP+D, represents an opportunity to partially solve the energy and water supply problems of these areas.

This chapter analyses the integration of Multi-Effect Distillation plants with Thermal Vapour Compression (MED-TVC) into Parabolic Trough Concentrating Solar Power plants (PT-CSP), based on the electricity and fresh water demands in Spain, which are variable during the year. The integration of the MED-TVC plant was made by taking steam from one of the extractions of the Power Block (PB) to feed the thermo-compressor. The comparison of the electricity production penalties and the fresh water production in different periods of the year, along with the suitability of using one coupling arrangement or another, is presented and discussed in this paper.

4.2 Methodology

The model of the whole system, PT-CSP+MED-TVC plant, has been developed by modelling the three subsystems: the solar field, the power block and the desalination unit. The details of each one are explained in the following sections. Two possible coupling arrangements between the PT-CSP plant and the MED-TVC unit have been considered (as shown in Figure 4.1): the first option consists in using steam from one of the extractions from the low pressure turbine of the power block (E1 to E4) to feed the MED-TVC while the second uses steam from one of the extractions from the high pressure turbine (E5 and E6). Once the whole model has been developed, the simulation tool have been used to assess the thermal efficiency, the electricity and the water production of the integrated plant during three representative days in summer and three representative days in winter.

4.2.1 Solar field

The solar field considered is a parabolic trough solar field for a CSP plant of 50 MW_e similar to that of Andasol-2 commercial power plant, Therminol VP-1 oil (Eastman Chemical Company, 2015) as the Heat Transfer Fluid (HTF), and Thermal Energy Storage (TES, formed by two tanks with molten salts). The solar field consists of 156 collector loops, with 4 Solar Collector Assemblies (SCA) each one. One SCA is composed by 12 Solar Collector Elements (SCE) with 28 glass facets each. The solar field has a North-South orientation for obtaining the maximum energy on a yearly basis. The collector is a Eurotrough 150 model with the characteristics described in Table 4.1.

Table 4.1. Characteristics of the ET-150 solar collector (Llorente García et al., 2011).

Concept	Value
Gross length, m	150
Net length, m	142.8
Gross aperture width, m	5.77
Net aperture area, m^2	817.5
Focal length, m	1.71
Absorber radius, m	0.035
Mirror reflectivity (ρ)	0.932
Receiver glass transmissivity (τ)	0.96
Absorbance of the metallic pipe (selective coating, α)	0.95
Reduction of the effective absorbing receiver length	0.954
Reduction in the energy absorbed by the receiver due to	1

inaccuracies in the assembly	
Peak optical efficiency ($\eta_{opt,0}$)	0.81
Spacing between rows, m	17.2
Spacing between consecutive SCAs in a row, m	1.5
Spacing between consecutive SCEs in a SCA, m	0.25
Number of SCAs in a row	2
Number of SCEs in a SCA	12

The modelling of the solar field has been taken from Llorente García et al. (2011), which has been validated with actual data from Andasol-2, showing excellent agreement. It consists basically in applying an energy balance on a receiver control volume assuming a linear and discrete approximation over the governing differential equations in order to simplify the problem. Thus the time step must be small enough, lower than 10 s, otherwise the error committed in the temperatures calculation would be significant. This model considers the solar field as a closed circuit with all the collectors equally disposed and an insulated pipe network for the HTF distribution. Each day is divided into four periods: a night time period before the sunrise, a start-up period for warming the HTF and initiate the power block operation, a full operation period up to the sunset, and a second night time period. The HTF temperatures in each collector and in the insulated pipes are supposed to be uniform and they are obtained by iteration starting from the initial guesses.

The model uses data of the direct normal irradiance, ambient temperature and wind velocity from a Typical Meteorological Year (TMY) generated by the software Meteonorm (2015), being the average yearly solar irradiation and ambient temperature in good agreement with actual data provided by a solar station located in the selected area. The plant was considered to be located in Almería, SE of Spain (longitude 2.215W and latitude 37.06N). The design inlet and outlet HFT temperatures in the solar field were 296 °C and 390 °C, respectively. It was considered a maximum limit for the thermal energy absorbed by a collector loop (1.8 MW_{th}), which guarantees not to surpass the maximum design value of the outlet HTF temperature, and for the thermal power sent to the power block (140 MW_{th}), which corresponds to a maximum net electric power of 50 MW_e. Notice that during the only-TES operation there is a decrease in the electricity production since the maximum limit for the energy sent to the PB was established at 119 MW_{th} because the temperature of the salts is lower than the nominal HTF temperature. Following the same operation strategy as in Llorente García et al. (2011), it was assumed that the steam generator starts to produce steam for the electricity generation once the HTF outlet temperature is 310 °C.

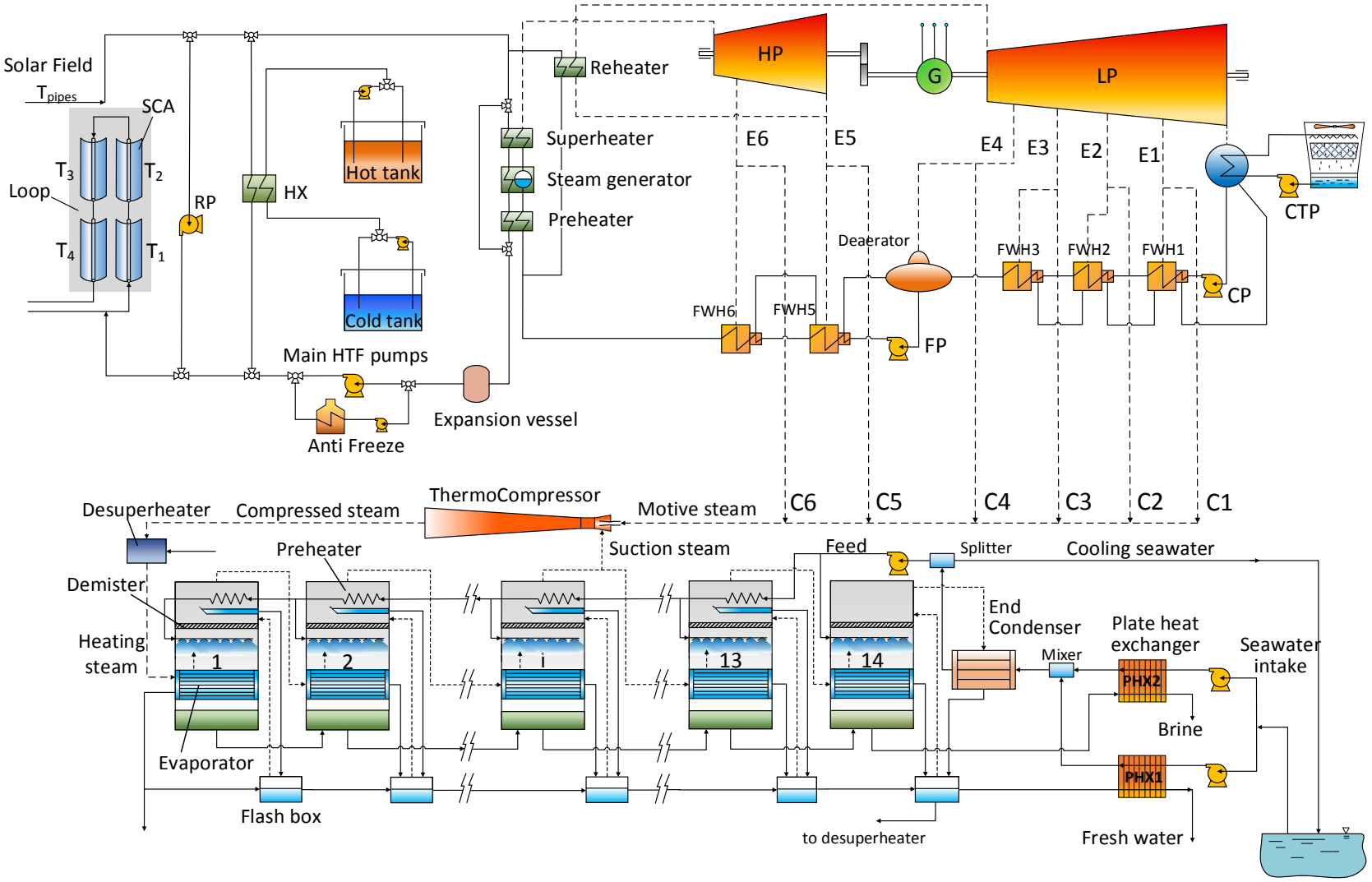

Figure 4.1. Scheme of the overall system where the different alternatives of feeding the thermocompressor (C1 to C6) are represented.

Nomenclature: AF=Anti-Freeze system; C=Cold tank; CP=Condensate Pump; CTP=Cooling Tower Pump; DSH=Desuperheater; E1-E6=turbine steam extractions; EV=Expansion Vessel; FP=Feeding Pump; FWH=Feed Water Heater; G=Electric Generator; HX=Heat Exchanger; HP=High Pressure turbine; H=Hot tank; LP=Low Pressure turbine; PH=Preheater; RP=Recirculating Pump; RH=Reheater; SF=Solar Field; SG=Steam Generator; SH=Superheater; T=Temperature

4.2.2 Multi-effect distillation plant with thermal vapour compression

The design of this system is based on the MED-TVC plant located in Trapani (Italy) (Temstet et al., 1996). The plant consists basically of 14 effects, 13 preheaters and 14 flashing boxes, in parallel-cross feeding arrangement (see Figure 4.1). The process is based on the evaporation of the seawater and subsequent condensation of the vapour formed, considered free of salts. This process takes place inside pressurized vessels, called effects, which are composed by three main elements: an evaporator, a demister and a preheater. The thermal input required by the process is exclusively supplied in the first effect, called heating steam, which flows inside the tube bundle of the evaporator. The seawater is sprayed over the outer surface of the evaporator tubes, evaporating part of it due to the heat released by the condensation of the heating steam. The vapour formed goes through the demister, where the droplets are retained, and part of it condenses in the preheater, warming up the feed seawater. The rest of the vapour is driven inside the tubes of the next evaporator, repeating the process. The vapour condensed (from the evaporator and preheater) is collected inside the flashing boxes, where additional flash vapour is produced. The last effect does not have preheater associated but a final condenser. The thermal efficiency of the system can be improved by recompressing part of the vapour formed, using a thermo-compressor. This device is very simple and robust. It uses high pressure steam (called motive steam) to compress low pressure vapour (called suction steam) taken from one of the MED plant effects by the Venturi effect. The vapour at the outlet (called compressed vapour) is a mixture of both vapour and it is at an intermediate pressure.

The mathematical model was developed at steady state and was implemented in the Engineering Equation Solver (EES) (Klein, 2013) environment. It is based on the mass and energy balances applied to the different elements of the plant, along with the heat transfer equations corresponding to the heat exchangers. The input data for the model are detailed in Table 4.2. As output data, the areas of the heat exchangers, the distillate production and the efficiency of the plant were obtained. The latter parameter is defined by the Gain Output Ratio (GOR) which is determined as the ratio of total distillate mass flow rate produced (q_D) to the mass flow rate of motive steam entering the thermo-compressor (q_m):

$$GOR = \frac{q_D}{q_m} \qquad \text{(Eq. 4.1)}$$

For the model of the thermo-compressor, the correlations obtained by Hassan and Darwish (2014), which are suitable for a wide range of operation conditions of the motive steam pressure, were used.

Moreover, a parametric study as function of the motive steam and suction steam pressures was carried out in order to obtain the best coupling arrangement with a PT-CSP plant, in terms of the GOR of the MED-TVC unit and the efficiency in the electricity production of the PT-CSP plant. The motive steam pressures studied were selected from the CSP plant referenced in Montes et al. (2009). Such study was made for optimum values of the specific heat transfer areas (that ones that minimize the heat transfer areas of the effects located after of the thermo-compressor location). Two scenarios were selected in order to match with the variability in the electricity demand: steam extracted from E2 (1.224 bar) and from E5 (20.6 bar) bleeds, namely C2 and C5 streams, as motive steam to feed the MED-TVC plant (see Figure 4.1). The nominal values of the different variables of the MED-TVC unit using both coupling arrangements are presented in Table 4-A.1 in Appendix 4-A**.**

For the simulation of the integrated PT-CSP+MED-TVC plant at partial load operation, it has been supposed that the change in the motive steam mass flow rate is directly proportional to the steam cycle mass flow rate and that the GOR is maintained constant and equal to that one obtained from the parametric analysis in each scenario.

Table 4.2. Main inputs for the design of the MED-TVC plant.

Parameter	**Value**
Design capacity*, m^3/d	10,000
Number of effects	14
Heating steam temperature, °C	70
Intake seawater temperature, °C	25
Intake seawater salinity, ppm	35,000
Rejected brine temperature, °C	37
Maximum brine salinity, ppm	60,000
Temperature difference in final condenser, °C	10
Desuperheater outlet temperature, °C	73
Diameter of the tubes between the effects, mm	600
Tube longitude between the effects, m	2
Tube longitude in evaporators, m	7
External diameter of evaporator tubes, m	0.038
Internal diameter of evaporator tubes, m	0.031
Wire diameter of demisters, mm	0.28
Density of demisters, kg/m^3	280
Mesh pad thickness, m	0.15

* Taking as suction steam that one from the last effect of the MED plant

4.2.3 Power block

The power block corresponds to a regenerative Rankine cycle with reheating and six extractions, for a net power production of 50 MW_e (see Figure 4.2). It consists of two turbines, referenced as high pressure and low pressure, coupled to an electrical generator (at different rotational speeds), a steam generator composed of a preheater, an evaporator, a superheater and a reheater, five closed feedwater heaters, one open feedwater heater (deaerator), a water-cooled condenser (with evaporative tower), two centrifugal pumps: the condensate and feeding pumps, and a condensate mixer. The model, which was implemented in Engineering Equation Solver environment, takes into account the part load operation of the cycle using the equations reported by Montes et al. (2009).

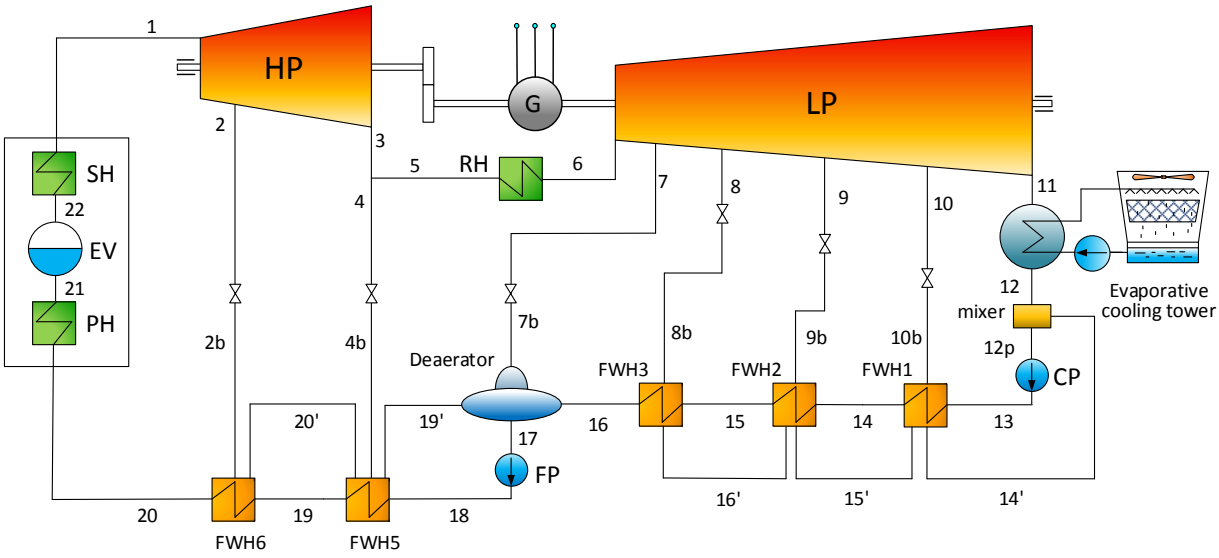

Figure 4.2. Scheme of the power block.

Nomenclature: CP=Condensate Pump; FP=Feeding Pump; FWH=Feed Water Heater; G=Electric Generator; HP=High Pressure turbine; LP=Low Pressure turbine; PH=Preheater; RH=Reheater; SH=Superheater.

Firstly, the cycle was solved under nominal conditions using the inputs of the Table 4.3. For this purpose each point of the cycle was defined by calculating its thermodynamic properties, temperature, pressure, specific enthalpy and specific entropy, along with the steam mass flow rate (see Table 4-A.2 in Appendix 4-A). The thermal efficiency of the cycle at nominal conditions was also determined as follows:

$$\eta_{th} = \frac{W_u}{(h_1 - h_{20}) + (h_6 - h_5) \cdot (1 - \alpha_2 - \alpha_4)} \qquad \text{(Eq. 4.2)}$$

where W_u is the useful mechanical energy generated in the cycle (equal to the energy obtained in the HP and LP turbines minus the energy consumption of the pumps), in kJ/kg, h is the specific enthalpy of the steam, in kJ/kg and α is the fraction of the total mass flow rate used in each extraction.

Table 4.3. Characteristics of the power block at nominal conditions (Montes et al., 2009).

Parameter	**Value**
Turbine	
Inlet temperature (°C)	370
Inlet pressure (bar)	90
High pressure turbine efficiency (%)	85.5
Low pressure turbine efficiency (%)	89.5
Electro-mechanical efficiency (%)	98
Condenser	
Pressure (bar)	0.08
Extraction point pressures	
Point 2 (bar)	45.4
Point 4 (bar)	20.6
Point 7 (bar)	8.75
Point 8 (bar)	3.627
Point 9 (bar)	1.224
Point 10 (bar)	0.346
Pressure drop	
Extraction line no. 1 (%)	2.5
Extraction line no. 2 (%)	3
Extraction line no. 3 (%)	4.5
Extraction line no. 4 (%)	3
Extraction line no. 5 (%)	3
Extraction line no. 6 (%)	3.5
Reheating line (%)	11.75
Condenser pump	
Isentropic efficiency (%)	75
Electro-mechanical efficiency (%)	98
Feedwater pump	
Isentropic efficiency (%)	78
Electro-mechanical efficiency (%)	98
Closed feedwater heaters	
Terminal temperature difference (°C)	1.5
Drain cooling approach (°C)	5
Steam generator	
Thermal efficiency (%)	98
Total pressure drop (water side) (bar)	4.5

At part load conditions, the efficiencies of all the elements of the cycle are reduced. Particularly, the turbine efficiency was determined according to Bartlett's equation (Bartlett, 1958):

$$\%Reduction = 0.191 - 0.409\left(\frac{q_v}{q_{v,ref}}\right) + 0.218\left(\frac{q_v}{q_{v,ref}}\right)^2 \quad \text{(Eq. 4.3)}$$

$$\eta_{s,t} = (1 - \%Reduction) \cdot \eta_{s,t,ref} \quad \text{(Eq. 4.4)}$$

Where q_v and $q_{v,ref}$ are the total steam mass flow rates flowing in the cycle in actual and nominal operation, in kg/s, respectively. On Eq. (4.4) $\eta_{s,t}$ and $\eta_{s,t,ref}$ are the isentropic efficiencies of the turbine in actual and nominal operation, respectively.

There are several control strategies for a steam turbine working in *off-design* conditions. The sliding pressure method has been established, which maintains fixed the steam temperature at the inlet of the turbine and varies the mass flow rate with the steam pressure in the steam generator, using wide open control valves at the governing stage. Therefore, when the power block is working at part load conditions the steam pressure and the mass flow rate of steam decrease, along with the extraction pressures. This pressure drop can be obtained using the *Law of the Ellipse* of Stodola (Stodola and Loewenstein, 1945), rearranged as function of the steam pressures and mass flow rates between any two points of the turbines 1 and 2:

$$\frac{p_1^2 - p_2^2}{p_{1,ref}^2 - p_{2,ref}^2} = \left(\frac{q_v}{q_{v,ref}}\right)^2 \quad \text{(Eq. 4.5)}$$

The generator efficiency also changes at part load operation, and it was obtained using the equation reported by Patnode (2007) for the SEGS VI power plant:

$$\eta_{gen} = 0.908 + 0.258 \cdot Load - 0.3 \cdot Load^2 + 0.12 \cdot Load^3 \quad \text{(Eq. 4.6)}$$

where *Load* is the fraction from nominal operation (expressed in parts per unit).

The closed feedwater heaters have lower efficiency when the load decreases. Patnode (2007) derived the following expression to calculate the UA factor working at part load operation, assuming constant fluid properties, neglecting the fouling and thermal resistance through the tubes, fully developed and turbulent flow inside the tubes and same proportion of the mass flow rates of inner and outer fluids at nominal and part load operation:

$$\frac{UA}{UA_{ref}} = \left(\frac{q_v}{q_{v,ref}}\right)^{0.8} \quad \text{(Eq. 4.7)}$$

Finally, the efficiency of the pumps at the part-load operation was determined as function of the mass flow rate (equation reported by Lippke (1995)):

$$\frac{\eta_s}{\eta_{s,ref}} = e_{m,ref} + 2\left(1 - e_{m,ref}\right)\frac{q_v}{q_{v,ref}} - \left(1 - e_{m,ref}\right)\left(\frac{q_v}{q_{v,ref}}\right)^2 \quad \text{(Eq. 4.8)}$$

where $\eta_{s,ref}$ is the isentropic efficiency of the pumps at nominal conditions and $e_{m,ref}$ a parameter related to the efficiency curves of the pumps (Lippke, 1995) (for constant speed pumps $e_{m,ref} = 0$).

Notice that there is a technical minimum of the thermal input from the solar field below which the turbine is stopped and the electricity production is zero. In this work this value was chosen to be roughly 41 MW_{th} (30% of the nominal load). The results of the power block performance at nominal and part load operation, in only-electricity mode, can be seen in Table 4-A.3 of Appendix 4-A.

4.3 Results

As preliminary results from the parametric analysis mentioned in Section 4.2, needed to perform the simulations of the integrated PT-CSP+MED-TVC plant, it was found that for a motive steam pressure of 20.6 bar, corresponding to the steam extraction at the outlet of the high pressure turbine (C5), the maximum GOR of the TVC-MED unit (17.08) resulted for the case that the thermo-compressor takes the suction steam from the 12th effect of the MED plant. For a motive steam pressure of 1.224 bar, taken from an intermediate extraction of the low pressure turbine (C2), the maximum GOR (13.81) was obtained for the case that the suction steam is taken from the 8th effect of the MED plant (see Table 4.4).

Table 4.4. Parametric analysis of the GOR as function of the motive steam pressure and thermo-compressor location.

p_m	N							
bar	6	7	8	9	10	11	12	13
20.6	16.37	16.45	16.57	16.71	16.86	17	17.08	17.04
1.224	13.71	13.79	13.81	13.68	13.65	13.58	13.44	13.23

The results of the simulations of the integrated PT-CSP+MED-TVC plant are shown in Figs. 4.4 – 4.9. Note that the results and discussion presented here are totally dependent on the location selected. They can be representative for locations with ambient conditions similar to that one selected (Mediterranean area) but they would be different for other locations with other climatic conditions. Figure 4.3 shows the thermal efficiency of the Rankine cycle in only-electricity and electricity plus water modes, being the MED-TVC plant fed by the C2 or C5 steam extractions from the LP and HP turbines, respectively. As it can be seen, in both cases the electricity generation is penalized when the MED-TVC is integrated into the power block of the CSP plant due to the use of steam extracted from the turbine, which is not further expanded in the following turbine stages, to feed the MED-TVC unit. In the case of using the C2 extraction for the MED-TVC plant, the efficiency of the Rankine cycle under nominal conditions is approximately decreased two percentage points in comparison with the efficiency in the only-electricity mode. In the case in which the C5 extraction is taken for the MED-TVC plant, the reduction is doubled with respect to the previous case resulting in a decrease of four percentage points compared to the only-electricity mode.

This analysis suggests that, if the electricity demand is high, the MED-TVC unit should be fed by the C2 extraction as it produces the lower decrease in the thermal efficiency of the cycle and the penalization in the electricity production is minimal. On the contrary, if the electricity demand is low and there is high pressure steam available to feed the MED-TVC plant, the optimum integration would be using the C5 extraction as the GOR is significantly improved.

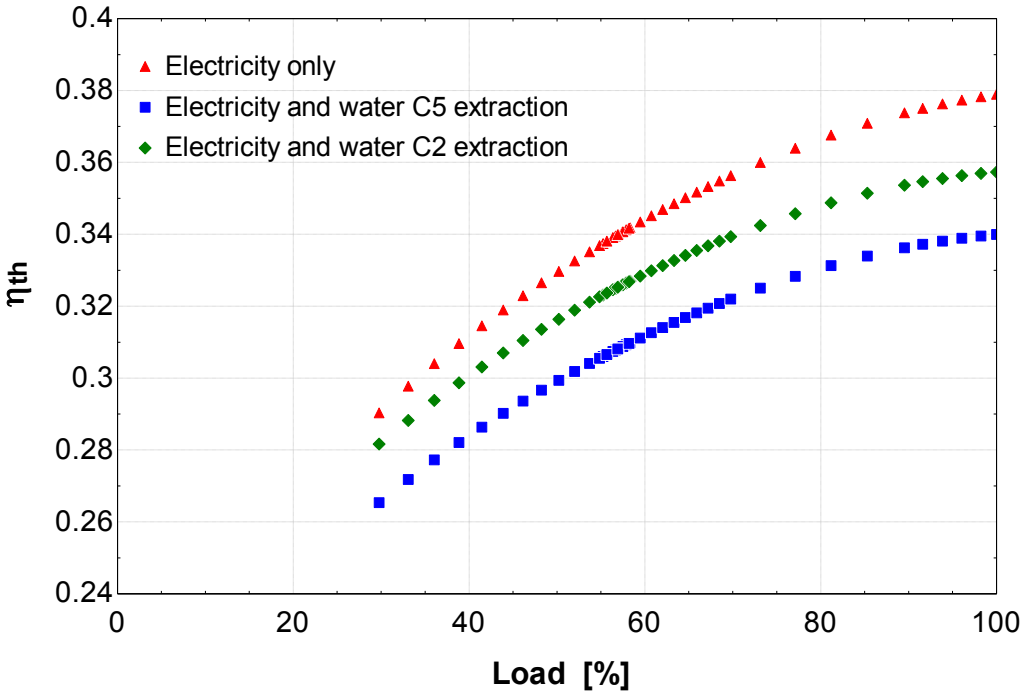

Figure 4.3. Comparison of the thermal efficiency of the power block as function of the load for electricity-only and electricity plus water operation modes (with the MED-TVC fed by the C2 and C5 extractions).

The simulation of the solar field for three days in summer (21st–23rd June) is depicted in Figure 4.4 by considering the starting point with no energy stored. In this figure, the HTF temperatures in the four collectors of each loop are represented (T_1 to T_4), along with the HTF temperature in the insulated pipes (T_{pipes}), the direct normal irradiance (E_b), the excess of thermal power generated by the solar field ($P_{PBexcess}$), which is sent to the thermal storage system), the energy stored in the TES (E_{stored}), the useful thermal power produced by the solar field ($P_{SFuseful}$), the useful thermal power sent to the PB ($P_{PBuseful}$) and the mass flow rate of HTF flowing in each loop (q_{loop}).

It can be observed that the irradiance profile of the first day was irregular, which was caused by the presence of clouds. However, the useful thermal power sent to the PB reached nominal values (140 MW_{th}). The sunrise took place at 5:47 UT and the useful thermal power sent to the power block started to be generated at 7:28 UT. Nevertheless, the electricity was generated only when this thermal power was above the technical minimum for the turbines, 41 MW_{th}, at 8:45 UT (see Figure 4.5). As can be seen, during this day, the TES was charged up to around 200 MWh, which means a 20% of its full capacity, 1010 MWh. The TES is charged only when there is excess of thermal power in the collectors (cyan line in Figure 4.4) and discharged only when the useful thermal power collected in the solar field (green line) is below the nominal value, if possible. From 17:39 UT to approximately 20:45 UT, the TES started to be discharged and the operation was mixed with the operation of the solar field. The other two days simulated showed a better irradiance profile resulting in a nearly constant operation and more electricity production as a result of the useful thermal energy sent to the power block (red line), which is increased by the only-TES operation mode after the sunset (extending the electricity production up to 7.5 hours until 3 AM approximately).

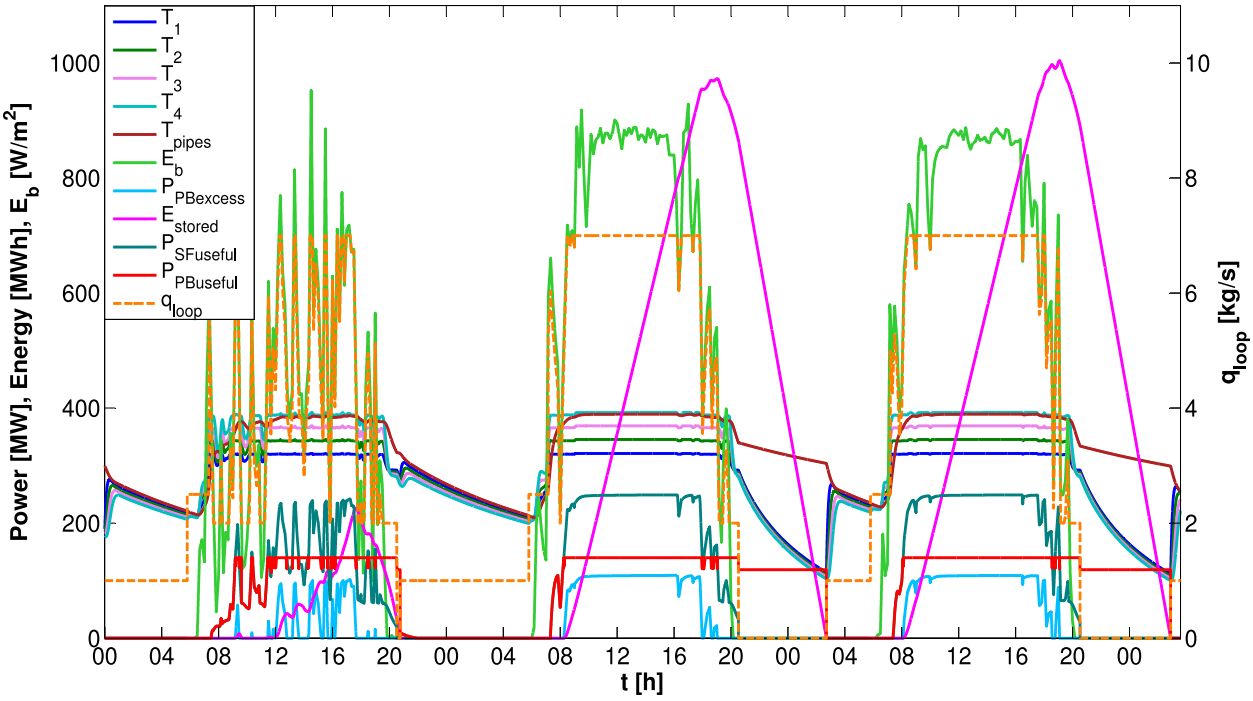

Figure 4.4. Simulation of the solar field for three days in summer: 21st-23rd June.

Figs. 4.5 and 4.6 show the electrical energy and fresh water production during the mentioned summer days (W_{eT} and q_{DT}) along with the daily fresh water production (q_{Dm3d}) and the electrical power ($\dot{W}_e$) with the MED-TVC fed by the low (C2) and high (C5) pressure extractions, respectively. As can be observed, the maximum values of electricity production are reached during the daylight hours (from 8 AM UT up to 20 PM UT approximately) due to the high irradiance values that are obtained in these periods (see Figure 4.5). The maximum electricity production using C2 extraction was 47.63 MW_e (a 5% less than in the electricity-only operation mode) while it was 45.05 MW_e when C5 extraction was considered (a 10% less in comparison with the electricity-only operation mode). For the fresh water, the maximum production was 8872.6 m^3/d using the C2 extraction and 9938.6 m^3/d when the C5 extraction was used (11.27% and 0.6% less than the nominal value, respectively). On June 21st, the operation of the integrated plant did not continue after the sunset because the TES was discharged before that moment. However, on 22nd and 23rd of June, the integrated PT-CSP+MED-TVC plant continued operating after the sunset thanks to the TES (see Figure 4.5), although the electricity production was lower due to the lower thermal input to the power block from the TES. As it can be seen, the water production followed the same trend as the electricity production.

The total electricity and fresh water production during the three days was 2228 MWh and 17,243 m^3 when the C2 extraction was considered and 2108 MWh and 19,293 m^3 when using the C5 extraction, respectively. Therefore, the electricity production was penalized a 5.38%

when the high pressure steam from the turbine is used to feed the MED-TVC plant with respect to the case of taking low pressure steam. However, the water production was improved by 11.89% regarding the low pressure extraction and, as mentioned above, in this case the efficiency of the plant was higher (with a GOR of 17.08). As in Spain the electricity demand is lower in summer than in winter and the fresh water demand has the opposite trend, it seems suitable to use the C5 extraction in summer when the desalination plant produces higher amount of water at a higher efficiency, at the expense of reducing the electricity production. The daily power and fresh water production using C2 and C5 steam extractions and their comparison can be seen in Appendix 4-B.

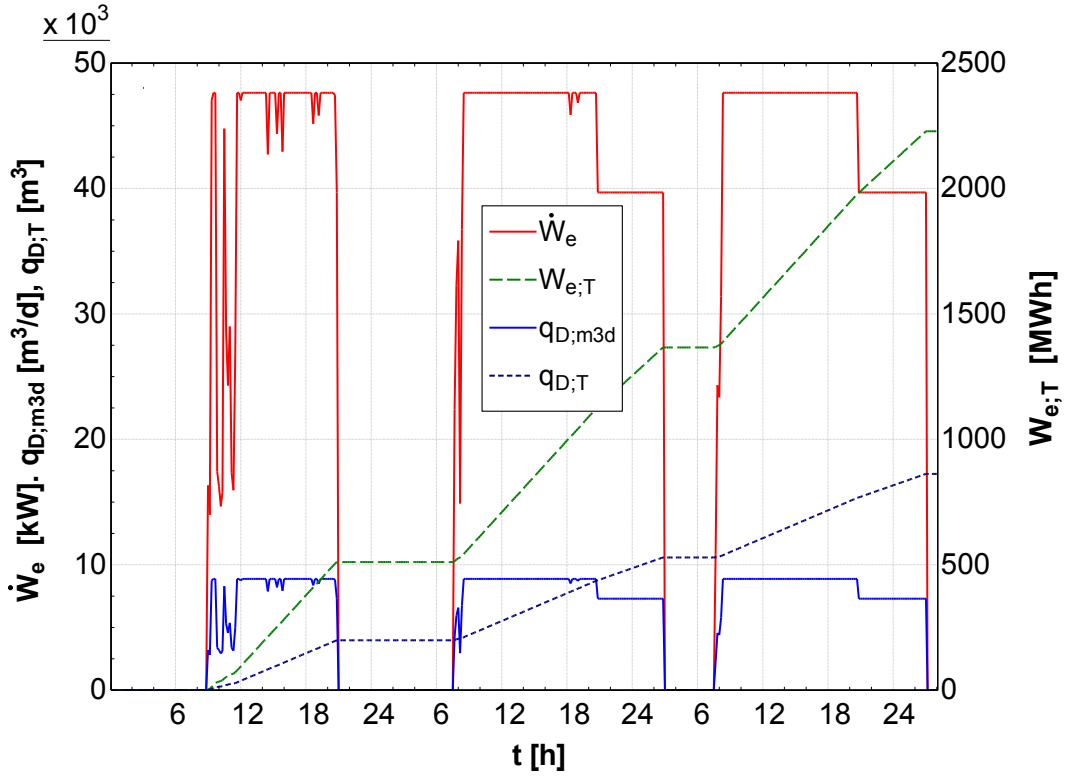

Figure 4.5. Electricity and water production for three days in summer (21st–23rd June) (with the MED-TVC fed by the C2 extraction).

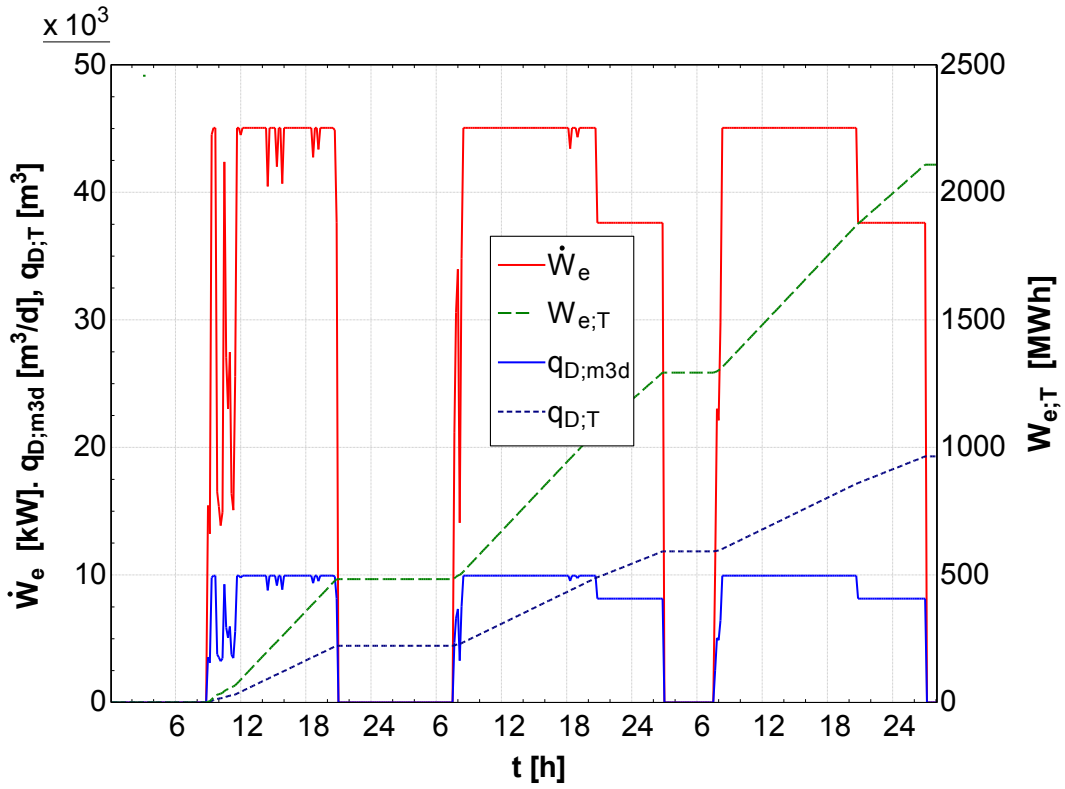

Figure 4.6. Electricity and water production for three days in summer (21st–23rd June) (with the MED-TVC fed by the C5 extraction).

Similar analysis was carried out for three days in winter (21st–23rd December). Figure 4.7 shows the output parameters of the solar field for these three days. As depicted, the irradiance profiles were very irregular, and the useful thermal power generated by the solar field in this period was quite low. The TES system was not charged in any of the days, being the daily operation reduced to the period up to few hours as long as there was useful thermal power to be sent to the power block and it was above the technical minimum considered for the turbine operation (41 MW_{th}). The sunrise took place at 8:17 UT in this period but there was not useful thermal power until 12:56 UT in the first day. However, the electricity production started only when the useful thermal power sent to the PB reached 41 MW_{th} at 16:27 (see Figure 4.8). The turbines were stopped at 17:09 UT in this first day because the useful thermal power fell below 41 MW_{th} at that time. In this day the plant generated electricity only during roughly half an hour. The plant's operation during the other two days followed similar behaviour.

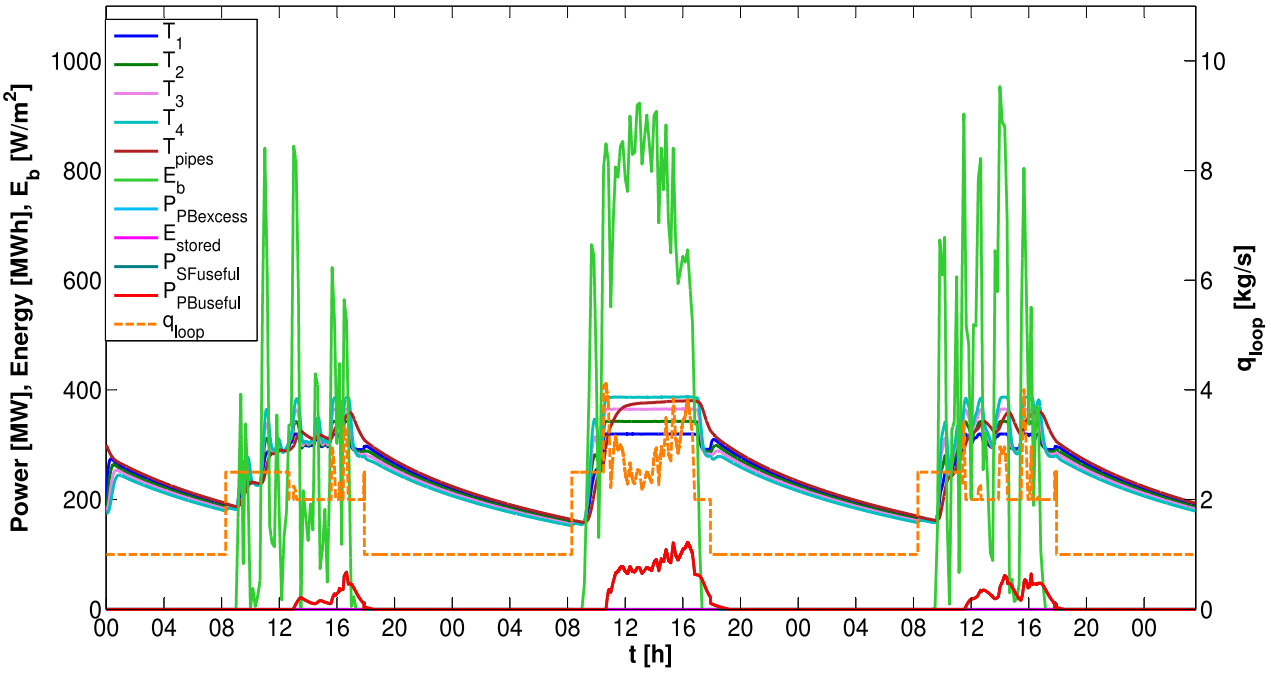

Figure 4.7. Simulation of the solar field for three days in winter: 21st–23rd December.

Figs. 4.8 and 4.9 show the electricity and fresh water production during this period for both the C2 and C5 coupling arrangements. When the MED-TVC plant is coupled to the PT-CSP plant by the C2 extraction, the total electricity production was 202.6 MWh and the maximum electrical power was 40.72 MW_e, while in the case of using the C5 extraction, the electricity production decreased to 191.8 MWh and the maximum value reached was 38.57 MW_e. Regarding the total fresh water production, it was 1605 m^3 and 1782 m^3 for the C2 and C5 arrangements, and the maximum values obtained were 7480.3 and 8352.9 m^3/d, respectively. The daily power and fresh water production using C2 and C5 steam extractions are shown in Appendix 4-B.

From the results obtained in this period, it follows that using the high pressure extraction to feed the MED-TVC plant, the electricity production was penalized by 5.33% with respect to the use of the low pressure extraction. The fresh water generated was increased by 11%. As the electricity demand in Spain is higher in winter and during this period there is less high pressure steam available to feed the MED-TVC (because the power block works almost all the day at part load operation and consequently the pressures and mass flow rates of steam are lower) it would be more convenient to use low pressure steam from the C2 extraction of the turbine as the heat source of the MED-TVC unit.

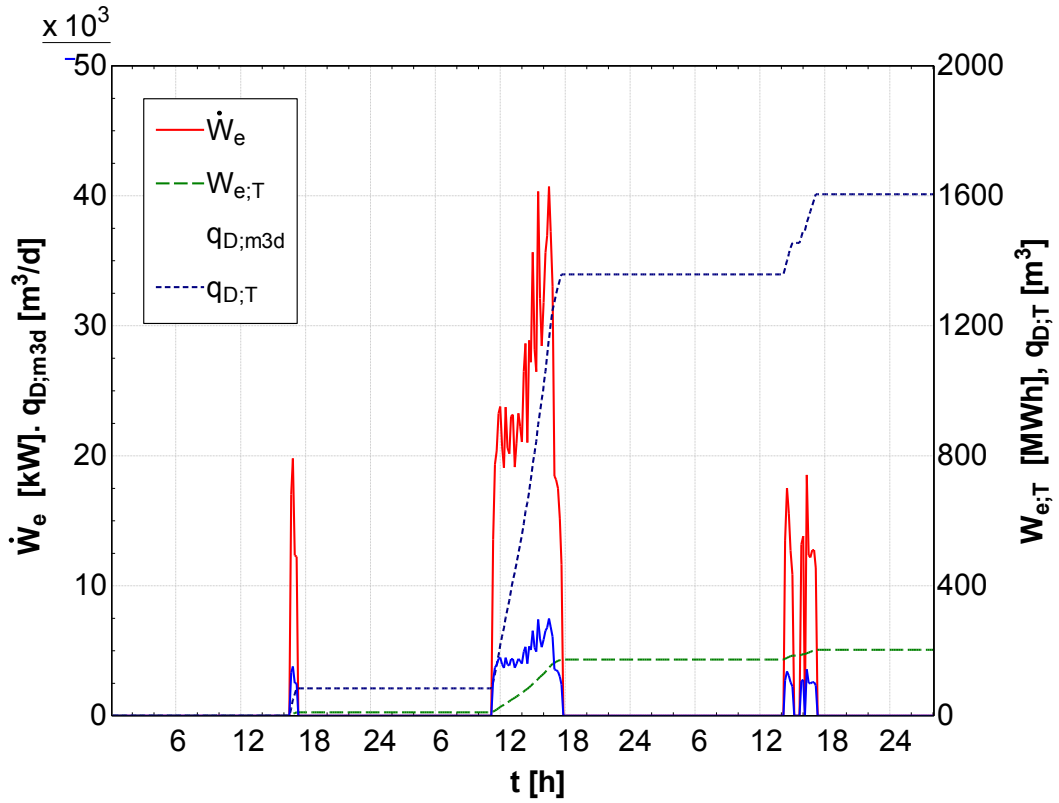

Figure 4.8. Electricity and water production for three days in winter (21st–23rd December) (with the MED-TVC fed by the C2 extraction).

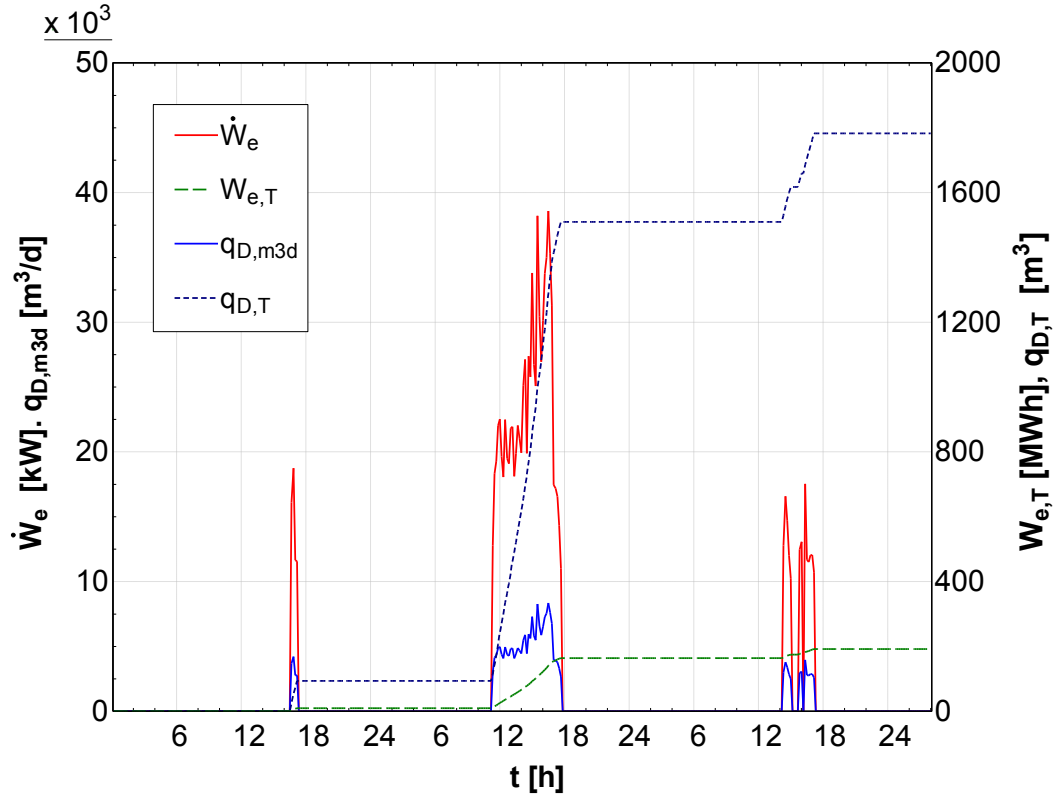

Figure 4.9. Electricity and water production for three days in winter (21st–23rd December) (with the MED-TVC fed by the C5 extraction).

4.4 Conclusions

It has been developed a simulation tool for a preliminary estimation of the fresh water production and power generation with MED-TVC desalination processes integrated into CSP plants, that is useful to select, depending on the electricity and fresh water demand profile, which is the optimal coupling arrangement from the energetic point of view (maximum GOR of the MED-TVC unit and thermal efficiency in the electricity generation).

The model has been used to simulate the electricity and fresh water production of a PT-CSP-MED-TVC plant during three representative days of summer (21st–23rd June) and winter (21st–23rd December). Firstly, parametric study of the GOR of the MED-TVC unit as function of the motive steam pressure and thermo-compressor location was carried out, using data from Andasol-2 power plant. Two scenarios were selected as result of the parametric analysis: the first coupling arrangement considered was to feed the MED-TVC with a high pressure steam extraction of 20.6 bars and with the thermo-compressor located in the 12th position, which produced a maximum GOR of 17.08, but at the same time penalized considerably the electricity production. The second coupling arrangement consisted in using a low pressure steam extraction of 1.226 bars and with the thermo-compressor located in the 8th position (which maximized the GOR to 13.81), and produced a lower impact on the electricity generation.

The results of the simulations showed that, when the MED-TVC unit was fed by the high pressure steam extraction from the turbine, the fresh water production was improved by 11.89% for the three days of summer and by 11% during the three days of winter compared to the case of using the low pressure steam extraction. In the case of the electricity production, it was penalized a 5.38% and a 5.33% in summer and in winter, respectively, when using steam at 20.6 bars compared with the use of steam at 1.226 bars. Although the results were similar for the two periods analysed, the selection of one or another coupling arrangement for the PT-CSP-MED-TVC plant depends on the electricity and water demands in the location considered. During the three days of summer it was produced 2228 and 2108 MWh of electrical energy using the C2 and C5 steam extractions, respectively, while in the three days of winter the production was 202.6 and 191.8 MWh, which mean a 90.9% and a 91% lower than in summer. Particularly, in Spain, the highest electricity consumption takes place in winter, when the weather conditions are worse and the fresh water demand is low. During this period it is then recommended the use of a low pressure extraction of the LP turbine, which produces the lower penalization in the electricity generation although the fresh water production is reduced. On the contrary, in summer in Spain the electricity demand is lower and the water demand is higher. It is recommended thus for this period to integrate the MED-TVC unit into the PT-CSP plant using a high pressure steam extraction from the HP turbine, which produces more fresh water at the expense of penalizing the electricity production.

Acknowledgments

The authors wish to thank the European Commission (DG for Research & Innovation) for its financial assistance within the Integrated Research Programme in the field of Concentrated Solar Power (CSP) (STAGE-STE Project; Grant Agreement No. 609837).

Appendix 4-A

Table 4-A.1. MED-TVC performance in nominal operation mode for the C2 and C5 steam extractions.

Concept	Extraction C5	Extraction C2
Suction effect, N	12	8
Motive steam pressure, bar	20.6	1.224
Gain output ratio	17.08	13.81
Specific heat transfer area, m^2s/kg	609.5	601.6
Evaporator areas (1 to N), m^2	4882	4882
Evaporator areas (N+1 to 14), m^2	3482	3302
Preheater areas, m^2	55.13	55.13
Motive steam mass flow rate, kg/s	6.517	7.386
Suction steam mass flow rate, kg/s	3.803	3.383
Compress steam mass flow rate, kg/s	10.32	10.77
Desuperheater water mass flow rate, kg/s	0.3539	0.1
Heating steam flow rate, kg/s	10.67	10.87
Distillate production, m^3/d	9693.6	8881.9
Suction steam temperature, °C	41.16	49.97
Suction steam pressure, bar	0.0785	0.1233
Compressed steam temperature, °C	116.8	84.79
Heating steam temperature, °C	70	70
Heating steam pressure, bar	0.3118	0.3118
Entrainment ratio	1.714	2.183
Compression ratio	3.972	2.529

Table 4-A.2. Stream data of the power block in nominal conditions.

Point	**p**	**T**	**h**	**s**	**q**	**x**
	bar	°C	kJ/kg	kJ/kgK	kg/s	-
1	90	370	3026	6.147	60.17	100
2	45.4	283.5	2891	6.188	6.29	100
3	20.6	213.9	2756	6.241	53.88	0.977
4	20.6	213.9	2756	6.241	4.386	0.977
5	20.6	213.9	2756	6.241	49.5	0.977
6	18.18	370	3186	7.077	49.5	100
7	8.75	279.7	3012	7.114	2.916	100
8	3.627	188	2838	7.167	2.865	100
9	1.224	105.4	2664	7.238	2.571	0.991
10	0.346	72.41	2490	7.313	2.065	0.94
11	0.08	41.51	2316	7.401	39.08	0.892
12	0.08	41.51	173.8	0.596	39.08	0
12p	0.131	51.24	214.5	0.72	46.58	0
13	8.356	51.34	215.7	0.721	46.58	-100
14	8.356	70.07	294	0.956	46.58	-100
15	8.356	103	432.3	1.34	46.58	-100
16	8.356	137.5	578.9	1.713	46.58	-100
17	8.356	172.2	728.8	2.063	60.17	-100
18	94.5	174	741.2	2.07	60.17	-100
19	94.5	210.8	904.1	2.42	60.17	-100
20	94.5	254.9	1110	2.826	60.17	-100
21	94.5	306.9	1384	3.322	60.17	0
22	90	303.3	2743	5.679	60.17	1
14’	0.334	56.34	426.6	1.342	7.5	0.05
15’	1.187	75.07	314.4	1.017	5.436	-100
16’	3.518	108	453	1.396	2.865	-100
19’	19.98	179	759.1	2.128	10.68	-100
20’	44.27	215.8	925.1	2.475	6.29	-100

100 = superheated vapour; -100 = subcooled liquid

Table 4-A.3. Power block performance in on-design and off-design for only-electricity mode.

Concept	**Load=100%**	**80%**	**50%**	**30%**
Thermal efficiency (%)	37.89	36.6	32.94	29.09
Electrical power production (MW_e)	50	38.61	21.53	11.23
Steam mass flow rate (kg/s)	60.17	46	26.91	15.36
Steam generator thermal power (MW_{th})	115.32	93.99	60.23	36.73
Reheater thermal power (MW_{th})	21.25	15.27	8.05	4.24
Solar field thermal power (MW_{th})	140	112	70	42
Condenser thermal power (MW_{th})	83.72	68.36	45.32	28.80
Condenser pump electrical power (MW_{th})	0.052	0.033	0.016	0.008
Feeding pump electrical power (MW_{th})	0.742	0.454	0.207	0.103

Appendix 4-B

Daily comparison of the daily electric energy generation and fresh water production, using the C2 and C5 steam extractions to feed the MED-TVC unit, during 21st–23rd June (Figures (a) and (b)) and during 21st–23rd December (Figures (c) and (d)).

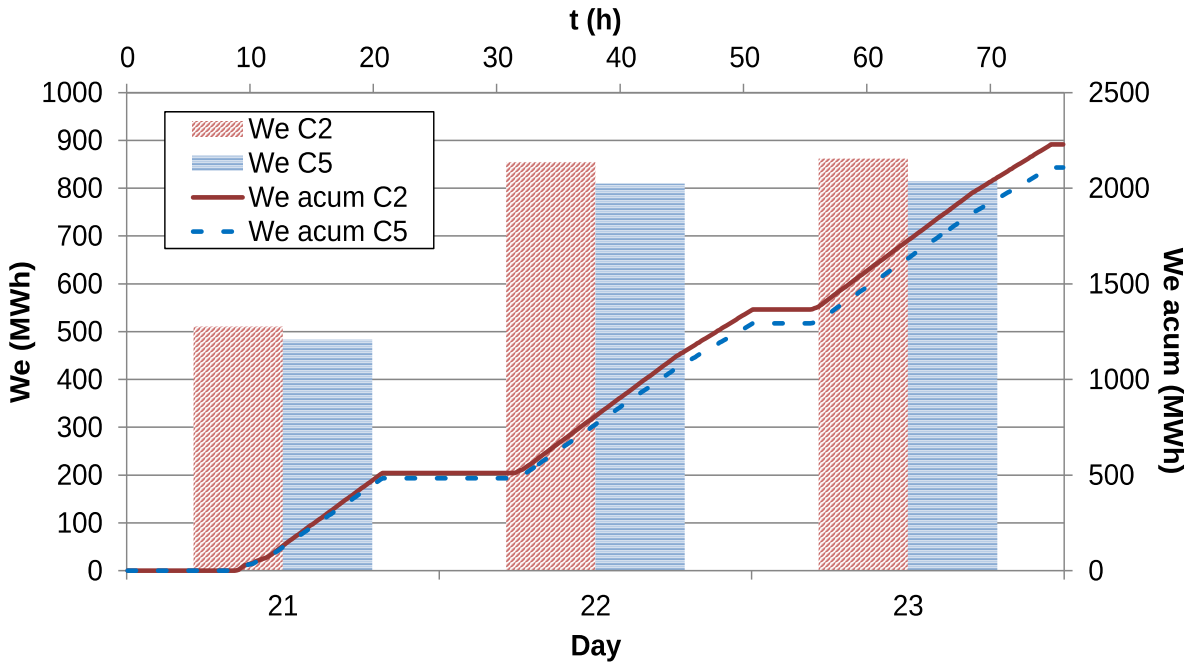

(a)

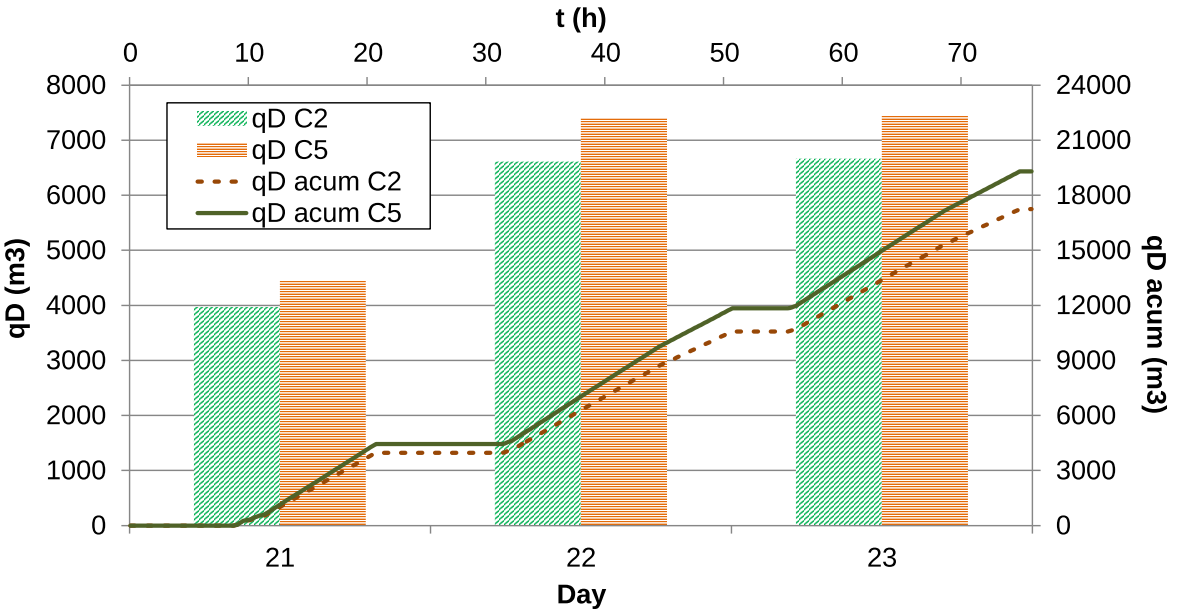
t (h)
0
10
20
30
40
50
60
70
8000
7000
6000
5000
4000
3000
2000
1000
0
qD (m3)
24000
21000
18000
15000
12000
9000
6000
3000
0
qD acum (m3)
qD C2
qD C5
qD acum C2
qD acum C5
21
22
23
Day

(b)

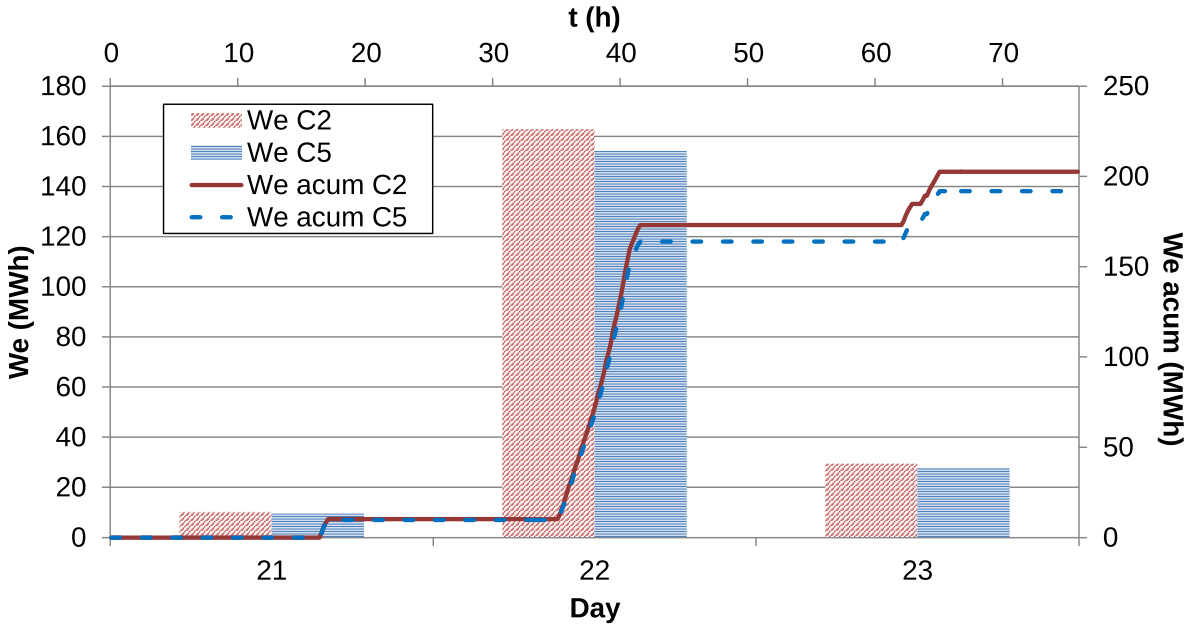
t (h)
0
10
20
30
40
50
60
70
180
160
140
120
100
80
60
40
20
0
We (MWh)
250
200
150
100
50
0
We acum (MWh)
We C2
We C5
We acum C2
We acum C5
21
22
23
Day

(c)

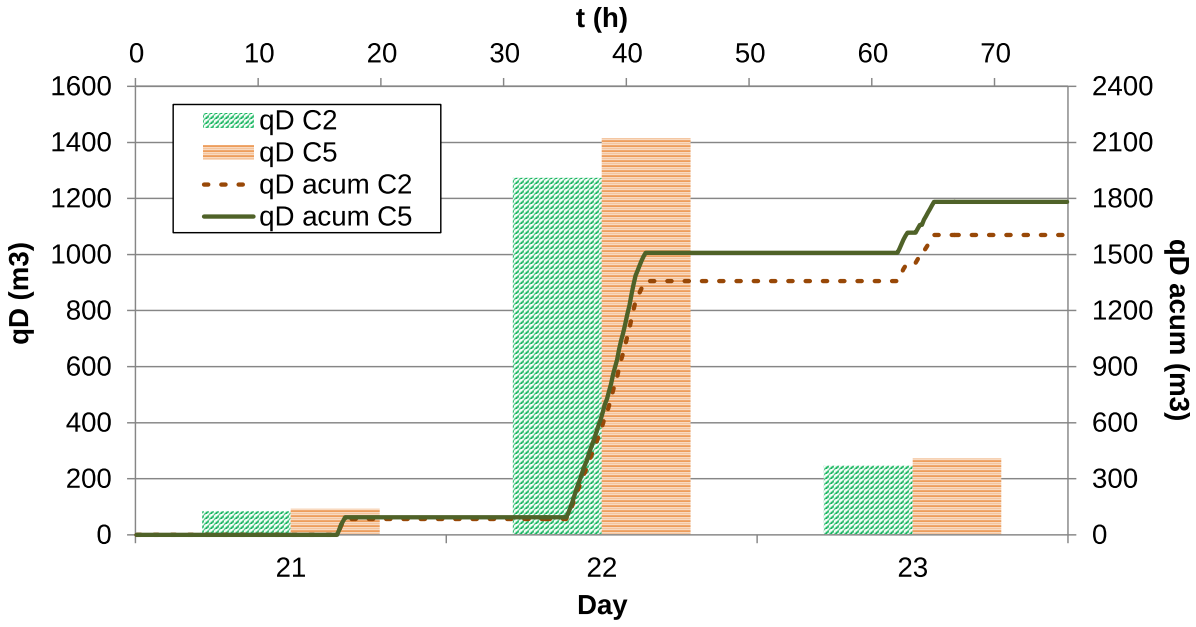

(d)

Figure 4-B.1. Daily comparison of the daily electric energy generation and fresh water production, using the C2 and C5 steam extractions to feed the MED-TVC unit, during 21st-23rd June (a) and (b) and during 21st–23rd December (c) and (d).

.

References

Bartlett, R.L., 1958. Steam turbine performance and economics. McGraw-Hill, New York.

Eastman Chemical Company, 2015. Therminol® VP-1 | Therminol [WWW Document]. URL http://www.therminol.com/products/Therminol-VP1 (accessed 3.23.15).

Hassan, A.S., Darwish, M.A., 2014. Performance of thermal vapor compression. Desalination 335, 41–46. doi:10.1016/j.desal.2013.12.004

Klein, S.A., 2013. Engineering Equation Solver Software (EES).

Lippke, F., 1995. Simulation of the part-load behavior of a 30 MWe SEGS plant. Tech. Rep.

Llorente García, I., Álvarez, J.L., Blanco, D., 2011. Performance model for parabolic trough solar thermal power plants with thermal storage: Comparison to operating plant data. Sol. Energy 85, 2443–2460. doi:10.1016/j.solener.2011.07.002

Meteonorm, 2015. Meteonorm: Irradiation data for every place on Earth [WWW Document]. URL http://meteonorm.com/ (accessed 7.4.15).

Montes, M.J., Abánades, A., Martínez-Val, J.M., Valdés, M., 2009. Solar multiple optimization for a solar-only thermal power plant, using oil as heat transfer fluid in the parabolic trough collectors. Sol. Energy 83, 2165–2176. doi:10.1016/j.solener.2009.08.010

NREL, 2015. NREL: TroughNet - U.S. Parabolic Trough Power Plant Data [WWW Document]. URL http://www.nrel.gov/csp/troughnet/power_plant_data.html (accessed 4.4.15).

Patnode, A.M., 2007. Simulation and Performance Evaluation of Parabolic Trough Solar Power Plants [WWW Document]. URL http://digital.library.wisc.edu/1793/7590

Stodola, A., Loewenstein, L.C., 1945. Steam and gas turbines, with a supplement on The prospects of the thermal prime mover,. P. Smith, New York.

Temstet, C., Canton, G., Laborie, J., Durante, A., 1996. A large high-performance MED plant in Sicily. Proc. 1st Symp. Eur. Desalin. Soc. 'Desalination Eur. 105, 109–114. doi:10.1016/0011-9164(96)00064-1

Torresol Energy, 2015. Torresol Energy - Gemasolar thermosolar plant [WWW Document]. URL http://www.torresolenergy.com/TORRESOL/gemasolar.html?swlang=en (accessed 4.4.15).

Chapter 5. Modelling of MED-TVC plants: parametric analysis

This chapter has been published as a scientific article in *Desalination*. 394 (2016) 18–29. doi:10.1016/j.desal.2016.04.020.

Title:

"Parametric study of a multi-effect distillation plant with thermal vapour compression for its integration into a Rankine cycle power block"

Authors:

Bartolomé Ortega-Delgado. Affiliation: CIEMAT-Plataforma Solar de Almería, Ctra. de Senés s/n, 04200 Tabernas, Almería, Spain. E-mail: bartolome.ortega@psa.es

Patricia Palenzuela. Affiliation: CIEMAT-Plataforma Solar de Almería, Ctra. de Senés s/n, 04200 Tabernas, Almería, Spain. E-mail: patricia.palenzuela@psa.es. Corresponding author.

Diego-César Alarcón-Padilla. Affiliation: CIEMAT-Plataforma Solar de Almería, Ctra. de Senés s/n, 04200 Tabernas, Almería, Spain. E-mail: diego.alarcon@psa.es

Abstract:

This work presents a parametric study of a multi-effect distillation plant with thermal vapour compression (MED-TVC) for the analysis of its coupling with a Rankine cycle power block. In particular, the effect of the motive and suction steam pressures on the Gain Output Ratio (GOR), fresh water production, the specific heat transfer area and other key variables in an MED-TVC unit has been analysed. For this purpose, a mathematical model of the MED-TVC system has been firstly developed and validated against actual data from Trapani MED-TVC industrial plant (Temstet et al., 1996). Different motive steam pressures corresponding to the turbine steam extractions available at a commercial power block have been taken, and the suction pressure has been varied by locating the thermocompressor in different effects. It was found an optimum value of the reduction of the heat transfer area of the evaporators after the suction point such that minimizes the specific heat transfer area. Moreover, results showed that there is an optimum position of the thermocompressor that maximizes the GOR for every motive steam pressure. The results of this work can be very useful to identify the best operation modes when a MED-TVC unit is integrated into a Rankine cycle power block.

Keywords: Solar desalination; Multi-effect distillation; Thermal vapour compression; Parametric study; Modeling

Contents

List of figures

List of tables

Nomenclature

Variables

c_p	Specific heat at constant pressure, in kJ/kg-°C
CR	Compression ratio
D	Diameter, m
h	Specific enthalpy, kJ/kg
L	Longitude, m
M	Mach number
N	Number of effects
p	Pressure, bar
q	Mass flow rate, kg/s
Q	Heat rate transfer in the evaporator, kW
Ra	Entrainment ratio
s	Salinity, g/kg
sA	Specific heat transfer area, $m^2/(kg \cdot s^{-1})$
t	Feedwater temperature in the preheaters, °C
T	Temperature, °C
T''	Temperature of the condensate exiting the distillate flash boxes, °C
t_{preh}	Preheated feed seawater temperature, °C
U	Overall heat transfer coefficient, $kW/(m^2 K)$
X	Salinity, ppm
y	Fraction of steam introduced in the thermocompressor

Acronyms and abbreviations

BPE	Boiling Point Elevation
CSP	Concentrating Solar Power
CSP+D	Concentrating Solar Power and Desalination
CV	Control Volume
EES	Engineering Equation Solver
GOR	Gain output ratio
IAPWS	International Association for the Properties of Water and Steam
LT-MED	Low Temperature Multi-Effect Distillation
LTMD	Log Mean Temperature Difference
MED	Multi-Effect Distillation
MENA	Middle East and North Africa
MSF	Multi-Stage Flash

NCG	Non-Condensable Gases
NEA	Non-equilibrium allowance, °C
PC	Parallel/Cross
PCF	Pressure Correction Factor
PF	Parallel Feed
PHX	Plate Heat Exchanger
RO	Reverse Osmosis
SAM	System Advisor Model
STPP	Solar Thermal Power Plants
SWCC	Seawater Cooling Circuit
TCF	Temperature Correction Factor
TL	Thermocompressor Location
TVC	Thermal Vapour Compression

Subscripts

B	Brine
C	Condensed in the flashing box
c	Condensed in the evaporator
cond	Condensation
comp	Compressed steam
cw	Cooling seawater
D	Distillate
ev	Evaporator
ext	External
dsh	Desuperheater
F	Feedwater
FB	Flashing box
FE	Flash of the brine in the effect
Fint	Feedwater entering the preheater
in	Seawater inlet of the end condenser
int	Internal
m	Motive/demister
pipe	Pipe connecting the effects
preh	Preheater
s	External steam
sat	Saturated
sh	Superheated

suc	Suction
sw	Seawater
T	Total
TC	Thermocompressor
V	Vapour
w	Wire

Superscripts

$'$	Conditions of the vapour/condensate after the demister
$''$	Conditions of the vapour/condensate in the flashing boxes

Greek

α	Fraction of vapor condensed in the preheater
β	Fraction of heat transfer area reduction in evaporators after the suction
γ	Isentropic expansion coefficient
δ	Diameter, mm
λ	Specific enthalpy of condensation/evaporation, kJ/kg
ρ	Density, kg/m^3

5.1 Thermocompressor models

5.1.1 Literature review

In general, the models for predicting the performance of thermocompressors can be divided in two groups: based on gas dynamics theory (physical models) and based on experimental data (empirical models). One of the earliest physical models for simple air ejectors was developed by Keenan & Neumann (1942), based on the gas dynamics theory and the mass, momentum and energy conservation equations. They assumed that the mixing of the motive and suction steam occurs at constant cross-sectional area (constant area method). This one-dimensional model did not consider the existence of the diffuser, neither the heat and friction losses. Later, they included other approach considering that the mix of both fluids occurred at constant pressure in the mixing chamber (constant pressure method) (Keenan et al., 1948). Eames et al. (1995) further extended the Keenan's model by accounting for the irreversibilities due to friction losses in the nozzle, mixing chamber and diffuser in a steam jet refrigerator, considering certain isentropic efficiencies in these sections in order to approximate the friction losses. Years after, Aly et al. (1999) presented two different models for steam ejectors in order to determine the pressure, velocity and Mach number at each section, based on conservation equations and previous works. They also compared their results with the empirical curves from Power (1994), and obtained good agreement with deviations between 10−15%.

El-Dessouky et al. (2002) developed a physical model for the evaluation of the performance and design of thermocompressors, based on previous works. They adopted the constant pressure methodology and used the following approximations:

1. The expansion of the motive steam in the nozzle is considered as an isentropic process. The same is applied for the mixing of the motive and suction steam in the diffuser.
2. Both motive and suction steam are supposed to be in saturation conditions and their velocities are neglected. The effect of the compressed mixture velocity is irrelevant.
3. The fluids are considered as ideal gases with constant expansion exponent and the flow as adiabatic.
4. The mixing of the motive and suction steam occurs at the suction space.
5. The losses due to friction are accounted using isentropic efficiencies in the nozzle, diffuser and mixing section.
6. The motive and suction steam have equal molecular weight and specific heat ratio.
7. The flow is considered at steady-state conditions and one-dimensional.

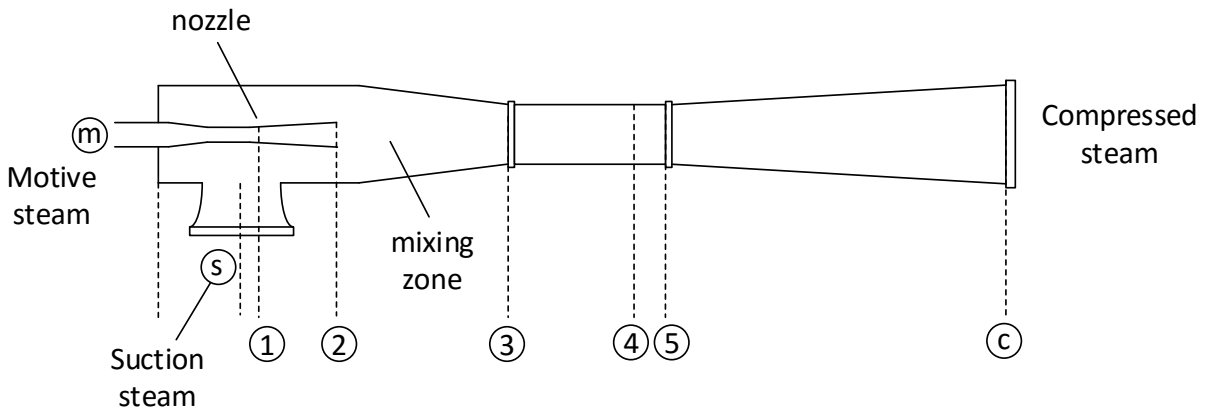

Figure 5.1. Thermocompressor scheme.

The physical model is defined by the equations described below:

- The mass balance in the control volume defined by the thermocompressor itself:

$$q_m + q_s = q_c \quad \text{(Eq. 5.1)}$$

- The entrainment ratio is defined as the flow rate of suction (or entrainment) steam divided by the flow rate of the motive (or primary) steam. For convenience, this variable was named as w, while the inverse relationship was named by Ra:

$$w = \frac{q_s}{q_m} = \frac{1}{\mathrm{Ra}} \quad \text{(Eq. 5.2)}$$

- The compression and expansion ratios of the thermocompressor are defined by:

$$CR = \frac{p_c}{p_s} \quad \text{(Eq. 5.3)}$$

$$ER = \frac{p_m}{p_s} \quad \text{(Eq. 5.4)}$$

- The expansion of the motive steam in the nozzle is described by the Mach number of the fluid at the outlet section:

$$M_{m2} = \sqrt{\frac{2\eta_n}{\gamma - 1}\left[\left(\frac{p_m}{p_2}\right)^{\frac{\gamma-1}{\gamma}} - 1\right]} \quad \text{(Eq. 5.5)}$$

where M is the Mach number, p is the pressure, γ is the isentropic expansion coefficient (also known as heat capacity ratio), and η_n the efficiency of the nozzle (defined as the real enthalpy change divided by the enthalpy change under isentropic conditions).

- The isentropic expansion of the suction steam entering the thermocompressor is also modelled by means of the Mach number of the fluid at the nozzle outlet:

$$M_{s2} = \sqrt{\frac{2}{\gamma - 1}\left[\left(\frac{p_s}{p_2}\right)^{\frac{\gamma-1}{\gamma}} - 1\right]} \quad \text{(Eq. 5.6)}$$

- The mixing of both fluids are expressed by the critical or sonic Mach number (the flow velocity is equal to the speed of sound in the fluid) of the mixture at section 4 (end of the constant section and beginning of the diffuser), as function of the critical Mach number of the motive and suction steam at the outlet of the nozzle (section 2):

$$M_4^* = \frac{M_{m2}^* + wM_{s2}^*\sqrt{T_s/T_m}}{\sqrt{(1+w)(1+wT_s/T_m)}} \quad \text{(Eq. 5.7)}$$

- The Mach number and the critical Mach number dependence at any section of the thermocompressor is given by:

$$M^* = \sqrt{\frac{(\gamma+1)M^2/2}{1+(\gamma+1)M^2/2}} \quad \text{(Eq. 5.8)}$$

- When fluids reach supersonic velocities is usual the occurrence of normal shocks, that accounts for discontinuities in the properties of the fluid, such as a significant pressure difference. In this case, the mixture is supersonic at the constant section of the thermocompressor, therefore a normal-shock is produced as consequence of the irreversible process. The Mach number of the mixture after occurring the shock wave is expressed as:

$$M_5^2 = \frac{M_4^2 + \frac{2}{\gamma - 1}}{\frac{2\gamma}{\gamma - 1} M_4^2 - 1} \quad \text{(Eq. 5.9)}$$

- According to White (2014), for flow through a normal-shock wave, the upstream Mach number must be supersonic, that is, $p_5 > p_4$ only if $M_4 > 1$. In this case, from Eq. 5.9, M_5 must be subsonic, that is, $M_5 < 1$. As a result, a normal-shock wave decelerates the fluid from supersonic to subsonic velocities.

- The constant pressure method assumes that the pressure of the mixture between sections 2 and 4 is kept constant. On the other hand, the pressure at section 4 is related to the pressure at section 5, after the shockwave, by the following relationship:

$$\frac{p_5}{p_4} = \frac{1 + \gamma M_4^2}{1 + \gamma M_5^2} \quad \text{(Eq. 5.10)}$$

- The relationship of the mixture pressure between the inlet and the outlet of the diffuser is given by:

$$\frac{p_c}{p_5} = \left(\frac{\eta_d(\gamma - 1)}{2} M_5^2 + 1\right)^{\frac{\gamma}{\gamma - 1}} \quad \text{(Eq. 5.11)}$$

- The cross sectional area of the nozzle throat is obtained with:

$$A_1 = \frac{q_m}{p_m} \sqrt{\frac{RT_m}{\gamma \eta_n} \left(\frac{\gamma + 1}{2}\right)^{\frac{\gamma+1}{\gamma-1}}} \quad \text{(Eq. 5.12)}$$

- The cross sectional area ratio of the nozzle throat and diffuser constant area is obtained by:

$$\frac{A_1}{A_3} = \frac{p_c}{p_m} \left(\frac{1}{(1 + w)(1 + w((T_s/T_m))}\right)^{1/2} \frac{\left(\frac{p_2}{p_c}\right)^{1/\gamma} \left(1 - \left(\frac{p_2}{p_c}\right)^{\gamma - 1/\gamma}\right)^{1/2}}{\left(\frac{2}{\gamma + 1}\right)^{1/(\gamma - 1)} \left(1 - \frac{2}{\gamma + 1}\right)^{1/2}} \quad \text{(Eq. 5.13)}$$

- Finally, the cross sectional area ratio between the nozzle throat and the nozzle outlet is given by:

$$\frac{A_2}{A_1} = \sqrt{\frac{1}{M_{m2}^2}\left(\frac{2}{\gamma+1}\left(1+\frac{\gamma-1}{2}M_{m2}^2\right)\right)^{\frac{\gamma+1}{\gamma-1}}} \qquad \text{(Eq. 5.14)}$$

The mentioned equations could be solved either for the thermocompressor sizing or for the performance assessment, depending on the selection of the input and output parameters. In the first case, the entrainment ratio, flow rate of compressed steam and pressures of the motive, suction and compressed steam are required (along with the efficiencies at the nozzle and diffuser) in order to determine the cross-sectional areas of the nozzle throat, nozzle outlet and diffuser constant section (A_1, A_2 and A_3, respectively). On the second approach, the geometrical features (cross-sectional areas) in addition to the motive and suction steam pressures are used to obtain the compressed and suction steam flow rates, which define the entrainment ratio of the thermocompressor.

However, the scientific literature is also full of empirical models that predict the performance of steam ejectors. Power (1994) obtained empirical curves of the entrainment ratio (kg of motive steam per kg of suction steam) adjusting the operational data taken from thermocompressors in different process industries, as function of the expansion and compression ratio. The model showed good agreement with real data from manufacturers, and it was generally accurate within 20% of the compression ratio to 5, expansion ratio to 1000 and entrainment ratio from 0.25 to 5. This method has better results for motive steam pressures above 5 bar and low compression ratios.

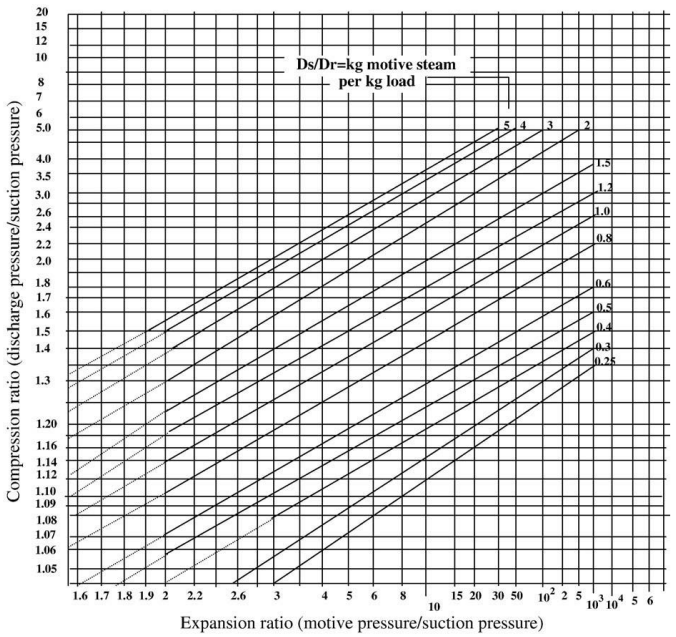

Figure 5.2. Empirical curves of the entrainment ratio as function of the compression and expansion ratios (Power, 1994).

A widely used correlation for estimating the entrainment ratio of a thermocompressor was published by El-Dessouky (1997), as function of the motive, suction and compressed steam pressures and the temperature of the suction steam. Notice that the entrainment ratio is defined here as motive steam mass flow rate divided by the suction steam mass flow rate. This relation was obtained with the data and approach provided by Power (1994):

$$Ra = \frac{q_m}{q_s} = 0.296 \frac{p_c^{1.19}}{p_s^{1.04}} \left(\frac{p_m}{p_s}\right)^{0.015} \left(\frac{PCF}{TCF}\right) \quad \text{(Eq. 5.15)}$$

where p_m, p_s and p_c are the motive, suction and compressed steam pressures, respectively, in kPa, and the terms PCF and TCF (Pressure and Temperature Correction Factors, respectively) are determined by the following equations:

$$PCF = 3 \cdot 10^{-7} p_m^2 - 9 \cdot 10^{-4} p_m + 1.6101 \quad \text{(Eq. 5.16)}$$

$$TCF = 2 \cdot 10^{-8} T_s^2 - 6 \cdot 10^{-4} T_s + 1.0047 \quad \text{(Eq. 5.17)}$$

where p_m is in kPa and T_s in °C. This equation is valid for the following ranges of variation of the variables involved: $Ra < 4$, $10 < T_s < 500$ °C, $1 < p_m < 35$ bar and $CR > 1.81$.

Also, El-Dessouky et al. (2002) obtained a semi-empirical model for evaluating the performance of thermocompressors, which may be applied to different conditions of the streams, and it does not require the knowledge of geometrical parameters or the implementation of iterative procedures of calculation. They presented correlations for the motive steam pressure at the outlet of the nozzle and area ratios, using experimental data from several ejector manufacturers to solve the physical model.

Bin Amer (2009) modified the correlation obtained by El-Dessouky (1997) for the entrainment ratio, neglecting the temperature and pressure correction factors and changing the value of the constant parameter in (Eq. 5.15). This expression is valid in the range of motive steam pressures between 20 – 30 bar:

$$Ra = \frac{q_m}{q_s} = 0.235 \frac{p_c^{1.19}}{p_s^{1.04}} \left(\frac{p_m}{p_s}\right)^{0.015} \quad \text{(Eq. 5.18)}$$

More recently, Hassan & Darwish (2014) obtained equations from the empirical curves obtained by Power (1994) for different ranges of the expansion ratio: from 2–10, 10–100 and 100–1000. Three different correlations as function of the compression and expansion ratios were obtained (with the coefficients presented in Table 5.1), permitting to easily implement the Power's graphical method into any equation solving software. In addition, the model was

compared with the semi-empirical one from Al-Juwayhel et al. (1997) and the modification done by Bin Amer (2009).

For expansion ratios equal or higher than 100:

$$Ra_H = a_0 + a_1 \cdot CR + \frac{a_2}{ER} + a_3 \cdot CR^2 + \frac{a_4}{ER^2} + a_5 \cdot \frac{CR}{ER} + a_6 \cdot CR^3 + \frac{a_7}{ER^3} + a_8 \cdot \frac{CR}{ER^2} + a_9 \cdot \frac{CR^2}{ER} \quad \text{(Eq. 5.19)}$$

For $100 \geq ER \geq 10$:

$$Ra_H = b_0 + b_1 \cdot CR + \frac{b_2}{ER} + b_3 \cdot CR^2 + \frac{b_4}{ER^2} + b_5 \cdot \frac{CR}{ER} + b_6 \cdot CR^3 + \frac{b_7}{ER^3} + b_8 \cdot \frac{CR}{ER^2} + b_9 \cdot \frac{CR^2}{ER} \quad \text{(Eq. 5.20)}$$

For $10 \geq ER \geq 2$:

$$Ra_H = c_0 + c_1 \cdot \ln(CR) + \frac{c_2}{ER} + c_3 \cdot \ln(CR)^2 + \frac{c_4}{ER^2} + c_5 \cdot \frac{\ln(CR)}{ER} + c_6 \cdot \ln(CR)^3 + \frac{c_7}{ER^3} + c_8 \cdot \frac{\ln(CR)}{ER^2} + c_9 \cdot \frac{\ln(CR)^2}{ER} \quad \text{(Eq. 5.21)}$$

Table 5.1. Coefficients used in the correlations obtained by Hassan & Darwish (2014) for the entrainment ratio.

i	a_i	b_i	c_i
0	−1.93422581403321	−3.20842210618164	−1.61061763080868
1	2.152523807931	3.93335312452389	11.0331387899116
2	113.490932154749	27.2360043794853	13.5281254171601
3	−0.522221061154973	−1.19206948677452	−14.9338191429307
4	−14735.9653361836	−141.423288255019	−34.4397376531113
5	−31.8519701023059	−22.5455184193569	−48.4767172051364
6	0.047506773195604	0.125812687624122	6.46223679313751
7	900786.044551787	348.506574704109	29.9699902855834
8	−495.581541338594	41.7960967174647	70.8113406477665
9	10.0251265889018	6.43992939366982	46.9590107717394

5.1.2 Models comparison

In order to compare the performance of a thermocompressor related to a Multi-Effect Distillation with Thermal Vapour Compression (MED-TVC) desalination process, four different models have been selected and implemented in Engineering Equation Solver (EES) environment (Klein, 2013). Particularly, the models considered were: the semi-empirical model from El-Dessouky (1997), the implicit physical model from El-Dessouky et al. (2002), the curves from Power (1994) written down into equations by Hassan & Darwish (2014) and the modified El-Dessouky's empirical correlation by Bin Amer (2009). The inputs for the models have been partially taken from the Trapani MED-TVC commercial plant (Italy), and are presented in Table 5.2:

Table 5.2. Inputs used in the comparison of the thermocompressor's models.

Parameter	Unit	Value
Motive steam pressure, p_m	Pa	4.415E6
Suction steam pressure, p_s	Pa	5904
Nozzle efficiency, n_n	-	0.85
Diffuser efficiency, n_d	-	0.85
Heat capacity ratio (steam), γ	-	1.33
Specific gas constant (steam) , R	J/kgK	461.5

Firstly, the physical model of El-Dessouky et al. (2002) is used for the thermocompressor sizing, that is, to obtain the cross-sectional areas of the nozzle throat, nozzle outlet and diffuser throat (see Table 5.3). Then, the model is used for the performance assessment in order to determine the entrainment ratio and the rest of the operational variables as function of the motive steam pressure. The results obtained from this algorithm are shown in Table 5.4. Since the rest of models use the motive, suction and compressed steam pressures as inputs, the comparison has been performed considering the compressed and suction steam pressures equal to the ones obtained in the physical model of El-Dessouky, along with the motive steam mass flow rate (it is required to specify one mass stream at least for solving the physical model, contrary to empirical correlations that are function of pressures only). Notice that the algorithm of the physical model of El-Dessouky et al. (2002) that determines the performance will be reliable and feasible only for motive steam pressures near to the design value since it is based on a fixed geometry previously defined.

Table 5.3. Results of the design algorithm of El-Dessouky's physical model.

Parameter	Unit	Value
Nozzle's throat cross sectional area	m^2	0.001123
Nozzle's outlet cross sectional area	m^2	0.0501
Diffuser's throat cross sectional area	m^2	0.5913

The comparison between models was carried out by the evaluation of the influence of the variation of the motive steam pressure (between 10 – 45 bar) in the entrainment, according to their corresponding validity ranges. The results obtained are shown in Figure 5.3. Lower values of the motive steam pressure lead to a compression ratio lower than one, that is, the suction steam is not compressed.

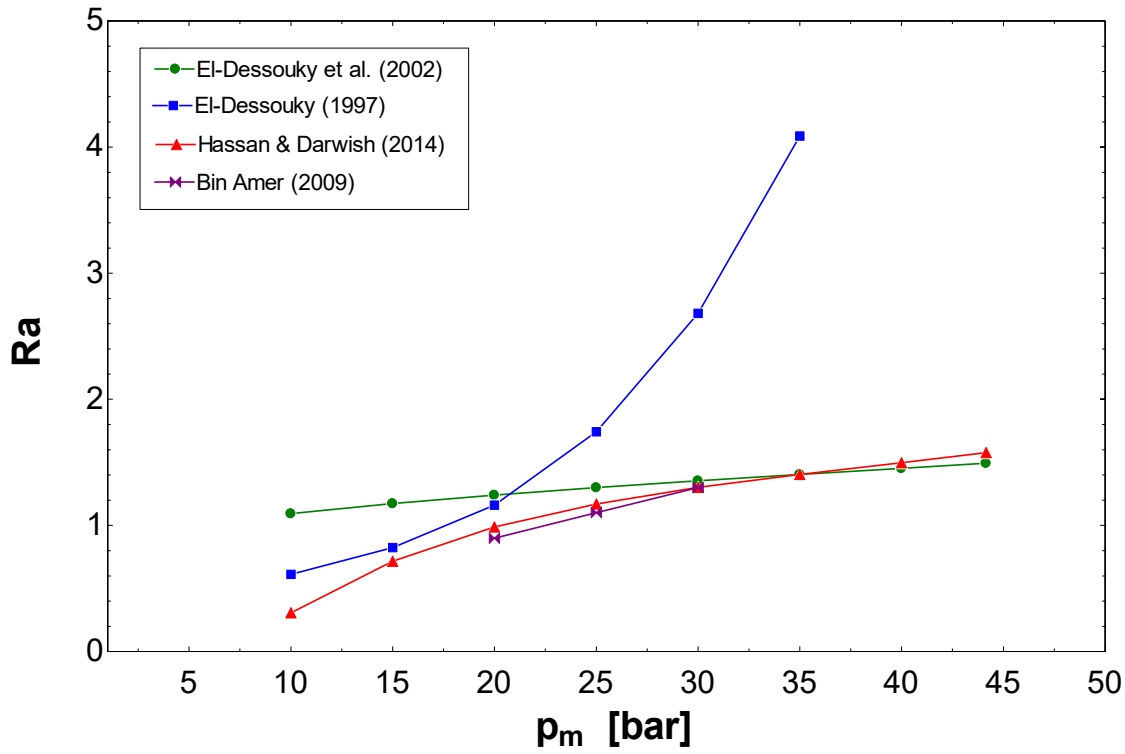

Figure 5.3. Entrainment ratio as function of the motive steam pressure for the different models considered.

As it can be seen, the physical model and the empirical model from Hassan & Darwish (2014) have a similar trend and fairly agree for motive steam pressures near to the nominal (45 bar). The physical model from El-Dessouky et al. (2002) seems to predict better the performance of the steam ejector as is based on a specific geometry and uses the governing equations of the compressible flow. Regarding the other models, it can be said that the semi-empirical one

developed by El-Dessouky (1997) has a very different behaviour from the rest, increasing quadratically with the motive steam pressure. Finally, the model from Bin Amer (2009) shows a good match with the model of Hassan & Darwish (2014).

In conclusion, it can be extracted from the analysis done that the empirical model obtained by Hassan & Darwish (2014) fits very well with the results obtained from the physical model from El-Dessouky et al. (2002) in a range of motive steam pressures close to the design one. For the purpose of this thesis, the model from Hassan & Darwish (2014) has been selected to be implemented in the MED-TVC model as it is more flexible than the physical model from El-Dessouky et al. (2002), allowing us to simulate larger motive steam pressure ranges.

Table 5.4. Parametric study of Ra and other variables as function of the motive steam pressure, using the performance algorithm of El-Dessouky's physical model.

p_m	p_s	A_1	A_2	A_3	Ra	w	CR	ER	q_m	q_s	q_c	p_2	p_3	p_4	p_5	M_{m2}	M_{s2}	M_4	M_5	M^*_{m2}	M^*_{s2}	M^*_4
(Pa)	(Pa)	(m^2)	(m^2)	(m^2)	-	-	-	-	(kg/s)	(kg/s)	(kg/s)	(Pa)	(Pa)	(Pa)	(Pa)	-	-	-	-	-	-	-
2E5	5904	0.001123	0.051	0.591	0.8748	1.143	0.39	33.9	0.327	0.374	0.701	122.3	122.3	122.3	2064	5.21	3.13	3.86	0.42	2.40	2.09	2.24
5E5	5904	0.001123	0.051	0.591	0.9841	1.016	0.79	84.7	0.786	0.799	1.59	305.8	305.8	305.8	4194	5.21	2.56	3.48	0.43	2.40	1.92	2.17
10E5	5904	0.001123	0.051	0.591	1.094	0.914	1.35	169.4	1.523	1.393	2.92	611.6	611.6	611.6	7122	5.21	2.14	3.21	0.45	2.40	1.74	2.11
15E5	5904	0.001123	0.051	0.591	1.173	0.852	1.84	254.1	2.239	1.908	4.15	917.3	917.3	917.3	9677	5.21	1.89	3.06	0.46	2.40	1.62	2.07
20E5	5904	0.001123	0.051	0.591	1.24	0.806	2.29	338.8	2.942	2.373	5.32	1223	1223	1223	12007	5.21	1.70	2.95	0.46	2.40	1.51	2.04
25E5	5904	0.001123	0.051	0.591	1.299	0.77	2.71	423.4	3.635	2.798	6.43	1529	1529	1529	14176	5.21	1.55	2.87	0.47	2.40	1.42	2.02
30E5	5904	0.001123	0.051	0.591	1.353	0.739	3.11	508.1	4.319	3.192	7.51	1835	1835	1835	16219	5.21	1.43	2.81	0.47	2.40	1.33	2.00
35E5	5904	0.001123	0.051	0.591	1.404	0.712	3.49	592.8	4.996	3.558	8.56	2140	2140	2140	18157	5.21	1.32	2.75	0.48	2.40	1.25	1.98
40E5	5904	0.001123	0.051	0.591	1.453	0.688	3.85	677.5	5.667	3.9	9.57	2446	2446	2446	20005	5.21	1.22	2.70	0.48	2.40	1.18	1.96
44.15E5	5904	0.001123	0.051	0.591	1.493	0.67	4.14	747.8	6.22	4.167	10.39	2700	2700	2700	21477	5.21	1.14	2.66	0.48	2.40	1.12	1.95

5.2 Introduction to the parametric analysis

The increase of the world population along with the rising in the industrial activities of the developing countries make the electricity and water demand grow considerably (approximately 37% of increase in electricity consumption from 2000 to 2011 (International Energy Agency, 2013)). On the other hand, some regions of the world suffer from severe water stress and the fresh water necessity is expected to expand in the next decades (UNESCO and World Water Assessment Programme, 2014). At the same time, the zones that present water scarcity usually have high levels of solar irradiation, thus, the coupling between solar thermal power plants and desalination plants (Concentrating Solar Power and Desalination, CSP+D) results as a great opportunity to partially solve the energy and water sustainable production in these areas of the world (DLR, 2009). On one hand, CSP plants can help to reduce the greenhouse gas emissions to the atmosphere by avoiding the use of fossil fuels. Although their major drawbacks are the natural intermittence of the solar resource and its daily variability, appropriate thermal energy storage systems permit to continue the operation even in nightly or cloudy periods (Romero and González-Aguilar, 2014). On the other hand, seawater desalination is one of the usual technologies used for fresh water supply in arid regions.

The co-production of water and electricity may be performed either by integrating a thermal desalination technology into a CSP plant or by utilizing the electricity produced by a Reverse Osmosis (RO) unit. In arid regions, thermal desalination is the most preferred technology. Although Multi-Stage Flash (MSF) is the most widespread in the Middle East, Multi-effect Distillation (MED) has been proved to be more efficient thermodynamically than MSF (Darwish and Darwish, 2014). MED plants can be integrated into CSP plants either by reusing the low-grade energy released to the ambient in the CSP plant cooling system (it corresponds to the integration of a Low Temperature MED plant, LT-MED) or using the medium/high pressure steam of the power system to feed a steam ejector coupled to a MED unit (which corresponds to the integration of a MED-TVC plant). In both cases, the integration of the MED contributes to increase the sustainability of the CSP+D concept since the cooling requirements decrease. However, the first case implies the fully replacement of the condenser of the power plant, which might mean a large risk towards the implementation of a CSP+D demonstration plant, since the power production would be entirely dependent on the desalination system. Moreover, the exhaust steam is not expanded to a pressure as low as in the case of standalone CSP plants, which decrease the power cycle efficiency. The second case offers a series of advantages against the first one: i) it allows the use of the power cycle condenser in case of failure or maintenance in the desalination plant; ii) it allows the expansion of the exhaust steam up to a lower pressure; iii) it allows the decoupling of the fresh water production from the electricity production. The coupling of MED has already been considered for studies of CSP+D in the literature. Palenzuela et al. (2011, 2013) compared RO and diverse MED

desalination technologies coupled to a parabolic trough CSP plant in the MENA (Middle East and North Africa) region. Results showed that the coupling of CSP and MED plants is technically feasible and more efficient than the CSP+RO option under certain conditions (high ambient temperature and high electrical consumption) that are usually present in arid and semi-arid areas. More specifically, a novel arrangement of MED with thermal vapour compression was introduced, named LT-MED-TVC, where the motive steam comes from a high/medium pressure extraction of the power block while the entrainment vapour is taken from the exhaust steam of the low pressure turbine. In this case, when the pressure of the motive steam is low (2 bar), the efficiency of this system is similar to that one of the CSP+RO case and the cooling requirements are considerably reduced. Also, Casimiro et al. (2014) studied the integration of a parallel feed MED-TVC into a CSP, developing a model implemented as an add-on to the SAM (System Advisor Model) software from NREL. An analysis of four different cooling systems was carried out: a Seawater Cooling Circuit (SWCC) along with the MED, dry cooling, wet cooling (evaporative) and a standalone SWCC. Among them, the option that generated more electricity (up to a 30%) was the wet cooling, followed by the standalone SWCC with respect to the CSP+MED/SWCC case. However, this latter option had the advantage of producing fresh water as a secondary product, apart from the electricity.

Despite the potential of the CSP+MED-TVC concept, the main problem faced is the penalty in the power production because of the use of an intermediate steam extraction from the power cycle. Therefore, it is important to study the system at the MED-TVC level, analysing the influence of the steam pressures required in the thermal vapour compressor on the performance, fresh water production and costs of the MED plant. Several authors have carried out parametric analyses of MED-TVC plants to study their performance under different conditions. Shen et al. (2011) developed a steady-state mathematical model for a 10,000 m^3/day MED-TVC plant and studied the influence of the motive steam pressure and suction steam temperature over the Gain Output Ratio, GOR (that is defined as the mass flow rate of distillate produced per unit of mass flow rate of motive steam supplied to the thermocompressor), the entrainment ratio, Ra (defined here as the entrained steam mass flow rate per unit of motive steam mass flow rate) and the specific heat transfer area, sA, (that is the sum of the evaporators, preheaters and end condenser areas per unit of distillate production). The results showed that the increase of the motive steam pressure enhanced the GOR, the Ra and the specific exergy consumption, while decreased the condenser inlet seawater mass flow rate, the specific energy consumption and the specific heat transfer area. Also, it was found that the GOR and Ra increased with the suction steam temperature. Kouhikamali et al. (2011) developed a mathematical model to investigate different MED-TVC configurations in order to find the suction pressure of the thermocompressor that maximizes the GOR and minimizes the sA. It was concluded that moving the thermocompressor from the latter effects to the middle ones caused an increase of the Ra, maximized the GOR and reduced the sA. More recently,

Dahdah & Mitsos (2014) did a multi-objective structural optimization of MED-TVC systems maximizing the GOR and minimizing the sA required. The results indicated that intermediate extractions of the suction steam maximized the distillate production and decreased the sA.

Most of the parametric studies deal with MED-TVC models developed for design purposes (i.e. assuming the heat transfer areas of all evaporators and preheaters as outputs), while in this study the geometry of the MED-TVC plant is previously fixed by a base case and only the heat transfer area of the evaporators after the position of thermocompressor is variable. Moreover, this work introduces a totally novel concept which has not been previously shown in other MED-TVC studies. It is the optimization of the reduction of the heat transfer area of the mentioned evaporators, which minimize the total heat transfer area of the plant and consequently the investment costs. Another contribution of this work is the study of the influence of the motive steam pressures equal to those ones of the turbine steam extractions available at the power block of a commercial CSP plant on the performance and specific heat transfer area requirements of a MED-TVC plant, which help to choose the best arrangements for the integration of a MED-TVC unit into a Rankine power block depending on the electricity and water demands. For all these purposes, a detailed model of a parallel/cross (PC) feed MED-TVC plant is firstly developed and validated with data from the MED-TVC plant in Trapani; then a study of the reduction of the heat transfer area of the evaporators after the position of the steam ejector such that minimizes the sA is carried out, and finally, an exhaustive parametric study is performed in which the results obtained are discussed.

5.3 Process description

The system consists basically of N effects, $N-1$ preheaters and N flashing boxes in parallel/cross feeding arrangement (see Figure 5.4). The design is based on the MED-TVC plant located in Trapani (Italy) (Temstet et al., 1996). Each effect has a horizontal tube falling film evaporator, a demister to catch the water droplets, and a shell and tube preheater (with the exception of the last one, which has no preheater associated but a larger shell and tube heat exchanger called end condenser). The MED system consists basically in a sequence of evaporation-condensation processes, being the steam generated in one effect the heat source for the seawater evaporation in the next effect, at lower temperature and pressure.

The thermal energy source required by the entire process, called heating steam, is added exclusively in the first effect. The external steam releases the heat to the feedwater, which is sprayed over the tube bundle, evaporating part of it. The generated vapour is driven through a demister to the preheaters, where a small part condenses warming up the feedwater before entering into the next effect. The saturation temperature of the generated vapour decreases due to the pressure losses in the demister, connecting lines and condensation inside the evaporator,

and the remaining vapour leaving the preheater at a lower temperature flows inside the evaporator tubes of the following effect taking place the same process as before, and so with the rest of effects. On the other hand, the unevaporated brine, deposited in the bottom of the effect, is directed to the following effect producing additional vapour by flashing. Finally, the vapour generated in the last effect is cooled in the end condenser, where the intake seawater flowing inside the tubes is used as the cooling source. Part of the seawater leaving the end condenser is used as feedwater in the distillation process and the rest is rejected back to the sea. Two plate heat exchangers in which the rejected brine and produced distillate release the remaining heat to the intake seawater are used before the end condenser. They allow regulating the temperature of the seawater and are switched on/off depending on the season.

The condensed vapour (distillate), both in the preheaters and the evaporators, is led to the distillate flash boxes, where additional vapour is generated by flashing, as the temperature of the condensate entering the flash box is higher than the saturation temperature at the steam pressure. Part of the condensed heating steam flow rate enters the first flash box, which is needed to keep the distillate production constant.

The thermocompressor takes low pressure vapour (called suction or entrained steam) from a certain effect of the MED plant and re-compresses it by a higher pressure vapour, called motive steam, producing vapour at an intermediate pressure (called compressed steam) which is addressed to the evaporator of the first effect. Also, a desuperheater is needed at the outlet of the thermocompressor in order to reduce the temperature of the heating steam to a temperature close to saturation. This device uses water from the last distillate flash box for cooling the steam, which is re-introduced in the distillate line to maintain the overall distillate production.

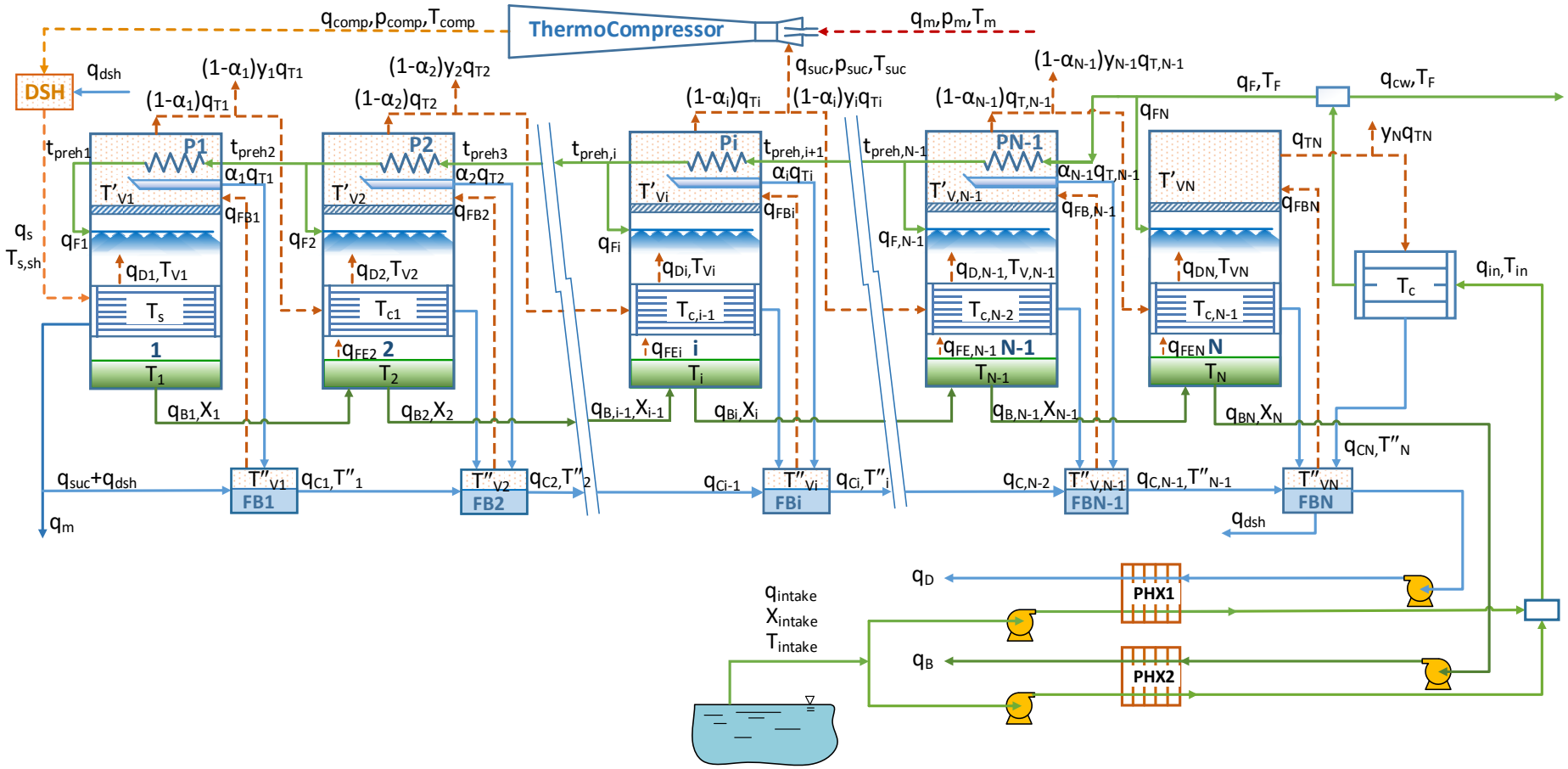

Figure 5.4. Scheme of the PC-MED-TVC plant.

5.4 Methodology

5.4.1 Mathematical model

A steady state mathematical model of a parallel/cross MED-TVC plant shown in Figure 5.4 has been developed, which is based on the mass and energy balances applied to the different elements of the plant, along with the heat transfer equations corresponding to the heat exchangers. The assumptions and approximations stablished in the model are the following:

1. Kinetic and potential energy are neglected in comparison with the other energy terms.
2. Heat losses to the environment are not considered.
3. The thermodynamic losses are taken into account. These losses are referred to the Boiling Point Elevation (BPE), the Non-Equilibrium Allowance (NEA) and the pressure losses in the demister, connecting lines and condensation inside the evaporator tubes. The effect of the pressure drop in the vapour condensation process on the external surface of the tubes is neglected (El-Dessouky et al., 1998).
4. The vapour entering the evaporators 2 to N is assumed to be in saturation conditions, as well as the distillate exiting all the preheaters and the evaporators.
5. The vapour generated by boiling is supposed to be superheated due to the BPE and its temperature is assumed to be equal to the unevaporated brine ($T_{Vi} = T_i$). The energy associated with the temperature increase due to the BPE is transferred to the feedwater inside the tubes of the preheaters in the condensation process.
6. The external steam is assumed to be superheated at a temperature 3°C above the saturation temperature, thus releasing sensible and latent heat to the feedwater.
7. The effect of Non-Condensable Gases (NGC) is not accounted.
8. The produced distillate is free of salts.

The model has been implemented in Engineering Equation Solver (Klein, 2013) software environment which permits to solve non-linear equation systems simultaneously using the Newton-Raphson method. A proper initialization and bound of the variables is needed for the convergence of the model. This software also contains libraries for the thermo-physical properties of the pure water and steam according the IAPWS Formulation 1995 (Wagner and Pruß, 2002) and for the properties of the seawater, which correspond to the correlations obtained by Sharqawy et al. (2010).

The temperature of the brine in each effect (T_i) is equal to the vapor saturation temperature ($T_{Vsat,i}$) plus the boiling point elevation (calculated through the expression proposed by El-Dessouky & Ettouney (2002a)), due to the presence of salts:

$$T_i = T_{Vsat,i} + BPE_i \quad \text{(Eq. 5.22)}$$

The condensation of the vapor generated in the evaporator i takes place in the evaporator $i+1$, at a lower temperature (T_{ci}) than the boiling temperature in the evaporator i due to the thermodynamic losses.

$$T_{ci} = T_i - BPE_i - \Delta T_{ti} \quad \text{(Eq. 5.23)}$$

$$\Delta T_{ti} = \Delta T_{m,i} + \Delta T_{pipe,i} + \Delta T_{cond,i} \quad \text{(Eq. 5.24)}$$

$$\Delta T_{m,i} = T_{Vsat,i} - T'_{Vsat,i} \quad \text{(Eq. 5.25)}$$

$$\Delta T_{pipe,i} = T'_{Vsat,i} - T'_{c,i} \quad \text{(Eq. 5.26)}$$

$$\Delta T_{cond,i} = T'_{c,i} - T_{c,i} \quad \text{(Eq. 5.27)}$$

where ΔT_{ti} is the total drop in the saturation temperature of the vapor formed in the effect i, defined as the sum of the saturation temperature drop in the demister ($\Delta T_{m,i}$), the connecting pipes ($\Delta T_{pipe,i}$) and the evaporator ($\Delta T_{cond,i}$). The saturation temperature drop in the demister is defined as the difference of the saturation temperature of the vapor formed before the demister (T_{Vsat}) and the saturation temperature of the vapour after the demister (T'_{Vsat}). The decrease in the saturation temperature of the vapor in the connecting pipes is obtained as the difference between T'_{Vsat} and the saturation temperature of the vapour at the entrance of the following evaporator (T'_c). Finally, the saturation temperature drop in the evaporator is defined as the variation between T'_c minus the saturation temperature inside the tube bundle in the heat transfer process (T_c). The temperature drops in the demister are determined by the correlation proposed in El-Dessouky & Ettouney (2002a), while the temperature drops in the connecting pipes are estimated by means of the Unwin's equation (Nayyar, 2006). The temperature drops in the evaporator are calculated by the procedure described in Engineering Sciences Data Unit (ESDU) (1993) which is based on Friedel's correlation (Friedel, 1979).

For the global system, the following equations are considered taking the MED-TVC plant as a single control volume. The general mass balance is:

$$q_{in} = q_F + q_{cw} \quad \text{(Eq. 5.28)}$$

being q_{in} the mass flow rate of seawater entering the end condenser, q_F the total feed seawater distributed in the effects, and q_{cw} the cooling seawater rejected to the sea. Moreover, the total mass flow rate of distillate produced (q_D) is calculated as the sum of mass flow rate of steam produced by boiling ($q_{Di}\ i = 1, N$) plus the mass flow rate of steam produced by flashing ($q_{FEi}\ i = 2, N$), or equivalently:

$$q_D = \sum_{i=1}^{N} q_{Di} + \sum_{i=2}^{N} q_{FEi} \quad \text{(Eq. 5.29)}$$

5.4.1.1 Effects and flash boxes analysis

The first effect diagram is shown in Figure 5.5. Mass and energy conservation equations are applied to the Control Volume (CV) corresponding to this effect, along with the heat transfer equations of the evaporator and preheater. The mass balance equation establishes:

$$q_{F1} = q_{D1} + q_{B1} \quad \text{(Eq. 5.30)}$$

where q_{F1} is the mass flow rate of feed seawater entering the first effect, q_{D1} is the mass flow rate of steam obtained by boiling and q_{B1} is the mass flow rate of unevaporated brine. The salt balance is as given:

$$q_{F1}X_F = q_{B1}X_1 \quad \text{(Eq. 5.31)}$$

where X_F is the feed seawater salt concentration, and X_1 is the salt concentration of the un-evaporated brine in the first effect.

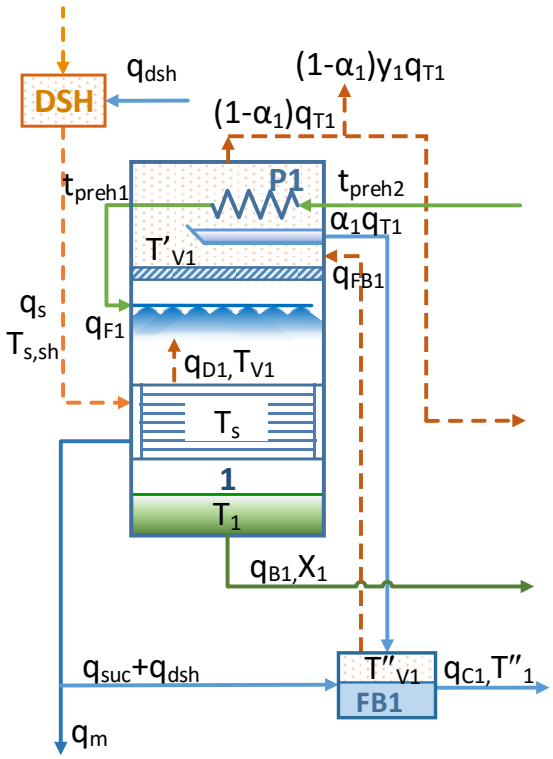

Figure 5.5. First effect flow diagram.

Applying an energy balance to the CV it is obtained:

$$q_s\lambda_s + q_s\bar{c}_{ps,sh}\left(T_{s,sh} - T_s\right) + q_{F1}h_{preh2} + q_{FB1}h''_{V1} = (1-\alpha_1)q_{T1}h'_{V1} + \alpha_1 q_{T1}h'_{C1} + q_{B1}h_{B1} \quad \text{(Eq. 5.32)}$$

where q_s is the mass flow rate of the heating steam, λ_s its specific enthalpy of condensation, $\bar{c}_{ps,sh}$ the specific heat at constant pressure and mean temperature between $T_{s,sh}$ and T_s, $T_{s,sh}$ the temperature of the superheated steam, T_s the temperature of the saturated heating steam, h_{preh2} the specific enthalpy of the feed seawater entering the preheater 1, at t_{preh2}, q_{FB1} the mass flow rate of flashing steam produced in the distillate flash box, h''_{V1} the specific enthalpy of the flashing vapor at T''_{V1}, α_1 is the fraction of the total steam that condenses in the outer surface of the preheater 1, h'_{V1} is the specific enthalpy of condensation of the steam in the vapor zone at T'_{V1} (vapor temperature after passing through the demister), h'_{C1} is the specific enthalpy of the condensed distillate in the preheater 1 at T'_{V1}, h_{B1} is the specific enthalpy of the un-evaporated brine produced is the first effect, at T_1, and q_{T1} is the steam mass flow rate produced by boiling in the first evaporator and in the first distillate flash box, respectively:

$$q_{T1} = q_{D1} + q_{FB1} \quad \text{(Eq. 5.33)}$$

The heat transfer equation associated with the first evaporator establishes that the heat released by the heating steam Q_1 is transferred to the seawater by convection and conduction through the tube walls, and it is characterized by the overall heat transfer coefficient U_1 which is determined by the correlation obtained by Al-Juwayhel et al. (1997):

$$Q_1 = q_{D1}\lambda_{V1} + q_{F1}\bar{c}_{p1}\left(T_1 - t_{preh1}\right) = A_1 U_1 (T_s - T_1) \quad \text{(Eq. 5.34)}$$

where λ_{V1} is the specific enthalpy of vaporization at T_{V1sat}, $\bar{c}_{p1}$ is the specific heat at constant pressure and mean temperature between T_1 and t_{preh1}, and A_1 is the heat transfer area of the first evaporator tube bundle.

The mass balance applied to the first distillate flash box is given by:

$$(q_{suc} + q_{dsh}) + \alpha_1 q_{T1} = q_{C1} + q_{FB1} \quad \text{(Eq. 5.35)}$$

where q_{suc} is the mass flow rate of suction vapour, q_{dsh} is the mass flow rate of condensate used to reduce the temperature of the compressed steam in the desuperheater, and q_{C1} is the mass flow rate of distillate exiting the flash box. The energy balance is described as follows:

$$(q_{suc} + q_{dsh})h_{sc} + \alpha_1 q_{T1} h'_{C1} = q_{C1} h''_{C1} + q_{FB1} h''_{V1} \quad \text{(Eq. 5.36)}$$

where h_{sc} is the specific enthalpy of both the condensed suction vapor and desuperheated distillate and h''_{C1} is the specific enthalpy of the distillate exiting the flash box.

For a generic effect i (see the diagram flow in Figure 5.6), with i varying from 2 to $N-1$, the following energy balance results when applying to the CV:

$$\begin{aligned}(1 - y_{i-1})(1 - \alpha_{i-1}) q_{T,i-1}\lambda_{c,i-1} + q_{FBi}h''_{Vi} + q_{B,i-1}h_{B,i-1} + q_{Fi}h_{Fi} \\ = (1 - \alpha_i) q_{Ti} h'_{Vi} + \alpha_i q_{Ti} h'_{Ci} + q_{Fint,i}\bar{c}_{pi}\left(t_{preh,i} - t_{preh,i+1}\right) \\ + q_{Bi}h_{Bi}\end{aligned} \quad \text{(Eq. 5.37)}$$

where y_{i-1} is the fraction of vapour from the effect $i-1$ used as suction vapor in the thermocompressor, $\lambda_{c,i-1}$ is the specific enthalpy of condensation of the steam inside the tube bundle of the evaporator i at $T_{c,i-1}$, h_{fi} is the specific enthalpy of the feedwater before entering the preheater i, $q_{Fint,i}$ is the mass flow rate of feedwater entering the preheater $i-1$, $\bar{c}_{pi}$ is the specific heat at constant pressure and mean temperature between $t_{preh,i}$ and $t_{preh,i+1}$

and q_{Ti} is sum of the flow rates of vapour produced by evaporation (q_{Di}), flashing of the distillate collected in the flashing box (q_{FBi}) and flashing of the brine coming from the previous effect (q_{FEi}), as indicated in the following equation:

$$q_{Ti} = q_{Di} + q_{FBi} + q_{FEi} \qquad \text{(Eq. 5.38)}$$

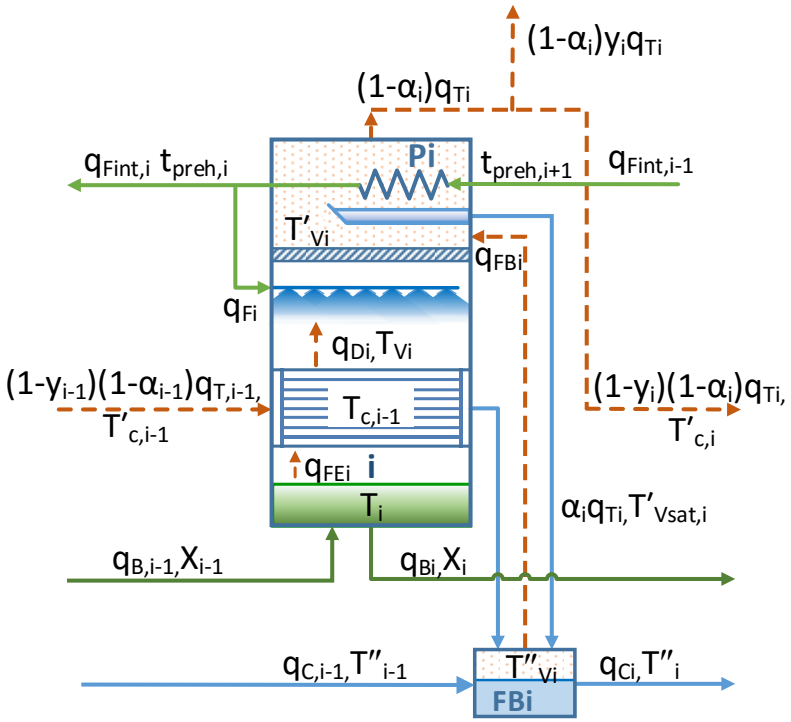

Figure 5.6. Generic effect i flow diagram.

The mass flow rate of feedwater leaving the preheater i is obtained with the expression below:

$$q_{Fint,i} = q_F - \sum_{k=i+1}^{N} q_{F,k} \qquad \text{(Eq. 5.39)}$$

The mass and salinity balances in the generic effect i are:

$$q_{B,i-1} + q_{Fi} = q_{Bi} + q_{Di} + q_{FEi} \qquad \text{(Eq. 5.40)}$$

$$q_{B,i-1}X_{i-1} + q_{Fi}X_F = q_{Bi}X_i \qquad \text{(Eq. 5.41)}$$

The mass flow rate of vapour produced by flashing in the effect is given by:

$$q_{FEi}\lambda_{FEi} = q_{B,i-1}\bar{c}_{p,FEi}\left(T_{i-1} - T_{B,FEi}\right) \qquad \text{(Eq. 5.42)}$$

where λ_{FEi} is the specific enthalpy of condensation of the steam produced by the flashing brine in the effect, $\bar{c}_{p,FE,i}$ is the specific heat at constant pressure and mean temperature between T_{i-1} and $T_{B,FEi}$ of the flashing brine in the effect and $T_{B,FEi}$ is the temperature of the unevaporated brine after the flashing process.

The flashing process is inherently of non-equilibrium and the temperature of the unevaporated brine from this process ($T_{B,FEi}$) is greater than the temperature of the brine in the effect (T_i) by the non-equilibrium allowance (NEA):

$$T_{B,FEi} = T_i + NEA_i \quad \text{(Eq. 5.43)}$$

This parameter is estimated through the correlation proposed by Miyatake et al. (1973) as function of the temperature difference of the boiling brine between the effects $i-1$ and i (ΔT_i) and the vapor temperature in the effect i (T_{Vi}).

$$NEA_i = 33\frac{\Delta T_i^{0.55}}{T_{Vi}} \quad \text{(Eq. 5.44)}$$

The heat transfer equation for evaporators from $i = 2\ to\ N$ is given by:

$$Q_i = (1-y_{i-1})(1-\alpha_{i-1})q_{T,i-1}\lambda_{c,i-1} = A_i U_i\left(T_{c,i-1} - T_i\right) \quad \text{(Eq. 5.45)}$$

The mass and energy balances applied to the control volumes delimited by the distillate flash boxes from $i = 2$ to $N-1$ are:

$$q_{C,i-1}h''_{C,i-1} + (1-y_{i-1})(1-\alpha_{i-1})q_{T,i-1}h_{c,i-1} + \alpha_i q_{Ti}h'_{Ci} = q_{FBi}h''_{Vi} + q_{Ci}h''_{Ci} \quad \text{(Eq. 5.46)}$$

with:

$$q_{Ci} = q_{C,i-1} + (1-y_{i-1})(1-\alpha_{i-1})q_{T,i-1} - q_{FBi} + \alpha_i q_{Ti} \quad \text{(Eq. 5.47)}$$

It is assumed that the temperature of the steam in the flash box (T''_{Vi}) is equal to the temperature of the steam in the effect after passing through the demister (T'_{Vi}). In this case, the condensate temperature is related with the temperature of steam in the flash box by the non-equilibrium allowance:

$$T''_i = T''_{Vi} + NEA''_i \quad \text{(Eq. 5.48)}$$

Finally, the mass and energy balances of the last effect are shown below. Figure 5.7 depicts a flow diagram of this effect with all the corresponding upstream and downstreams.

The mass, salinity and energy balances applied to the CV delimited by this effect are given by:

$$q_{B,N-1} + q_{FN} = q_{BN} + q_{DN} + q_{FEN} \quad \text{(Eq. 5.49)}$$

$$q_{B,N-1}X_{N-1} + q_{FN}X_F = q_{BN}X_N \quad \text{(Eq. 5.50)}$$

$$(1 - y_{N-1})(1 - \alpha_{N-1})q_{T,N-1}\lambda_{c,N-1} + q_{FBN}h''_{VN} + q_{B,N-1}h_{B,N-1} + q_{FN}h_{FN} = q_{TN}h'_{VN} + q_{BN}h_{BN} \quad \text{(Eq. 5.51)}$$

The equation that describes the flash process that takes place when the brine from the effect $N-1$ enters the effect N is:

$$q_{FEN}\lambda_{FEN} = q_{B,N-1}\bar{c}_{p,FEN}\left(T_{N-1} - T_{B,FE,N}\right) \quad \text{(Eq. 5.52)}$$

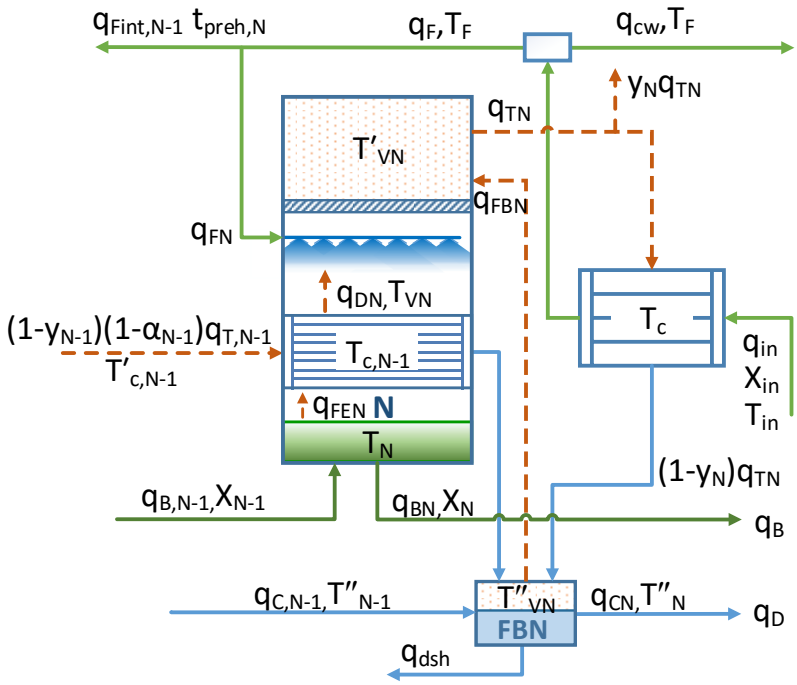

Figure 5.7. Last effect N flow diagram.

The temperature of the un-evaporated brine after the flashing process is higher than the brine temperature in the bottom of the effect by the non-equilibrium allowance:

$$T_{B,FEN} = T_N + NEA_N \quad \text{(Eq. 5.53)}$$

The heat transfer equations associated with the last evaporator is:

$$Q_N = (1 - y_{N-1})(1 - \alpha_{N-1}) q_{T,N-1} \lambda_{c,N-1} = A_N U_N \left(T_{c,N-1} - T_N\right) \quad \text{(Eq. 5.54)}$$

The energy and mass balances in the flash box N can be written as follows, taking into account that part of the distillate collected here is driven to the desuperheater:

$$q_{C,N-1} h''_{c,N-1} + (1 - y_{N-1})(1 - \alpha_{N-1}) q_{T,N-1} h_{c,N-1} + (1 - y_N) q_{TN} h_c - q_{FBN} h''_{VN} - q_{dsh} h''_{cN} = q_{CN} h''_{cN} \quad \text{(Eq. 5.55)}$$

$$q_{C,N} = q_{C,N-1} + (1 - y_{N-1})(1 - \alpha_{N-1}) q_{T,N-1} + (1 - y_N) q_{TN} - q_{FBN} - q_{dsh} \quad \text{(Eq. 5.56)}$$

As showed before, the temperature of the flashing condensate T''_{cN} is obtained through the non-equilibrium allowance parameter.

5.4.1.2 End condenser

The energy balance applied to the last condenser is defined by the following equation:

$$q_{in}(h_F - h_{in}) = (1 - y_N)(q_{DN} + q_{FEN} + q_{FBN}) \lambda_c \quad \text{(Eq. 5.57)}$$

being h_F the specific enthalpy of the feedwater (at T_F) at the exit of the end condenser, h_{in} the specific enthalpy of the seawater before entering the end condenser (at T_{in}) and λ_c the specific enthalpy of condensation of the total vapor at T_c.

The heat transfer equation associated with the end condenser is:

$$Q_c = A_c U_c LTMD_c \quad \text{(Eq. 5.58)}$$

where the overall heat transfer coefficient of the condenser (U_c) is calculated using the correlation obtained by El-Dessouky & Ettouney (2002b). The log mean temperature difference in the final condenser is given by:

$$LTMD_c = \frac{T_F - T_{in}}{ln\left(\frac{T_c - T_{in}}{T_c - T_F}\right)} \quad \text{(Eq. 5.59)}$$

5.4.1.3 Preheaters

The energy balance applied to the preheaters is given below, from $i = 1$ to $N - 1$:

$$q_{Fint,i}\bar{c}_{p,preh,i}\left(t_{preh,i} - t_{preh,i+1}\right) = \alpha_i q_{Ti}\lambda'_{Vi} + \alpha_i q_{Ti}\bar{c}_{p,BPE,i}\left(T'_{Vi} - T'_{Vsat,i}\right) \quad \text{(Eq. 5.60)}$$

where $\bar{c}_{p,preh,i}$ is the specific heat at constant pressure and mean temperature between $t_{preh,i}$ and $t_{preh,i+1}$, λ'_{Vi} is the specific enthalpy of vaporization at $T'_{Vsat,i}$, $T'_{Vsat,i}$ is the saturation temperature of the vapor after passing through the demister and $\bar{c}_{p,BPE,i}$ is the specific heat at constant pressure and mean temperature between T'_{Vi} and $T'_{Vsat,i}$ of the vapor. The latter term of the equation corresponds to the sensible heat associated with the BPE.

The heat transfer equation for the generic preheater i is:

$$Q_{preh,i} = A_{preh,i}U_{preh,i}LTMD_{preh,i} \quad \text{(Eq. 5.61)}$$

being $LTMD_{preh,i}$ the log mean temperature difference between the condensing vapor at T'_{Vi} and the preheating seawater:

$$LTMD_{preh,i} = \frac{t_{preh,i} - t_{preh,i+1}}{ln\left(\frac{T'_{Vi} - t_{preh,i+1}}{T'_{Vi} - t_{preh,i}}\right)} \quad \text{(Eq. 5.62)}$$

The overall heat transfer coefficient for a preheater is calculated using a correlation obtained by El-Dessouky & Ettouney (2002b).

5.4.1.4 Plate heat exchangers

The energy balance applied to the brine and distillate plate heat exchangers are presented below, respectively.

$$q_{sw,in,HX1}\bar{c}_{p,sw,HX1}(T_{sw,out,HX1} - T_{intake}) = q_D\bar{c}_{p,D}(T''_N - T_{D,out}) \quad \text{(Eq. 5.63)}$$

$$q_{sw,in,HX2}\bar{c}_{p,sw,HX2}(T_{sw,out,HX2} - T_{intake}) = q_B\bar{c}_{p,B}(T_N - T_{B,out}) \quad \text{(Eq. 5.64)}$$

where $q_{sw,in,PHX1}$ and $q_{sw,in,PHX1}$ are the mass flow rates of seawater entering each plate heat exchanger, which are assumed equal, $T_{sw,out,HX1}$ and $T_{sw,out,HX2}$ are the seawater temperature at the outlet of each plate heat exchanger, T_{intake} is the seawater temperature at the inlet of the plate heat exchangers, $\bar{c}_{p,sw,HXi}$ is the specific heat at constant pressure and mean temperature between $T_{sw,out,HXi}$ and T_{intake}, $T_{B,out}$ and $T_{D,out}$ are the brine and distillate outlet temperature

after the plate heat exchangers, respectively, $\bar{c}_{p,D}$ is the specific heat at constant pressure and mean temperature between T_N'' and $T_{D,out}$ of the distillate and $\bar{c}_{p,B}$ is the specific heat at constant pressure and mean temperature between T_N and $T_{B,out}$ of the exiting brine. The two seawater streams after the plate heat exchangers are mixed before entering the condenser at T_{in}.

5.4.1.5 Thermocompressor model

In Section 5.1 were defined the main parameters that characterize a thermocompressor; the entrainment ratio (Ra), or mass of motive steam (q_m) required per unit mass of the entrained vapor (q_{suc}), the compression ratio (CR), the pressure ratio of the compressed (p_{comp}) and suction vapour (p_{suc}), and expansion ratio (ER), or pressure ratio between motive (p_m) and suction vapour (see Eqs. 5.2, 5.3, and 5.4).

As it was previously analysed in Section 5.1 there are a limited number of methods available in the literature to determine Ra. However, these methods require tedious and lengthy calculation procedures which are not suitable for implementing in this model. For the model presented in this chapter, correlations for Ra developed by Hassan & Darwish (2014) (based on the Power's graphical method (Power, 1994)) that are a function on the compression and expansion ratios (pressure ratio of the motive steam and suction vapour) have been used due to its flexibility, allowing us to simulate wide range of operation conditions for the motive steam pressure, as explained in Section 5.1.

Applying the mass and energy balances to the thermocompressor, it results in:

$$q_{comp} = q_m + q_{suc} \quad \text{(Eq. 5.65)}$$

$$q_{comp} h_{comp} = q_m h_m + q_{suc} h_{suc} \quad \text{(Eq. 5.66)}$$

5.4.2 Plant performance

The plant performance has been evaluated by two parameters: the GOR and the sA. The GOR in a MED-TVC is determined as follows:

$$GOR = \frac{q_D}{q_m} \quad \text{(Eq. 5.67)}$$

The specific surface area (sA) is related directly to the cost of the plant since the evaporators represent one of the main shares (roughly 40%) of the total capital cost (Sommariva, 2010), and it is obtained by:

$$sA = \frac{\sum_{i=1}^{N} A_i + \sum_{i=1}^{N-1} A_{preh,i} + A_c}{q_D} \quad \text{(Eq. 5.68)}$$

5.4.3 Validation of the mathematical model

The model has been validated with available data of the Trapani MED-TVC plant in Sicily (Italy) (Temstet et al., 1996), which consists of four identical units of 9000 m^3/d each and twelve effects. The main fixed variables in the model were the number of effects, fresh water production, position of the thermocompressor, the motive steam pressure, temperature and salinity of the seawater intake, temperature of the external vapour introduced in the first evaporator, salinity of the brine in the first effect and the temperature of the seawater entering the end condenser after passing through the plate heat exchangers. The rest of the input data together with the mentioned ones are described in Table 5.5. The main output variables were the GOR, area of evaporators, preheaters, end condenser, temperature and salinity profiles along the effects and mass flow rates of all the streams. It is important to note that the thermodynamic losses have been minimized in the model in order to match the performance of the actual plant.

Table 5.5. Input data used to run the model (Temstet et al. (1996) except otherwise indicated.)

Inputs	Symbol	Value
Number of effects	N	12
Position of the thermocompressor	N_{effect}	12
Daily distillate production (m^3/d)	q_D	9000
Motive steam pressure (bar)	p_m	44.145
Motive steam temperature (ºC)	T_m	257
Heating steam temperature (ºC)	T_s	64.5
Intake seawater temperature (ºC)	T_{intake}	22
End condenser inlet seawater temperature ^ (ºC)	T_{in}	25.7
Feed seawater salinity (g/kg)	s_{in}	40
Brine in the first effect * (g/kg)	s_B	66.9
Vapor temperature in the last cell (ºC)	T_{VN}	37
Feed seawater temperature (ºC)	T_F	35
Feed seawater temperature to the first effect (ºC)	t_{preh1}	55
Tube longitude in evaporators (m)	L_{ev}	7
External diameter of evaporator tubes[1] (m)	D_{ext}	0.022
Internal diameter of evaporator tubes* (m)	D_{int}	0.018

Diameter of the tube lines between effects* (mm)	δ_i	1000
Tube longitude between effects* (m)	L_{pipes}	2
Wire diameter of demisters[2] (mm)	δ_w	0.32
Vapour velocity in demisters[2] (m/s)	v_{vapor}	1
Demister density[2] (kg/m^3)	ρ_m	100
Mesh pad thickness[2] (m)	L_m	0.1
Vessel diameter♣ (m)	D_{vessel}	5.5

^ Selected to match cooling requirements

* Assumption

♣ Selected to adjust the vapour velocity inside the effects

[1] Cipollina et al. (2005)

[2] El-Dessouky & Ettouney (2002a)

The validation was carried out by the comparison of the results obtained from the model with data of Trapani plant found in the literature. The results from the validation are shown in Table 5.6, which present a good agreement with the actual data, since the relative errors obtained were below 5% in all cases except in the number of tubes. This could be explained by the calculation method used, which might be different from the selected in the real design procedure. As observed, the vapour temperatures in several effects and the mass flow rates of intake, feed, cooling seawater, motive steam and brine blowdown are very close to the actual data.

Table 5.6. Comparison between actual data and model results. Reference: Temstet et al. (1996) used except otherwise indicated.

Variable	Trapani	Model	Error (%)
Vapour temperature in the 1st effect (ºC)	62.2	62.67	0.75
Vapour temperature in the 5th effect (ºC)	53	52.61	-0.73
Vapour temperature in the 11th effect (ºC)	39.3	39.47	0.43
Intake seawater mass flow rate (T/h)	1280	1272	-0.59
Feed seawater mass flow rate (T/h)	1130.4	1125	-0.49
Brine blowdown mass flow rate (T/h)	755	752.8	-0.29
Brine blowdown salinity (g/kg)	59.9	59.77	-0.22
Cooling mass flow rate (T/h)	149.6	147.6	-1.37
Motive steam flow rate (T/h)	22.5	22.83	1.45
GOR (-)	16.7	16.3	-2.40
Number of tubes in evaporators[1]	11,000	11,697	6.34

[1] Cipollina et al. (2005)

5.5 Parametric study

In order to find the best arrangement for the coupling with the power block of a CSP plant (see a schema of this integration in Figure 5.8), the model of the MED-TVC unit, once has been validated against real data, has been used to carry out a parametric study so as to analyse the influence of motive and suction vapour pressures on the GOR, the fresh water production, the exergetic power consumed and the specific heat transfer area of a MED-TVC unit.

The parametric study has been performed taking a base case that corresponds to a MED-TVC plant with 12 effects, a nominal capacity of 10,000 m^3 per day and the inputs shown in Table 5.7. The brine salinity reached in the first cell has been imposed to 65,900 ppm to avoid scaling in the tube bundle evaporators, and the feedwater flow rates have been considered equally distributed along the effects. From the base case, a parametric analysis has been performed at different motive and suction steam pressures. The motive steam pressures studied correspond to the available steam extractions from the Rankine cycle power block of the commercial CSP plant Andasol-1 (Montes et al., 2009) (see Table 5.8). Regarding the suction steam pressure, it has been varied considering different thermocompressor locations (TL) for every motive steam pressure. The location has been varied from the 12^{th} effect to the 5^{th} effect due to the operation limit of the thermocompressor. In order to achieve a stable operation, the compression ratio must be kept above the critical conditions (El-Dessouky et al., 2000), which means a CR above 2 corresponding to the 5^{th} effect.

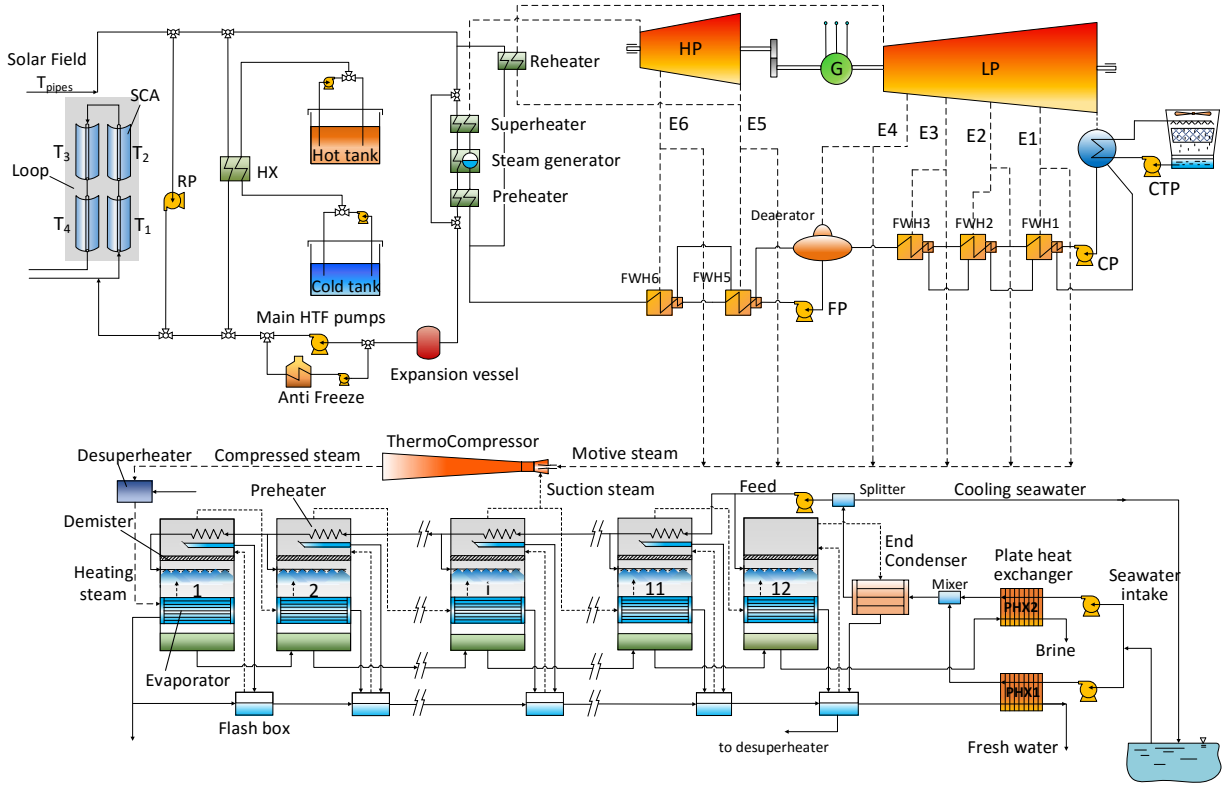

Figure 5.8. General scheme of the system: solar field, power block and multi-effect distillation plant.

Table 5.7. Main input data used in the MED-TVC base case study.

Variable	Symbol	Value	Reference
Plant capacity (m^3/d)	q_D	10,000	(Palenzuela, 2012)
Number of effects	N	12	(Cipollina et al., 2005)
Heating steam temperature (°C)	T_s	70	Assumption
Motive steam pressure (bar)	p_m	45.4	(Montes et al., 2009)
Intake seawater temperature (°C)	T_{intake}	22	(Temstet et al., 1996)
Seawater salinity at the inlet of the condenser (ppm)	X_{in}	40,000	(Temstet et al., 1996)
Rejected brine temperature (°C)	T_N	37	(Temstet et al., 1996)
Temperature of the seawater at the inlet of the condenser (°C)	T_{in}	25.9	Assumption
Temperature of the feed seawater (°C)	T_F	35	Assumption
Temperature of the preheated feed seawater entering the first effect (°C)	t_{preh1}	60	Assumption
Temperature of the distillate (°C)	$T_{D,out}$	25	Assumption
Brine salinity in the first effect (ppm)	X_1	65,900	Assumption

Table 5.8. Motive steam pressures used in the parametric study (Montes et al., 2009).

	E3	E4	E5	E6
Motive steam pressure (bar)	3.627	8.75	20.6	45.4

More importantly, a first analysis has been carried out in order to determine the optimum reduction in the heat transfer area of the subsequent effects to each location of the thermocompressor, $A_{afterTL}$. For this purpose, it has been assumed that the heat transfer area of such effects is a proportion (β) of the heat transfer area of the effects located before the position of the thermocompressor, as indicated in the following equation:

$$A_{after\,TL} = A_{before\,TL} \cdot \beta \tag{5.69}$$

The parameter β has been varied from 0.2 to 0.9 in order to find an optimum value of β such sA is minimum, and it has been performed for every motive steam pressure and every TL. Notice that the areas of the evaporators before the thermocompressor location, $A_{beforeTL,}$ and the area of all preheaters are equal to those determined in the base case and the feedwater mass flow rates entering the effects after the TL, which are imposed to be equal, are reduced in the same proportion than the heat transfer areas. According to this Equation, the lower β the higher is the reduction of the area of the evaporators after the thermocompressor location.

Then, for every optimum β, the thermocompressor location that leads to the maximum GOR is determined for each motive pressure. All of these results can be very useful when considering the coupling of a MED-TVC unit with a power block since they help to choose the most efficient desalination plant with the minimum costs depending on the pressure of the vapor extracted from the turbine that is used as motive steam in the MED-TVC plant.

5.6 Results and discussion

5.6.1 Base case

The results obtained from the computation of the model for the base case (taking the inputs from Table 5.7) are shown in Table 5.9 and Figure 5-A.1 in Appendix 5-A, which include the heat transfer area of evaporators, preheaters, end condenser, the GOR and distillate production.

Table 5.9. Results obtained in the base case simulation.

Variable	Symbol	Value
Heat transfer area of the evaporators (m^2)	A_{ev}	4839
Heat transfer area of the preheaters (m^2)	A_{preh}	149.9
Heat transfer area of the end condenser (m^2)	A_c	2045
GOR	-	14.35
Distillate production (m^3/d)	q_D	10,000

5.6.2 Parametric results

One of the main results found in this study is the existence of a β optimum (β_{opt}), which is that one which minimizes the sA, for every motive steam pressure and each thermocompressor location (TL). As an example, the variation of sA with β, for a motive steam pressure of 45.4 bar is depicted in Figure 5.9, for different TL. As observed, the higher TL the higher β_{opt}, which is due to the fact that lower number of subsequent effects to TL have a reduced heat transfer area, being the influence of β in the area reduction lower (according to Eq. (5.69)). It is expected that the total distillate production and the total area of the evaporators increase with β since lower area reduction after TL is given the higher the β. However, the existence of a minimum sA could be explained as follows: it has been checked that the total thermodynamic losses (determined by (Eq. 5.24)) increase with β as shown in Figure 5.10, which could cause a higher rate of growth in the distillate production than that in the area at initial values of β changing the trend to a lower rate of growth in the distillate production at higher values of β. It would result in a sA (that is the relation between the area and the distillate production) minimum as shown in Figure 5.9. The rest of values of β_{opt} for each motive steam pressure and TL are shown in Table 5.10, and further variables are presented in Table 5-A.1 in Appendix 5-A.

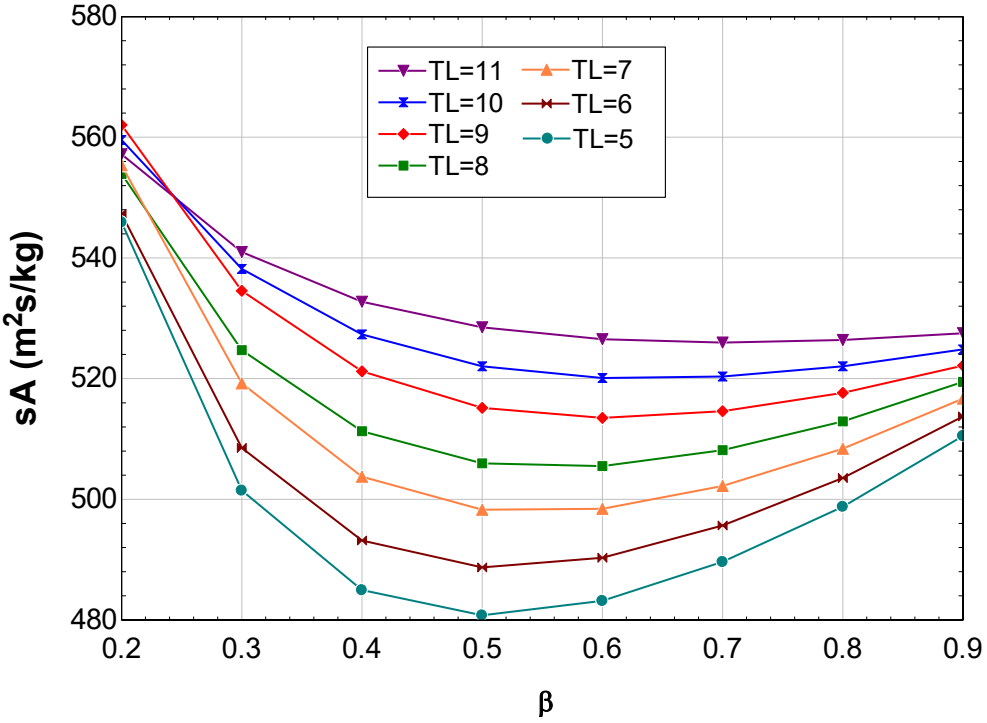

Figure 5.9. Variation of the total specific heat transfer area with the area reduction and thermocompressor location for a motive steam pressure of 45.4 bar.

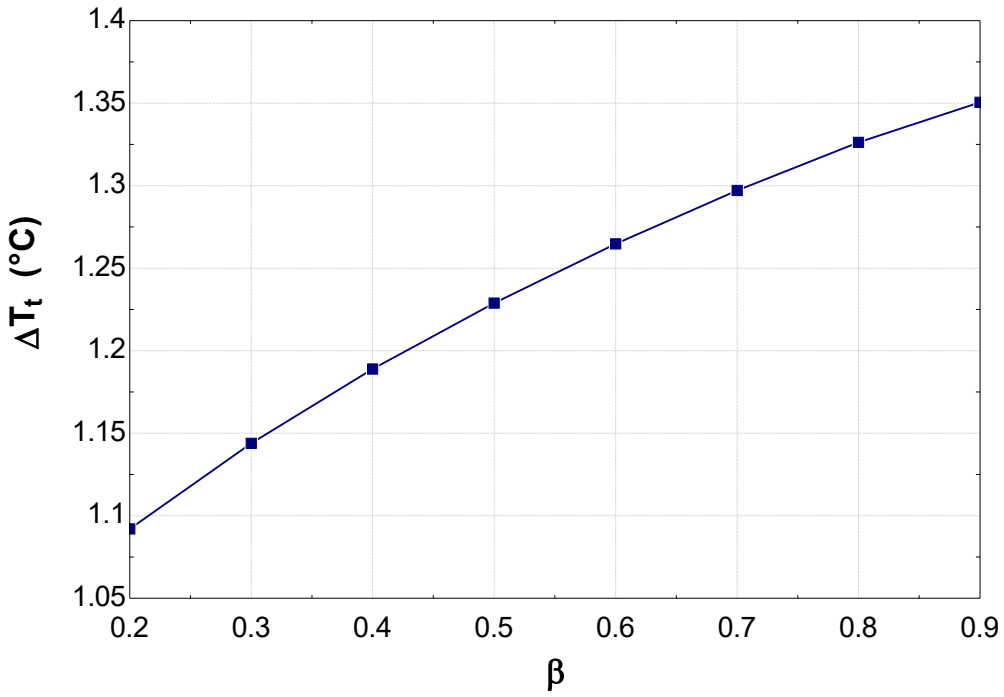

Figure 5.10. Change of the total sum of temperature losses with the area reduction for a motive steam pressure of 45.4 bar.

Table 5.10. Value of β_{opt} such minimizes the specific heat transfer area for every motive steam pressure and thermocompressor location.

Motive steam pressure (bar)	**TL**	$\boldsymbol{\beta_{opt}}$
45.4	11	0.7
45.4	10	0.6355
45.4	9	0.603
45.4	8	0.5631
45.4	7	0.5439
45.4	6	0.5166
45.4	5	0.5047
20.6	11	0.7171
20.6	10	0.6531
20.6	9	0.6178
20.6	8	0.5709
20.6	7	0.5506
20.6	6	0.5189
20.6	5	0.5057
8.75	11	0.7409
8.75	10	0.6747
8.75	9	0.6266
8.75	8	0.5903
8.75	7	0.5802
8.75	6	0.5608
8.75	5	0.5547
3.627	11	0.77
3.627	10	0.6981
3.627	9	0.6615
3.627	8	0.6208
3.627	7	0.6064
3.627	6	0.5824
3.627	5	0.5766

Figure 5.11 shows the trend of sA with respect to TL for each motive steam pressure, in which it can be observed that the minimum is always reached in the effect 5th (lowest limit permitted in TL) due to the fact that in this case the reduction in the heat transfer area is applied to a higher number of evaporators. Similar results were obtained in Kouhikamali et al. (2011), where the sA decreases with the increase in the suction pressure.

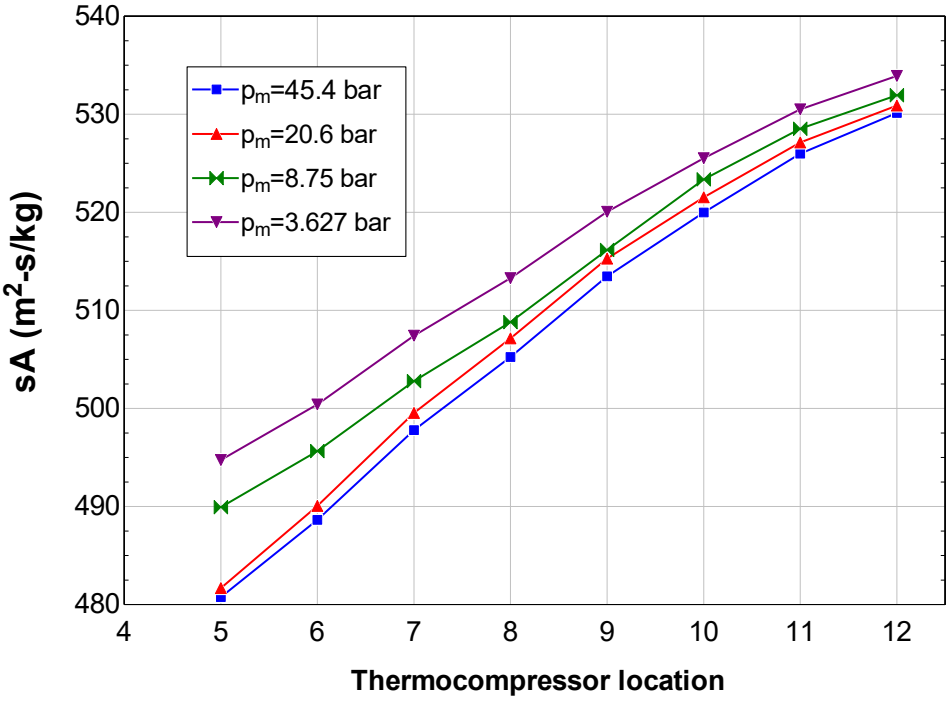

Figure 5.11. Specific heat transfer area versus the thermocompressor location and motive steam pressure.

Also, Figure 5.12 shows the results of the evolution of the GOR as function of the thermocompressor location for each motive steam pressure. As it can be seen, it is obtained an optimum position of the thermocompressor that maximizes the thermal efficiency of the desalination plant. This result is in accordance with those obtained by other authors (Kouhikamali et al., 2011; Liu et al., 2012). The existence of an optimum GOR could be explained by two different effects: on the right side of the figure, the GOR increases the lower the TL (that means higher suction pressure, since the steam ejector would be located further from the last effect) due to the fact that the steam ejector is able to entrain more amount of vapour the higher the suction pressure is, which leads to a decrease in the motive steam flow rate (to reach certain conditions at the outlet of the thermocompressor) and thus to an increase in the thermal efficiency of the plant. On the left side of the figure, the GOR decreases the lower the TL since it means the steam ejector must be located closer to the first effect, which causes an important decrease in the exploitation of energy by vapour recompression, resulting in a higher thermal consumption and therefore in a lower thermal efficiency of the desalination process. On the other hand, it can also be seen that for a fixed thermocompressor location, the GOR increases with the increase in the motive steam pressure. It is due to the fact that higher motive steam pressures lead to a higher amount of vapour entrained (because of the Venturi effect), which in turn results in lower motive steam flow rate required (keeping the outlet conditions of the thermocompressor roughly constant) and therefore in higher GOR**.** Finally, it can be observed that the position of the maximum GOR increases with the increase in the motive steam pressure. At higher motive steam pressures, the GOR increases the higher TL is

(thermocompressor located closer to the last effect) since on one hand, higher distillate production is obtained (more amount of vapour and higher specific heat transfer area is available to promote the evaporation/condensation processes as it will be shown later) and on the other hand, lower motive steam flow rate is required (as already mentioned before). At lower motive steam pressures, the decrease in the suction steam mass flow rate at higher TL is much higher than at high motive steam pressures, which lead to higher motive steam mass flow rates and therefore to lower GOR. Thus, it was obtained that for a motive steam pressure of 45.4 bar, the optimum thermocompressor location was the 11th effect, and for a motive steam pressure of 3.627 bar, the optimum was found in the 9th effect. The EES diagram outputs of these two optimized MED-TVC designs are presented in Figure 5-A.2 and Figure 5-A.3 (Appendix 5-A), respectively.

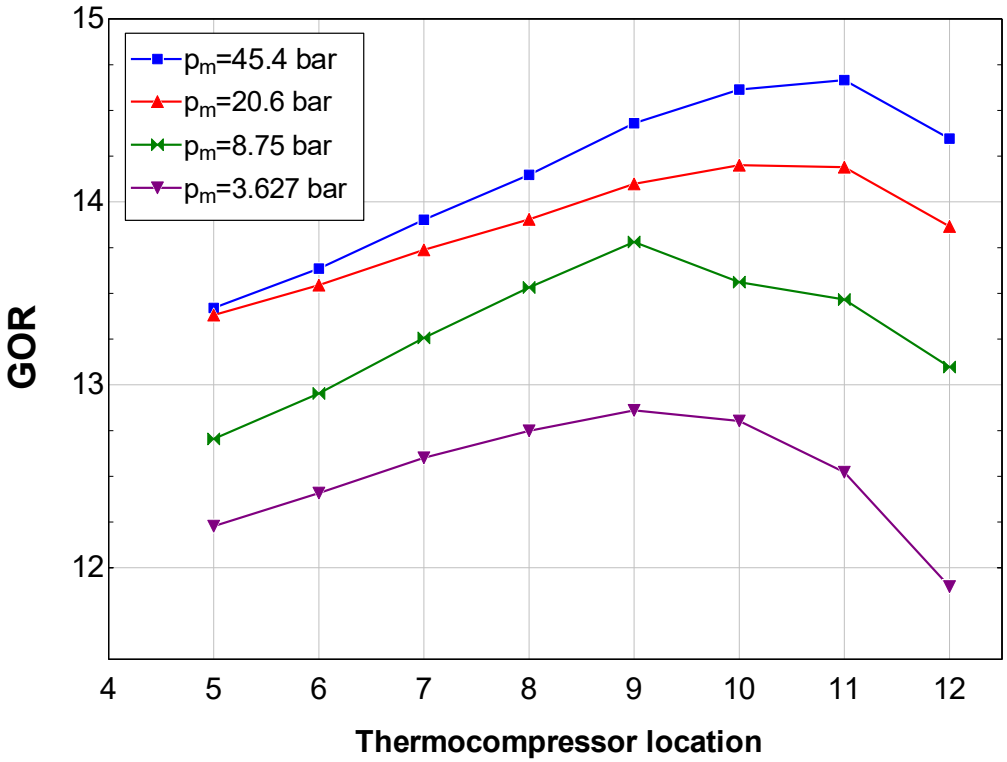

Figure 5.12. Gain output ratio as function of the thermocompressor location and motive steam pressure.

Figure 5.13 shows the effect of the thermocompressor location on the distillate production and the motive steam exergetic power. As observed, the distillate production increases the higher the TL (thermocompressor closer to the last effect) due to the fact that more amount of vapour and larger specific heat transfer area is available to promote the evaporation/condensation processes before the vapour entrainment by the thermocompressor. Also, it can be seen that, for a fixed TL, the distillate production is higher the lower the motive steam pressure. It could be explained due to the fact that the suction steam pressure decreases with the decrease in the

motive steam pressure which leads to a lower mass flow rate of entrained vapour. As a result, more steam after the steam ejector will be available to promote new evaporation/condensation processes and therefore more amount of distillate will be finally produced.

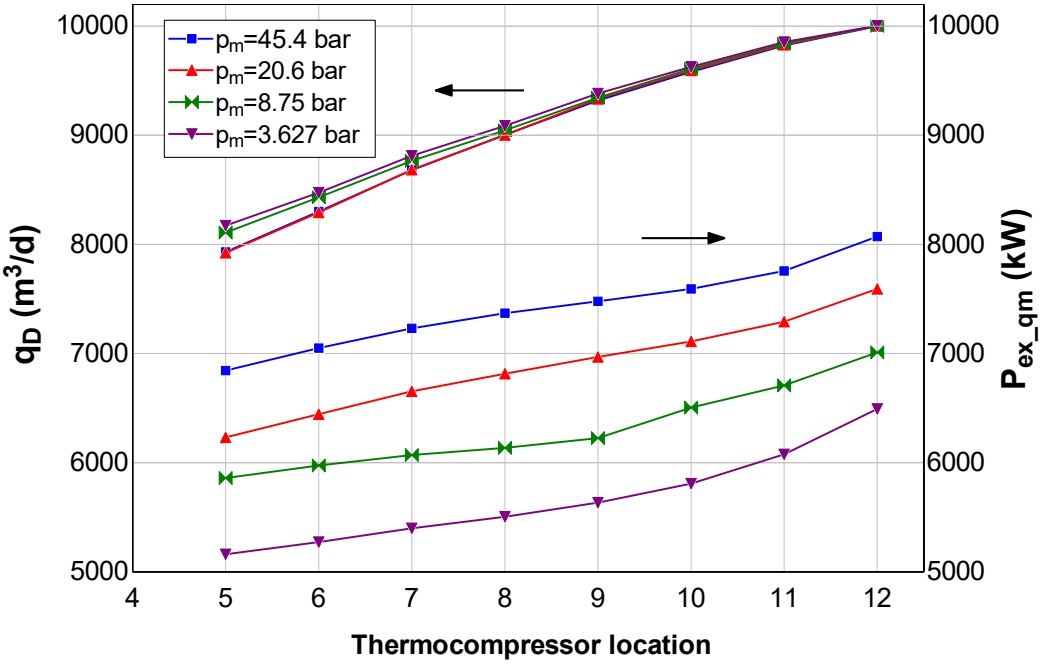

Figure 5.13. Freshwater production and exergetic power of the motive steam as function of the thermocompressor location and motive steam pressure.

With respect the exergetic power of the motive steam, it can be seen that higher motive steam pressures result in greater exergetic power, in accordance with Shen et al. (2011). It would mean a higher penalty in the electricity production of the power block in case a MED-TVC unit is coupled to a CSP plant. On the other hand, it is observed that the lower TL (higher suction steam pressure) the lower the exergetic power and therefore the lower the decrease in the electricity production in the case of a CSP+TVC-MED system. Particularly, for the particular MED-TVC design corresponding to a steam extraction pressure of 45.4 bar (TL=11), the exergetic power of the motive steam results of 7757 kW, while in the case of the MED-TVC design corresponding to a steam extraction pressure of 3.627 bar (TL=9), this value is of 5634 kW, that is, a reduction of 27%.

Figure 5.14 depicts the variation of the entrainment ratio (Ra, defined as the ratio between the motive steam mass flow rate and the suction steam mass flow rate) with the thermocompressor location. As it can be observed, Ra increases the higher the TL is (which means lower suction steam pressures). A decrease in the suction pressure leads to a decrease in the suction steam mass flow rate and therefore to an increase in the motive steam mass flow rate to reach certain conditions at the outlet of the thermocompressor. The effect in the decrease of suction steam mass flow rate is higher than that in the increase of the motive steam mass flow rate, which

results in higher entrainment ratios. For a fixed TL, the Ra decreases the higher the motive steam pressure is, which is also pointed out in Shen et al. (2011). This is due to the fact that, as mentioned before, higher motive steam pressures lead to higher suction steam flow rates and therefore to lower motive steam mass flow rates. The effect in the increase of the former is higher than that of the latter, giving place to lower entrainment ratios.

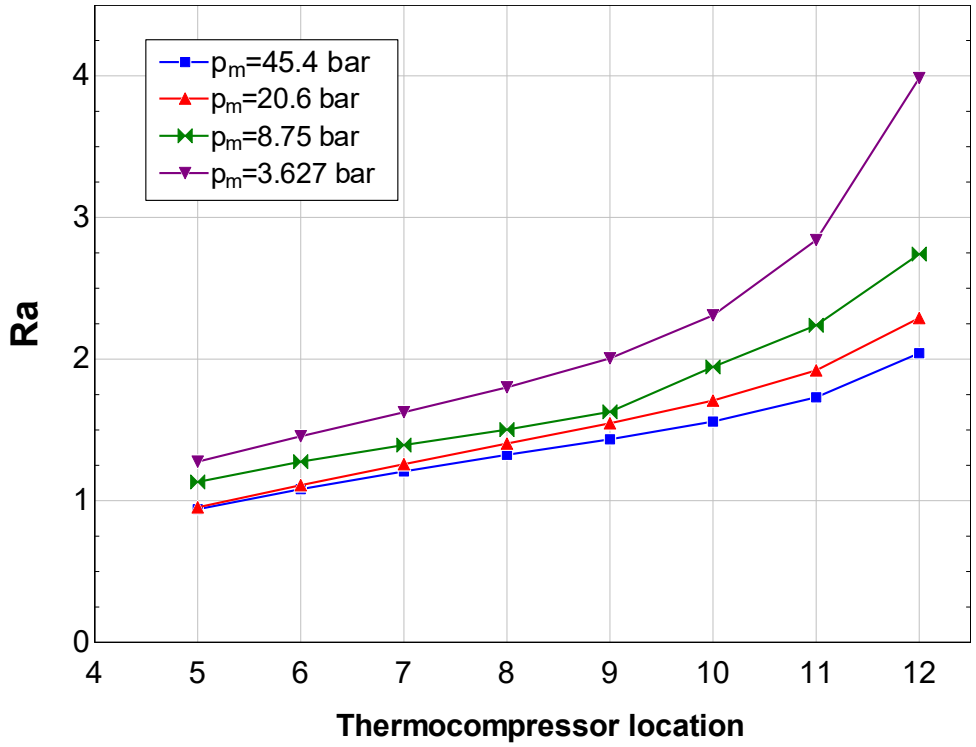

Figure 5.14. Entrainment ratio as function of the thermocompressor location and motive steam pressure.

The results above exposed can be very useful to determine the best arrangements when coupling a MED-TVC unit to a power block depending on the electricity and water demand curves. In a scenario where the electricity demand is high, the best arrangement which penalizes less the electricity production from the power block would be feeding the thermocompressor at effect number 9 with low pressure steam at 3.627 bar. In this case the GOR obtained would be 12.86 (a reduction of 10.38% respect to the base case, 14.35) and the distillate production 9384 m^3/d, 6.2% below the nominal production (10,000 m^3/d, when the thermocompressor is at the last effect). The specific heat transfer area required would be 520 m^2s/kg, 1.9% lower than the base case (530.1 m^2s/kg). On the other hand, if the electricity demand were low, the best coupling would be feeding the thermocompressor at effect number 11 with high quality steam at 45.4 bar. In this case, the GOR would be 14.67 (2.2% higher than the base case) and the distillate production 9823.4 m^3/d, 1.77% lower than the design daily production. The specific heat transfer area would be 526 m^2s/kg, which mean a decrease of 0.77% with respect to the nominal case.

5.7 Conclusions

A simulation tool for desalinated water production by multi-effect distillation with thermo-compression has been developed which allows to choose the best desalination plant from both an economic (optimal reduction in the heat transfer area of the evaporators located after the thermocompressor) and thermal efficiency (maximum GOR) point of view. Also, such tool allows selecting the best arrangements in the case of integrating a MED-TVC unit into a Rankine cycle power block, depending on the electricity and water demand profiles.

The possibilities of integration of the MED-TVC unit with a power block have been investigated, using actual data from the power cycle of a commercial CSP plant, reaching the following conclusions:

- For any given motive steam pressure, there is an optimal location of the thermocompressor such that the GOR is maximized. The higher the motive steam pressure, the higher GOR is reached and the steam ejector should be located closer to the last effect.
- There is an optimal reduction of the evaporator heat transfer areas after the thermocompressor position such minimizes the specific heat transfer area, for every motive steam pressure and each thermocompressor location. The closer to the last effect the steam ejector is located the lower the reduction in the evaporators' area of the desalination plant.
- The distillate production decreases considerably as the suction pressure increases, or equivalently, when the thermocompressor location is closer to the 5^{th} effect (lowest limit permitted in TL). The influence of the motive steam pressure on the distillate production is smaller although it is also observed that lower motive steam pressures lead to higher fresh water productions.

Regarding the influence on the integration of the MED-TVC unit into the power block, the following aspects are concluded:

- When the electricity demand is high, the best arrangement would be a MED-TVC unit taking a low pressure motive steam from the turbine extraction and locating the thermocompressor in one effect close to the 5^{th} effect, which would give more electricity production at the expense of decreasing the efficiency and the distillate production of the desalination plant (see Figure 5.12 and Figure 5.13).
- When the electricity demand is low, the best solution would be to use higher motive steam pressures from the turbine for the desalination plant and locate the steam ejector

in a position closer to the last effect, producing more amount of distillate at a higher efficiency (see Figure 5.12 and Figure 5.13).

Acknowledgement

The authors wish to thank the European Commission (DG for Research & Innovation) for its financial assistance within the Integrated Research Programme in the field of Concentrated Solar Power (CSP) (STAGE-STE Project; Grant Agreement No. 609837).

Appendix 5-A

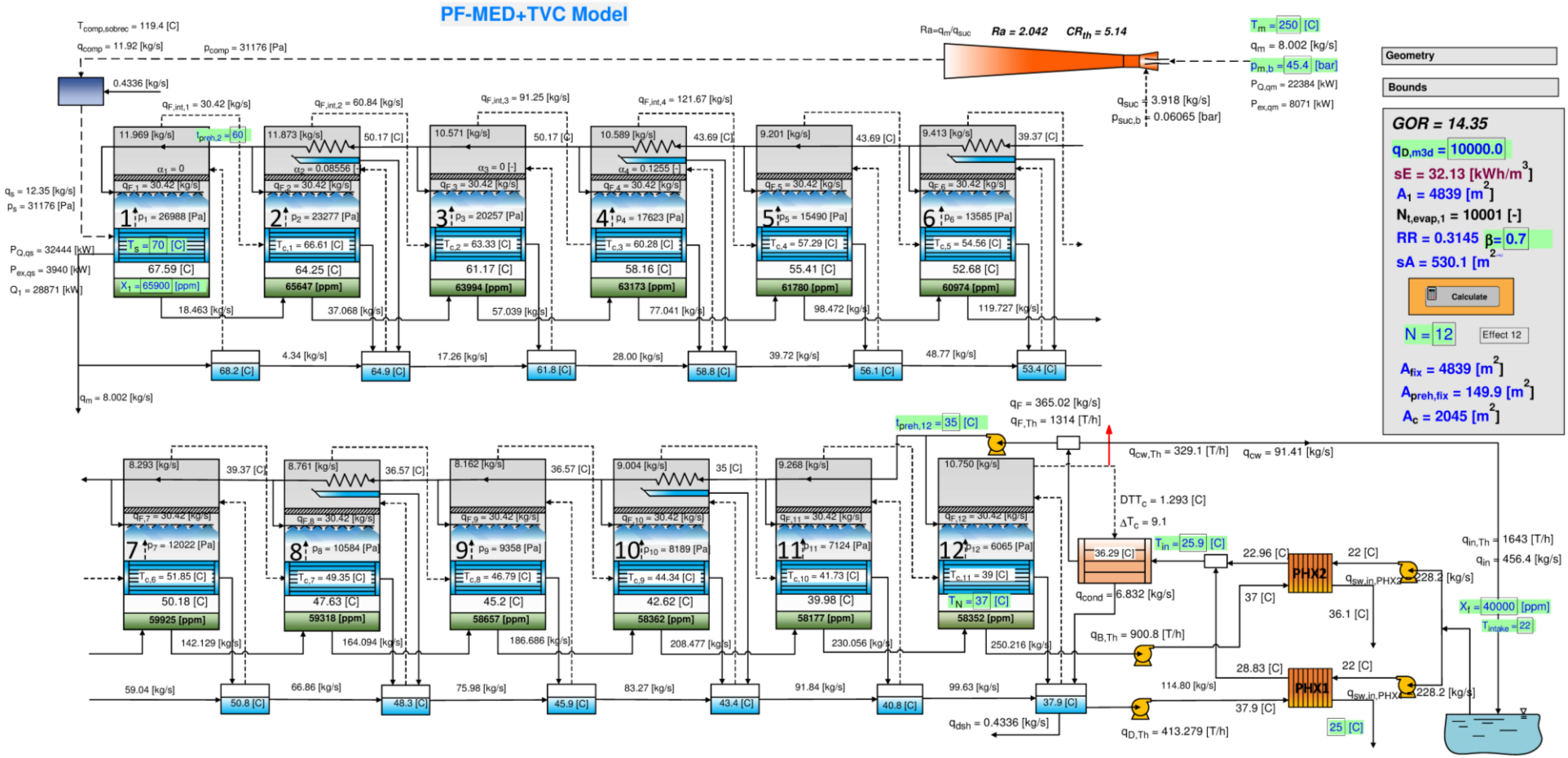

Figure 5-A.1. EES diagram window with the MED-TVC base case solved.

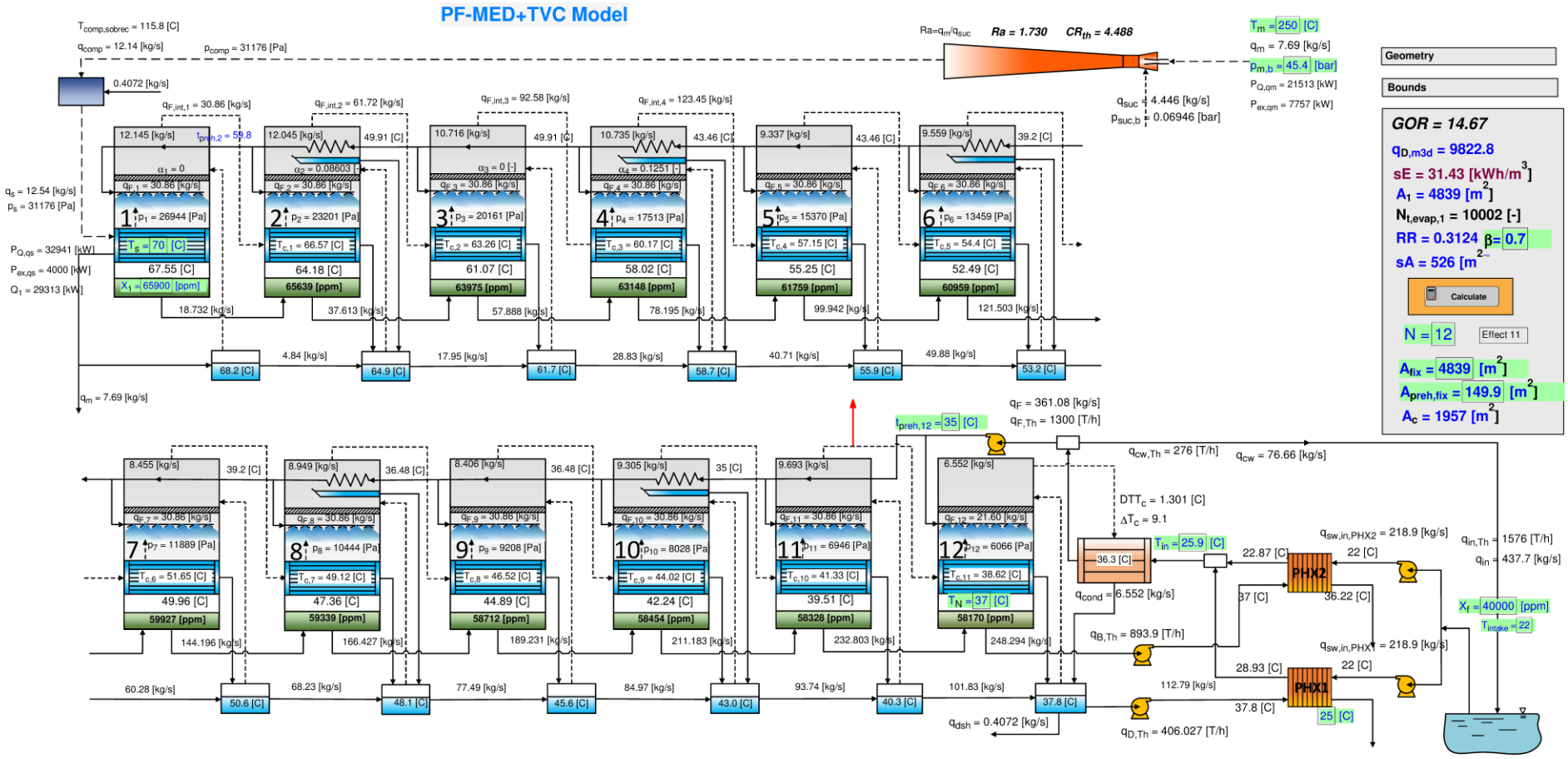

Figure 5-A.2. EES diagram window with the optimized MED-TVC fed by the high pressure steam extraction (45.4 bar).

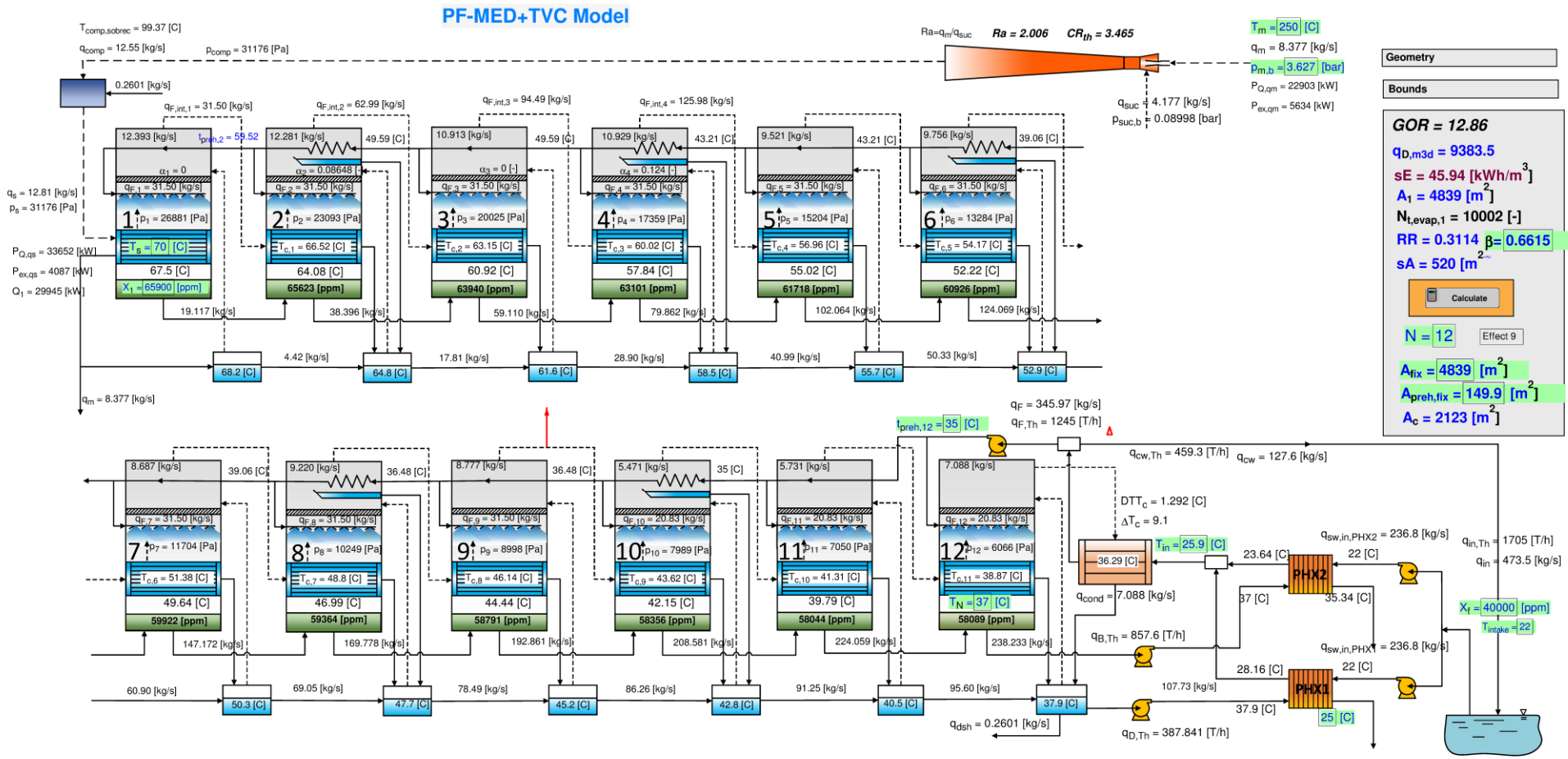

Figure 5-A.3. EES diagram window with the optimized MED-TVC fed by the low pressure steam extraction (3.623 bar).

Table 5-A.1. Main variables of the MED-TVC unit as function of the motive steam pressure and thermocompressor location

p_m	TC loc.	GOR	sA	A_c	q_D	q_m	q_{suc}	$P_{ex,qm}$	Ra
(bar)	-	-	(m^2/kg/s)	(m^2)	(m^3/d)	(kg/s)	(kg/s)	(kW)	-
45.4	12	14.35	530.1	2045	10001	8.003	3.919	8072	2.042
45.4	11	14.67	526	1957	9823	7.691	4.446	7757	1.73
45.4	10	14.61	520	1911	9581	7.528	4.83	7592	1.559
45.4	9	14.43	513.5	1884	9319	7.415	5.172	7479	1.434
45.4	8	14.15	505.2	1863	9003	7.306	5.519	7369	1.324
45.4	7	13.9	497.8	1831	8681	7.169	5.942	7231	1.207
45.4	6	13.63	488.6	1790	8302	6.99	6.465	7050	1.081
45.4	5	13.42	480.7	1733	7931	6.785	7.215	6843	0.9404
20.6	12	13.87	530.9	2137	10001	8.281	3.617	7591	2.289
20.6	11	14.19	527.1	2042	9830	7.954	4.141	7291	1.921
20.6	10	14.2	521.5	1986	9593	7.757	4.543	7111	1.707
20.6	9	14.1	515.3	1945	9333	7.601	4.916	6968	1.546
20.6	8	13.9	507.1	1906	9002	7.433	5.297	6814	1.403
20.6	7	13.74	499.5	1862	8685	7.258	5.767	6653	1.259
20.6	6	13.54	490.1	1805	8292	7.029	6.333	6443	1.11
20.6	5	13.38	481.7	1740	7923	6.797	7.13	6231	0.9534
8.75	12	13.1	531.9	2265	10003	8.768	3.198	7010	2.741
8.75	11	13.47	528.5	2153	9841	8.39	3.748	6708	2.238
8.75	10	13.56	523.4	2079	9610	8.136	4.185	6505	1.944
8.75	9	13.78	516.2	1977	9344	7.785	4.784	6224	1.628
8.75	8	13.53	508.8	1954	9046	7.674	5.107	6135	1.503
8.75	7	13.26	502.8	1938	8766	7.592	5.449	6069	1.393
8.75	6	12.95	495.7	1913	8432	7.473	5.858	5974	1.276
8.75	5	12.7	489.9	1873	8109	7.328	6.466	5858	1.133
3.627	12	11.9	533.9	2504	10005	9.654	2.423	6492	3.984
3.627	11	12.52	530.5	2314	9854	9.035	3.181	6076	2.841
3.627	10	12.8	525.5	2195	9628	8.634	3.739	5807	2.309
3.627	9	12.86	520	2123	9384	8.377	4.177	5634	2.006
3.627	8	12.75	513.3	2075	9088	8.184	4.546	5504	1.8
3.627	7	12.6	507.4	2037	8811	8.028	4.942	5399	1.625
3.627	6	12.41	500.4	1991	8474	7.84	5.388	5273	1.455
3.627	5	12.23	494.7	1944	8172	7.673	6.017	5160	1.275

References

Al-Juwayhel, F., El-Dessouky, H., Ettouney, H., 1997. Analysis of single-effect evaporator desalination systems combined with vapor compression heat pumps. Desalination 114, 253–275. doi:10.1016/S0011-9164(98)00017-4

Aly, N.H., Karameldin, A., Shamloul, M.M., 1999. Modelling and simulation of steam jet ejectors. Desalination 123, 1–8. doi:10.1016/S0011-9164(99)00053-3

Bin Amer, A.O., 2009. Development and optimization of ME-TVC desalination system. Desalination 249, 1315–1331. doi:10.1016/j.desal.2009.06.026

Casimiro, S., Cardoso, J., Ioakimidis, C., Farinha Mendes, J., Mineo, C., Cipollina, A., 2014. MED parallel system powered by concentrating solar power (CSP). Model and case study: Trapani, Sicily. Desalin. Water Treat. 1–14. doi:10.1080/19443994.2014.940222

Cipollina, A., Micale, G., Rizzuti, L., 2005. A critical assessment of desalination operations in Sicily. Desalination 182, 1–12. doi:10.1016/j.desal.2005.03.004

Dahdah, T.H., Mitsos, A., 2014. Structural optimization of seawater desalination: II novel MED–MSF–TVC configurations. Desalination 344, 219–227. doi:10.1016/j.desal.2014.03.026

Darwish, M.A., Darwish, A., 2014. Solar cogeneration power-desalting plant with assisted fuel. Desalin. Water Treat. 52, 9–26. doi:10.1080/19443994.2013.797674

DLR, 2009. Global Potential of Concentrating Solar Power [WWW Document]. URL http://www.dlr.de/tt/desktopdefault.aspx/tabid-2885/4422_read-16596/

Eames, I.., Aphornratana, S., Haider, H., 1995. A theoretical and experimental study of a small-scale steam jet refrigerator. Int. J. Refrig. 18, 378–386. doi:10.1016/0140-7007(95)98160-M

El-Dessouky, H., 1997. Modeling and simulation of thermal vapor compression desalination plant, in: Symposium on Desalination of Seawater with Nuclear Energy. Republic of Korea.

El-Dessouky, H., Alatiqi, I., Bingulac, S., Ettouney, H., 1998. Steady-state analysis of the multiple effect evaporation desalination process. Chem. Eng. Technol. 21, 437–451. doi:10.1002/(SICI)1521-4125(199805)21:5<437::AID-CEAT437>3.0.CO;2-D

El-Dessouky, H., Ettouney, H., Alatiqi, I., Al-Nuwaibit, G., 2002. Evaluation of steam jet ejectors. Chem. Eng. Process. 41, 551–561.

El-Dessouky, H.T., Ettouney, H.M., 2002. Thermodynamic Losses, in: El-Dessouky, H.T., Ettouney, H.M. (Eds.), Fundamentals of Salt Water Desalination. Elsevier Science B.V., Amsterdam, pp. 565–583. doi:10.1016/B978-044450810-2/50014-2

El-Dessouky, H.T., Ettouney, H.M., Al-Juwayhel, F., 2000. Multiple Effect Evaporation—Vapour Compression Desalination Processes. Process Control 78, 662–676. doi:http://0-dx.doi.org.fama.us.es/10.1205/026387600527626

Engineering Sciences Data Unit (ESDU), 1993. Condensation inside tubes: pressure drop in straight horizontal tubes. ESDU Heat Transf. Ser. Sect. 10 Condens.

Friedel, L., 1979. Improved friction pressure drop correlations for horizontal and vertical two-phase pipe flow. Eur. Two-Phase Flow Gr. Meet.

H&C Heat Transfer Solutions, 2014. Heat Transfer Coefficients, in: El-Dessouky, H.T., Ettouney, H.M. (Eds.), Fundamentals of Salt Water Desalination. Elsevier Science B.V., Amsterdam, pp. 585–598. doi:10.1016/B978-044450810-2/50015-4

Hassan, A.S., Darwish, M.A., 2014. Performance of thermal vapor compression. Desalination 335, 41–46. doi:10.1016/j.desal.2013.12.004

International Energy Agency, 2013. IEA Key World Energy Statistics 2013 (RPRT). Paris, France.

Keenan, J.H., Neumann, E.P., 1942. A simple air ejector. ASME J. Appl. Mech. A75–A81.

Keenan, J.H., Neumann, E.P., Lustwerk, F., 1948. An Investigation of Ejector Design by Analysis and Experiment, Meteor report. Massachusetts Institute of Technology, Guided Missiles Program.

Klein, S.A., 2013. Engineering Equation Solver Software (EES).

Kouhikamali, R., Mehdizadeh, M., Sanaei, M., 2011. Process investigation of different locations of thermo-compressor suction in MED-TVC plants. Desalination 280, 134–138. doi:10.1016/j.desal.2011.06.070

Liu, X.H., Cao, G.J., Shen, S.Q., Zhao, G. Bin, 2012. Performance Analysis of Parallel Feed LT-MED Desalination System with Thermal Vapor Compressor. Adv. Mater. Res. 347–353, 3058–3063. doi:10.1080/19443994.2012.682966

Miyatake, O., Murakami, K., Kawata, Y., Fujii, T., 1973. Fundamental experiments with flash evaporation. Heat Transf. Jpn. Res. 2, 89–100.

Montes, M.J., Abánades, A., Martínez-Val, J.M., Valdés, M., 2009. Solar multiple optimization for a solar-only thermal power plant, using oil as heat transfer fluid in the parabolic trough collectors. Sol. Energy 83, 2165–2176. doi:10.1016/j.solener.2009.08.010

Nayyar, M.L., 2006. Piping handbook [WWW Document]. URL http://site.ebrary.com/id/10226666

Palenzuela, P., 2012. Coupling assessment of multi-effect distillation plants and solar thermal power plants (THES). Universidad de Almería y Plataforma Solar de Almería, Almería.

Palenzuela, P., Zaragoza, G., Alarcón-Padilla, D.C., Blanco, J., 2013. Evaluation of cooling technologies of concentrated solar power plants and their combination with desalination in the mediterranean area. Appl. Therm. Eng. 50, 1514–1521. doi:10.1016/j.applthermaleng.2011.11.005

Palenzuela, P., Zaragoza, G., Alarcón-Padilla, D.C., Guillén, E., Ibarra, M., Blanco, J., 2011.

Assessment of different configurations for combined parabolic-trough (PT) solar power and desalination plants in arid regions. Energy 36, 4950–4958. doi:10.1016/j.energy.2011.05.039

Power, R.B., 1994. Steam jet ejectors for the process industries. McGraw-Hill, New York.

Romero, M., González-Aguilar, J., 2014. Solar thermal CSP technology. Wiley Interdiscip. Rev. Energy Environ. 3, 42–59. doi:10.1002/wene.79

Sharqawy, M.H., Lienhard V, J.H., Zubair, S.M., 2010. Thermophysical properties of seawater: A review of existing correlations and data. Desalin. Water Treat. 16, 354–380. doi:http://dx.doi.org/10.5004/dwt.2010.1079

Shen, S., Zhou, S., Yang, Y., Yang, L., Liu, X., 2011. Study of steam parameters on the performance of a TVC-MED desalination plant. Desalin. Water Treat. 33, 300. doi:10.5004/dwt.2011.2653

Sommariva, C., 2010. Desalination and advance water treatment : economics and financing. Balaban Desalination Publications, Hopkinton, MA.

Temstet, C., Canton, G., Laborie, J., Durante, A., 1996. A large high-performance MED plant in Sicily. Proc. 1st Symp. Eur. Desalin. Soc. 'Desalination Eur. 105, 109–114. doi:10.1016/0011-9164(96)00064-1

UNESCO and World Water Assessment Programme, 2014. The United Nations World Water Development Report 2014: Water and Energy (RPRT). París.

Wagner, W., Pruß, A., 2002. The IAPWS formulation 1995 for the thermodynamic properties of ordinary water substance for general and scientific use. J. Phys. Chem. Ref. Data 31, 387–535.

White, F.M., 2014. Fluid Mechanics, McGraw-Hill international editions. McGraw-Hill. doi:10.1007/b138775

Chapter 6. Operational analysis of the coupling between a MED-TVC unit and a Rankine cycle power block using variable nozzle thermocompressors

Contents

List of figures

List of tables

Nomenclature

Variables

A	Area, m^2
k_s	Heating steam constant
p_m	Motive steam pressure, bar
Q_1	Heat rate in first effect, kW
q_{comp}	Compressed steam mass flow rate, kg/s
q_{cw}	Cooling seawater mass flow rate, T/h
q_{design}	Design mass flow rate of steam in PB, kg/s
q_D	Flow rate of distillate produced, m^3/d
q_F	Feedwater mass flow rate, T/h
q_{in}	Intake seawater mass flow rate, T/h
q_{LP1}	Mass flow rate of steam in FWH LP1, T/h
q_m	Motive steam mass flow rate, kg/s
sA	Specific heat transfer area, $m^2 \cdot s/kg$
T_s	Heating steam temperature, °C
X_1	Brine salinity in the first effect, ppm

Acronyms and abbreviations

CR	Compression Ratio
DEA	Deaerator
EES	Engineering Equation Solver
FHW	Feedwater Heater
GOR	Gain Output Ratio
HP	High Pressure
LP	Low Pressure
LT	Low Temperature
MED	Multi-Effect Distillation
PB	Power Block
TC	Thermocompressor
TVC	Thermal Vapour Compression

Subscripts

act	Actual
c	End condenser
comp	Compressed
cw	Rejected cooling seawater
D	Distillate
F	Feedwater
in	Intake or inlet
lim	Limit
m	Motive steam
nom	Nominal
opt	Optimum
preh	Preheater

Greek

β	Reduction of evaporator area
Δ	Variation step

6.1 Introduction

Among the different thermal desalination technologies suitable for coupling with a Rankine cycle power block, the Multi-Effect Distillation (MED) represents the most efficient one from a thermodynamic point of view (Darwish and El-Dessouky, 1996). One of the most feasible coupling arrangements is the integration of a Low Temperature MED (LT-MED) unit replacing the condenser of the power block, which uses heating steam from the outlet of the turbine at a maximum temperature of 70 °C in order to reduce the risk of scale formation on the tubes of the evaporators. However, in this case the freshwater production cannot be decoupled from the load of the turbine and there are not possibilities of regulation according to the electricity and water demands of the location. The integration of Thermal Vapour Compression (MED-TVC) units into CSP plants has a major advantage with respect that one: the possibility of decoupling the fresh water and power productions, which provides more flexibility to the operation of the plant and permits to adapt both productions to the daily or seasonal demands. In addition, there is no need to replace the condenser of the power cycle as in the case of the LT-MED and it allows the steam to be expanded completely through the turbine. Moreover, the thermal efficiency the MED-TVC unit is significantly increased with respect the LT-MED plants. In the CSP+MED-TVC configuration, the coupling with a power block is made through one of the steam extractions of the turbines, being the steam used as motive steam for the ejectors.

Most of the MED-TVC plants use conventional thermocompressors, which are designed for a fixed motive steam pressure and can only operate at an acceptable efficiency with motive steam pressures close to the nominal. When these plants are integrated into a power plant, it is needed to adapt the steam ejectors to the operation of the power block (the part load operation of the power block leads to changes in the pressure of the steam extractions from the turbine), which is only possible with the use of variable nozzle thermocompressors. They are able to modify the motive steam mass flow rate with a spindle located inside the nozzle, which changes its cross sectional area. Thus, the mass flow rate of motive steam can be kept constant or varied for convenience when the motive steam pressure changes at part load conditions, operating always with the maximum possible efficiency.

Although the literature related with the use of variable nozzle thermocompressors is scarce, the advantages of this kind of ejectors in MED desalination plants using steam from a power plant have been already pointed out by several authors. Desportes (2006) showed its use in the Huanghua Project in China. In that project, which was aimed to produce both power and water, a combined cycle power plant with two generation blocks of 600 MW fed two MED-TVC units with 4 effects and a capacity of 10,000 m^3/d each, using steam from the medium pressure turbines of the power plant. A variable nozzle thermocompressor was implemented for the MED-TVC units, permitting to adjust or keep the motive steam mass flow rate constant when

the pressure of the steam extracted from the turbines varies. In such way, the thermocompressor could be operated always with the maximum efficiency possible at the given pressure. Also, Shemer (2011) described the issues found in the operation process of a MED-TVC unit integrated with a coal-fired power plant in Tianjin (China), particularly the changes in the motive steam pressure as result of the decrease in the power demand, being the power block controlled with the sliding pressure method. This was solved by introducing variable nozzle thermocompressors that could handle the variable pressures maintaining always a high efficiency. Efrat and Haimiao (2013) also presented the benefits of the design of the MED-TVC plant in the above-mentioned power plant in Tianjin, which integrates the production of power, freshwater and brine. They underlined the great flexibility of operation achieved thanks to the variable nozzle thermocompressors, providing a high efficiency in the power, freshwater and brine production. The importance of using thermocompressors with adjustable cross sectional area of the nozzle has been also highlighted by other authors (Yang et al., 2013; Zhang et al., 2013), because of their capacity of working with high efficiency in a wide range of motive steam pressure conditions.

None of the above studies have analysed deeply the operation of a MED-TVC unit integrated into a CSP plant using variable nozzle thermocompressors. This chapter analyses the operation limits and the performance of the desalination unit at different loads of a Rankine cycle power block. To that end, a parametric study of the MED-TVC unit at part load operation has been carried out, taking into account the variation of the motive steam pressure as a result of the decrease in the power demand. Moreover, the strategy followed to simulate the off-design operation of the MED-TVC unit and its effect on the main performance variables is presented.

6.2 Modelling of the system

6.2.1 Rankine cycle power block

A 50 MW_e Rankine cycle power block has been modelled in Thermoflex® (Thermoflow, 2016), a software which enables to investigate the power production with high accuracy at design and off-design conditions. The power block (see Figure 6.1) is a single reheat, regenerative Rankine cycle with six feedwater heaters (FWH) with the same configuration as the commercial solar thermal power plant Andasol-1 (Montes et al., 2009). Table 6.1 shows the main parameters of the power block. The feedwater is preheated in three low-pressure feedwater heaters (LP P1, LP P2, LP P3), in a deaerator and in two high-pressure feed water heaters (HP P1, HP P2). The steam generator, which integrates the economizer, boiler and super-heater, has an efficiency of 98% and a 4.5 bar pressure drop and it delivers the superheated steam at 90 bar and 370 °C to a high pressure (HP) turbine. The second high

pressure preheater (HP P2) is fed by a 45.4 bar steam extraction from the HP expansion line. The remaining stream expands until 20.6 bar. A second extraction point, which feeds HP P1, matches the HP turbine outlet. A reheater increases the steam temperature to 370 °C before the low pressure (LP) expansion line. Both HP and LP turbines are regulated with the *sliding pressure* mode, thus maintaining the temperature of the steam entering the HP turbine constant at partial load while decreasing the pressure and mass flow rate of steam. Therefore, the steam generator and reheater are modelled to provide the nominal steam temperature of 370 °C in both design and off-design conditions. Four steam extractions from the LP turbine feed the deaerator and three LP feedwater heaters. LP expansion line is split in five turbine stages in which steam expands from 18.18 bar and 370 °C to 0.08 bar (water-cooled condenser operative pressure). The inlet pressure for each stage of the turbines is set according to Stodola law, where the following ratio is determined as follows:

$$q \cdot \frac{\sqrt{T_{in}}}{p_{in}} = const \qquad \text{(Eq. 6.1)}$$

being q the steam mass flow rate at the inlet of each stage, T_{in} and p_{in} are the inlet steam temperature and pressure in each turbine stage, respectively.

Different configurations have been selected for the integration of the MED-TVC unit into the power block. Each one considers that part of the steam extracted from the turbine is taken as motive steam to feed the thermocompressor coupled to the desalination plant, returning the condensed vapour from the first effect of the MED plant to the condenser of the power block as subcooled liquid. In this way, four configurations results from integrating the MED-TVC unit to the following steam extractions of the power block: 45.4, 20.6, 8.75 and 3.627 bar, corresponding to HP2, HP1, DEA and LP3, respectively. In all cases, the steam mass flow rate entering in the HP turbine at design conditions has been considered as input of the model (63.42 kg/s), which has been taken equal to that used in a plant similar to Andasol-1 (Montes et al., 2009).

Simulations of the power block have been performed for a wide range of load, from 120% to 20% (the technical minimum of the steam turbines operation is about 15–20% (MHPS, 2016)), in order to study the limit load that allows a constant motive steam mass flow rate for the thermocompressor equal to the one at nominal conditions, and therefore an on-design operation of the MED-TVC plant. From the limit load onwards, the motive steam mass flow rate to the thermocompressor of the MED-TVC unit was reduced and the simulations of the power block were performed until the minimum achievable load of the power block was obtained (that one that allows the convergence of the model).

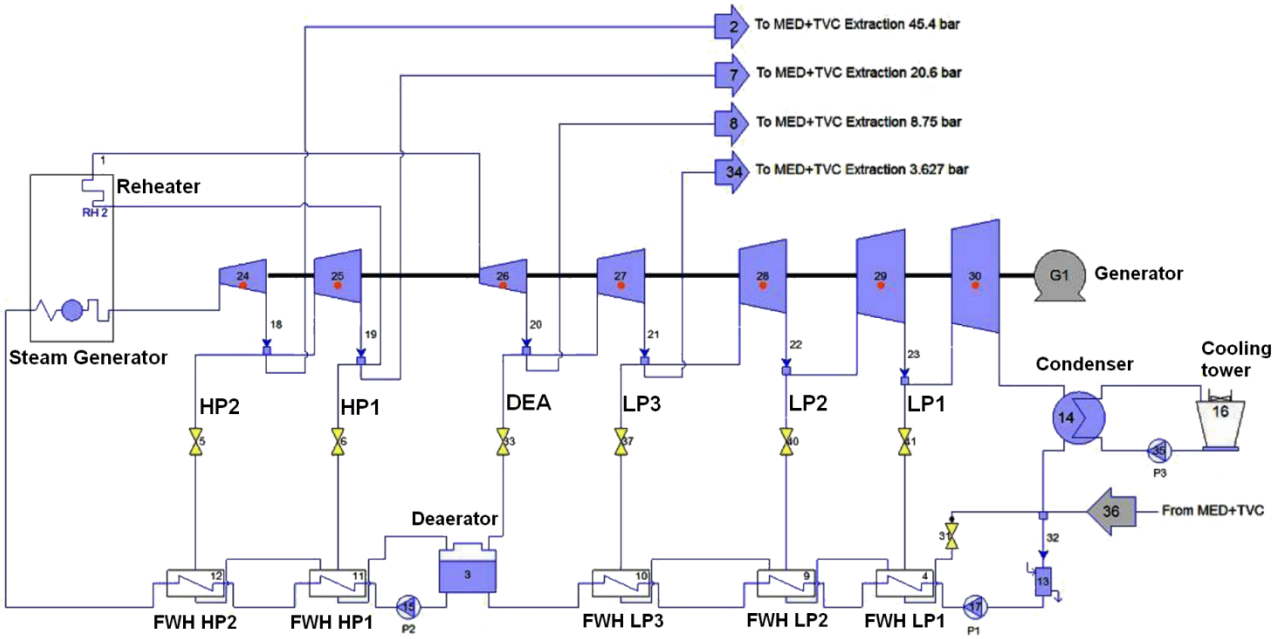

Figure 6.1. Diagram of the power block model in Thermoflex.

Table 6.1. Main parameters of the power block at nominal conditions (Montes et al., 2009).

Parameter	**Value**
Turbines	
HP inlet temperature (°C)	370
HP inlet pressure (bar)	90
High pressure turbine efficiency (%)	85.5
Low pressure turbine efficiency (%)	89.5
Electro-mechanical efficiency (%)	98
Condenser	
Pressure (bar)	0.08
Extraction point pressures	
Extraction line HP2 (bar)	45.4
Extraction line HP1 (bar)	20.6
Extraction line DEA (bar)	8.75
Extraction line LP3 (bar)	3.627
Extraction line LP2 (bar)	1.224
Extraction line LP1 (bar)	0.3461
Pressure drop	
Extraction line HP2 (%)	2.5
Extraction line HP1 (%)	3

Extraction line DEA (%)	4.5
Extraction line LP3 (%)	3
Extraction line LP2 (%)	3
Extraction line LP1 (%)	3.5
Reheating line (%)	11.75
Condenser pump	
Isentropic efficiency (%)	75
Electro-mechanical efficiency (%)	98
Feedwater pump	
Isentropic efficiency (%)	78
Electro-mechanical efficiency (%)	98
Closed feedwater heaters	
Terminal temperature difference (°C)	1.5
Drain cooling approach (°C)	5
Steam generator	
Thermal efficiency (%)	98
Total pressure drop (water side) (bar)	4.5

6.2.2 Multi-effect distillation with thermal vapour compression unit

6.2.2.1 Process description

The multi-effect distillation technology for seawater desalination is based on consecutive processes of evaporation of the seawater and subsequent condensation of the generated vapour. These processes take place inside connected vessels, called effects, each one at a pressure lower than the previous one, in order to be able to reuse the latent heat of the vapour. In general, each effect is comprised of a falling film evaporator, a demister, a preheater and a flash box. In the parallel/cross feed configuration (the one used in this study), the feedwater enters each effect at the same time, after being warmed up in the preheaters. The only external thermal energy addition occurs in the first evaporator, usually using saturated vapour (called heating steam) at a temperature below 70 °C to avoid the appearance of scaling over the external surface of the tubes. The feedwater entering the first effect is sprayed over the tube bundle of the evaporator, generating a thin falling film that boils as consequence of the heat released by the condensation of the heating steam inside the tubes. On one hand, vapour, which is considered free of salts, is produced, and on the other hand, concentrated brine is deposited

at the bottom of the effect and driven to the next effect, where is mixed with the brine of such effect. In this process a small amount of flash vapour is produced, which contributes to the total amount of vapour generated in the effect. Part of the total vapour generated condenses in the preheater, warming up the feedwater, and the rest is directed inside the tubes of the next evaporator and used as the driving force of the following evaporation-condensation process, at lower temperature and pressure. For a generic intermediate effect, the steam condensed in the associated preheater along with the steam condensed inside the evaporator are driven to the corresponding flash box, where they are collected, generating additional vapour by flash. This sequence is repeated until the last effect, where the remaining vapour releases its latent heat in the end condenser, which is used as the refrigeration system of the process.

One important component of a MED-TVC unit is the thermocompressor, which is a simple device that compresses low pressure vapour (suction or entrainment steam) using high pressure vapour (motive steam) by means of the well-known Venturi effect. It has three main sections: in the first convergent section, the fluid is accelerated creating a pressure decrease that drags the entrainment vapour into the middle section, called mixing zone. After that, in the divergent section, the mixed vapour is decelerated and its pressure elevated up to an intermediate pressure between the motive steam pressure and the entrainment vapour pressure. Variable nozzle thermocompressors (Figure 6.2) are able to cope with a wide broad of operating conditions maintaining a good performance, because of their ability to keep the motive steam flow rate constant when the pressure decreases. This is done with a spindle inside the nozzle that moves back and forth and changes the cross sectional area, letting pass a higher/lower amount of motive steam. That is why the concept of variable nozzle thermocompressors is so interesting in dual purpose power plants.

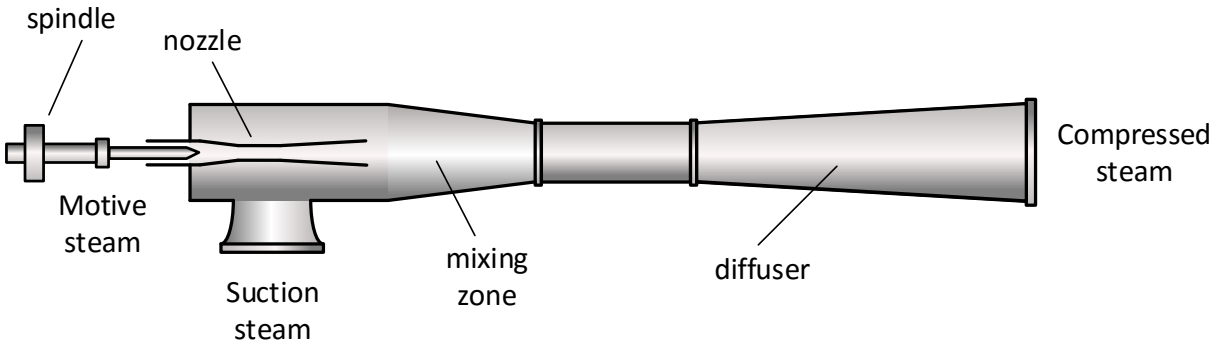

Figure 6.2. Scheme of variable nozzle thermocompressors.

6.2.2.2 Model of the MED-TVC unit

The desalination plant considered is a parallel/cross multi-effect distillation system with thermal vapour compression based on the MED-TVC commercial plant located in Trapani (Italy) (Temstet et al., 1996) (see Figure 6.3). This plant comprises four MED-TVC units of 12 effects and a preheater every two effects, and it is fed with high pressure steam at 45 bar from a boiler. In addition, it has two plate heat exchangers at the inlet of the plant in order to deal with the different temperatures of the intake seawater during the year (22 – 10 °C). All the design data of the plant modelled are indicated in Table 6.2. The unit has been designed in order to minimize the thermodynamic losses of the vapour during the condensation process, selecting appropriate values of the geometrical features, such as: the diameter of the connecting lines between the effects, diameter of the tubes in the evaporators, density of the demisters, etc. Notice that the maximum salinity of the brine in the design has been limited to 65,900 ppm in order to avoid scaling in the tubes.

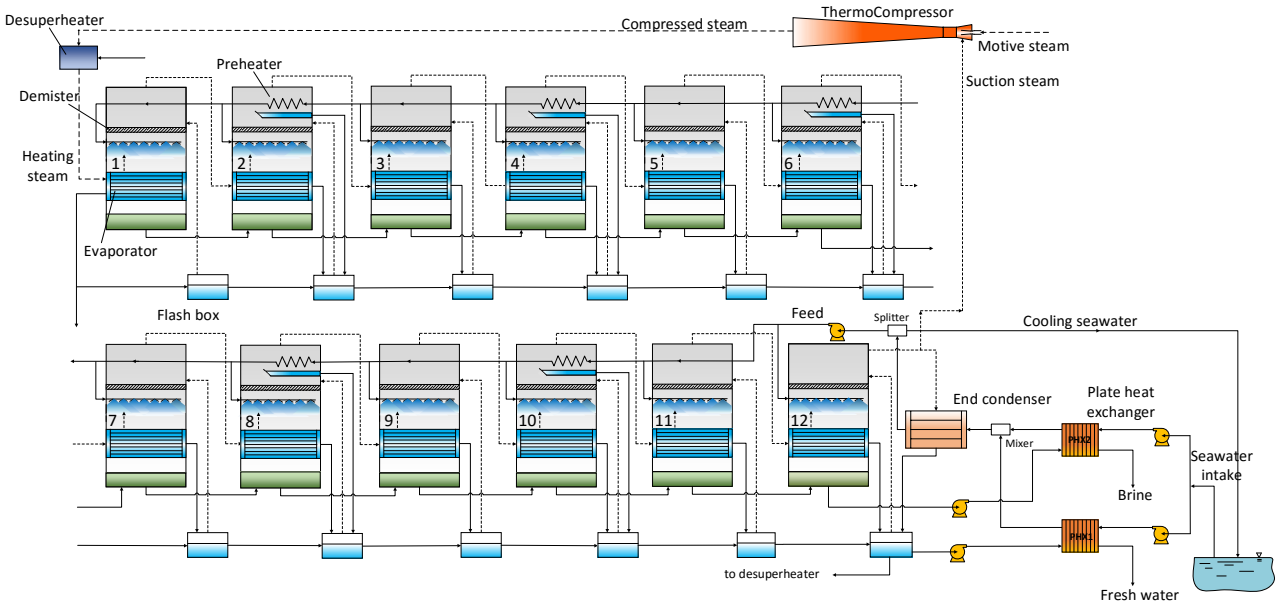

Figure 6.3. Diagram of the MED-TVC unit considered.

Table 6.2. Design data of the MED-TVC unit. Reference (Temstet et al., 1996) except otherwise indicated.

Concept	Value
Design and operational parameters	
Design capacity (m^3/d)	10,000
Number of effects	12
Thermocompressor location	12^{th}
Motive steam pressure (bar)	45.4
Heating steam temperature (°C)	70
Brine temperature in the last effect (°C)	37
Intake seawater temperature (°C)	22
Intake seawater salinity (ppm)	40,000
Maximum salinity in the first effect (ppm)	65,900
Feed seawater temperature (°C)	35
Inlet seawater temperature (°C)	25.9
Feedwater temperature at 1^{st} effect[a] (°C)	60
Distillate temperature[a] (°C)	25
Connecting lines	
Diameter of the connecting lines (mm)	1000
Tube longitude between effects (m)	2
Tube bundle evaporators	
Tube longitude of the evaporators (m)	7
External diameter of evaporator tubes (m)	0.022[a]
Internal diameter of evaporator tubes (m)	0.018[a]
Demisters	
Wire diameter of the demister (mm)	0.32
Density of the demister (kg/m^3)	100
Mesh pad thickness of the demister (m)	0.1
Vessel diameter [a] (m)	4.8

[a] Assumption
[b] (Cipollina et al., 2005)
[c] (El-Dessouky and Ettouney, 2002)

In order to perform the simulations of the MED-TVC unit coupled to the power block, a design and an operational model for the MED-TVC unit are required, which are described below. The first one is used to size and characterize the different components of the plant, such as the areas of the evaporators, preheaters and end condenser, the location of the thermocompressor, the nominal motive steam mass flow rate, etc., for each configuration. Once those parameters are obtained, the operational model permit to simulate the unit in operation, based on a fixed geometry, with changing conditions of the motive steam.

Regarding the model of the thermocompressor, the curves from Power (Power, 1994), which provides the entrainment ratio (ratio between the motive steam and suction steam mass flow rates) as function of the compression and expansion ratios, have been selected. The equations from these curves have been obtained by Ashraf and Darwish and are shown in (Hassan and Darwish, 2014). This model is particularly appropriate for simulating variable nozzle thermocompressors as it is valid for a wide range of motive steam pressures.

6.2.2.3 Design model of the MED-TVC unit

As mentioned above, four different coupling arrangements of the MED-TVC unit with the power block have been considered, corresponding to four steam extractions (namely HP2, HP1, DEA and LP3). For each coupling arrangement, the location of the thermocompressor that provides a maximum GOR and a minimum specific heat transfer area (determining the optimum reduction of the area of the evaporators after the thermocompressor location) was obtained in an exhaustive study presented in Chapter 5 and published in Ortega-Delgado et al. (2016). In that Chapter, a complete and detailed description of the design model of the MED-TVC unit developed and implemented in Engineering Equation Solver (EES) environment (Klein, 2013), along with the assumptions and approximations made, can be found. The main results obtained from this study can be seen in Table 6.3. The nominal motive steam mass flow rate (q_m) obtained in the design model was used in the model of the power block for the simulations. Also, this variable together with the thermocompressor location, the optimum reduction of the evaporators area after the thermocompressor location (β_{opt}), the area of the evaporators before the thermocompressor location (A_{bef}), the area of preheaters (A_{preh}), the area of end condenser (A_c), the feedwater mass flow rate (q_F) and the rejected cooling seawater mass flor rate (q_{cw}) were used as inputs for the operational model of the MED-TVC unit.

Table 6.3. MED-TVC nominal design for the four motive steam pressures considered.

p_m (bar)	TC (-)	sA (m^{2}s)/kg	GOR (-)	q_D (m^3/d)	q_m (kg/s)	q_F (T/h)	q_{cw} (T/h)	CR (-)	β_{opt} (-)	A_{bef} (m^2)	A_{preh} (m^2)	A_c (m^2)
45.4	11	526	14.67	9823	7.691	1300	275.9	4.49	0.7	4839	149.9	1957
20.6	10	521.5	14.2	9593	7.757	1273	325.6	3.95	0.653	4839	149.9	1986
8.75	9	516.2	13.78	9344	7.785	1243	349.7	3.5	0.627	4839	149.9	1977
3.627	9	520	12.86	9384	8.377	1245	459.3	3.47	0.662	4839	149.9	2123

6.2.2.4 Operational model of the MED-TVC unit

In order to simulate the off-design conditions (also called partial load) of the MED-TVC unit, an operational model based on the design model was developed. The MED-TVC plant operates at partial load when the mass flow rate or pressure of the motive steam changes, since it results in a variation of the external thermal energy supplied to the plant (heating steam mass flow rate and temperature). This occurs either when the motive steam pressure is reduced as consequence of the sliding pressure regulation of the power block or when there is not enough steam available in the power block to feed the MED-TVC unit with the nominal motive steam mass flow rate. It was considered that there was not available motive steam to feed the MED-TVC unit at nominal conditions when the mass flow rate of steam entering the LP P1 feedwater heater is lower than 0.1 kg/s. At these conditions, the mass flow rate of motive steam has to be decreased. The operation of the MED-TVC unit has been considered between 100 and 40% of the rated load, in accordance with Shemer (2011).

As explained before, in the operational model, the heat transfer areas have been taken as input variables and equal to those ones obtained from the design model (Table 3). Also, the feedwater mass flow rate (q_F) obtained by the design model for each case has been taken as initial value for the operational model. This variable, along with the heating steam temperature, have been considered as control variables in the operational model to adjust the salinity of the brine in the first effect and the brine temperature in the last effect, respectively. Their variation is consequence of the off-design operation of the power block, which is explained hereafter.

In order to see the effect of the partial load operation of the power block on the feedwater mass flow rate and this one on the brine salinity, the case of the MED-TVC unit operating with motive steam pressure at 45.4 bar has been investigated. As observed in Figure 6.4, a decrease of the motive steam mass flow rate from its nominal value (7.691 kg/s) results in an increase in the brine salinity in the first effect up to a limit of 120,000 ppm (it is the validity limit of the correlation used for the calculation of the seawater's thermo-physical properties), which can provoke serious scale formation risks. The increase in the brine salinity is due to the reduction of the feedwater flow rate entering the plant, which is caused by the decrease in the motive steam mass flow rate. This reduction leads to a decrease in the heat rate in the evaporator of the first effect and therefore in the compressed steam mass flow rate (as shown in Figure 6.5), reducing the feedwater flow rate needed in the process. On the other hand, the end condenser temperature is also affected by the decrease in the motive steam mass flow rate, since the lower amount of vapour produced in each effect (as a consequence of a lower heat rate in the first evaporator) leads to lower cooling needs in the end condenser of the MED plant (as depicted in Figure 6.6) and therefore to an increase of the condensation temperature. It can have a significant effect on the distillate produced (as seen in Figure 6.6) since the temperature

differences between effects are reduced and therefore the driving force of the evaporation process is decreased.

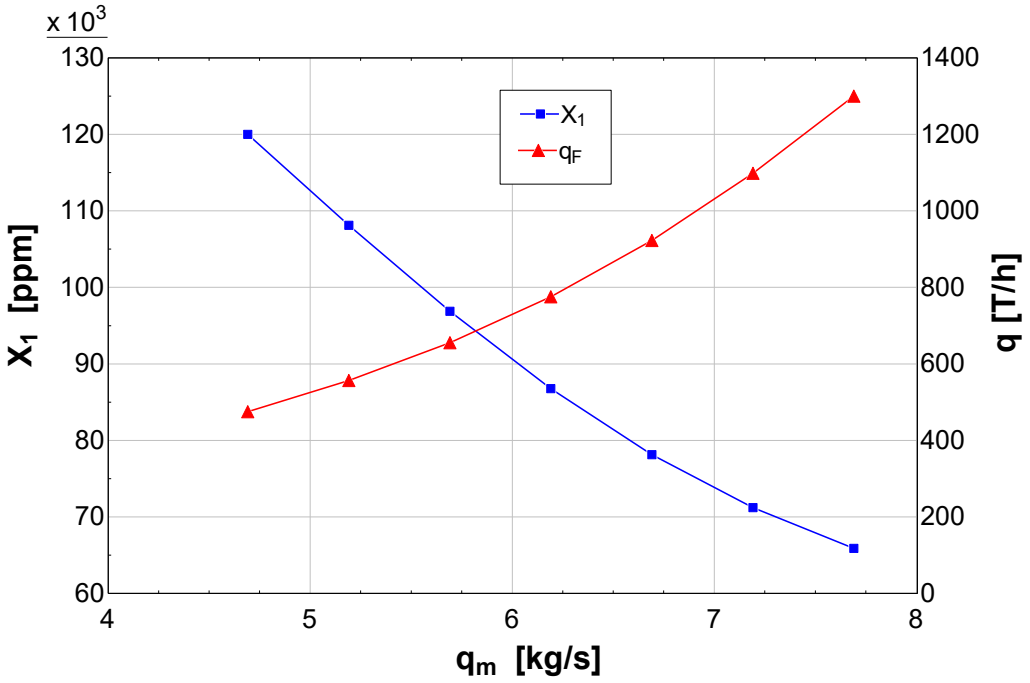

Figure 6.4. Variation of the brine salinity in the first effect and feedwater mass flow rate with the motive steam mass flow rate, for $p_m = 45.4$ bar.

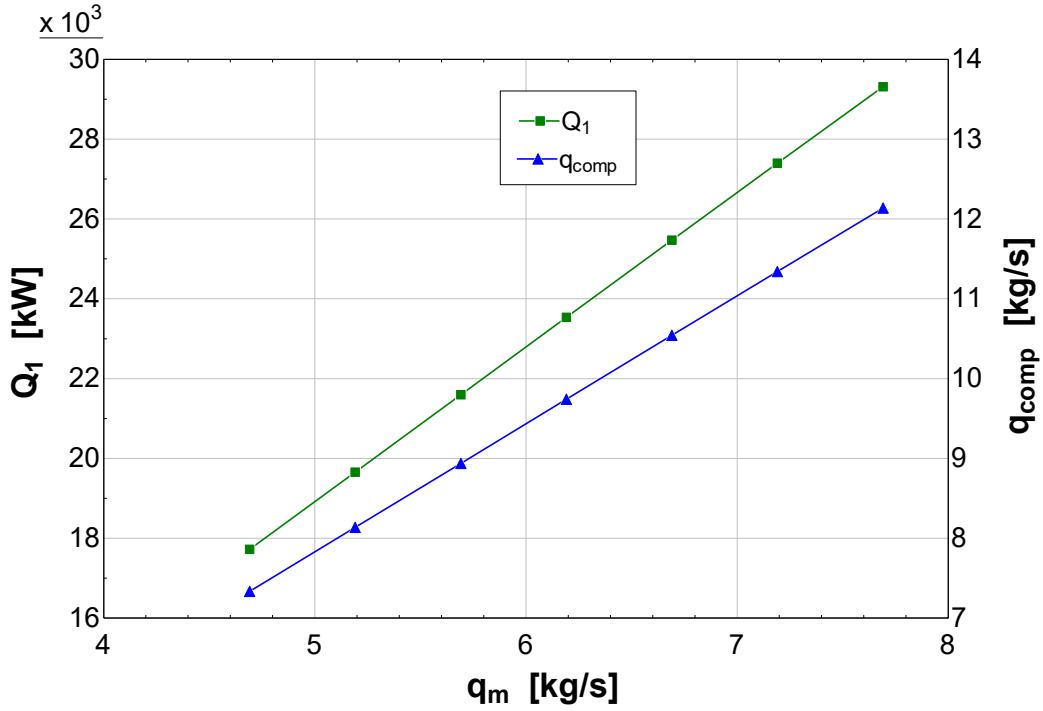

Figure 6.5. Variation of the heat rate in the first effect (Q_1) and the compressed steam mass flow rate (q_{comp}) with the motive steam mass flow rate, for $p_m = 45.4$ bar.

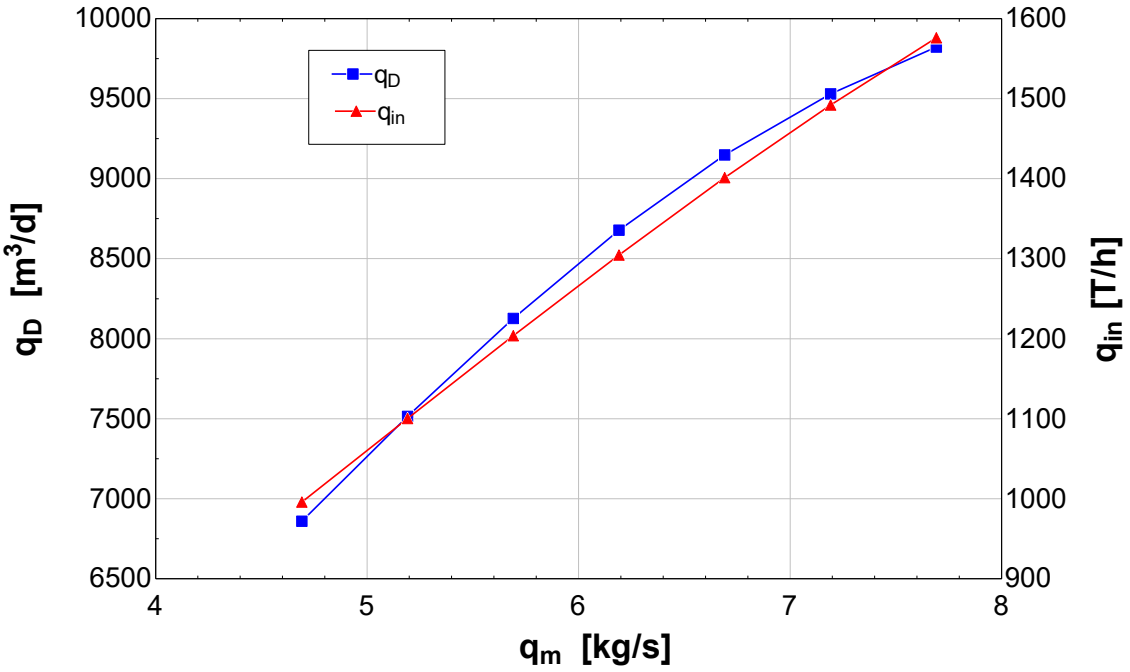

Figure 6.6. Variation of the daily freshwater production and mass flow rate of intake seawater with the motive steam mass flow rate, for $p_m = 45.4$ bar.

In order to avoid scale formation and a decrease in the distillate production, both variables (brine salinity and end condenser temperature) have to be controlled by a proper variation in the feedwater flowrate and heating steam temperature, respectively. Accordingly, on one hand q_F is adjusted in order to maintain the brine salinity in the first and second effects below a certain limit (70,000 ppm). On the other hand, the heating steam temperature (T_s) is adjusted within 70 and 60 °C (minimum temperature which leads to a reasonable temperature difference between effects, close to 2 °C) in order to maintain the condensation temperature around its design value, 37 °C.

The adjustment of q_F has been done by developing an algorithm (see Figure 6.7) that has been implemented in the operational model. The control of the heating steam temperature has been carried out as follows: it is linearly reduced in a quantity proportional to the MED-TVC load according to the following expression:

$$T_s = T_{s,nom} - \left(1 - \frac{q_m}{q_{m,nom}}\right) \cdot k_s \qquad \text{(Eq. 6.2)}$$

where $T_{s,nom}$ is the nominal heating steam temperature, $q_{m,nom}$ is the nominal mass flow rate of motive steam and q_m is the motive steam mass flow rate at the different loads of the MED-TVC plant, from the nominal one to the value corresponding to 40%. Finally, k_s is a constant determined to obtain a heating steam temperature of 60 °C for the lowest load of the MED-

TVC unit (40%). Notice that the decrease of the heating steam temperature can be done in real desalination plants by adjusting the amount of distillate entering the desuperheater.

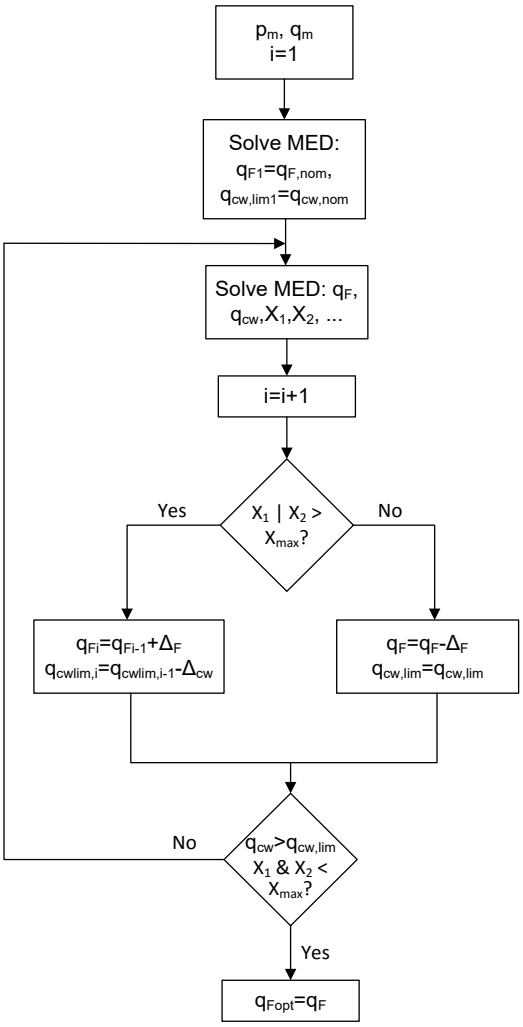

Figure 6.7. Algorithm developed for the operation control of the MED-TVC unit.

Notice that the rejected cooling mass flow rate is used in the algorithm as an internal control variable. Δ_F and Δ_{cw} are the step change in the feedwater (q_F) and rejected cooling (q_{cw}) mass flow rates, respectively.

Figure 6.8 shows an example of the MED-TVC unit operation in off-design conditions between 100% and 40% of the nominal mass flow rate of motive steam using the adjustment algorithms described above. This case corresponds to the integration of the MED-TVC unit into the power block using steam from the high pressure extraction HP2, and a load of 37.5% in the power block. As can be seen, the feedwater mass flow rate is perfectly controlled in order to maintain the brine salinity in the first effect below 70,000 ppm, keeping the temperature of the end condenser near to its design value (37 °C).

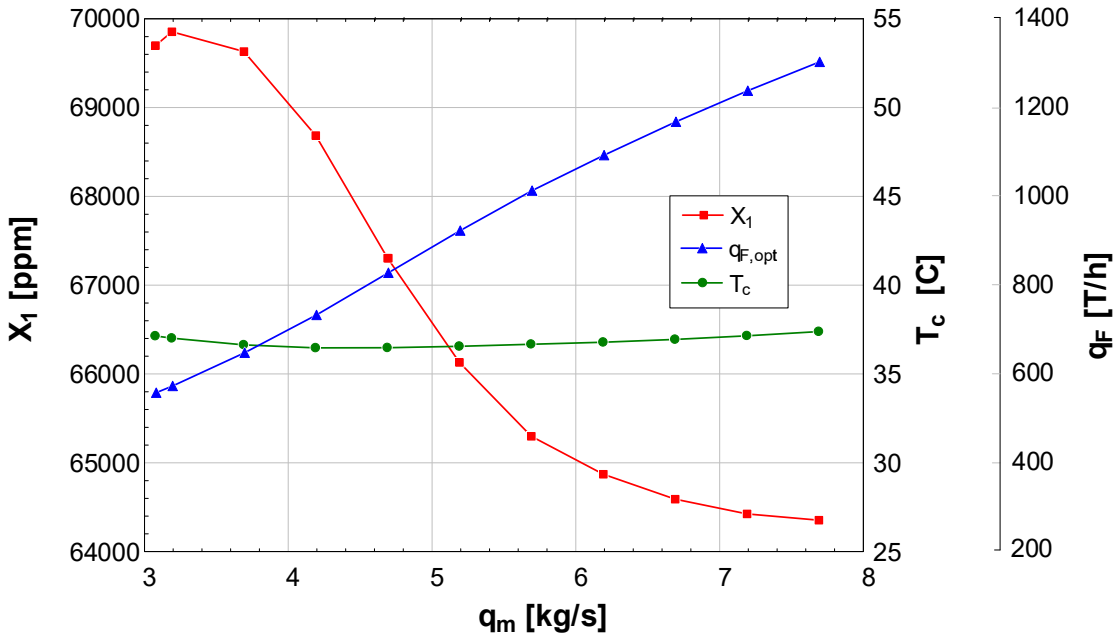

Figure 6.8. Variation of the brine salinity in the first effect, feedwater mass flow rate and temperature of the end condenser as function of the motive steam mass flow rate for the 37.5% of the load in the power block when the MED-TVC is integrated using steam from HP2.

6.3 Results

Figure 6.9 shows the variation of the steam mass flow rate entering the first feedwater heater (LP P1) with the load of the power block, for each coupling arrangement. In this figure, the limit loads that allow a constant motive steam mass flow rate for the thermocompressor equal to that at nominal conditions are shown. As mentioned above, this limit is established by the mass flow rate of steam available in the first low pressure feedwater heater LP P1 that becomes lower than 0.1 kg/s. As depicted, in all cases this happens for loads roughly less than 50% of the nominal value. Particularly, for the HP2, HP1, DEA and LP3 steam extractions the minimum feasible loads are 40%, 42.5%, 42.5% and 45%, respectively. The decrease of the steam supplied to LP P1 is due to the fact that the motive steam mass flow rate to the thermocompressor is kept constant while the steam in the power block decreases linearly with the load of the power block.

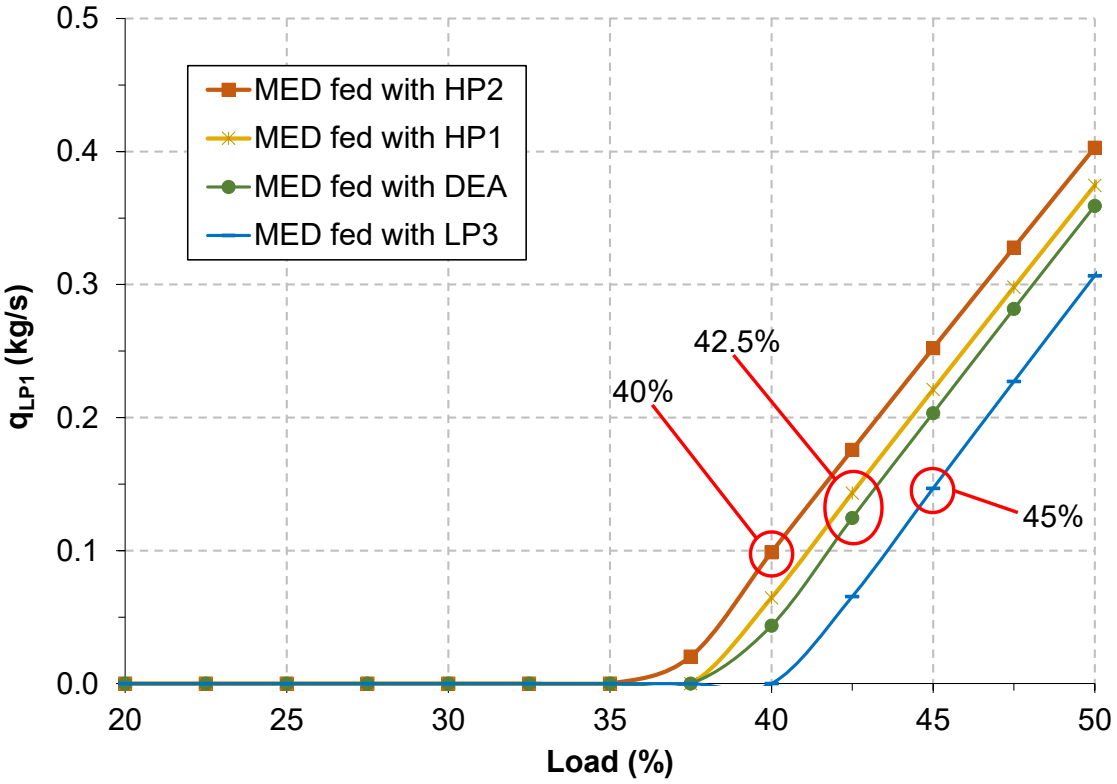

Figure 6.9. Variation of the mass flow rate of steam in the feedwater heater LP1 with the load.

Once the limit loads of the power block were achieved, the motive steam mass flow rate was reduced by steps of 0.5 kg/s until the steam to LP P1 was above 0.1 kg/s or the minimum load of the MED-TVC operation (40%) was reached. Simulations of the MED-TVC unit integrated into the power block also resulted in certain feasible minimum loads of the power block. These minimum limits are those ones that allowed the convergence of the model and were 25% for all steam extractions, except for LP3, that was 27.5%.

Table 6.4 shows some of the variables obtained from the simulations: motive steam pressure, motive steam mass flow rate, suction and compressed steam mass flow rates, mass flow rate of steam entering the LP P1 feedwater heater, net power generated, total fresh water produced, GOR, recovery ratio (RR), brine salinity in the first effect, heating steam temperature, temperature of the last effect, compression ratio (CR), expansion ratio (ER) and entrainment ratio (Ra), for six selected points of load of the power block in each coupling arrangement: over nominal conditions (120%), the nominal operation (100%), half-load operation (50%), the minimum load for which the motive steam nominal mass flow rate can be maintained (see Figure 6.9), the load from which the nominal motive steam mass flow rate has been decreased by steps of 0.5 kg/s, and finally the minimum load achievable by the power block. It can be seen that the freshwater production slightly decreases when the motive steam mass flow rate is kept constant. This is due to the fact that the decrease in the motive steam pressure causes a

Table 6.4. Selected operation points for the four coupling arrangements considered.

	Load (%)	p_m (bar)	q_m (kg/s)	q_{suc} (kg/s)	q_{comp} (kg/s)	q_{LP1} (kg/s)	P_{We} (kW)	q_D (m^3/d)	GOR (-)	RR (-)	X_1 (ppm)	T_s (°C)	T_{12} (°C)	CR (-)	ER (-)	Ra (-)
HP2	120	53.98	7.691	4.507	12.2	2.24	52464.1	9848.8	14.7	0.313	66024	70	36.91	4.51	781	1.706
	100	45.40	7.691	4.446	12.14	1.77	44094.4	9823.2	14.67	0.312	65899	70	37	4.49	653.6	1.73
	50	20.60	7.691	4.083	11.77	0.40	19692.9	9651.4	14.41	0.319	66476	70	37.36	4.40	290.4	1.884
	40	15.16	7.691	3.927	11.62	0.10	14238.2	9569.8	14.28	0.324	66969	70	37.5	4.36	212.0	1.959
	37.5	14.81	6.691	3.682	10.37	0.12	13552.9	8783	15.07	0.336	67604	67.8	37.09	4.09	213.7	1.817
	25	11.40	3.191	2.41	5.601	0.10	8979.2	5228.2	18.81	0.383	69785	60.3	37.88	2.91	164.4	1.324
HP1	120	24.58	7.757	4.612	12.37	2.24	53540.2	9640.7	14.27	0.313	66161	70	36.84	3.99	314.5	1.682
	100	20.60	7.757	4.543	12.3	1.76	45058.3	9593.5	14.2	0.312	65907	70	37	3.96	261.3	1.708
	50	8.99	7.757	4.105	11.86	0.37	20514.2	9370.3	13.87	0.323	66933	70	37.41	3.85	111.1	1.89
	42.5	7.15	7.757	4.161	11.92	0.14	16438.7	9385.6	13.89	0.324	67026	70	37.37	3.87	88.69	1.864
	40	6.78	7.257	4.009	11.27	0.12	15360.9	8999.8	14.24	0.331	67537	68.9	37.14	3.76	85.69	1.81
	25	5.11	3.103	2.318	5.421	0.11	9459.2	4853.9	17.96	0.380	69514	60	38.32	2.58	66.11	1.339
DEA	120	10.65	7.785	4.71	12.49	2.25	54853.4	9324.5	13.75	0.312	65942	70	37.03	3.49	119.2	1.653
	100	8.75	7.785	4.783	12.57	1.76	46341.3	9344.1	13.78	0.311	65918	70	37	3.50	98.24	1.628
	50	3.73	7.785	4.041	11.83	0.36	21641.3	8998.4	13.27	0.330	67476	70	37.6	3.36	40.15	1.926
	42.5	2.93	7.785	3.778	11.56	0.12	17569.4	8868.5	13.07	0.336	67876	70	37.85	3.30	31.03	2.061
	40	2.79	7.285	3.626	10.91	0.10	16419.4	8486.3	13.37	0.343	68399	68.9	37.64	3.22	30.14	2.009
	25	2.18	3.114	2.225	5.339	0.10	9886.2	4577.3	16.87	0.381	69479	60	38.66	2.32	25.34	1.4
LP3	120	4.43	8.377	4.358	12.73	2.22	55930.3	9498.4	13.02	0.315	66612	70	36.6	3.54	50.29	1.922
	100	3.63	8.377	4.178	12.55	1.73	47409.0	9384.6	12.86	0.312	65919	70	36.99	3.47	40.35	2.005
	50	1.50	8.377	3.02	11.4	0.31	22751.8	8857.5	12.13	0.340	68182	70	37.92	3.25	15.63	2.774
	45	1.27	8.377	2.776	11.15	0.15	20066.7	8737.2	11.97	0.345	68495	70	38.17	3.20	13.03	3.017
	42.5	1.22	7.877	2.691	10.57	0.12	18837.8	8387.2	12.22	0.354	69128	69.0	37.94	3.13	12.78	2.927
	27.5	0.97	3.877	1.997	5.874	0.10	11622.0	5050.8	14.96	0.383	69760	61.1	38.46	2.40	11.12	1.941

reduction in the suction steam, which leads to lower compressed steam flow rate and therefore to a lower distillate production.

However, the freshwater production suffers a rapid drop when the motive steam mass flow rate is diminished from its nominal value, as can be seen in Figure 6.10 where it has been represented the freshwater and power production for all the feasible operation points and for each steam extraction considered. As an example, in the case of using steam from HP2, if the power block load decreases from 100 to 40%, the freshwater production is reduced nearly 2.6% (from 9823.2 to 9569.8 m^3/d), while a reduction of the power block load from 100% to 25% generates a drop in the freshwater yield of 47% approximately, from 9823.2 to 5228.2 m^3/d (in this latter case the motive steam mass flow rate is reduced by 40%). Notice that the curves of water production for HP1 and DEA steam extractions suffer a change of tendency at power block loads of 47.5% and 105%, which is explained by a discontinuity in the correlations of the thermocompressor model (the performance equation changes at $ER = 100$), as reported as well in (Tamburini et al., 2015).

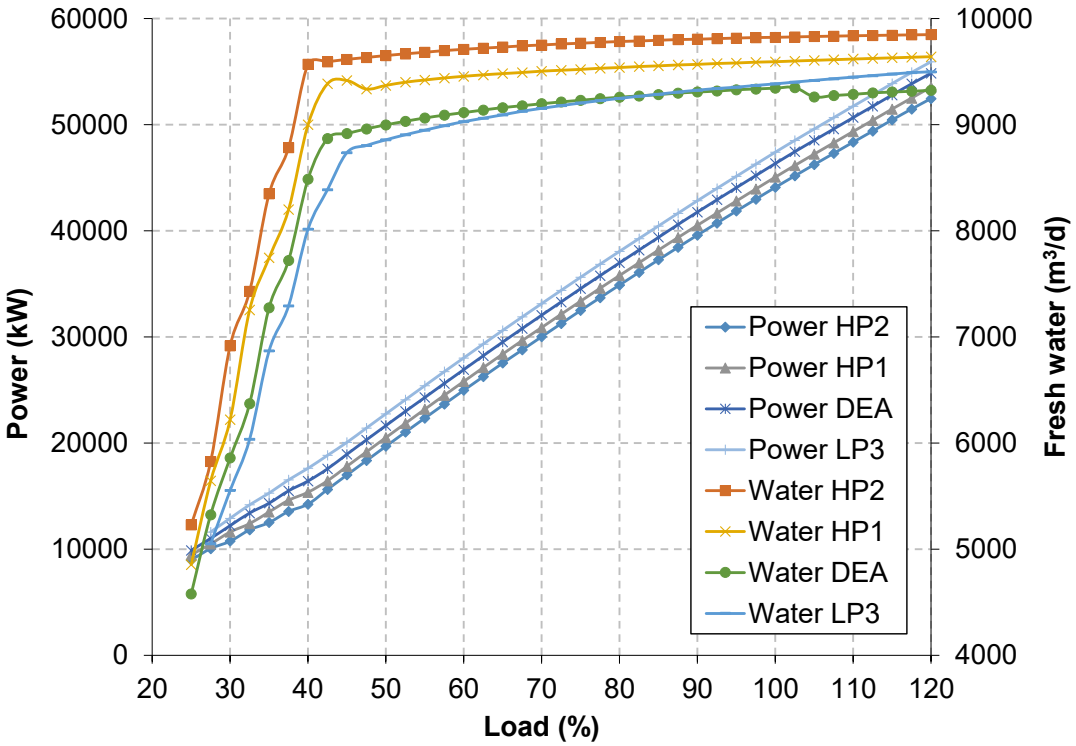

Figure 6.10. Power and freshwater production for each steam extraction considered as function of the power block load.

Regarding the power, it is observed that it decreases linearly with the load of the power block until the load limit of the power block at which the motive steam feeding the MED-TVC unit

has to be decreased. At this point, it is observed a trend change and the decrease in the power production becomes smaller. It can be due to the fact that the penalty rate in the power production decreases with the mass flow rate of the motive steam for the thermocompressor. For instance, a reduction of the thermal power load from 42.5 to 40% leads to a decrease in the power production from 15,624 to 14,238 kW (8.9%), while if the thermal power load is reduced from 40 to 37.5%, the decrease in the power production goes from 14,238 to 13,553 kW (4.8%). On the other hand, from a comparison between the coupling arrangements, it is seen that the use of high pressure steam from HP2 to feed the MED-TVC unit leads to the maximum amount of freshwater for all the loads of the power block but also to the lowest power production. On the contrary, as expected, the use of steam from the low pressure extraction LP3 generates the lowest freshwater production but the maximum power for all the load range.

Figure 6.11 depicts the variation of the motive steam mass flow rate and the Gain Output Ratio (GOR) with the load of the power block. As it can be seen, the GOR follows an evolution roughly constant from 120% to the limit load of the power block, when the motive steam mass flow rate has to be decreased. More importantly, variable area thermocompressors help to even increase the GOR when the motive steam flow is strongly decreased (power block load below 50%). As observed, the highest GOR was achieved using high pressure steam from HP2 extraction, while the lowest GOR was obtained using steam from the lowest pressure extraction LP3.

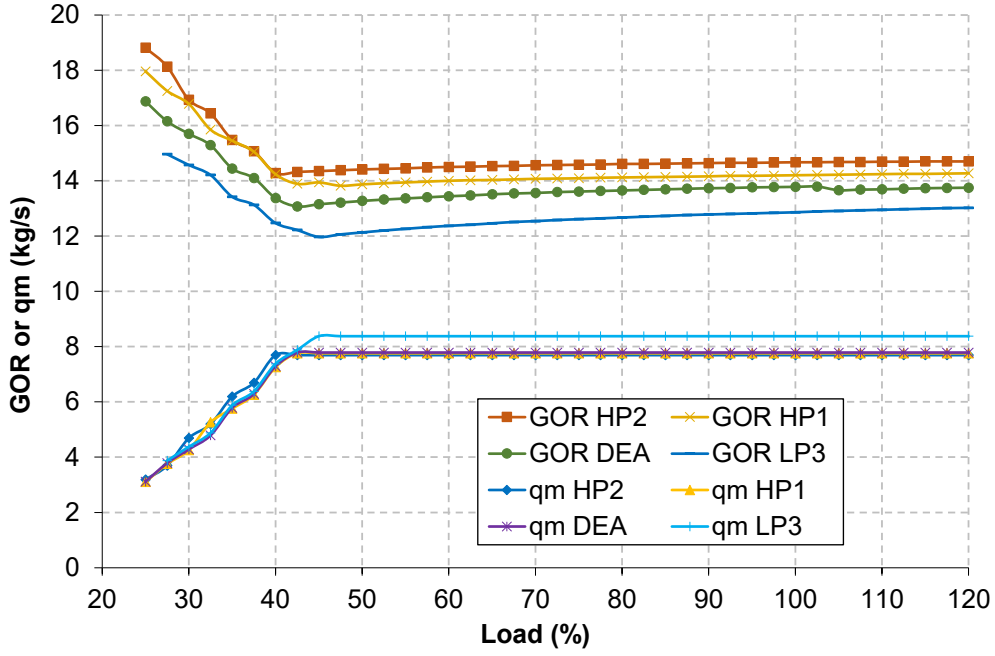

Figure 6.11. GOR and motive steam mass flow rate and as function of the power block load.

The variation of the feedwater mass flow rate and the brine salinity in the first effect as function of the load of the power block, for each steam extraction, is represented in Figure 6.12, where the control algorithm developed has been used.

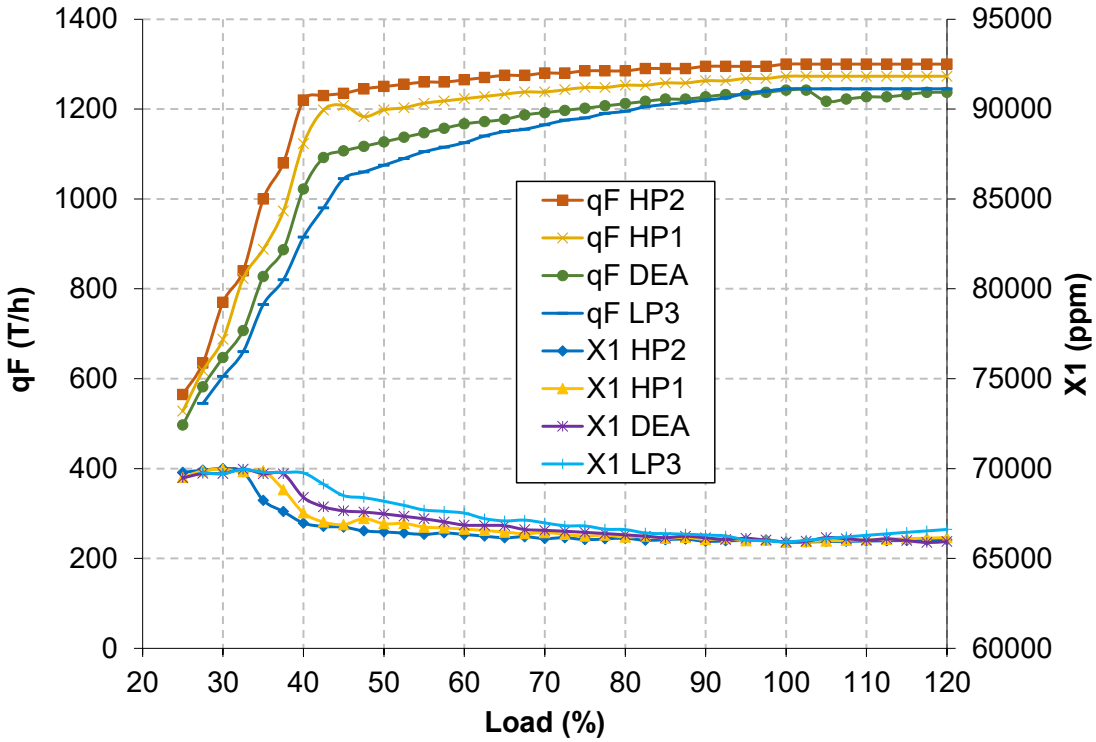

Figure 6.12. Feedwater mass flow rate and brine salinity in the first effect as function of the power block load.

On the other hand, as observed in Figure 6.13, the control loop also allows to maintain the last effect temperature (T_{12}) (which is equivalent to the end condenser temperature) around the nominal value (37 °C), as long as the mass flow rate of feedwater was enough to maintain the brine salinity in the first effect under the maximum limit. In the same figure it has been represented the variation of the heating steam temperature with the power block load. In this case, while the motive steam mass flow rate is equal to the nominal, the heating steam temperature is kept constant and equal to its nominal value (70 °C), but when the motive steam mass flow rate decreases, the heating steam temperature is reduced according to Eq. 6.2).

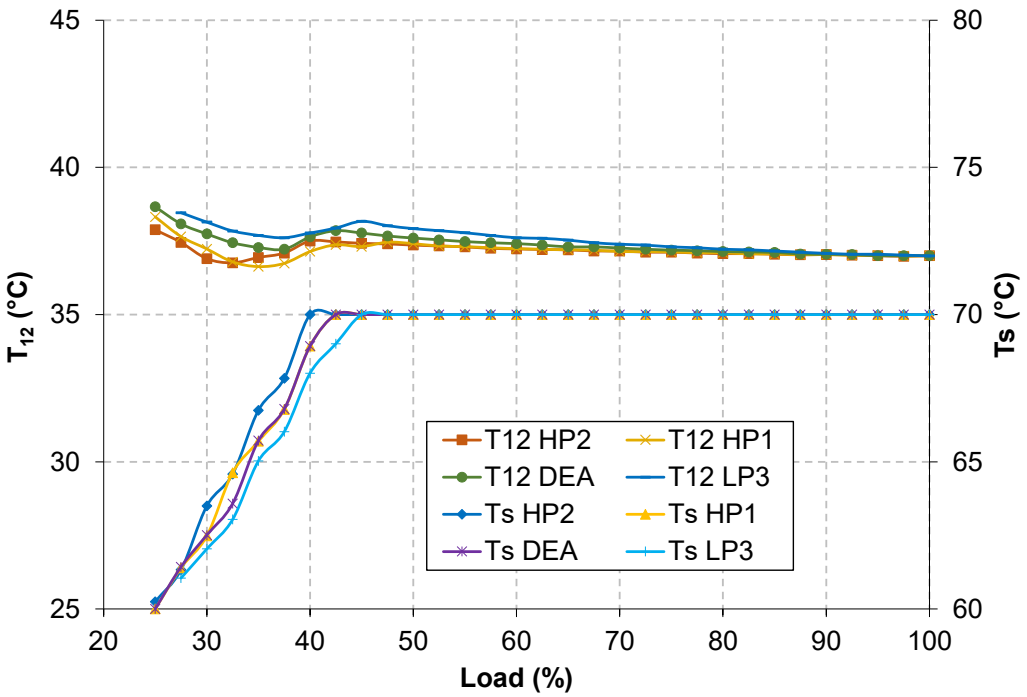

Figure 6.13. Last effect temperature and heating steam temperature as function of the power block load.

6.4 Conclusions

In this paper a parametric analysis of the coupling between a MED-TVC unit and a Rankine cycle power block with variable nozzle thermocompressors has been carried out, in order to investigate the operational limits of the integration of both systems. Four different coupling arrangements have been considered, corresponding with four steam extractions from the power block feeding the thermocompressor of the MED-TVC unit: two from the high pressure turbine (HP2, HP1) and two from the low pressure turbine (DEA, HP3). On one hand, the load of the power block has been decreased up to the technical limit. On the other hand, the MED-TVC unit has been simulated at part load conditions when there was not enough steam available in the power block.

The main conclusions reached in this study are the following:

- The use of variable nozzle thermocompressors in a MED-TVC unit coupled to a Rankine cycle power block would allow us to maintain the motive steam mass flow rate constant when the power load decreases (with sliding pressure regulation), thus operating the MED-TVC unit near to nominal conditions as long there is enough steam available in the power block .

- There are bottom limits of the load in each coupling arrangement considered for which the steam entering the last feedwater heater of the low pressure turbine (LP P1) is near to zero. In those cases, the motive steam mass flow rate has to be decreased and consequently the fresh water production is considerably reduced. However, variable area thermocompressors help to even increase the GOR in these cases. As an example, in the case of using steam from HP2, when the load decreases from 100% to 40% the freshwater reduction is of 2.6% and the GOR decreases 2.66%; when the load decreases from 100% to 25%, the freshwater reduction is of 47%, while the GOR decreases increases 28.8%. The operation limits of the power block are 40, 42.5, 42.5 and 45% of the load for the HP2, HP1, DEA and LP3 steam extractions of the high pressure and low pressure turbines, respectively. The nominal GOR are 14.67, 14.2, 13.78 and 12.86, and they are reduced only to 14.28, 13.89, 13.07 and 11.97 for those lowest operation points maintaining the nominal motive steam mass flow rate.

- When the motive steam mass flow rate of the thermocompressor is reduced from its nominal value, the MED-TVC unit works in off-design conditions and the brine salinity increases. In order to control the maximum value of the brine salinity in the unit and the brine temperature in the last effect, the feedwater mass flow rate and heating steam temperature need to be properly adjusted.

- Regarding the coupling arrangements considered in the study case, the use of steam from the highest pressure extraction considered (HP2) leads to the maximum freshwater production, ranging from 9823.2 to 5228.2 m^3/d for a variation of the power block load between 100% and 25% (steam extraction pressures of 45.4 and 11.4 bar, respectively), and the smallest power generation, from 44.094 to 8.979 MW_e in all the load range. The contrary occurs when using steam from the lowest pressure extraction selected (LP3), with water and power productions ranging from 9384.6 to 5050.8 m^3/d, and from 47.409 to 11.662 MW_e, respectively, for power block loads between 100% and 27.5% (steam extraction pressures of 3.63 and 0.97 bar, respectively).

Acknowledgments

The authors wish to thank the European Commission (DG for Research & Innovation) for its financial assistance within the Integrated Research Programme in the field of Concentrated Solar Power (CSP) (STAGE-STE Project; Grant Agreement No. 609837).

References

Cipollina, A., Micale, G., Rizzuti, L., 2005. A critical assessment of desalination operations in Sicily. Desalination 182, 1–12. doi:10.1016/j.desal.2005.03.004

Darwish, M.A., El-Dessouky, H., 1996. The heat recovery thermal vapour-compression desalting system: A comparison with other thermal desalination processes. Appl. Therm. Eng. 16, 523–537. doi:10.1016/1359-4311(95)00034-8

Desportes, C., 2006. Sea water desalination for the Bo-Hai Gulf: Case studies of MED desalination plants installed in Tianjin and Huanghua, in: IDA Desalination and Water Reuse International Forum & Exhibition. Tianjin (China).

Efrat, T., Haimiao, Y., 2013. Design Challenges and Operational Experience of a Mega MED Seawater Desalination Plant in Tianjin, in: IDA 2013 World Congress. Tianjin, China.

El-Dessouky, H.T., Ettouney, H.M., 2002. Thermodynamic Losses, in: El-Dessouky, H.T., Ettouney, H.M. (Eds.), Fundamentals of Salt Water Desalination. Elsevier Science B.V., Amsterdam, pp. 565–583. doi:10.1016/B978-044450810-2/50014-2

Hassan, A.S., Darwish, M.A., 2014. Performance of thermal vapor compression. Desalination 335, 41–46. doi:10.1016/j.desal.2013.12.004

Klein, S.A., 2013. Engineering Equation Solver Software (EES).

MHPS, 2016. Reduction of Minimum Load | MITSUBISHI HITACHI POWER SYSTEMS, LTD. [WWW Document]. URL https://www.mhps.com/en/technology/business/power/service/simulation/minimum_load.html (accessed 8.4.16).

Montes, M.J., Abánades, A., Martínez-Val, J.M., Valdés, M., 2009. Solar multiple optimization for a solar-only thermal power plant, using oil as heat transfer fluid in the parabolic trough collectors. Sol. Energy 83, 2165–2176. doi:10.1016/j.solener.2009.08.010

Ortega-Delgado, B., Palenzuela, P., Alarcón-Padilla, D.-C., 2016. Parametric study of a multi-effect distillation plant with thermal vapor compression for its integration into a Rankine cycle power block. Desalination 394, 18–29. doi:10.1016/j.desal.2016.04.020

Power, R.B., 1994. Steam jet ejectors for the process industries. McGraw-Hill, New York.

Shemer, H., 2011. Sliding Pressure Turbine Integrated with Seawater Desalination Facility (Multi-Effect Distillation - MED), in: IDA 2011 World Congress. Perth (Australia).

Tamburini, A., Cipollina, A., Micale, G., Piacentino, A., 2015. CHP (combined heat and power) retrofit for a large MED-TVC (multiple effect distillation along with thermal vapour compression) desalination plant: High efficiency assessment for different design options under the current legislative EU framework. doi:10.1016/j.energy.2016.03.066

Temstet, C., Canton, G., Laborie, J., Durante, A., 1996. A large high-performance MED plant in Sicily. Proc. 1st Symp. Eur. Desalin. Soc. 'Desalination Eur. 105, 109–114.

doi:10.1016/0011-9164(96)00064-1

Thermoflow, 2016. THERMOFLEX [WWW Document]. URL http://www.thermoflow.com/convsteamcycle_TFX.html (accessed 3.15.16).

Yang, Y., Shen, S., Zhou, S., Mu, X., Zhang, K., 2013. Research for the adjustable performance of the thermal vapor compressor in the MED–TVC system. Desalin. Water Treat. 1–10. doi:10.1080/19443994.2013.855946

Zhang, B., Yang, L., Shen, S., Liu, X., Zhang, K., 2013. Analysis of adjusting method for load performance of TVC-MED desalination plant. Desalin. Water Treat. 51, 857–862. doi:10.1080/19443994.2012.714579

Chapter 7. Yearly simulations of the water and power productions in CSP+D plants

Contents

List of figures

List of tables

Nomenclature

Variables

A	Area
C	Heat capacity rate
E	Thermal energy
E_b	Direct normal irradiance
p	Pressure
P	Power
q	Mass flow rate
T	Temperature
U	Overall heat transfer coefficient
W	Electric energy
X	Salinity

Acronyms and abbreviations

CSP	Concentrating Solar Power
DNI	Direct Normal Irradiance
EES	Engineering Equation Solver
HCE	Heat Collector Elements
HP	High Pressure
HTF	Heat Transfer Fluid
LP	Low Pressure
PB	Power Block
PT-CSP	Parabolic Trough Concentrating Solar Power
PC-MED-TVC	Parallel Cross Multi-Effect Distillation Thermal Vapour Compression
SCA	Solar Collector Assemblies
SCE	Solar Collector Elements
TES	Thermal Energy Storage
TMY	Typical Meteorological Year

7.1 Introduction

The aim of this chapter is to determine the annual power and freshwater production of a Parabolic Trough Concentrating Solar Power (PT-CSP) plant coupled with a Parallel Cross Multi-Effect Distillation Thermal Vapour Compression (PC-MED-TVC) unit located in Almería (Spain) by performing simulations with the different models developed for each subsystem considered. The complete system is comprised of three subsystems (see Figure 7.1): the solar field, the power block and the desalination unit. Each subsystem has been modelled individually using different software environments. MATLAB has been selected to implement the performance model of the parabolic trough solar field while the Rankine cycle power block and the MED-TVC unit models have been implemented using Engineering Equation Solver (EES) (Klein, 2013). These models have been developed to account both for the nominal and part load operation of the system, taking the operational limits of the power block and the desalination unit into consideration.

7.2 Solar Field

7.2.1 Characteristics of the solar field

This model has been adapted from Llorente García et al. (2011). The solar field characterization has been described in Chapter 4 and here is further described. The features of the solar field are similar to those of the commercial PT-CSP plant Andasol-1, with a power generation of 50 MW_e and a thermal power production of 144 MWth in the solar field at the design point. It consists of 156 loops of parabolic troughs collectors (Eurotrough with SOLEL absorber), each one composed of four Solar Collector Assemblies (SCA) in series (see Figure 7.2), arranged on a North-South axis. Every SCA has 12 Solar Collector Elements (SCE) comprised of 36 basic Heat Collector Elements (HCE). The characteristics of this collector are presented in Table 7.1. A thermal energy storage system consisting of two molten salts tanks is included which helps to meet the power production to the demand in hours with no insolation available. The Thermal Energy Storage system (TES) can provide up to 7.5 h of power block operation at the design conditions. When the Heat Transfer Fluid (HTF) reaches certain temperature in the solar field, electric energy begins to be generated in the Power Block (PB) thanks to the thermal energy transferred from the HTF to the water through a train of heat exchangers (preheater, steam generator, superheater and reheater). The implemented model has a high level of detail and it was the first model published with thermal storage that was validated with actual data from an existing plant, showing a good agreement between the results. In addition, this model was benchmarked within the *guiSmo* project (Eck et al., 2011).

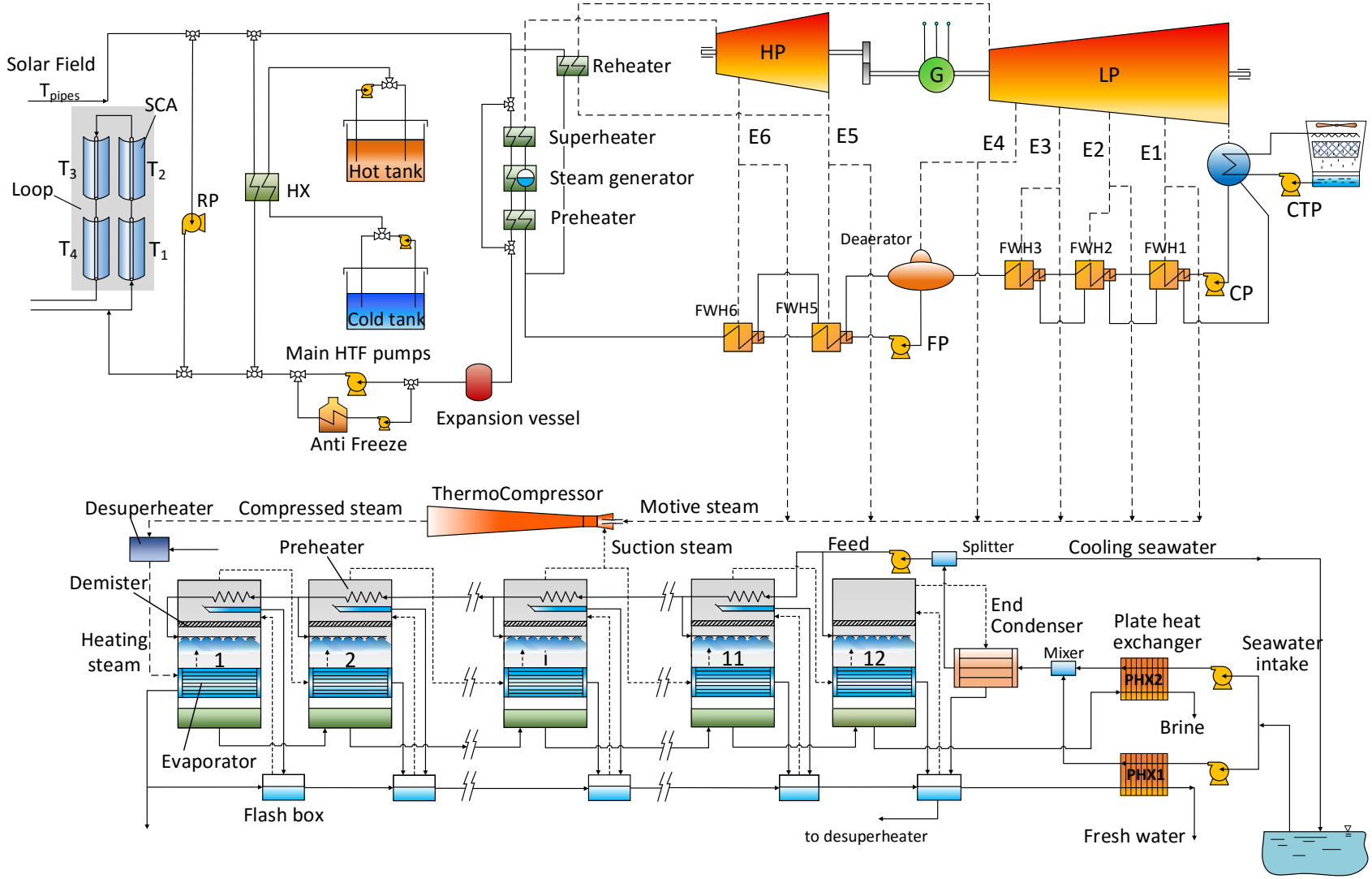

Figure 7.1. Scheme of the complete CSP+D plant with the three subsystems considered: solar field, power block and desalination plant.

Table 7.1. Characteristics of the ET-150 solar collector (Llorente García et al., 2011).

Concept	**Value**
Gross length, m	150
Net length, m	142.8
Gross aperture width, m	5.77
Net aperture area, m^2	817.5
Focal length, m	1.71
Absorber radius, m	0.035
Mirror reflectivity (ρ)	0.932
Receiver glass transmissivity (τ)	0.96
Absorbance of the metallic pipe (selective coating, α)	0.95
Reduction of the effective absorbing receiver length	0.954
Reduction in the energy absorbed by the receiver due to inaccuracies in the assembly	1
Peak optical efficiency ($\eta_{opt,0}$)	0.81
Spacing between rows, m	17.2
Spacing between consecutive SCAs in a row, m	1.5
Spacing between consecutive SCEs in a SCA, m	0.25
Number of SCAs in a row	2
Number of SCEs in a SCA	12

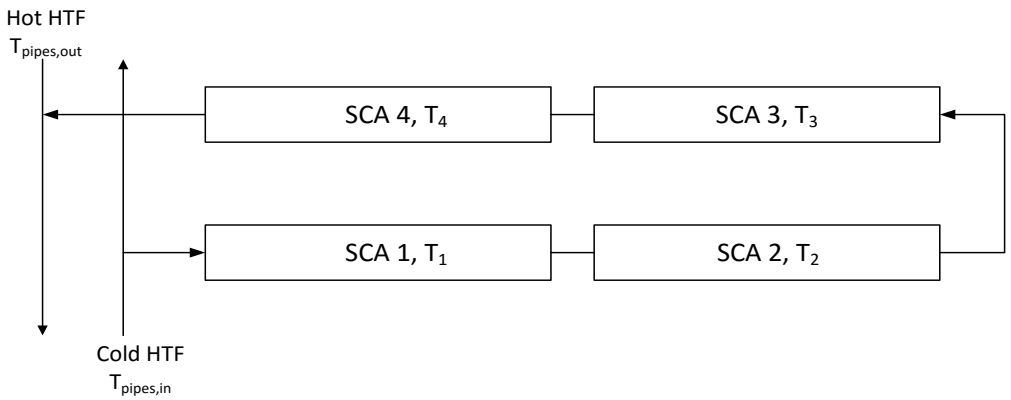

Figure 7.2. Scheme of a generic loop of the PT solar field.

7.2.2 Operation strategy

The algorithm developed by Llorente García et al. (2011) and adapted in this research work calculates for each day the HTF temperatures in a generic collector loop and uses them to obtain the rest of operation variables (thermal power absorbed, thermal losses, etc.). The whole solar field is considered as a number of consecutive and equivalent loops, each one composed of five sections: four pipes corresponding to the four SCAs and another for the insulated outlet pipe of the solar field. The HTF temperatures are calculated applying an energy balance to a pipe portion and assuming linear approximation on the resulting differential equations. The validity of the approximation is maintained for time steps below 10 sec.

The operation strategy followed, similar to that one of Llorente García et al. (2011), consists in considering four periods every day: a night time before sunrise where the solar field operates in recirculation mode (1 kg/s per loop) checking the status of the TES system, then, after the sunrise a HTF warm-up period begins with two stages: during the first one, the HTF is warmed up with a constant mass flow rate of 2.5 kg/s and by-pass the heat exchangers train of the power block, until the temperature of the HTF in the first SCA of the loop reaches a certain value, in this case 296 °C, as reported in the mentioned reference. After that, in the second stage, the HFT circulates through the heat exchangers until the temperature of the HTF in the insulated pipes reaches 310 °C, with the resulting mass flow rate calculated by the algorithm. After the warm-up period, a start-up of the turbine should be considered adding 20 minutes more of delaying, but in this work it has been neglected for simplicity. A *full operation* period is then applied until the sunset, where the power block generates electricity if there is enough thermal power provided by the solar field. The maximum thermal power absorbed by a loop is considered of 1.8 MW, with leads to HTF temperatures in the last SCA of 390 °C. Then, during this period, the thermal power delivered to the PB is calculated taking into account the resulting HTF solar field outlet temperature and 296 °C at the exit of the heat exchangers train. If there is an excess of thermal power, it is sent to the TES system. The maximum thermal energy absorbed by the TES is assumed to be 1010 MWh (which corresponds to 7.5 h of additional operation). The temperature of the hot tank has been established at 386 °C, and the cold tank temperature at 292 °C. In addition, a maximum limit of 1100 kg/s for the HTF mass flow rate has been imposed, which leads to 7 kg/s per loop as maximum. The last period considered, namely night period 2, takes place after the sunset and lasts until the beginning of the night period 1.

Basically, the performance model adapted for the parabolic trough solar field simulation has the algorithm structure shown in Figure 7.3: firstly, the geographical, meteorological data of the location considered and the features of the solar field are used to obtain the solar time and

incidence angle of the solar irradiation on a collector. Then the useful thermal power provided by the solar field is determined with the thermal power absorbed by a collector loop, the thermal losses and solar piping losses. This variable, together with the solar field temperature and state of the plant (storage tanks, irradiance levels, etc.), are used to decide the plant operation mode: night time period 1, HTF warm up, full operation and night time period 2. Also, it is calculated the thermal power sent to the power block and the thermal power delivered or added by TES system. Finally, the gross power output of the solar thermal power plant is obtained after solving the power block with the corresponding input of useful thermal power provided by the solar field.

The meteorological data have been obtained in form of a Typical Meteorological Year (TMY), with the software Meteonorm for Almería (southern of Spain). The time step between data point was 10 minutes, but the solar field model is valid for time steps below 10 s, therefore interpolation of the DNI has been performed between those intervals. The main variables extracted were the date, UTC time, Direct Normal Irradiance (DNI), ambient temperature and wind velocity. In general the methodology used to calculate the solar time and incidence angle has been taken from Stine and Geyer (2001).

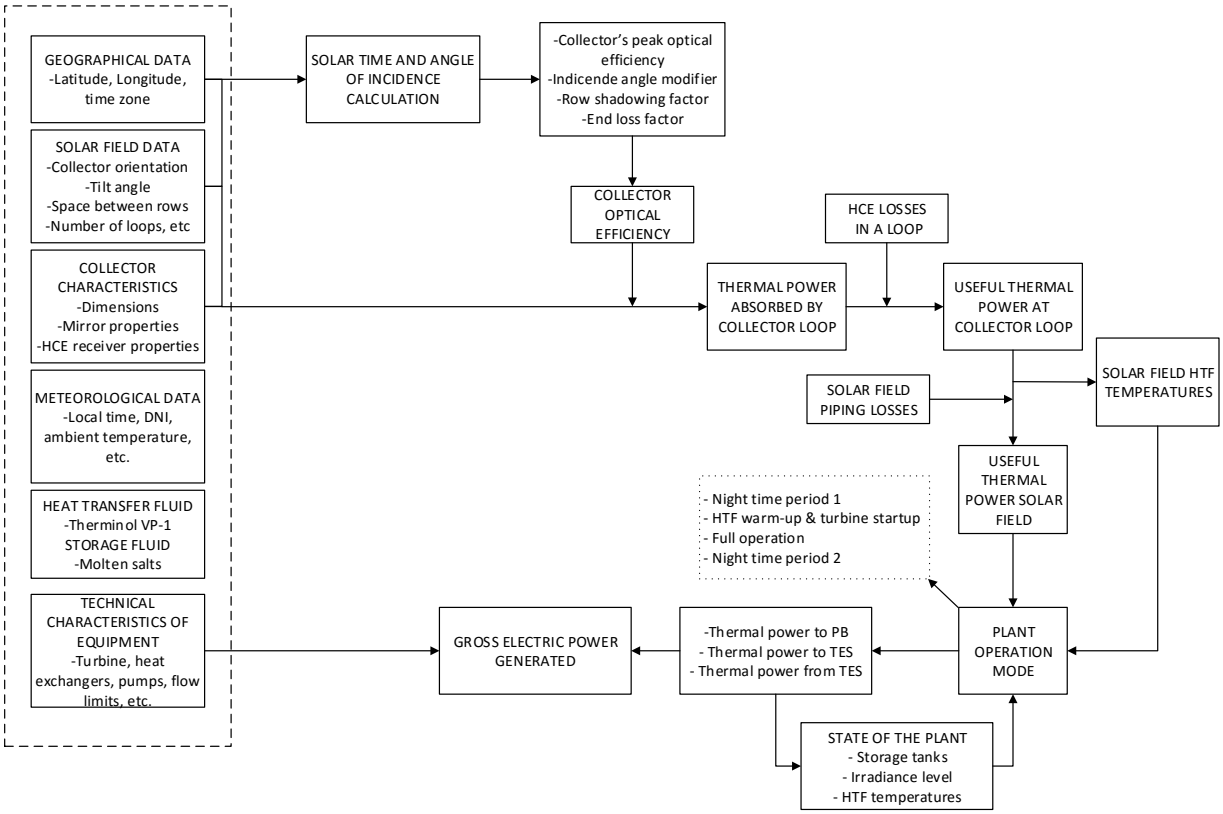

Figure 7.3. Diagram flow of the algorithm used for simulating the PT solar field.

7.3 Power block

The power block subsystem has been described in Chapter 4, which has been developed in order to simulate the part load conditions with the methodology proposed by Montes et al. (2009). The design characteristics of the power block at nominal conditions are presented in Table 4.3 of Chapter 4. Notice that in this analysis the heat exchangers of the steam generation train have been supposed with constant UA and C_{min}, in order to simplify the solving of the problem. The power block is thermodynamically solved for nominal conditions in order to obtain the required thermal power by the steam generation train. In Figure 7.4, the diagram output from the model of the power block implemented in EES software is shown, in nominal conditions. Also, the two different MED-TVC coupling arrangements considered, using a HP and LP steam extractions of the power block as motive steam, have been solved for nominal conditions (see Figs. 7.5 and 7.6), which is needed to simulate the off design operation of the integrated system. It is illustrative to compare the penalty in the thermal efficiency of the power block as result of the fresh water production, in nominal conditions. In the electricity only mode operation, the power block has a thermal efficiency of 37.7%, which is decreased to 33.6% if the HP steam extraction is used to feed the MED-TVC unit, and to 34.8% in the case of using the LP steam extraction.

7.4 Desalination unit

From Chapter 5 it was obtained the optimum coupling of a MED-TVC unit, based on the commercial Trapani plant, with a Rankine cycle power block with similar characteristics to that one of Andasol-1 (which are similar to Andasol-2), in terms of minimum specific heat transfer area and maximum GOR. The analysis was done for four different steam extractions of the power block: 45.4, 20.6 8.75 and 3.63 bar. Table 6.3 of Chapter 6 shows the main variables of the four different MED-TVC designs considered, corresponding to each steam extraction. The HP steam extraction of 45.4 bar (HP2) and the LP steam extraction of 3.63 bar (LP3) were identified as the most suitable steam extraction to feed the MED-TVC unit depending on the monthly power and water demands during the year on the location selected. In periods of the year with high electricity demand, the optimal coupling arrangement was found to be using the low pressure steam extraction of 3.63 bar to feed the MED-TVC unit, as the penalty on the electricity production was lower, although less water was produced. On the contrary, in periods of the year with low electricity demand, the high pressure steam extraction of 45.4 bar resulted the most suitable for increasing the water production and increase the efficiency of the desalination process, although the electricity generation was further penalised.

In the simulations performed in this chapter, the MED-TVC operational model developed in Chapter 6 has been used, in order to maintain the mass flow rate of motive steam in nominal

values at part load operation of the power block, as long as there is enough steam available in the cycle (which, similar to what was done in Chapter 6, has been considered when the steam mass flow rate entering the feedwater heater LP1 was below 0.1 kg/s). This could be done by using variable nozzle thermocompressors, as explained in Chapter 6. Also, the control algorithm implemented in the operational model of the MED-TVC unit, and described in detail in Chapter 6, has been used. This control algorithm adjusts the feedwater mass flow rate and the heating steam temperature so that the maximum brine salinity is always below 70,000 ppm and the end condenser temperature around its design value, 37 °C. Besides, the operation of the MED-TVC unit has been considered between 100 and 50% of the nominal load.

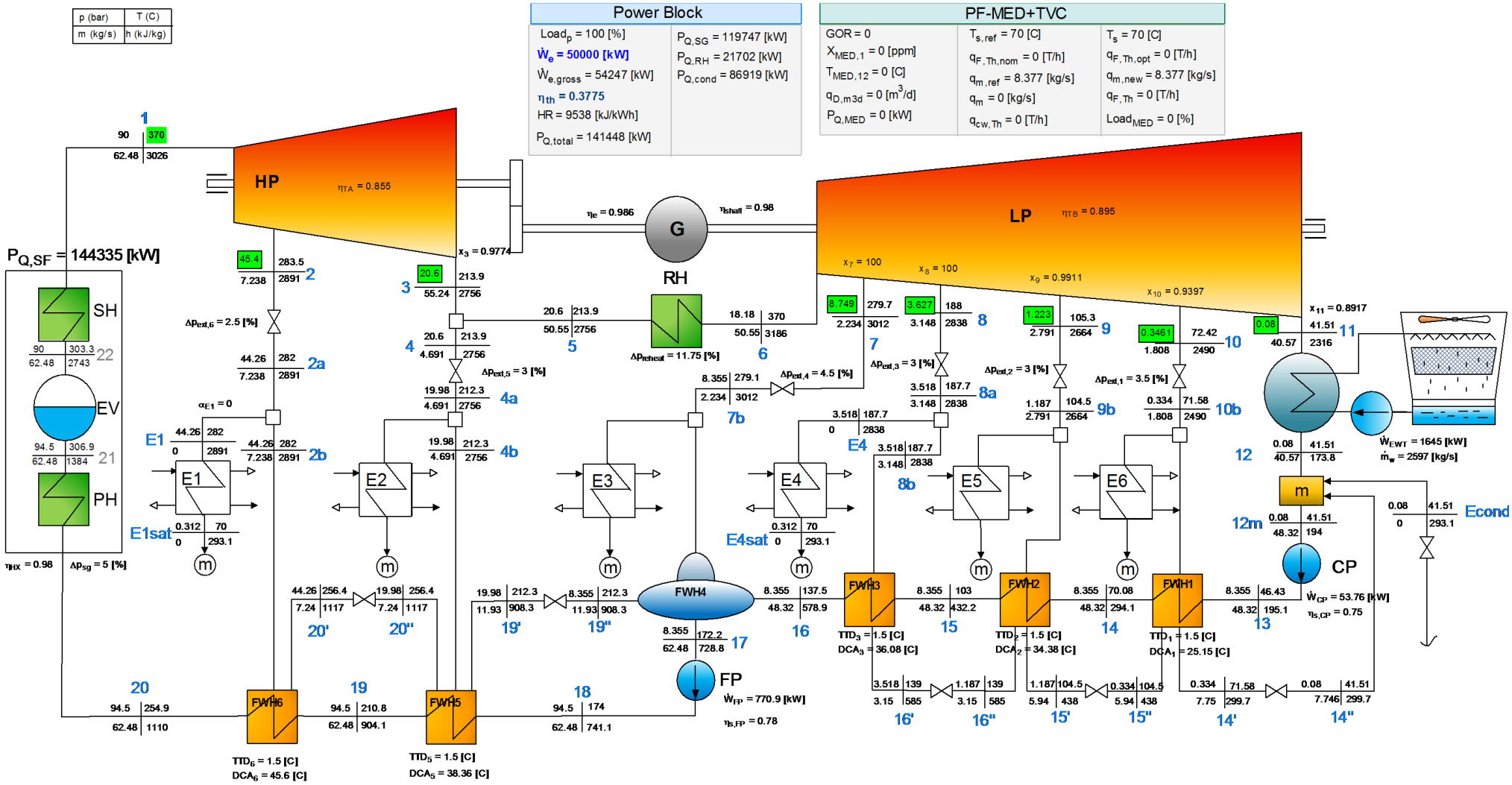

Figure 7.4. Scheme of the power block in nominal conditions.

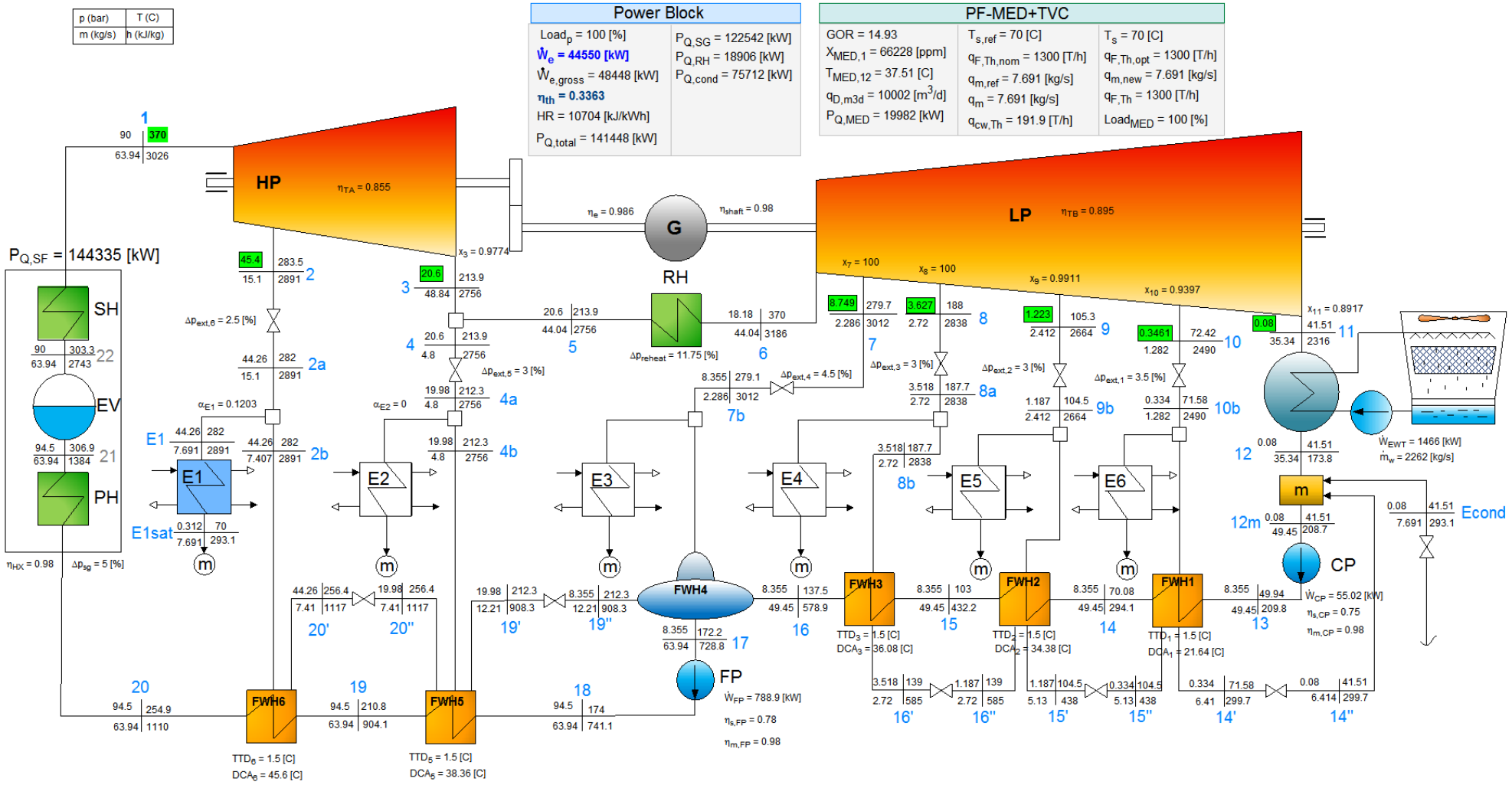

Figure 7.5. Scheme of the power block and MED-TVC unit coupled using the E1 (HP2) steam extraction, in nominal conditions.

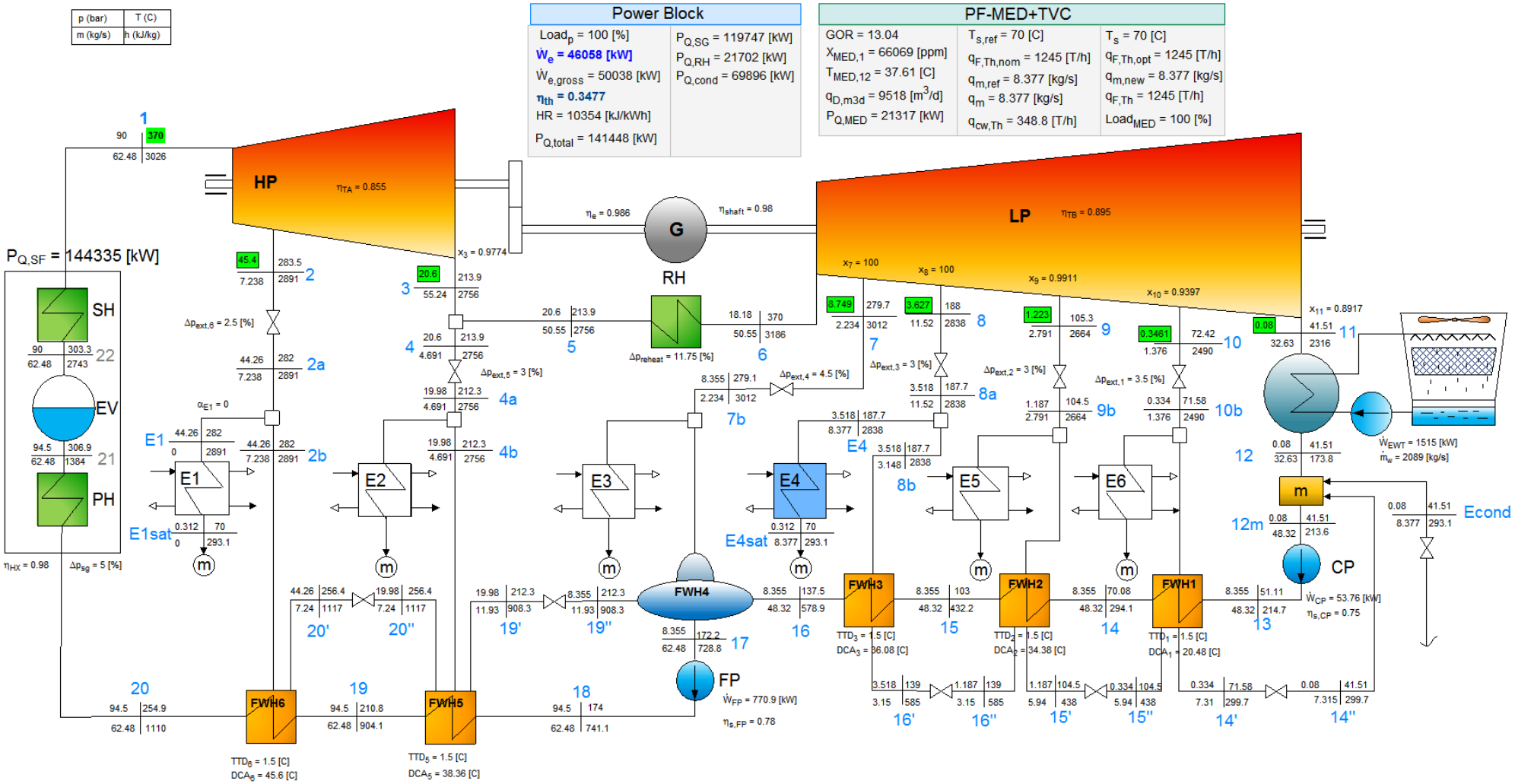

Figure 7.6. Scheme of the power block and MED-TVC unit coupled using the E4 (LP3) steam extraction, in nominal conditions.

7.5 Yearly simulations

7.5.1 Methodology

The location considered is Almería, in the southeast of Spain (longitude 2.22W and latitude 37.06N), which has high levels of solar irradiation over the year and access to the sea. The base year selected has been 2015, a non-leap year. Two integrated PB+MED-TVC models have been considered, for the HP2 and LP3 steam extractions. The selection of the former or the latter coupling arrangement has been done taking into account the monthly power demand in Almería. For this purpose, the monthly data for 2015 provided by Red Eléctrica Española (REE, 2016) for Andalusia have been taken, which are shown in Figure 7.7. Therefore, according to this power demand, the following coupling arrangement has been established for every month (see Table 7.2):

Table 7.2. Selection of the monthly coupling arrangement between the MED-TVC unit and CSP plant as function of the monthly power demand in Andalusia, during 2015.

J	F	M	M	J	J	A	S	O	N	D
LP3	HP2	HP2	LP3	LP3	LP3	LP3	HP2	HP2	HP2	LP3

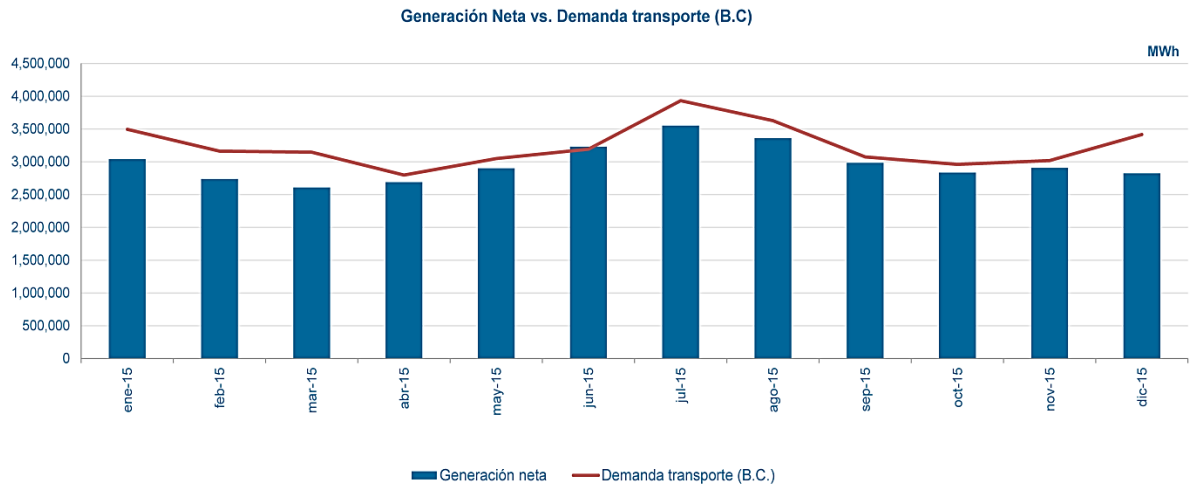

Figure 7.7. Monthly power demand profile for Andalusia region during 2015 (REE, 2016).

The simulations have been carried out as follows:

- Firstly, the solar field model uses the TMY to obtain the useful thermal power delivered to the power block among other key variables (HTF temperatures in each SCA of the loop and insulated pipes, HTF mass flow rate, useful thermal power absorbed by the solar field, thermal power losses, energy stored in the TES, etc.) for each time step selected (below 10 s) and during the period of time considered. In this case, weekly simulations have been done for each month, and the last week has been considered of 9 or 10 days, except in the case of February, that has 7 days. To that end, as the TMY provides 10-min data, the DNI has been interpolated. Therefore, 8640 points have been simulated for each day, which means 60,480 data points for each 7-day week and 3,153,600 points in the whole year. Of these, data points every 10 min have been extracted to create a vector file containing the useful thermal power transferred to the steam generator train of the power block, in order to reduce the calculation time.
- Secondly, the useful thermal power in 10-min intervals is introduced in the corresponding integrated PB+MED-TVC model, for every steam extraction, which calls to an external procedure where the MED-TVC model has been implemented. Therefore, for each step time the model solves the power block calculating in each point the main thermodynamic variables (pressure, temperature, enthalpy…) and also the integrated MED-TVC unit fed by the corresponding steam extraction, determining in this way the power and fresh water production. During the calculations a control algorithm implemented in the MED-TVC model determines the feedwater mass flow rate and heating steam temperature, as explained in Chapter 6, so that the maximum brine salinity is always below 70,000 ppm and the temperature of the end condenser closer to 37 °C. All the outputs are stored in an Excel file.
- Finally, the previous Excel file generated after solving the PB+MED-TVC integrated system, which contains the selected variables of interest, are passed to a MATLAB code for the elaboration of the different graphs.

7.5.2 Solar energy resource quantification

It is interesting to show the solar energy availability in the particular case studied. To this respect, firstly, the yearly DNI in the location considered is depicted in a colour map graph as function of the time of the day, using the data provided by the TMY file (see Figure 7.8). It can be seen how, although high values of the DNI are reached in different periods of the year, during the summer season there are more days with high values of the DNI in comparison with

the rest of the seasons. Also, the daylight hours are longer, which is the typical case of the latitude selected in the northern hemisphere.

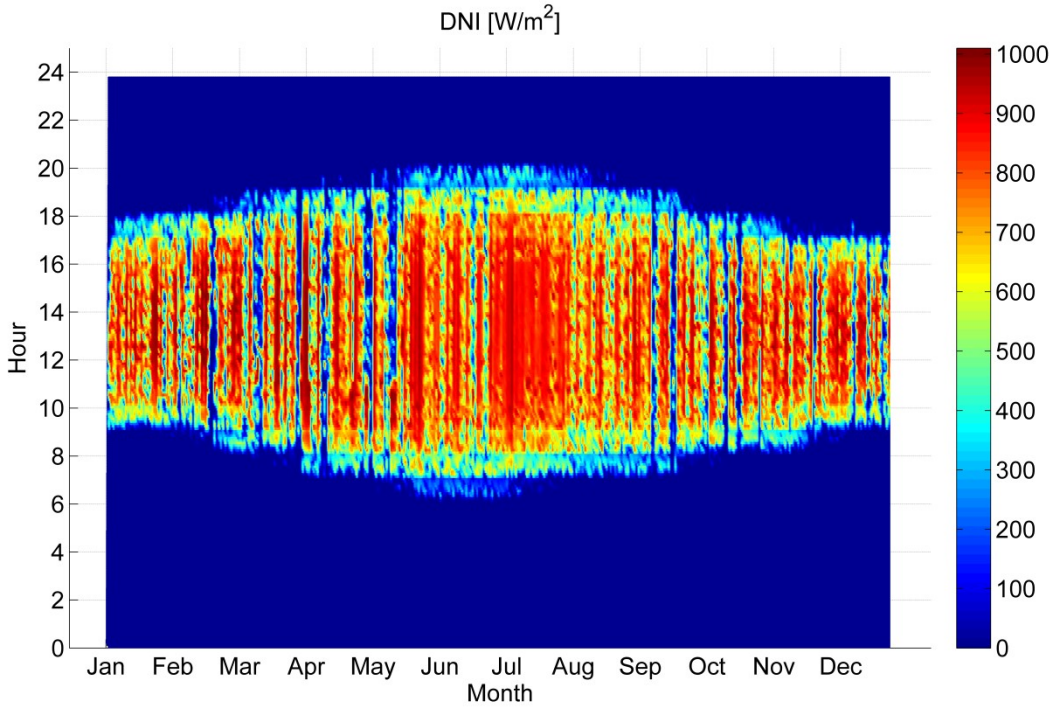

Figure 7.8. Yearly DNI as function of the time of the day.

Two important parameters are the sun incidence angle on the collectors and the sun's altitude. The first one is defined as the angle between the central ray of the sun and the normal vector to the aperture of the collector. The lower this angle the higher the thermal power absorbed by the collector, as more rays reach the receiver and transfer their energy to the heat transfer fluid. In Figure 7.9 the incidence angle versus the time of the day has been represented, for each day of the year. It is clear that the lower angles are obtained during the summer season in daylight hours, while during the winter season this angle is higher, which lead to a decrease in the thermal power absorbed by the HTF.

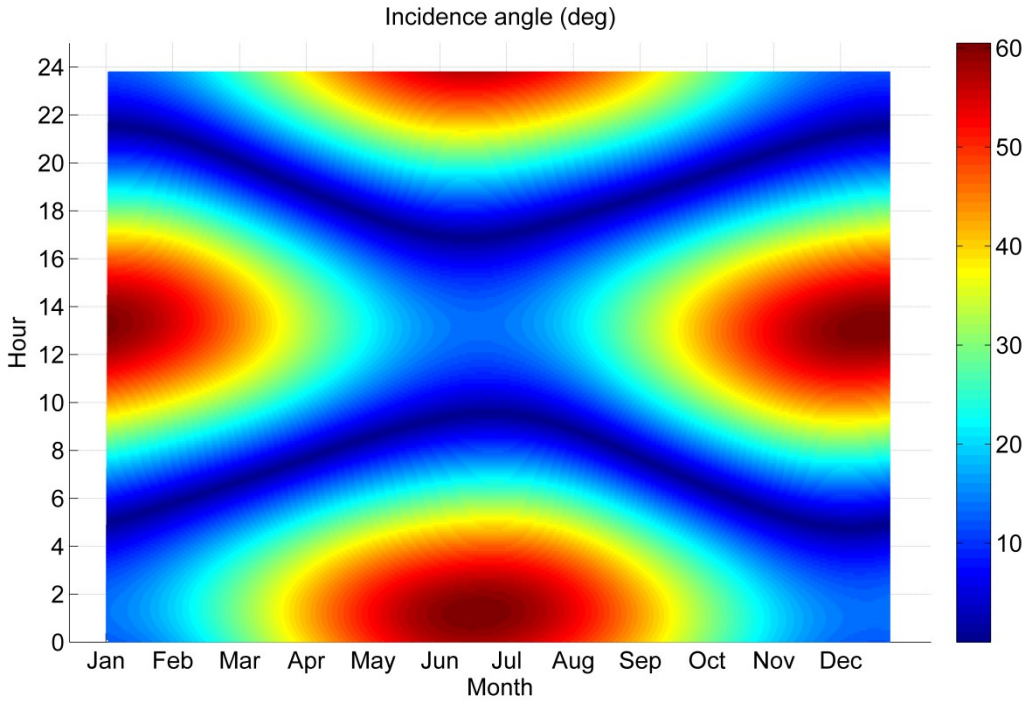

Figure 7.9. Yearly incidence angle as function of the time of the day.

On the other hand, the Sun's altitude, which is the angle between the central ray of the Sun and a horizontal plane containing the observer, is depicted in Figure 7.10. The higher this parameter the higher thermal energy absorbed by the collector, as the rays have better coincidence with the normal of the collector's aperture, that is, the incidence angle decreases. As can be seen, altitudes up to 70 degrees are achieved during the central hours of the day (12–14h) and for the summer season, which further improves the solar energy gathering.

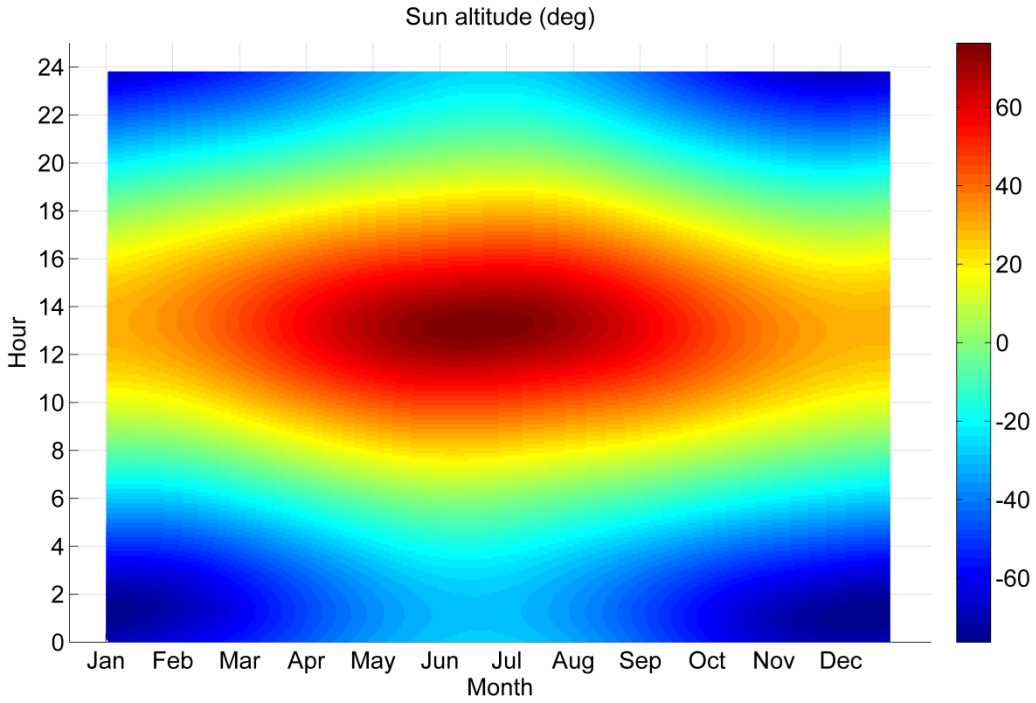

Figure 7.10. Yearly Sun's altitude as function of the time of the day.

Finally, the yearly thermal power absorbed by a generic loop as function of the time of the day is represented in Figure 7.11. As mentioned previously, there is a maximum limit imposed of 1.8 MW so that the HTF temperatures in the collectors are kept below 400 °C. The maximum amount of energy is collected during the summer season, mainly because of the abovementioned reasons. In particular, July and August are the months when more thermal power is absorbed by the collectors. In contrast to that, the winter season has the lower collection of thermal power, which suggests the necessity of a back-up system in order to continue the operation of the power plant.

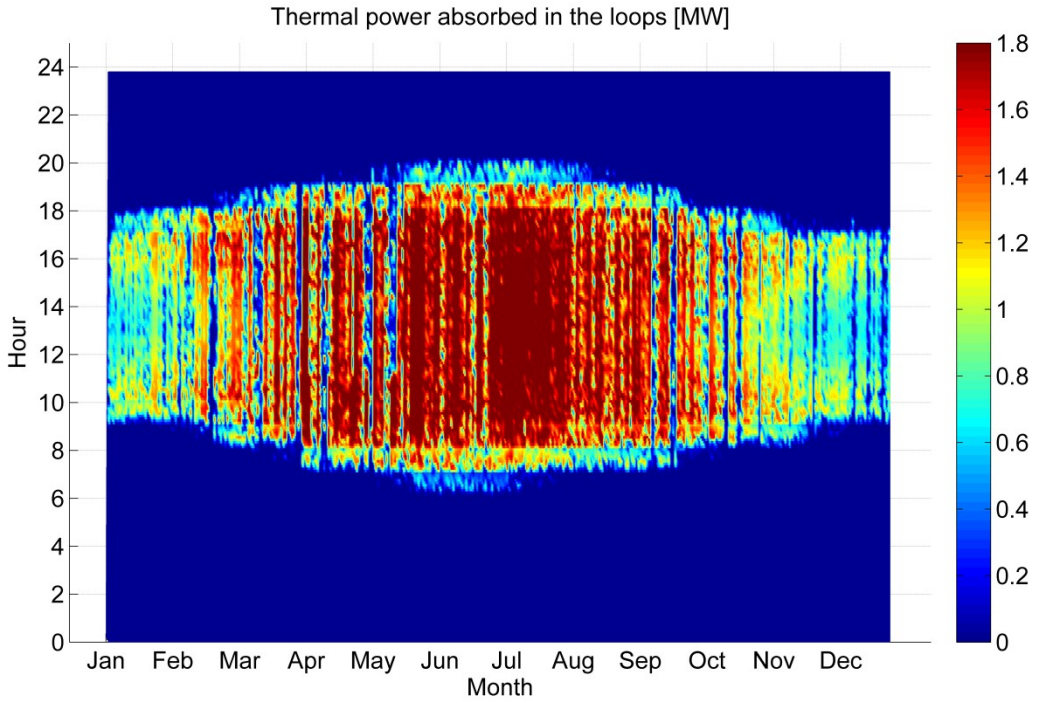

Figure 7.11. Yearly thermal power absorbed by a loop as function of the time of the day.

7.5.3 Yearly estimation of the power generation and fresh water production of the CSP+D plant

Figure 7.12 shows the estimated daily electric energy generation during the year, resulted from the simulations carried out with the integrated MED-TVC+PT-CSP model. It has a typical bell shape, with increasing electric generation starting from January, up to the central period of the year, in the summer season, when values up to 800 MWh_e are reached. In this period, the operation of the plant is possible during more days because of the larger number of clear days. From this period to December, the electric energy gradually decreases up to 100 – 200 MWh_e, when the plant availability is more dispersed. The daily fresh water production has a similar trend, as depicted in Figure 7.13. The values obtained range from 2000 to 7000 m^3 on average, for winter season and summer season, respectively.

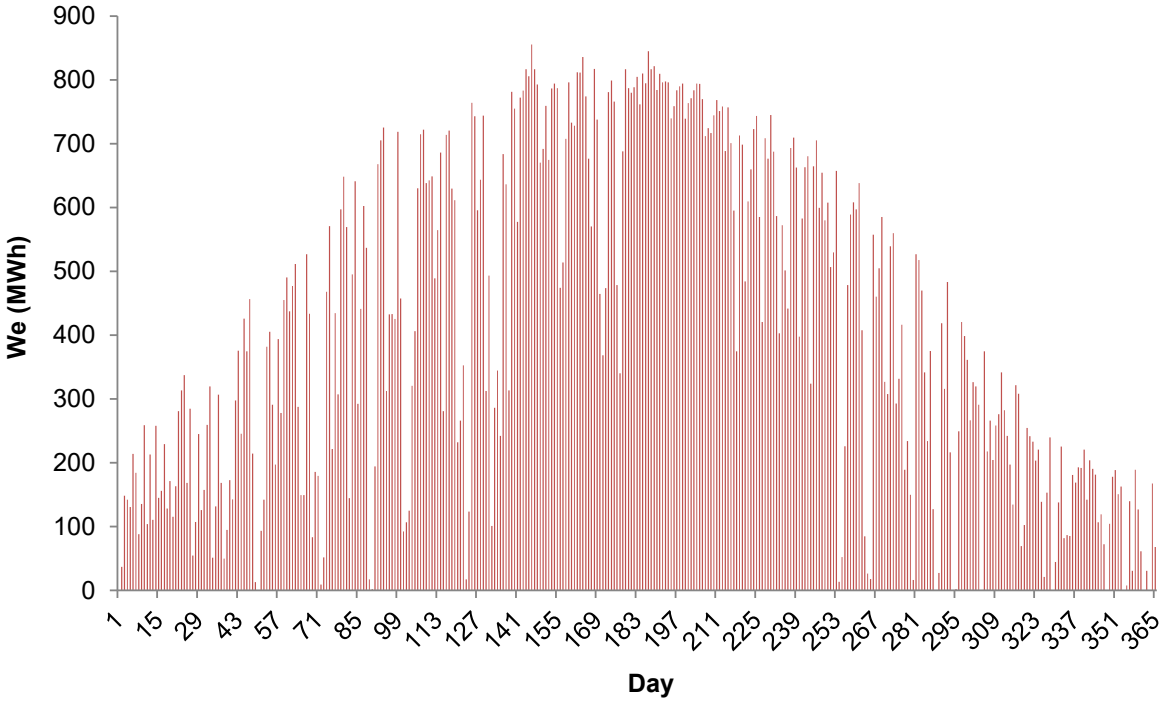

Figure 7.12. Daily electric energy generation.

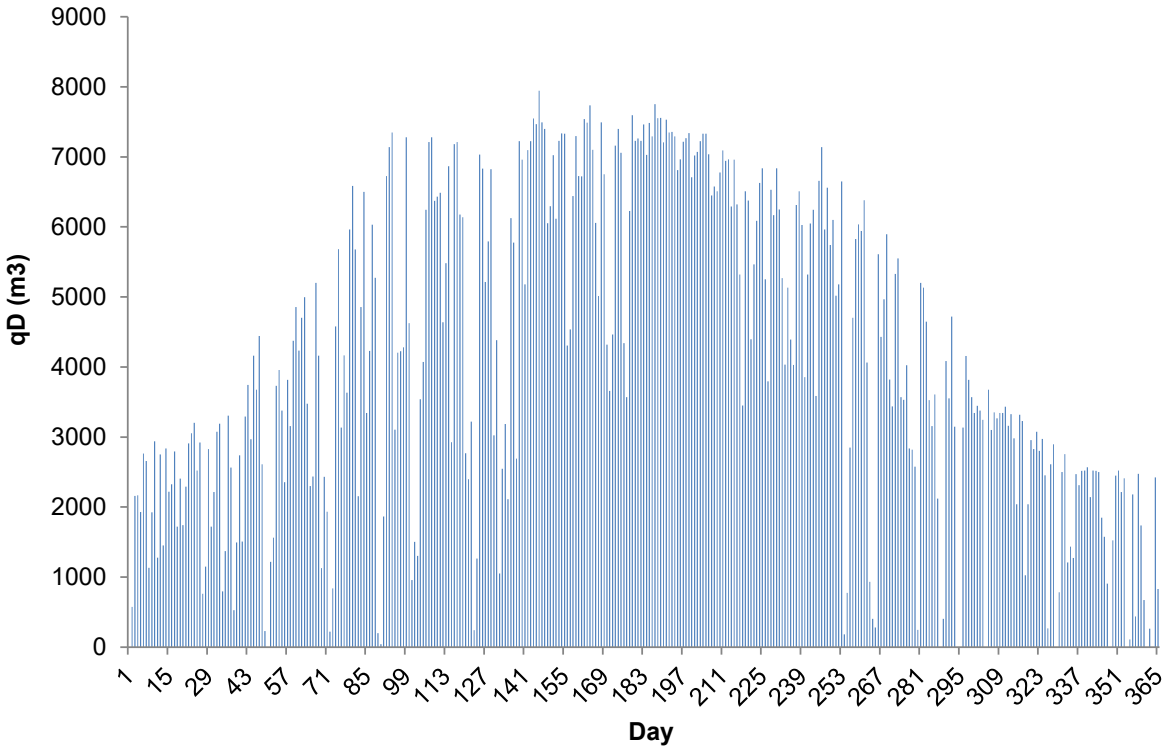

Figure 7.13. Daily fresh water production.

The monthly and total power and fresh water productions are presented in Table 7.3, along with the number of households that could be supplied with the generated electricity, if 4 MWh_e per household is taken as the average electricity consumption in Spain in the last years, according to World Energy Council (wec-indicators.enerdata.eu). Also, the number of inhabitants that could be supplied with water is presented, assuming a mean daily water consumption of 150 L (European Environment Agency, 2016). Particularly, the better month with higher electricity and water productions is July (24,122.7 MWh and 221,765.3 m^3), when up to 72,369 households could be fed with the power produced by the CSP+D plant. Winter season results the worse period, when only around 15,000 households could be supplied with electricity, on average.

Table 7.3. Monthly and total power and fresh water productions.

Month	W_e (MWh)	q_D (m^3)	**Number of households**	**Number of inhabitants**
January	5205.8	65,338.0	15,618	14,051
February	6736.3	73,243.1	20,209	17,439
March	10,959.3	114,964.9	32,878	24,724
April	15,045.6	151,593.3	45,137	33,687
May	17,539.6	160,622.6	52,619	34,542
June	20,569.7	189,489.8	61,710	42,109
July	24,122.7	221,765.3	72,369	47,691
August	19,219.9	175,602.3	57,660	37,764
September	13,407.0	135,999.2	40,221	30,222
October	8318.1	90,997.8	24,955	19,569
November	5877.7	76,187.0	17,633	16,930
December	3661.4	49,921.6	10,984	10,736
Total	150,663.2	1,505,725	37,666	27,501

7.5.4 Daily simulations for representative months on summer and winter

In this section the daily simulations of different variables of interest during two particular months of the year are shown: July and December, which are the months which have the higher and the lower electric energy generation during the year, respectively. The variables shown are the HTF temperatures in each collector of the generic loop (T_1, T_2, T_3 and T_4), the HTF temperature of the insulated pipes (T_{pipes}), the direct normal irradiance (E_b), the thermal power excess which has not been transferred to the power block ($P_{PB,excess}$), the thermal energy stored in the TES system (E_{stored}), the useful thermal power collected in the solar field

($P_{SF,useful}$), the useful thermal power transferred to the power block ($P_{PB,useful}$), the HTF mass flow rate in the generic loop (q_{loop}), the power generation, the daily fresh water production, the electric energy generation in 10-min steps, the daily fresh water production in 10-min steps, the motive steam pressure and mass flow rate, the specific energy consumption of the MED-TVC unit, the brine salinity in the first effect and the heating steam temperature.

7.5.4.1 Daily simulations for July

In this month the simulations were performed with the MED-TVC fed by the LP3 steam extraction (Figures 7.14 – 7.25), as selected previously. The month has been divided into four weeks, the first three comprising seven days and the last ten days. In general, it can be seen how due to the good climatic conditions (few cloudy days, high DNI levels) and Sun's position (small incidence angle, high Sun's altitude), the thermal power collected by the solar field is high and also the TES system is filled to values near to its maximum almost all the days. In addition, the longer daylight hours make the CSP+D plant operate near to 18 h per day (including the 7.5 h of TES discharge). The daily mean values of the electric energy generated and fresh water production are around 0.75 GWh and 7000 m^3. The motive steam conditions are kept near to nominal values during all the operation period, and the specific energy consumption of the MED-TVC process is maintained around 47 kWh/m^3. Finally, it can be seen how the brine salinity in the first effect is kept below 70,000 ppm, while the heating steam temperature and last effect temperature take values near to their design specifications, that is, 70 °C and 37 °C, respectively.

7.5.4.2 Daily simulations for December

During this month the simulations were carried out with the MED-TVC fed by the LP3 steam extraction, as stated previously (Figures 7.26 – 7.37). In contrast to the simulations performed in July, this month provides much less amount of electric energy and fresh water, because of the reason explained above. The month has been also divided into four weeks, the first three comprising seven days and the last ten days. The mean daily power produced during these weeks is around 0.25 GWh at best, and the fresh water production is kept below 2000 m^3 per day. Some days, such as 14th and 20th, the plant cannot operate because of the lack of solar resource.

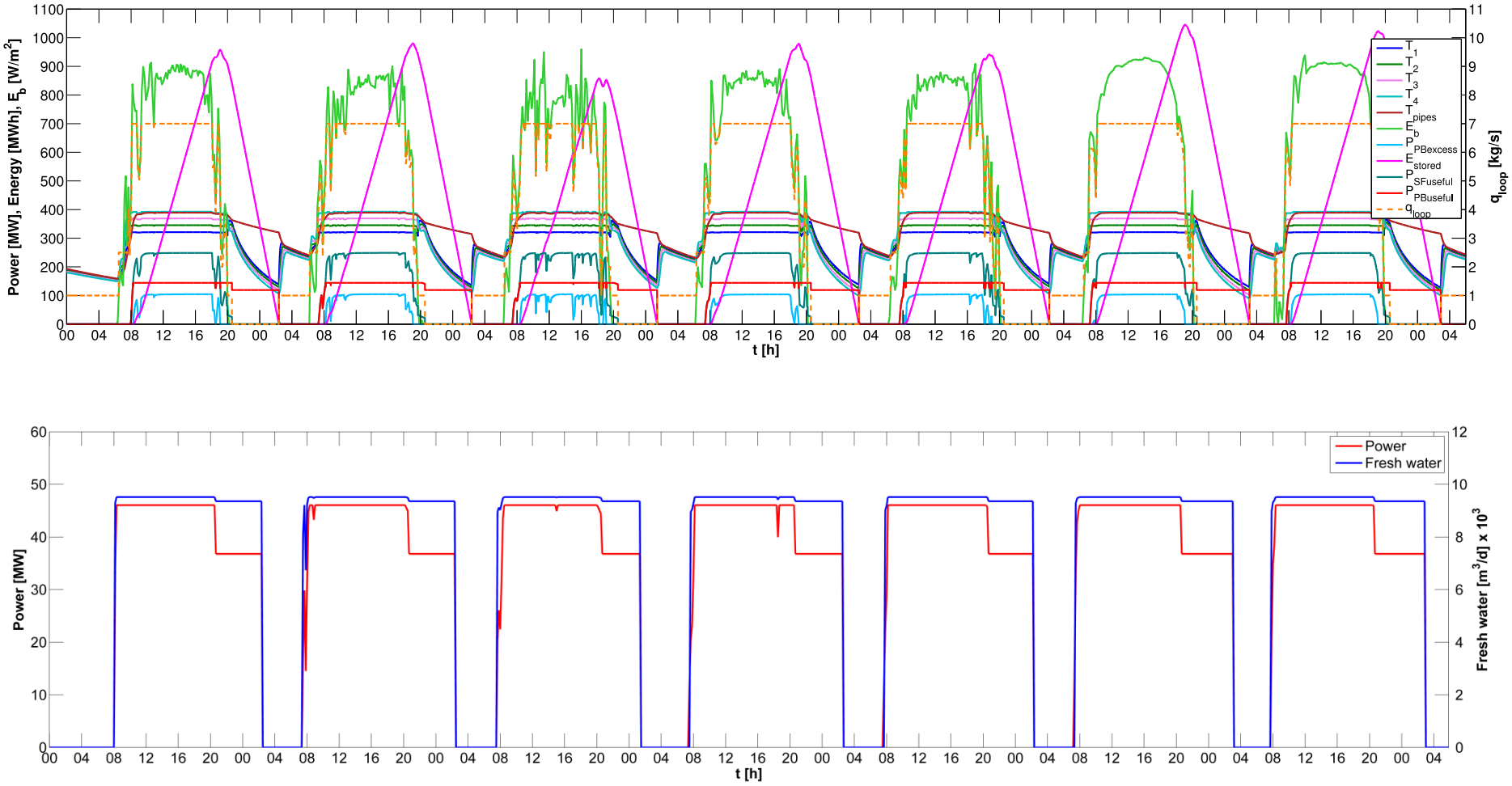

Figure 7.14. Solar field output, power and fresh water productions during July 1st-7th.

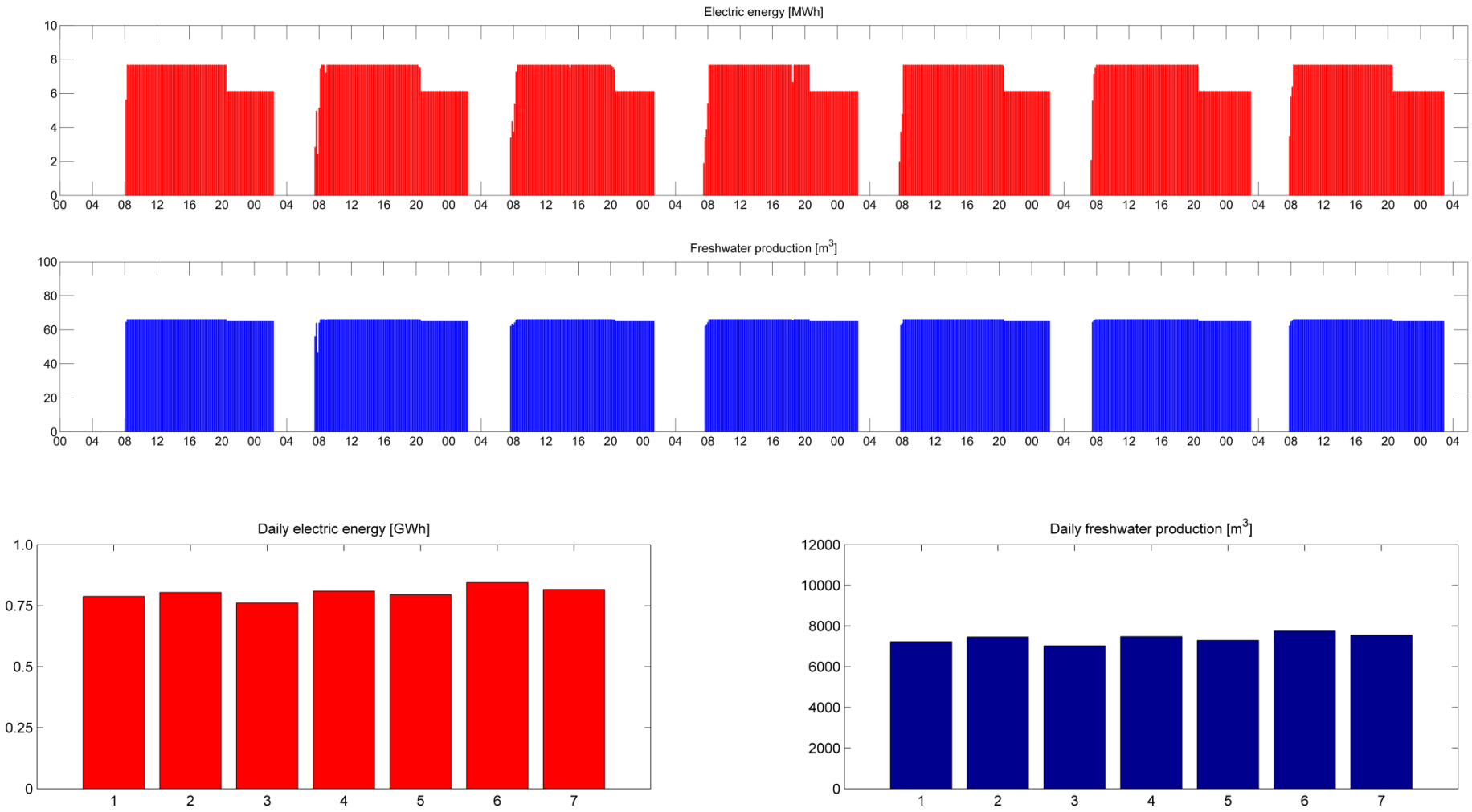

Figure 7.15. Electric energy and fresh water productions, for 10-min periods and daily periods, during July 1st-7th.

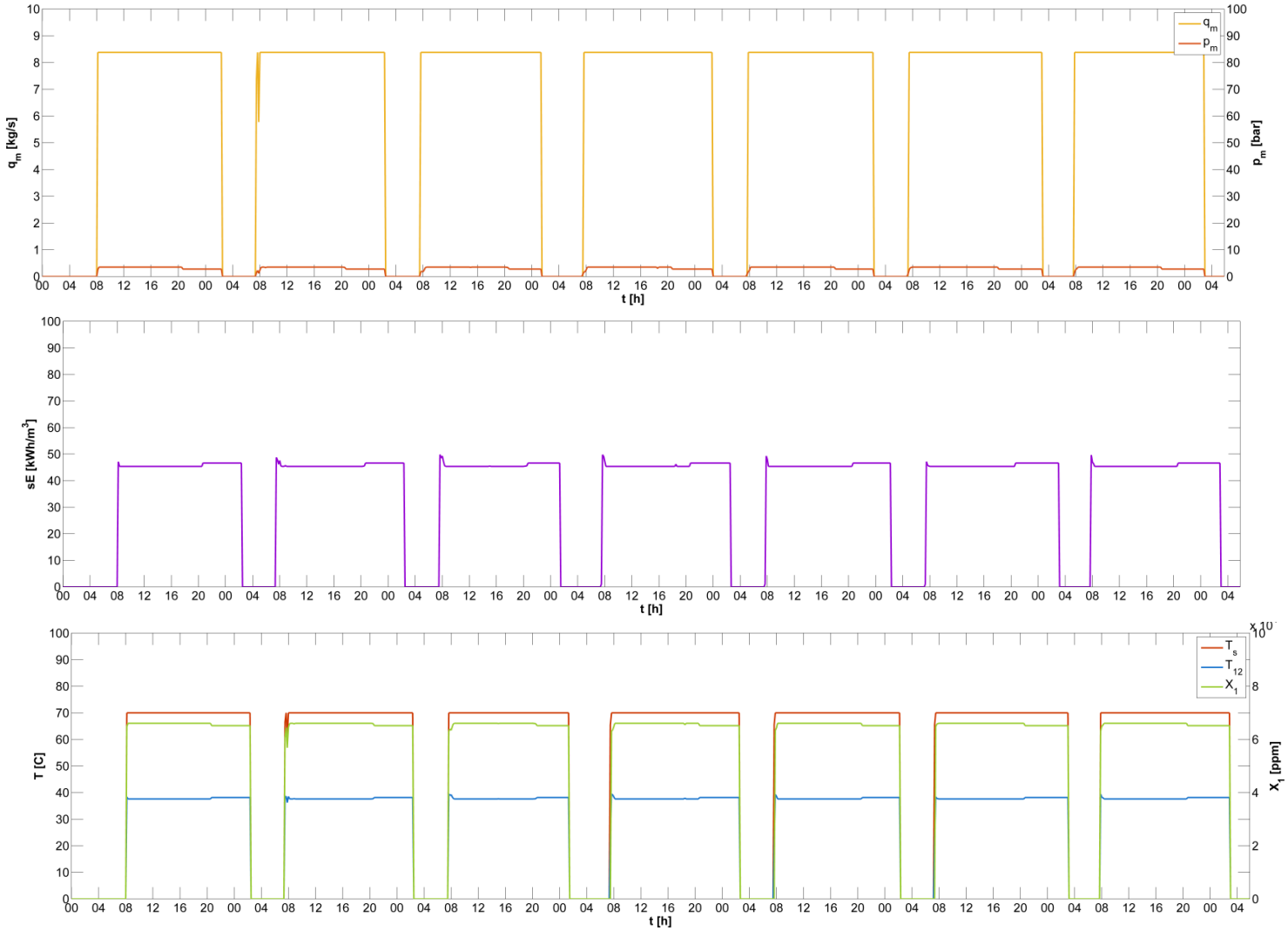

Figure 7.16. Motive steam pressure and mass flow rate, specific energy consumption, heating steam temperature, last effect temperature and brine salinity in1st effect, during July 1st-7th.

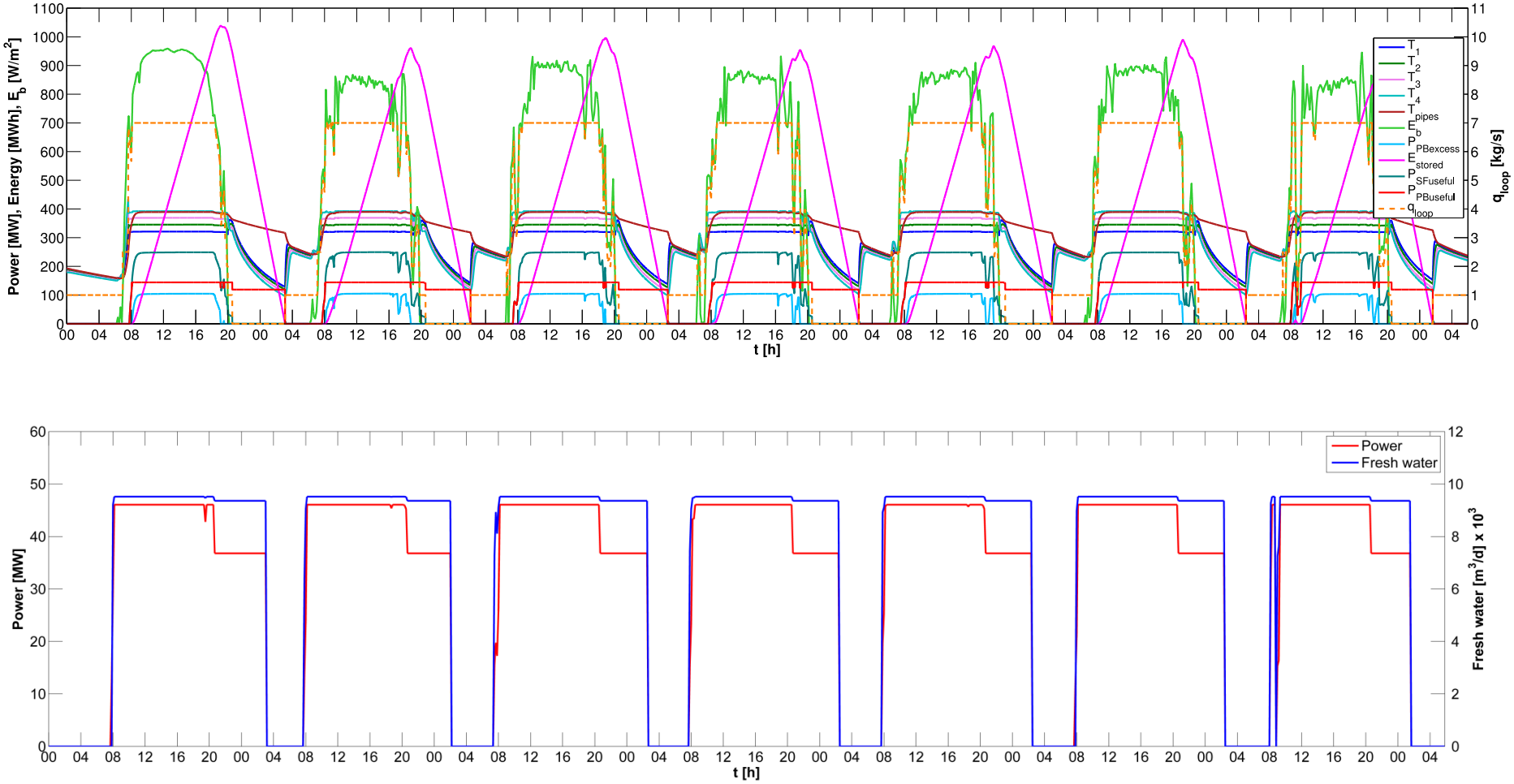

Figure 7.17. Solar field output, power and fresh water productions during July 8th-14th.

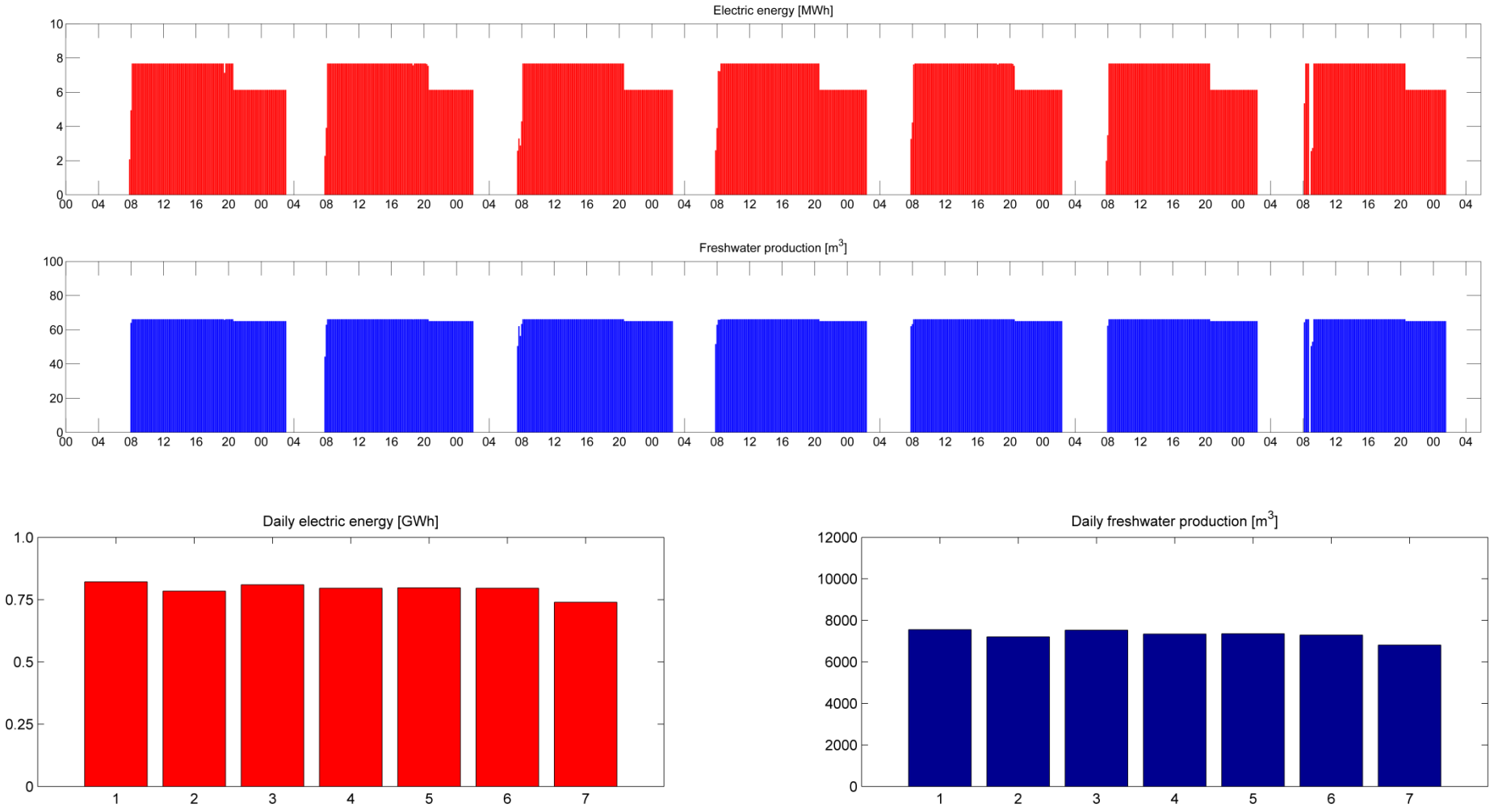

Figure 7.18. Electric energy and fresh water productions, for 10-min periods and daily periods, during July 8th-14th.

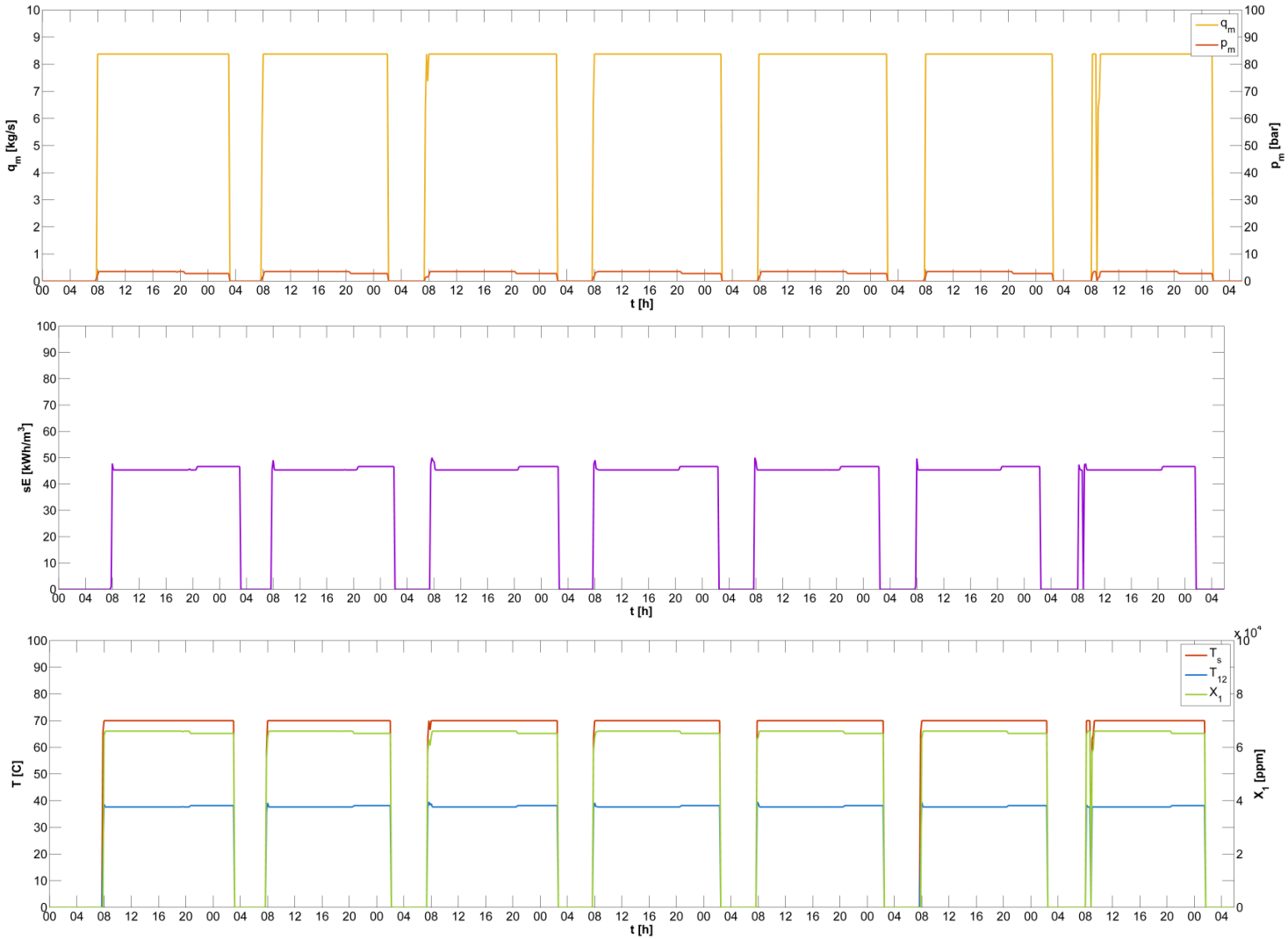

Figure 7.19. Motive steam pressure and mass flow rate, specific energy consumption, heating steam temperature, last effect temperature and brine salinity in1st effect, during July 8th-14th.

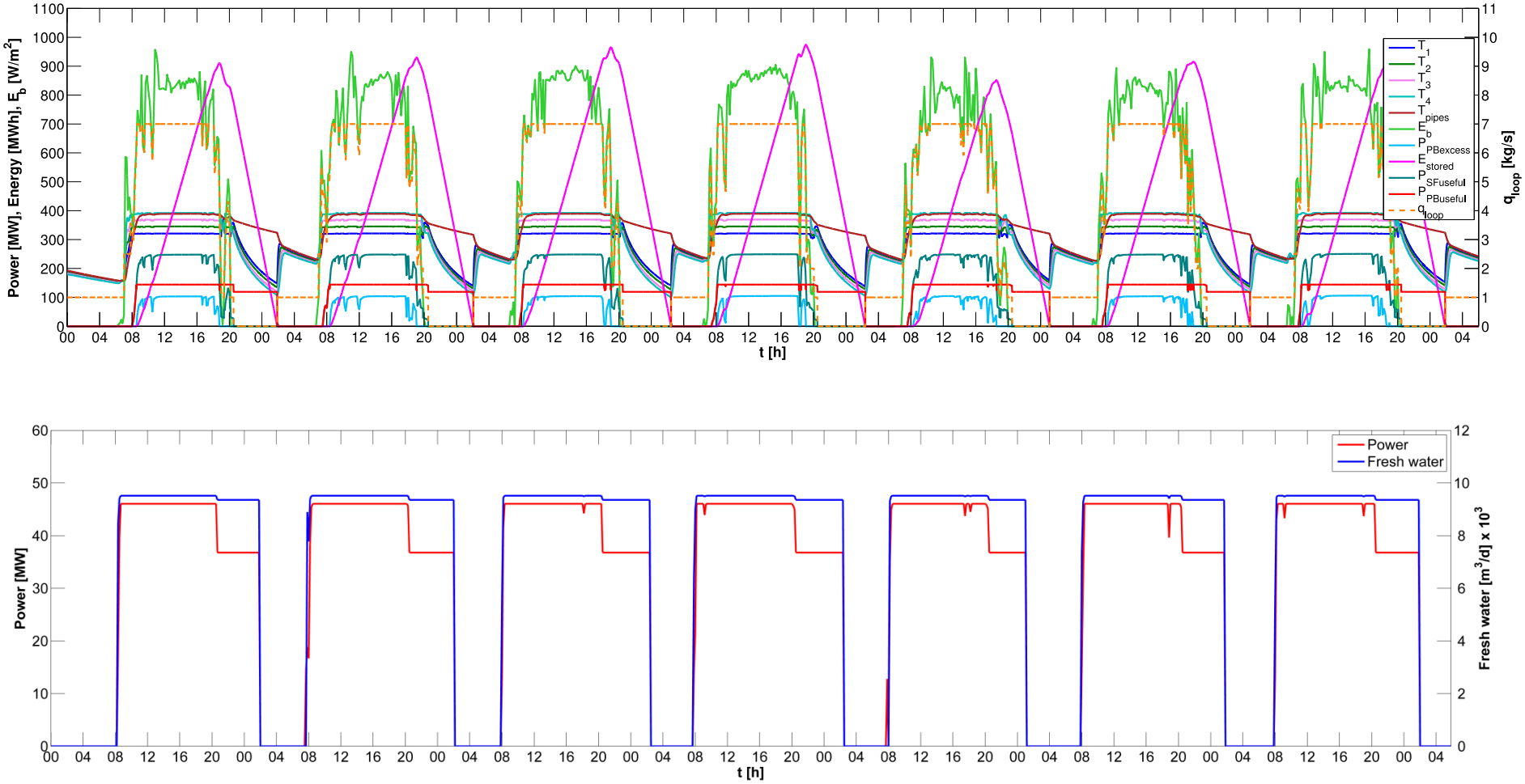

Figure 7.20. Solar field output, power and fresh water productions during July 15th-21st.

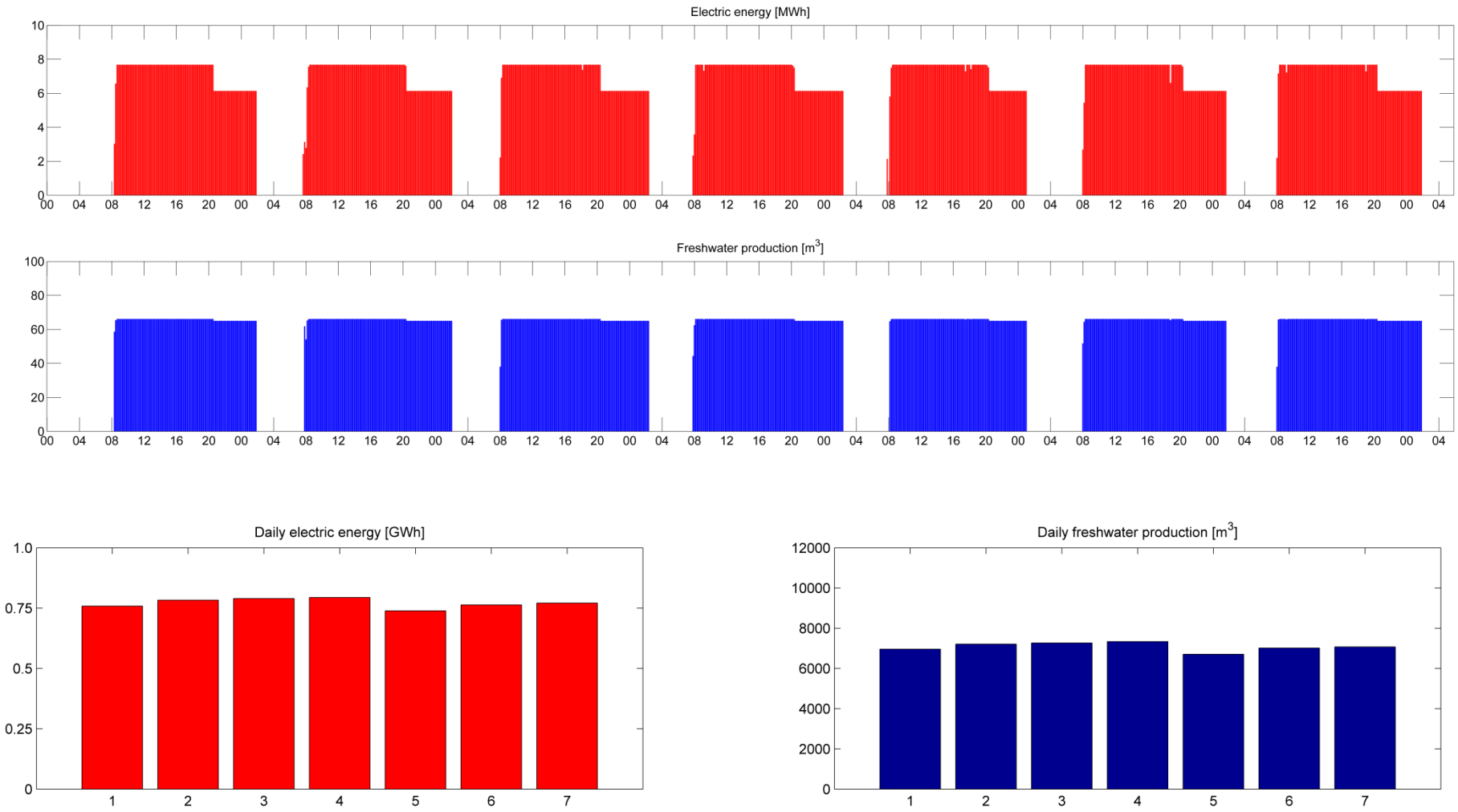

Figure 7.21. Electric energy and fresh water productions, for 10-min periods and daily periods, during July 15th-21st.

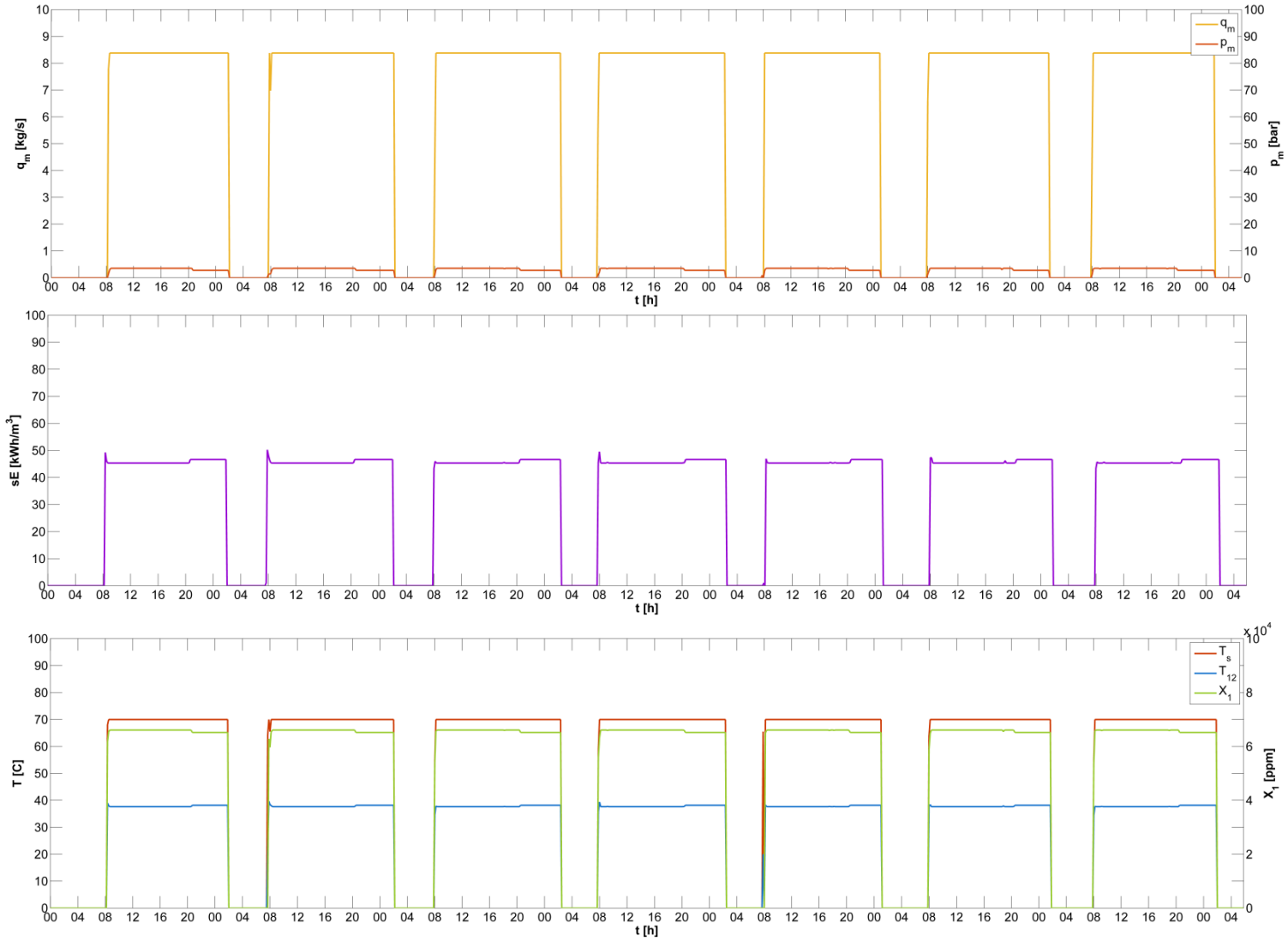

Figure 7.22. Motive steam pressure and mass flow rate, specific energy consumption, heating steam temperature, last effect temperature and brine salinity in1st effect, during July 15th-21st.

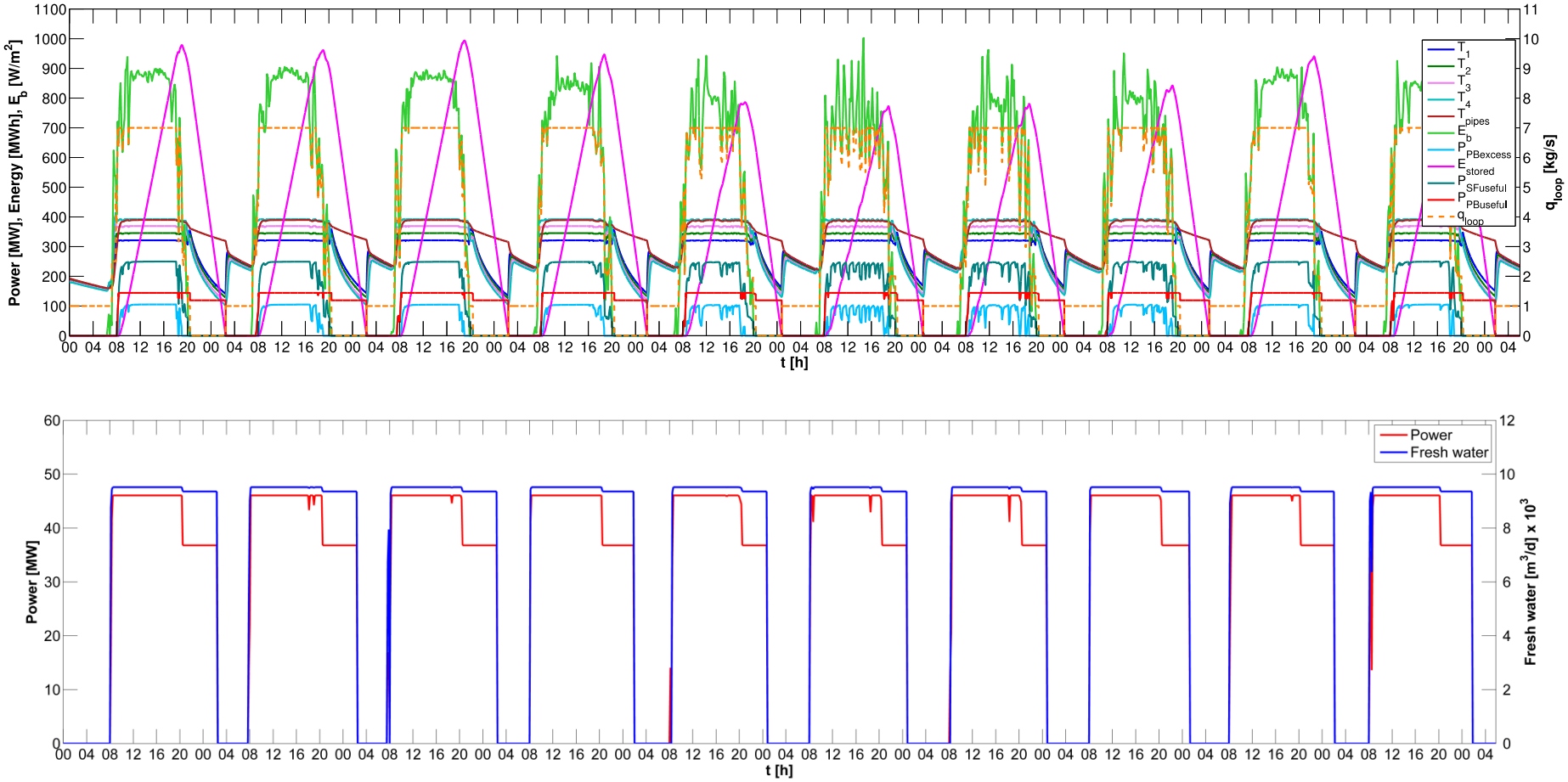

Figure 7.23. Solar field output, power and fresh water productions during July 22nd-31th.

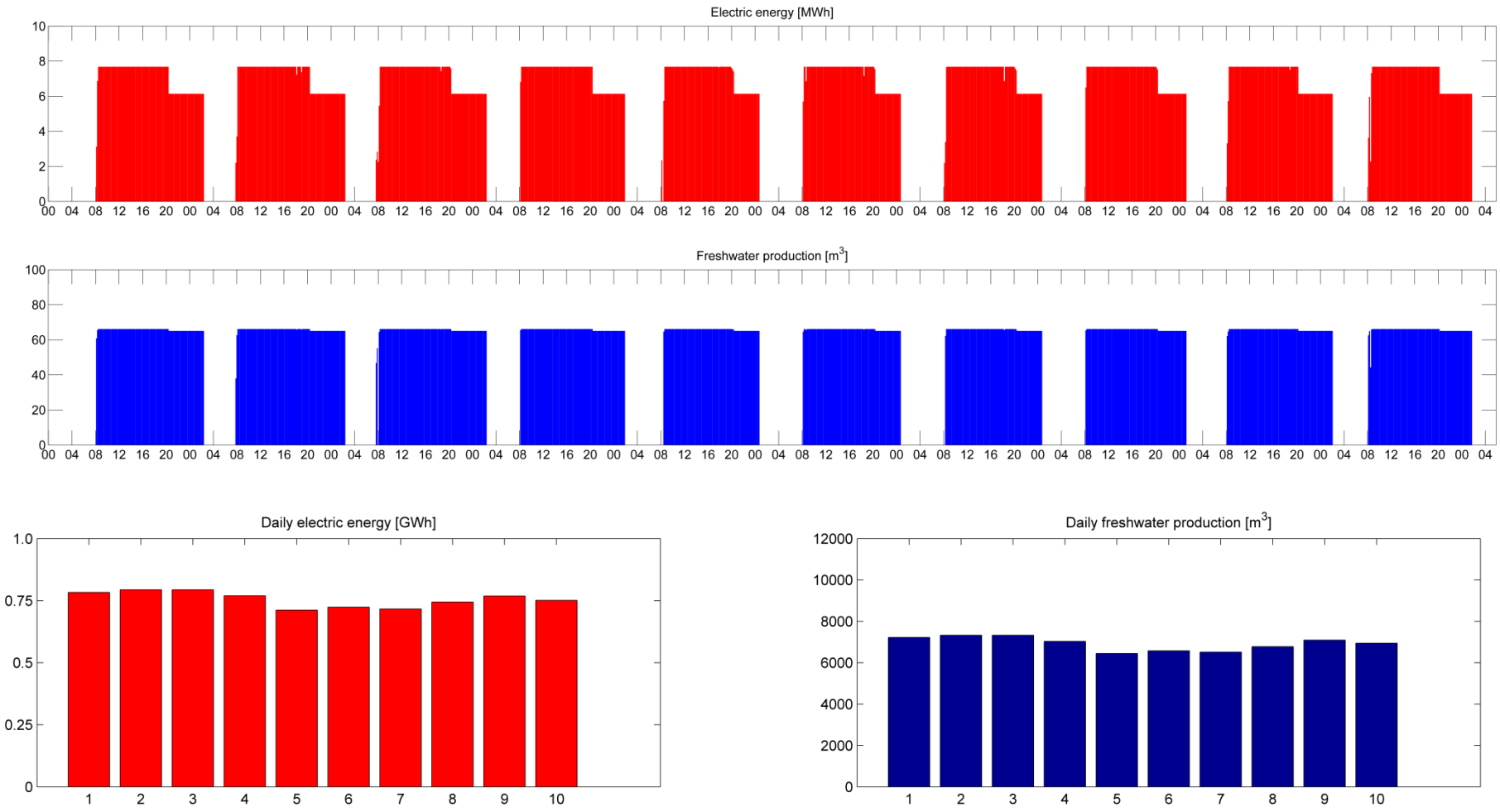

Figure 7.24. Electric energy and fresh water productions, for 10-min periods and daily periods, during July 22nd-31th.

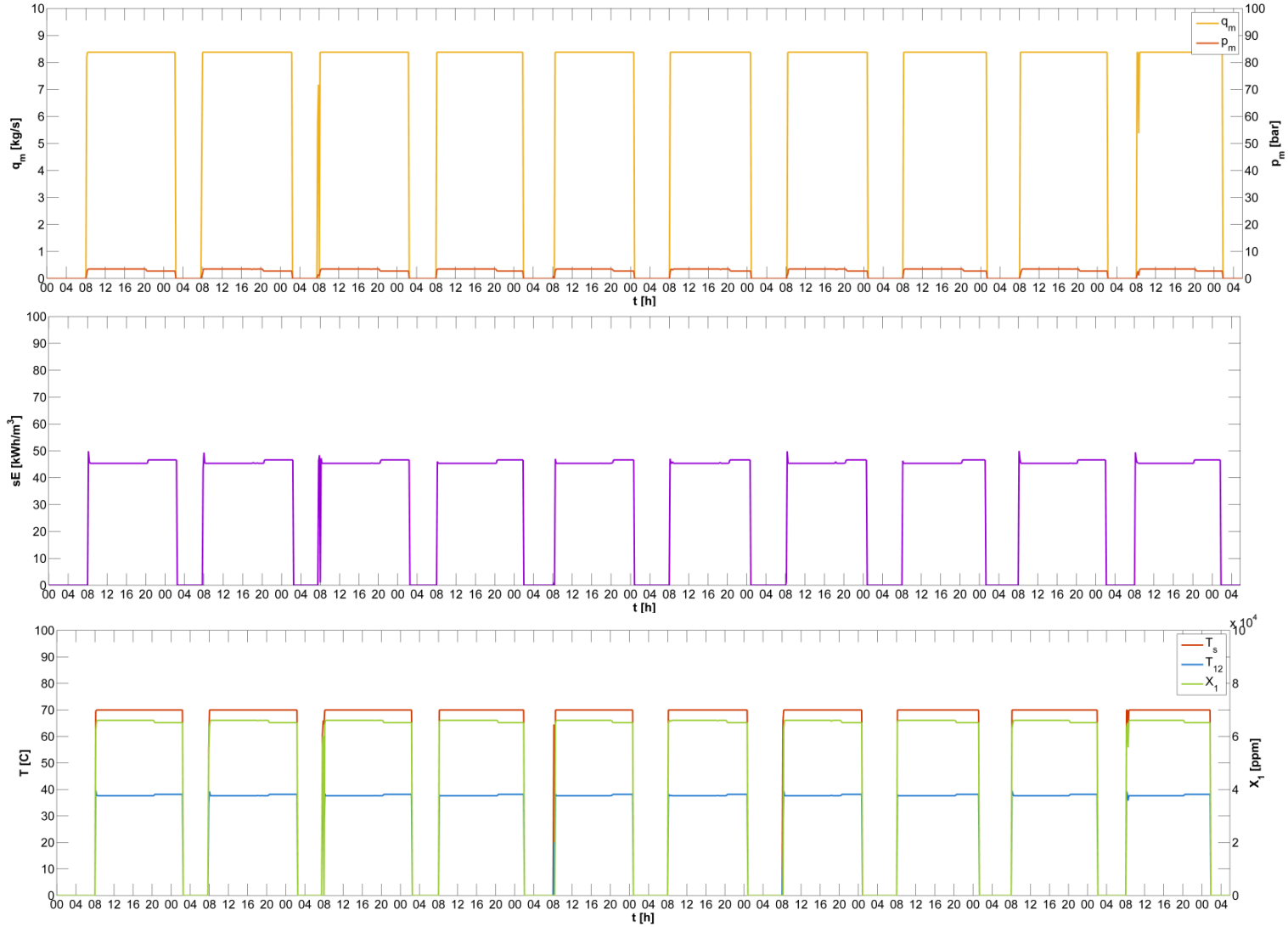

Figure 7.25. Motive steam pressure and mass flow rate, specific energy consumption, heating steam temperature, last effect temperature and brine salinity in1st effect, during July 22nd-31th.

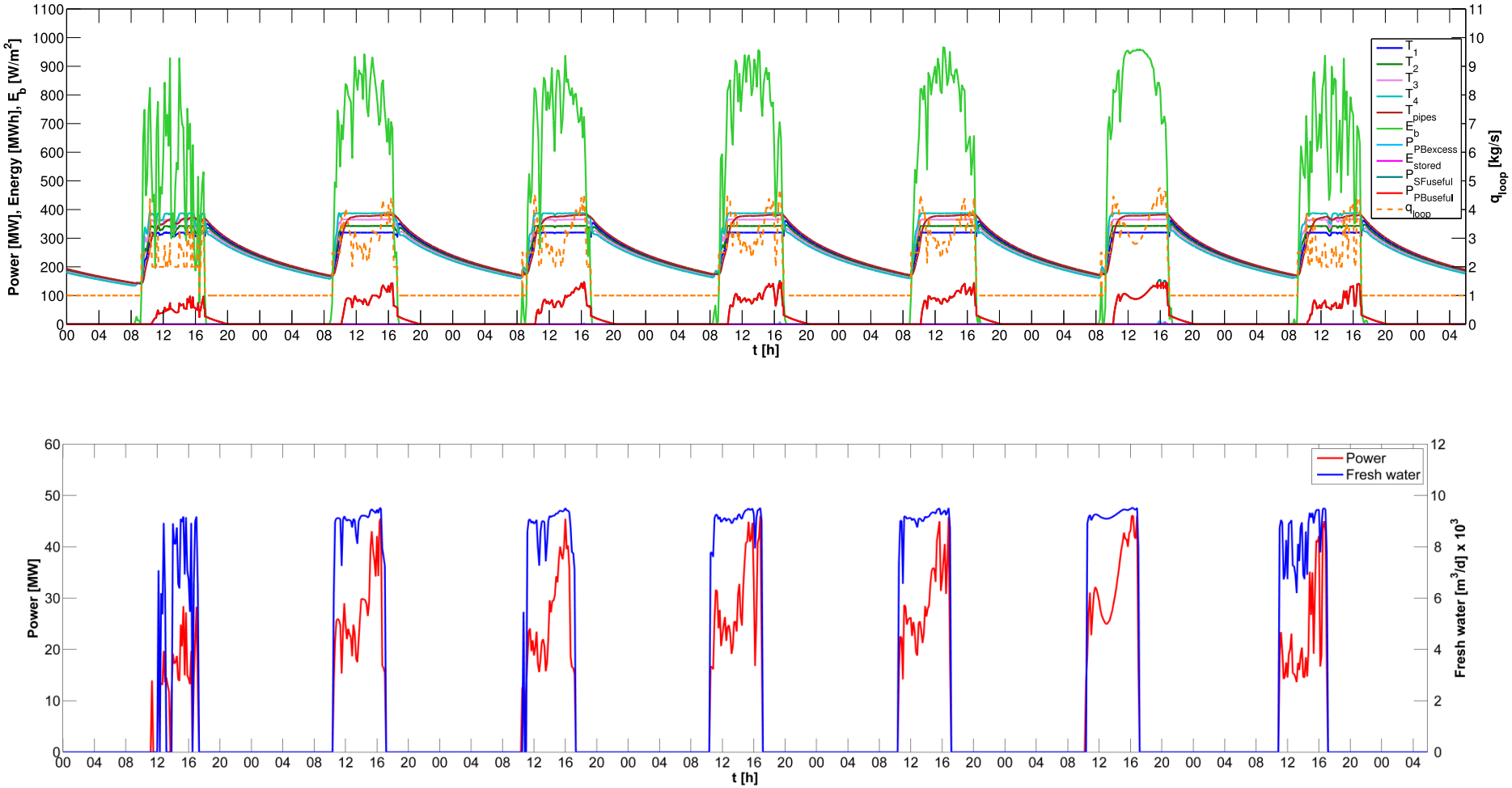

Figure 7.26. Solar field output, power and fresh water productions during December 1st-7th.

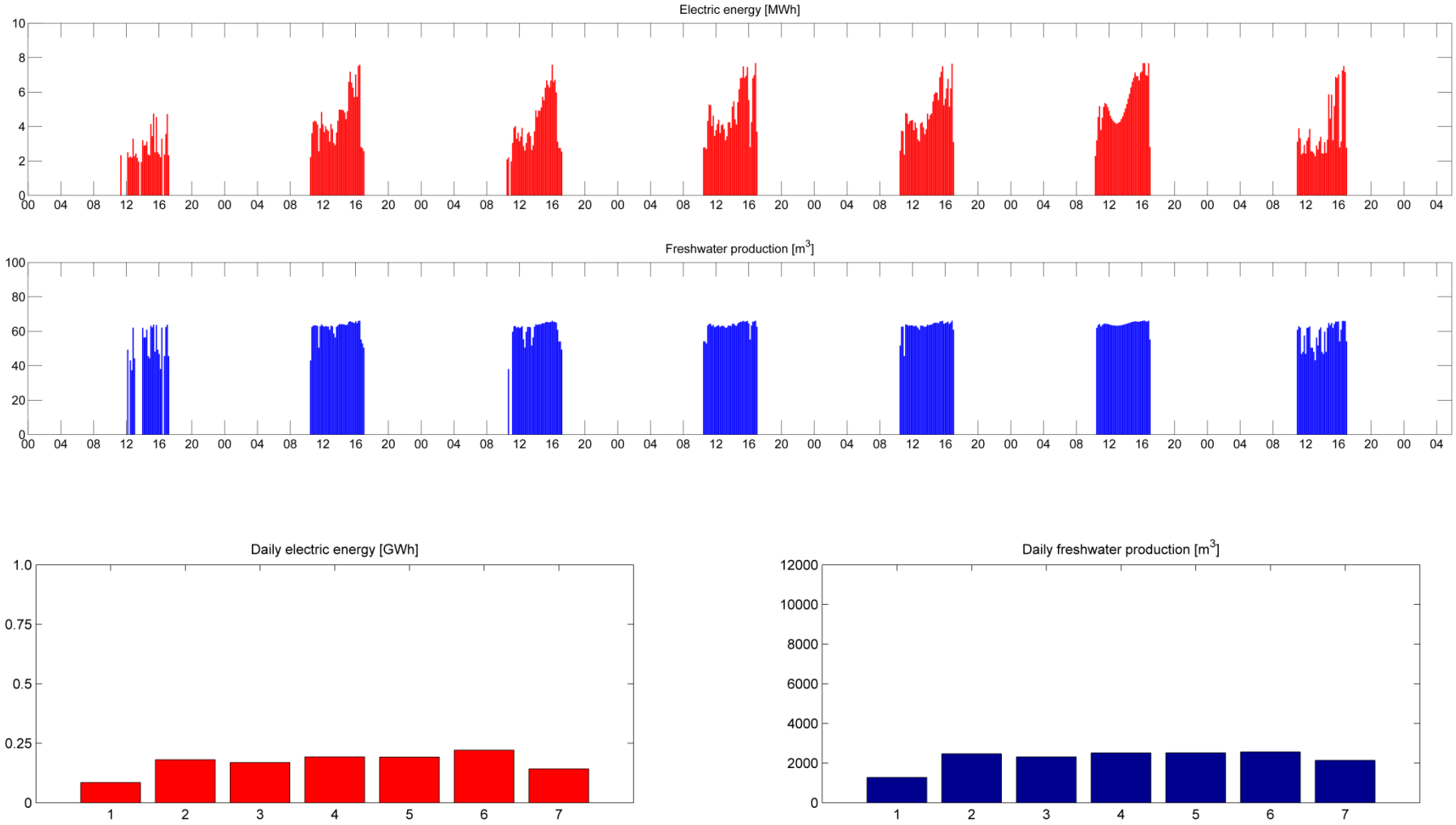

Figure 7.27. Electric energy and fresh water productions, for 10-min periods and daily periods, during December 1st-7th.

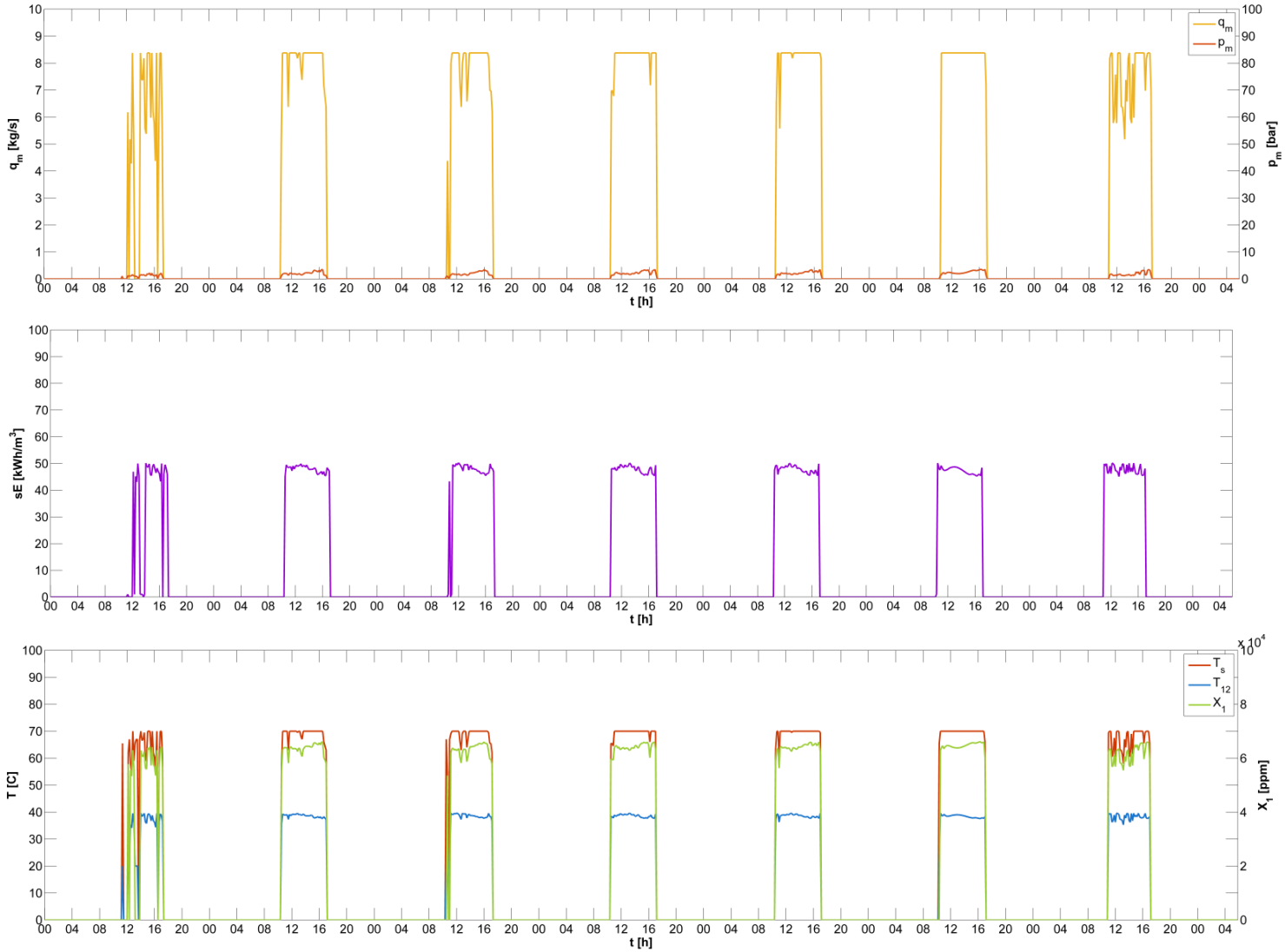

Figure 7.28. Motive steam pressure and mass flow rate, specific energy consumption, heating steam temperature, last effect temperature and brine salinity in1st effect, during December 1st-7th.

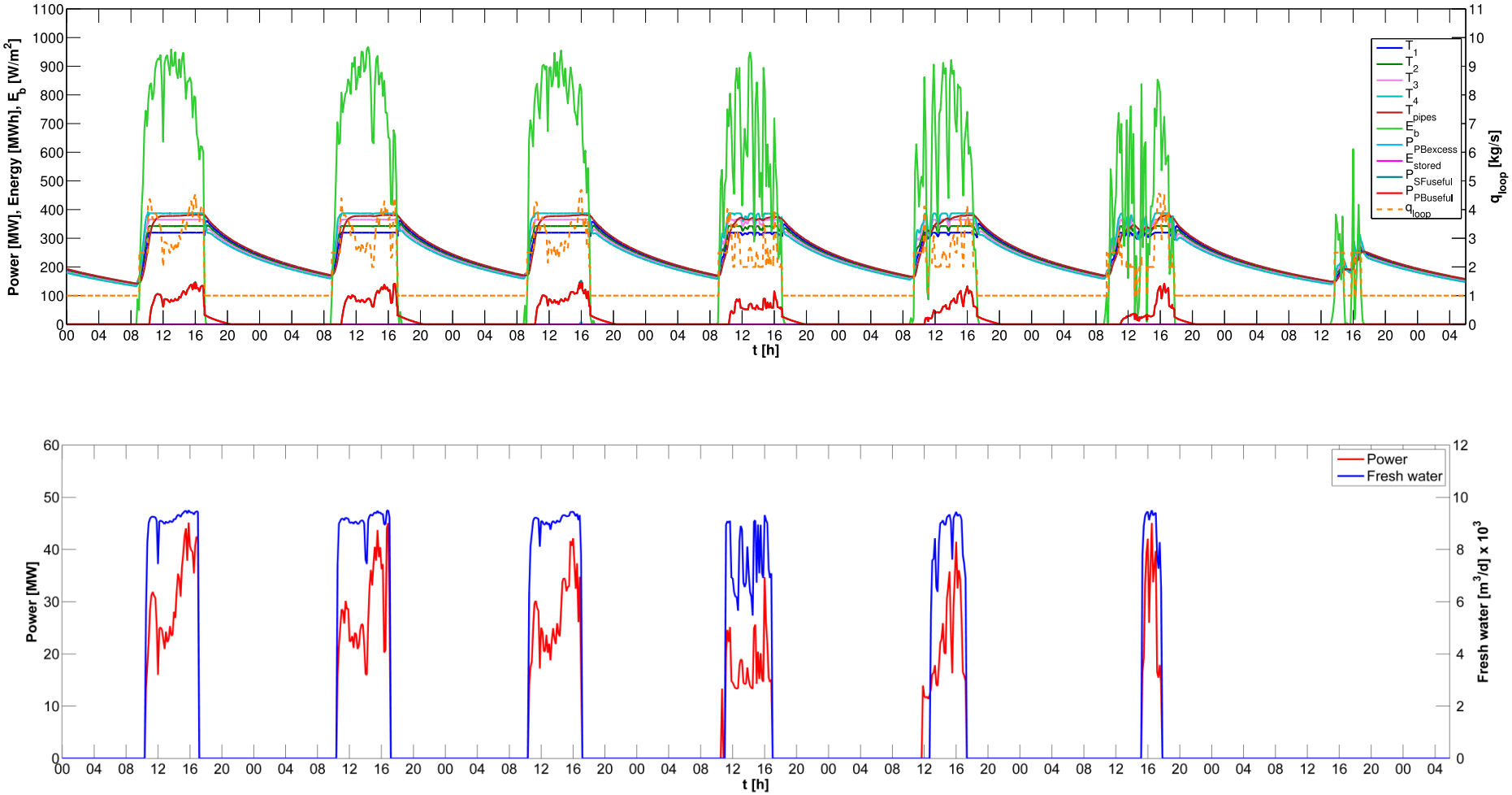

Figure 7.29. Solar field output, power and fresh water productions during December 8th-14th.

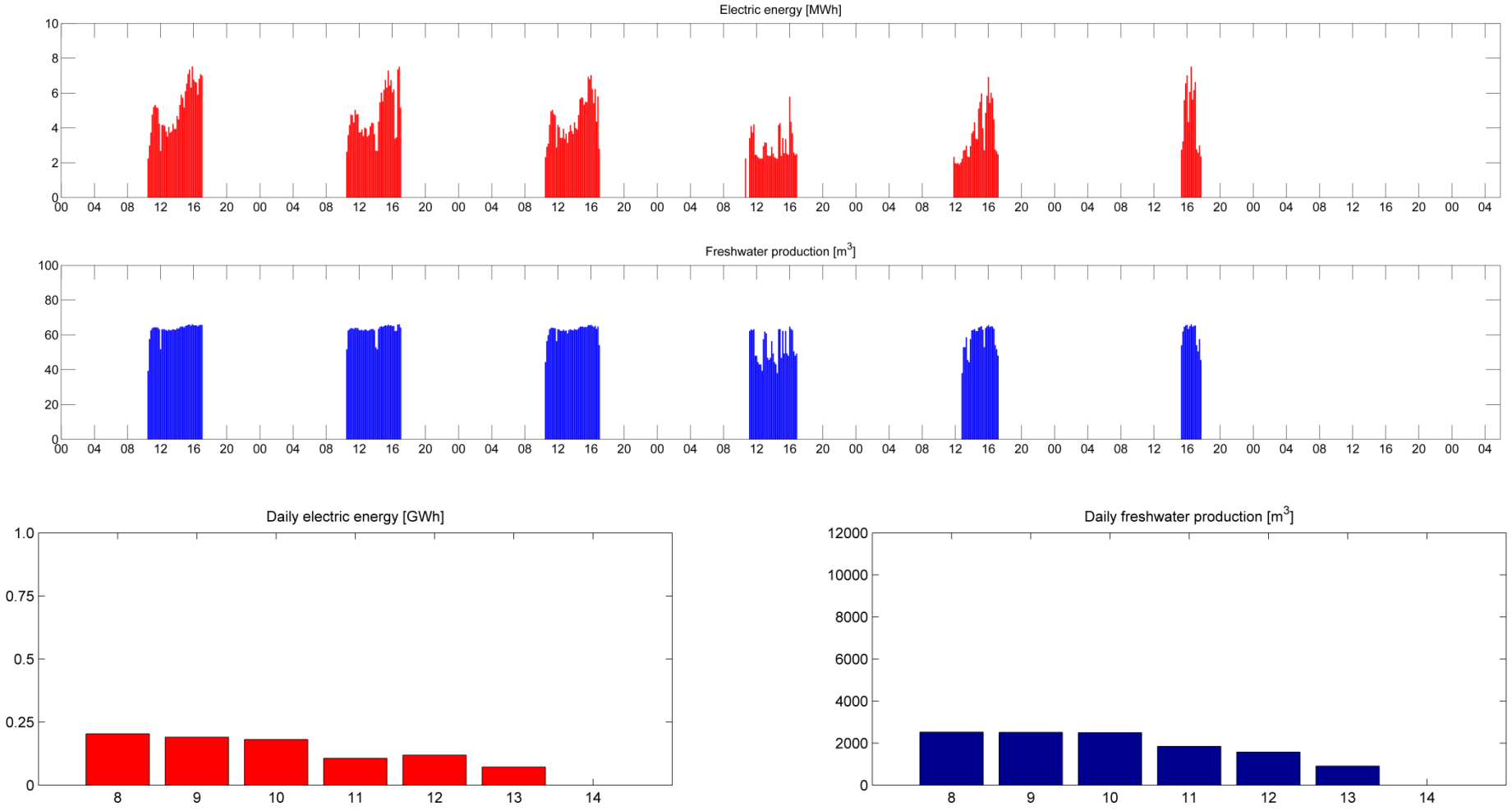

Figure 7.30. Electric energy and fresh water productions, for 10-min periods and daily periods, during December 8th-14th.

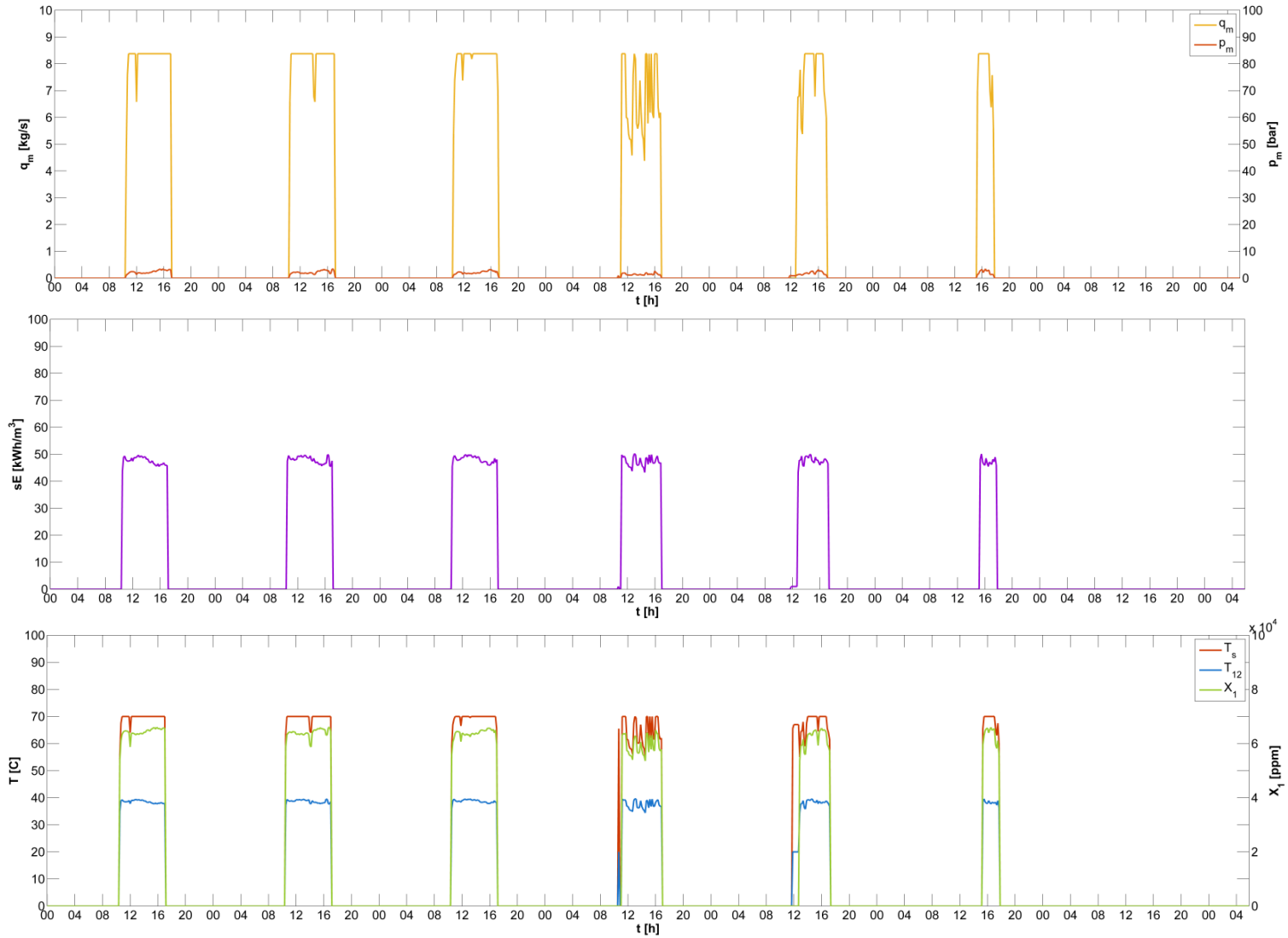

Figure 7.31. Motive steam pressure and mass flow rate, specific energy consumption, heating steam temperature, last effect temperature and brine salinity in1st effect, during December 8th-14th.

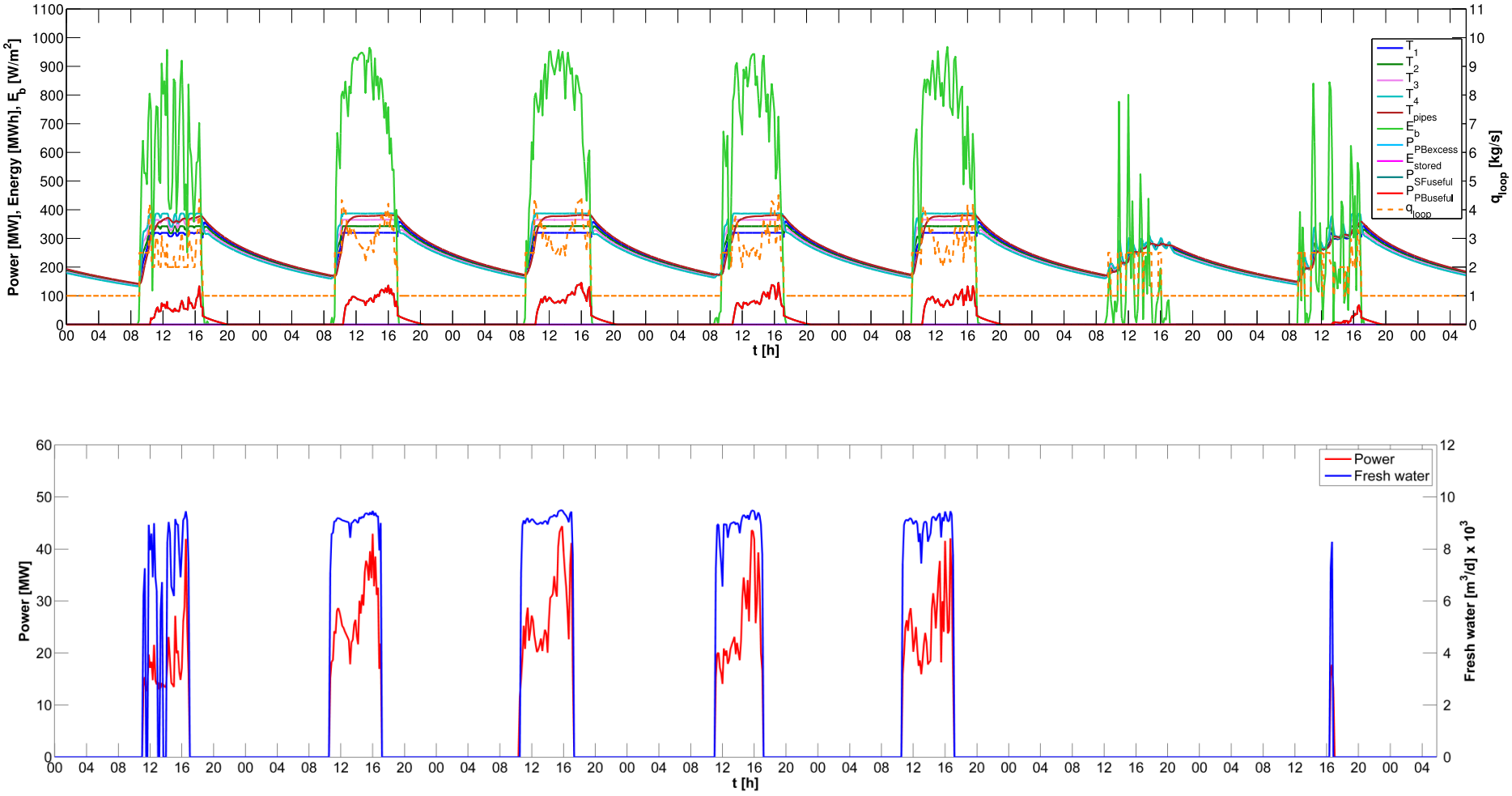

Figure 7.32. Solar field output, power and fresh water productions during December 15th-21st.

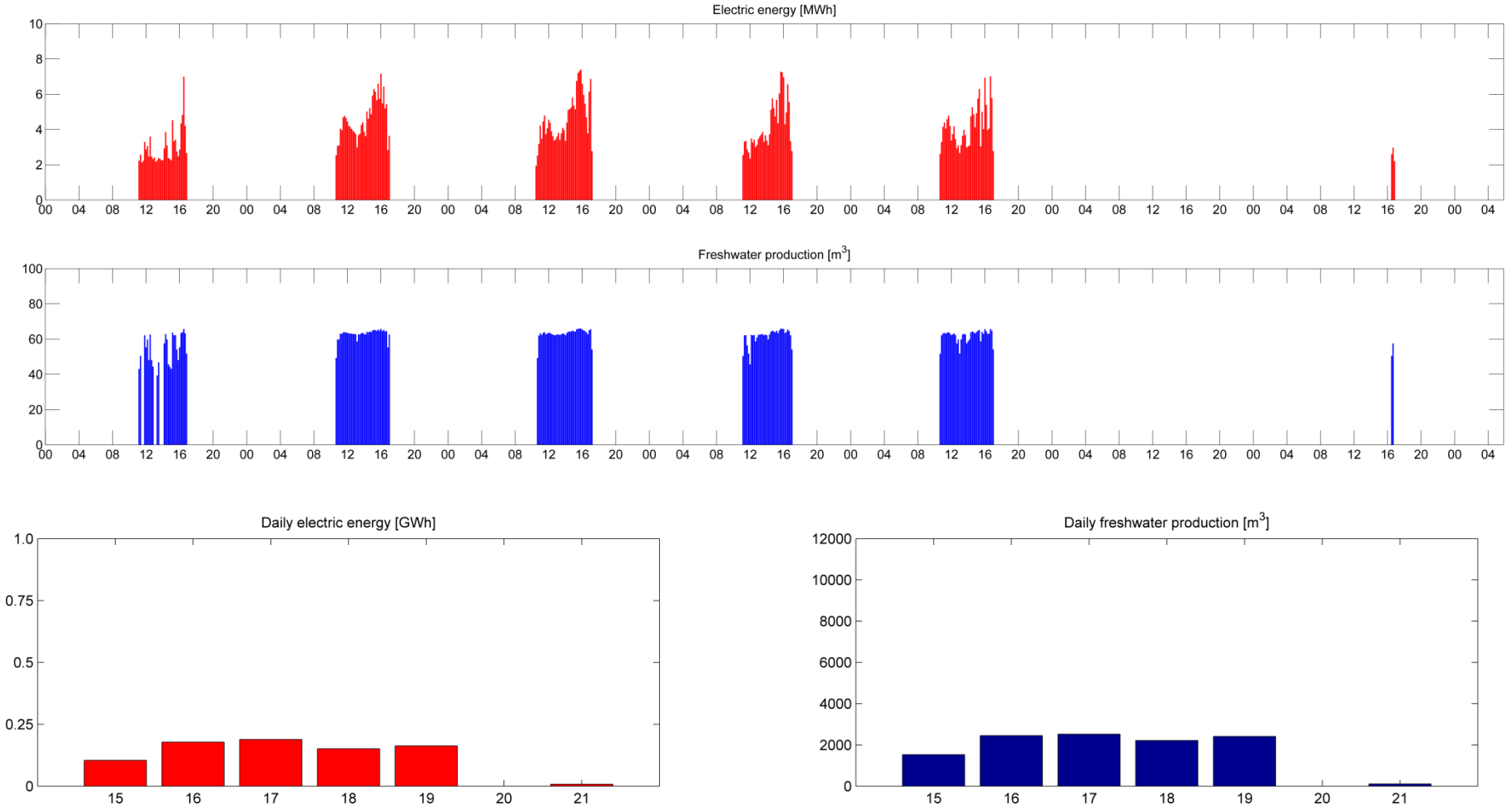

Figure 7.33. Electric energy and fresh water productions, for 10-min periods and daily periods, during December 15th-21st.

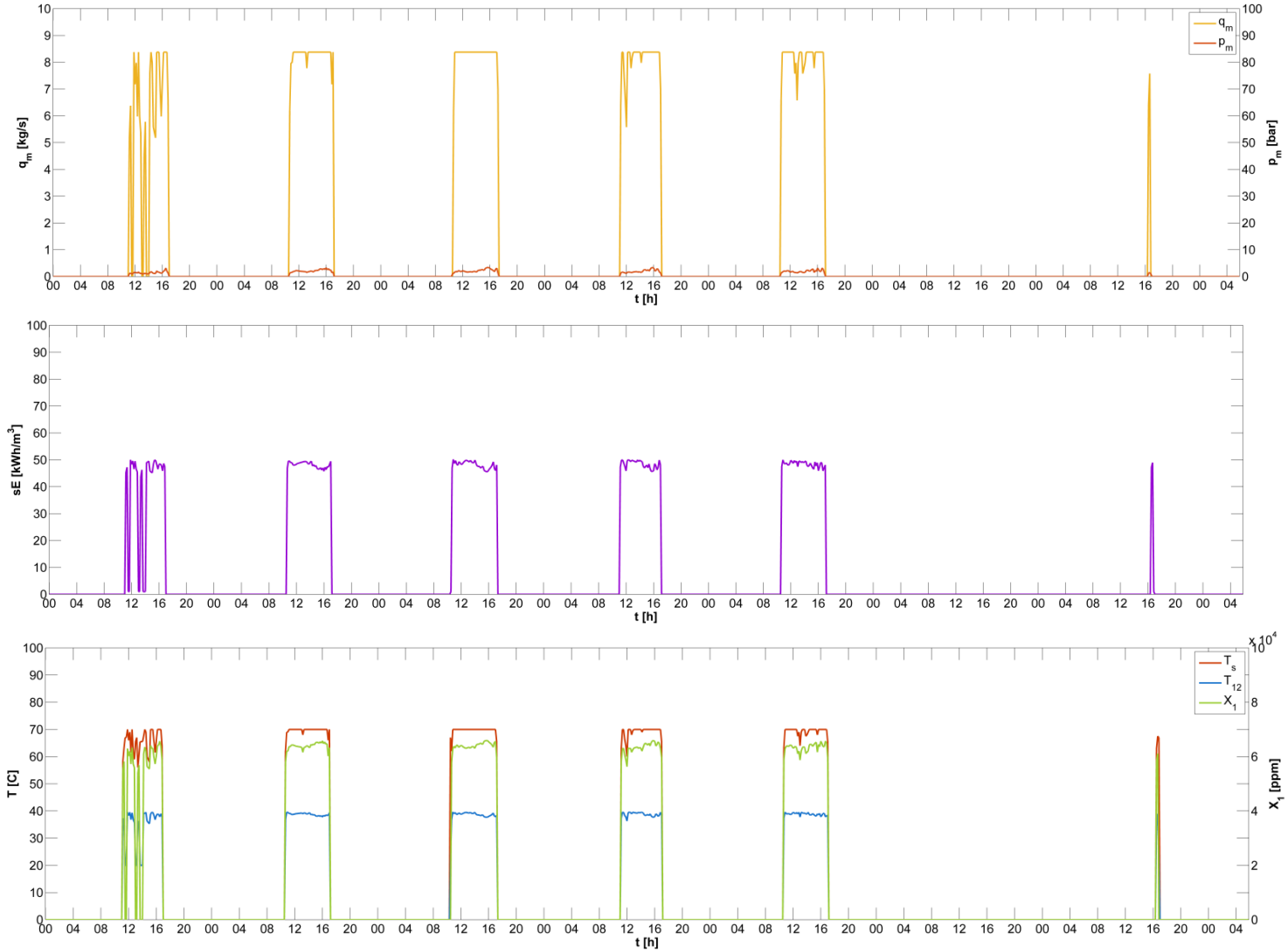

Figure 7.34. Motive steam pressure and mass flow rate, specific energy consumption, heating steam temperature, last effect temperature and brine salinity in1st effect, during December 15th-21st.

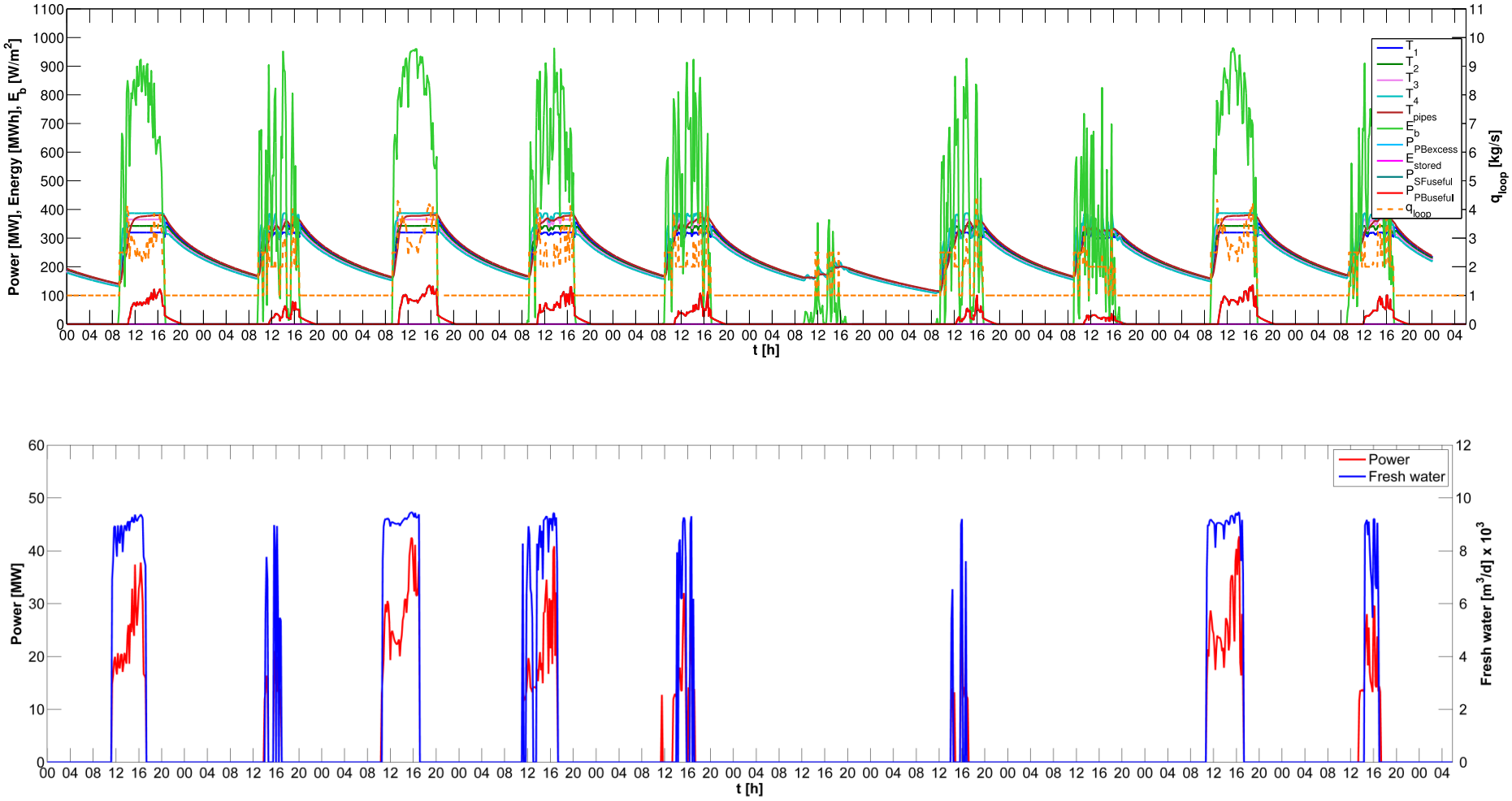

Figure 7.35. Solar field output, power and fresh water productions during December 22nd-31th.

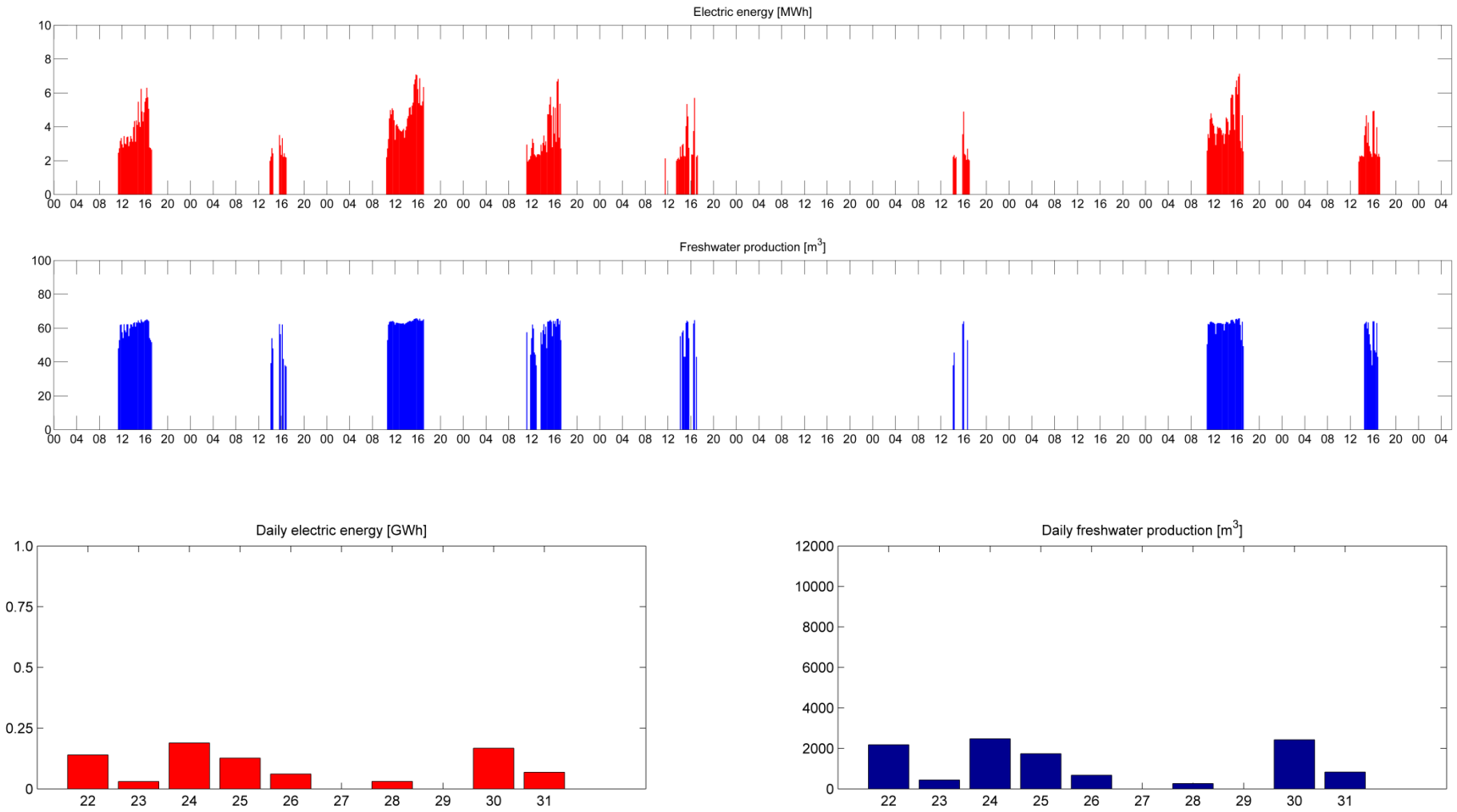

Figure 7.36. Electric energy and fresh water productions, for 10-min periods and daily periods, during December 22nd-31th.

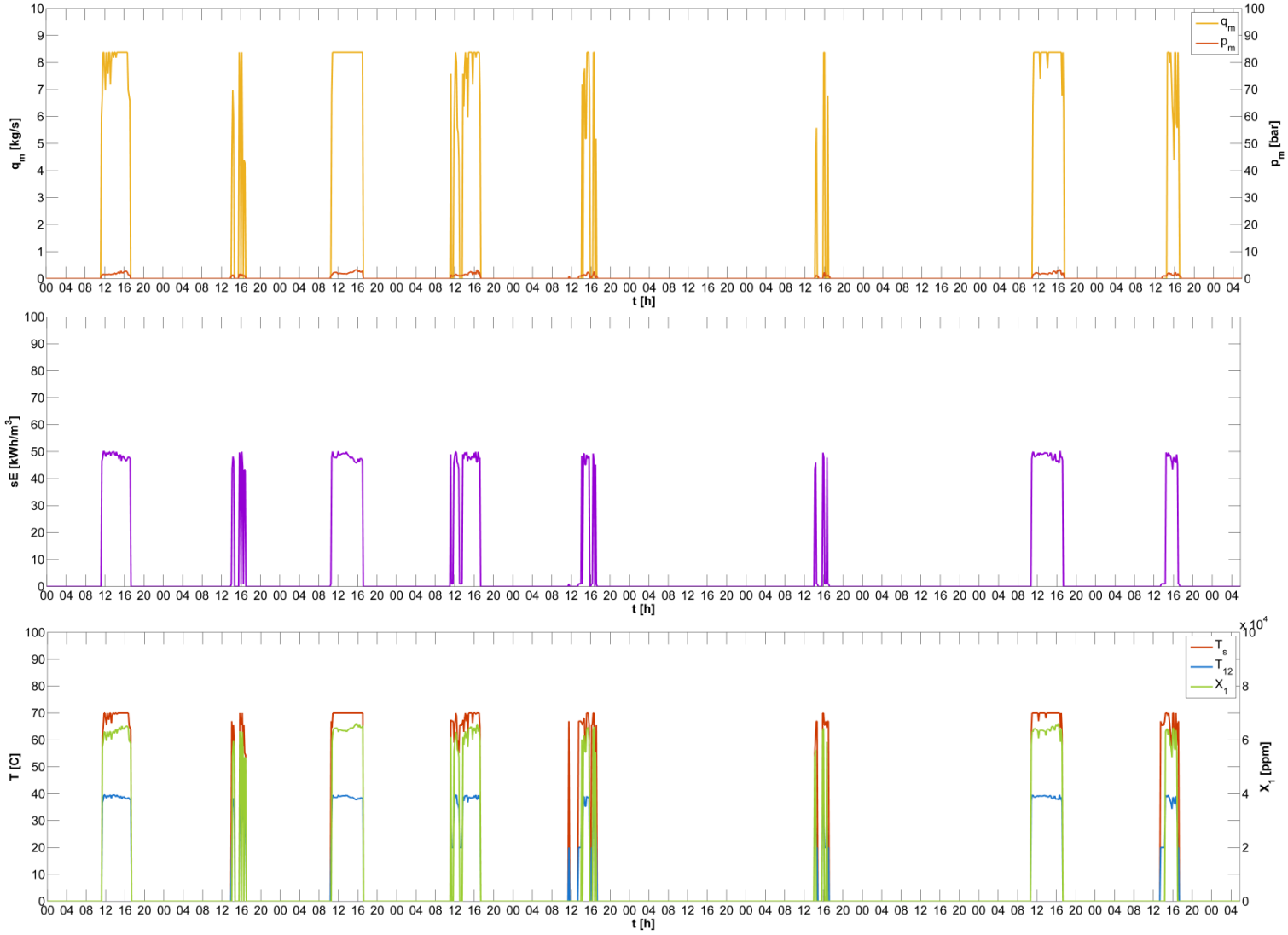

Figure 7.37. Motive steam pressure and mass flow rate, specific energy consumption, heating steam temperature, last effect temperature and brine salinity in1st effect, during December 22nd-31th.

7.6 Conclusions

In this chapter, the CSP+D simulation tool developed in previous chapters, comprising the models of the solar field, power block and desalination plant, has been used to estimate the yearly power and freshwater production for a hypothetic CSP+D plant located in Almería (Spain). Two coupling arrangements previously analysed (using a high pressure or low pressure steam extractions to feed the MED-TVC unit) have been alternatively used, depending on the monthly electric energy demand in the location considered. The features of the power block in nominal conditions, for three different scenarios: only electricity generation, electricity and water production using a high pressure steam extraction, and electricity and water productions using a low pressure steam extraction, have been also shown.

Results obtained for the particular case studied showed that the maximum electricity and fresh water productions estimated were simultaneously obtained during the summer period, being July the month with the higher production. In particular, 24,122.7 MWh and 221,765.3 m^3, for the electric energy and water productions, that may meet the needs of 72,369 households and 47,691 inhabitants, respectively.

Finally, two representative months of the summer and winter periods (July and December) have been selected in order to show the daily fresh water and electricity productions. In addition, other significant variables regarding the solar field, power block and desalination unit in operation have been represented, such as the HTF temperatures of the collectors, the useful thermal power absorbed in the solar field and transferred to the power block, the motive steam pressure and mass flow rate entering the thermocompressor, the specific energy consumption of the MED-TVC unit, or the brine salinity in the first effect and temperatures of the heating steam and in the last effect.

References

Eck, M., Barroso, H., Blanco, M., Burgaleta, Juan-Ignacio Dersch, J., Feldhoff, J.-F., Garcia-Barberena, J., Gonzalez, L., Hirsch, T., Ho, C., Kolb, G., Neises, T., Serrano, J.A., Tenz, D., Wagner, M., Zhu, G., 2011. guiSmo: Guidelines for CSP performance modeling – present status of the SolarPACES Task-1 project, in: Proceedings. 17th SolarPACES Conference. Granada, Spain.

Klein, S.A., 2013. Engineering Equation Solver Software (EES).

Llorente García, I., Álvarez, J.L., Blanco, D., 2011. Performance model for parabolic trough solar thermal power plants with thermal storage: Comparison to operating plant data. Sol. Energy 85, 2443–2460. doi:10.1016/j.solener.2011.07.002

Meteonorm, 2015. Meteonorm: Irradiation data for every place on Earth [WWW Document]. URL http://meteonorm.com/ (accessed 7.4.15).

Montes, M.J., Abánades, A., Martínez-Val, J.M., Valdés, M., 2009. Solar multiple optimization for a solar-only thermal power plant, using oil as heat transfer fluid in the parabolic trough collectors. Sol. Energy 83, 2165–2176. doi:10.1016/j.solener.2009.08.010

REE, 2016. Red Eléctrica de España | Series estadísticas por comunidades autónomas [WWW Document]. URL http://www.ree.es/es/estadisticas-del-sistema-electrico-espanol/series-estadisticas/series-estadisticas-por-comunidades-autonomas (accessed 7.15.16).

Stine, W.B., Geyer, M., 2001. Power from the sun [WWW Document]. URL http://www.powerfromthesun.net/book.html

Chapter 8. Conclusions and future works

Contents

Nomenclature

Acronyms and abbreviations

CSP	Concentrating Solar Power
EES	Engineering Equation Solver
GOR	Gain Output Ratio
MED	Multi-Effect Distillation
PT	Parabolic Trough
TVC	Thermal Vapour Compression

8.1 Conclusions

In this research work, a theoretical analysis of high efficient Multi-Effect Distillation (MED) processes for seawater desalination and their integration with concentrating solar power plants has been carried out. With the objective of increasing the thermal performance of the MED process and reducing its energy consumption, two different approaches have been taken into account: to increase the number of effects by rising the top brine temperature up to 120 °C, using seawater pretreatments such a nanofiltration, and to introduce Thermal Vapour Compression (TVC). Also, the coupling of a MED-TVC unit, based on the Trapani commercial plant, with a Parabolic Trough Concentrating Solar Power (PT-CSP) plant, similar to the commercial Andasol-2 plant, has been evaluated to find the best configuration arrangement that optimize the power and water production depending on the demand profiles (water & power) during the year in the location considered. For the first approach, a mathematical model for a forward feed MED process has been developed and implemented in Engineering Equation Solver, able to simulate high operation temperatures and a large number of effects. This model has been compared with others from the literature and includes a detailed calculation of the thermodynamic losses of the vapour. For the second approach, a design MED-TVC model has been developed and implemented in Engineering Equation Solver (EES). In addition, an operational model of the MED-TVC process has been built to be integrated into a CSP plant for yearly simulations of the CSP+MED-TVC system. Regarding the model of the CSP plant, on one hand, an accurate performance model of the parabolic trough solar field taken from the literature has been implemented in MATLAB, which can simulate the operation of the solar field with time steps of ten seconds. On the other hand, the power block, based on a Rankine cycle, has been implemented allowing also the simulation of part load conditions.

Specific conclusions are presented below:

1. There is not a clear agreement among the scientific community about the best seawater desalination technology to be coupled to a CSP plant for the combined production of power and water, particularly comparing membrane and thermal methods. Several factors influence this selection, as the location of the plant, the energy source availability, socio-economic issues, fuel prices, power and water demands, etc. However, reverse osmosis technology has lower energy consumption and the larger global desalination capacity installed in the last years. Due to the potential that the integration of MED units into CSP plants presents, further investigation for the increase of the thermal efficiency of MED processes must be accomplished.

2. The increase of the number of effects, by rising the top brine temperature (or equivalently, the heating steam temperature) in a forward feed MED process significantly improves the Gain Output Ratio (GOR) and consequently the specific

energy consumption, and reduces the specific heat transfer area. In the case study presented in this work, for a difference of temperature between effects of 2.5 °C, rising the heating steam temperature from 70 to 120 °C allows to increase the number of effects from 14 to 34, and leads to a 70% growth in the GOR (from 10.38 to 17.6) and a 11% reduction of the specific heat transfer area (from 518.2 to 463.9 m^2/ (kg/s)) and a 45% decrease in the specific thermal energy consumption (from 61.98 to 34.49 kWh/m^3). Also, it was identified that the terminal temperature difference of the preheater associated with the first effect ($TTD_{preh,1}$) has a significant influence on the thermal efficiency of the MED process: the lower this parameter is, the higher GOR is obtained. This improvement is constrained by the increase of the specific heat transfer area that low values of $TTD_{preh,1}$ imply. Particularly, for a $TTD_{preh,1}$ of 8 °C the GOR is 6.15 while in the case of a $TTD_{preh,1}$ of 2 °C, the GOR obtained is 7 (12% of increase). However, the specific heat transfer area is also increased, from 333.4 to 347.1 m^2/(kg/s) (an increase of 4% approximately). Moreover, the thermodynamic losses were found to greatly increase the specific heat transfer area.

3. It hast been identified the necessity of using different coupling arrangements of the MED-TVC unit to the CSP plant depending on the water and power local demands, optimizing the thermal efficiency of both the desalination system and the power block by using high pressure steam or low pressure steam from the turbines to feed the MED-TVC unit, respectively.

4. It has been developed a simulation tool for the fresh water production using a MED-TVC process which allows to select the optimum design for the desalination plant from both economic (minimum specific heat transfer area) and energetic (maximum thermal efficiency, GOR) point of views. The tool also permits to select the best coupling scheme with a Rankine cycle power block, as function of the available steam extractions and the thermocompressor location. For the particular case study analysed, it was concluded that for any given steam extraction pressure feeding the MED-TVC unit, there is an optimal location of the thermocompressor that maximizes the GOR. Higher motive steam pressures lead to higher GOR values, with the thermocompressor close to the last effect. Also, there is an optimal reduction of the evaporator's heat transfer areas after the thermocompressor suction point that minimizes the specific heat transfer area, for every motive steam pressure and thermocompressor location. Intermediate positions of the thermocompressor lead to lower specific heat transfer areas but also to lower fresh water production. Regarding the coupling with Rankine cycle power blocks, it was recommended that, when the electricity demand is high, the best integration scheme would be with the MED-TVC unit being fed with a low pressure steam extraction and with the thermocompressor suction in intermediate

effects, which increases the power generation (using steam of low exergy) but also decreases the fresh water production. On the contrary, when the electricity demand is low, the suggested coupling arrangement would be using high or medium pressure steam extraction to feed the MED-TVC unit, and with the thermocompressor closer to the last effect. By doing so, the fresh water production is improved but the power generation is further penalized (by using steam of higher exergy). Particularly, in the case study presented, using low pressure steam at 3.63 bar and with the thermocompressor in the 9th position, the exergetic power of the steam extraction from the low pressure turbine resulted 5634 kW and the water production 9384 m^3/d, 6.2% below the nominal value (10,000 m^3/d). Conversely, using high pressure steam to feed the MED-TVC unit at 45.4 bar and placing the thermocompressor suction closer to the last effect (11th), the fresh water production in this case resulted of 9823 m^3/d, 1.77% lower than the design value, and the exergetic power of the steam extraction 7757 kW, a 37.7% higher than in the case of the low pressure steam.

5. The use of variable nozzle thermocompressors in a MED-TVC unit coupled to a Rankine cycle power block allows to maintain the motive steam mass flow rate constant when the thermal power load decreases (with sliding pressure regulation method), thus operating the MED-TVC unit near to nominal conditions as long there is enough steam available in the power block. As an example, in the case of using steam from the high pressure turbine (namely HP2), when the load decreases from 100% to 40%, the freshwater reduction is only of 2.6% (from 9823.2 to 9569.8 m^3/d). However, there are certain limits in the thermal load of the power block that do not permit to maintain the motive steam flow rate constant. Instead, it has to be reduced leading to a considerable reduction in the fresh water production. Nevertheless, variable area thermocompressors help to even increase the GOR in these cases. In the same example, the decrease in the load from 100 to 25% leaded to a drop in the freshwater of 47% approximately (from 9823.2 to 5228.2 m^3/d), with a decrease in the motive steam mass flow rate of 40%, but to an increase in the GOR of 28.8%.

6. When the motive steam mass flow rate of the thermocompressor is reduced from its nominal value, the MED-TVC unit works in off-design conditions and key process variables like the brine salinity and the vapour temperature in the last effect increase. In order to control these variables and therefore to keep a feasible operation of the MED plant, the feedwater mass flow rate and heating steam temperature need to be properly adjusted.

7. The accurate estimation of the annual power and water production in CSP+D plants, by using appropriate modelling of the part load operation of the integrated system, would permit to carry out more detailed economic studies for checking the feasibility of this

kind of plants. In this regard, the use of different coupling schemes depending on the power and water profile demands during the year increases the efficiency of both the power and water production, and therefore reduces the production costs. As a particular case study, the yearly power and fresh water production for a hypothetic MED-TVC+PT-CSP plant located in Almería (Spain), with same features of the subsystems described previously, has been estimated using the developed models of the solar field, power block and desalination unit. Two integration schemes previously analysed have been alternatively used, depending on the monthly electric energy demand: using steam from the high pressure turbine to feed the MED-TVC unit, and using steam from the low pressure turbine. Results obtained showed that the maximum electricity and fresh water productions were achieved during the summer period. In particular, July was the best month, with 24,122.7 MWh and 221,765.3 m^3, which could supply electric energy and fresh water to 72,369 households and 47,691 inhabitants, respectively. Finally, the total yearly amount of electric energy and fresh water production were 150,663.2 MWh and 1,505,725 m^3. If it is compared with the published annual electricity generation of 175,000 MWh in Andasol-1, it would mean a 14% of decrease due to the fresh water production.

8.2 Future works

As a result of the different analyses performed in this thesis, further investigation on the improvement of the MED process and its integration with CSP plants are proposed. Particularly, reliable variable nozzle thermocompressor models are needed in order to make realistic estimations of their performance. To that end, a test bed facility recently installed at Plataforma Solar de Almería will be useful for obtaining empirical performance curves and for validating theoretical models. This facility consists in a train of four different thermocompressors operating in a wide range of motive and entrained vapour pressures and flow rates, which are fed by a steam generator powered by the thermal energy provided by a parabolic trough solar field.

Another investigation line suggested is to increase the operation temperature at the outlet of the ejectors in MED-TVC units, which could improve the thermal efficiency of the desalination process although a higher exergy motive steam is expected to be required.

Regarding the modelling of the MED process, the presence of non-condensable gases should be accounted in future works, along with a more exact calculation of the overall heat transfer coefficients.

Also, assessments of the integration of MED-TVC processes into higher temperature power cycles, such as Brayton, which are suitable for using in central receiver towers, may be carried out in order to investigate the potential of this kind of systems comparing with the ones already studied.

Finally, with the simulation tool developed for the detailed calculation of the annual power and water production in CSP+MED-TVC systems, the completion of thermo-economic analyses are proposed in order to provide realistic estimations of the levelised energy and water costs, if reliable cost data of the different components are obtained. The accurate assessment of these costs is fundamental for project feasibility analyses.